

**Effect of Precursor Anion in Alcohol/Water Solutions During
Hydro/Solvothermal Synthesis on Cobalt Oxide Morphology
and Catalytic Ability**

by Whitney Heuvel

Thesis submitted in fulfilment of the requirements for the degree

Master of Engineering in Chemical Engineering

in the Faculty of Engineering

Cape Peninsula University of Technology

District Six Campus

Supervisor: Prof. Veruscha Fester

Cape Town

March 2020

CPUT copyright information

The thesis may not be published either in part (in scholarly, scientific or technical journals),
or as a whole (as a monograph), unless permission has been obtained from the University

Declaration

I, WHITNEY EMBETH HEUVEL, declare that this thesis is my own unaided work. It is being submitted in fulfilment of the MEng Degree at Cape Peninsula University of Technology, District Six Campus. It has not been submitted before for any degree or examination in any other University.



(Signature)

Signed in Cape Town this 11 day of March 2020

Abstract

The textile industry requires water for practically every step during its manufacturing process, and would benefit from water reuse systems. This is challenging, as the reactive dyes used in this industry often escape the conventional wastewater treatment methods used. The use of advanced oxidation processes combats these challenges, as it allows for the conversion of organic toxic waste to harmless H₂O and CO₂. Potassium peroxymonosulphate (Oxone[®]) has become popular in these treatment methods, as highly active sulphate radicals are activated once in contact with a transition metal. Such reactions are dependent on the catalyst used, and therefore require control of its morphology for enhanced capabilities. Cobalt oxide is deemed the best activator of peroxymonosulphate. The use of alcohols in its synthesis has been studied, but a systematic study increasing the alcohol chain lengths, in addition to the cobalt anion during hydro/solvothermal synthesis, has not been studied. Although the cobalt complex formed from cobalt chloride in water and alcohol has been studied, the use of these complexes as a precursor to cobalt oxide nanoparticles has not been studied.

Cobalt hydroxide precursors were therefore synthesised in pure alcohol, pure water and alcohol/water solutions in the ratios 1:1 and 1:0. Five alcohols were selected, namely methanol, ethanol, propanol, butanol and octanol. and cobalt chloride hexahydrate and cobalt nitrate hexahydrate were used to study the effect of the anion. The effect of calcination temperature was also studied by varying it between 300°C and 500°C. The resulting particles were characterised using TEM, SEM, XRD, BET, EDS, FT-IR and ELNEFS, and its catalytic ability was tested treating a methylene blue solution in an in-house developed continuous reactor.

Both α - and β -cobalt hydroxide polymorphs were encountered as precursors from cobalt chloride. The β -phase was evident when the water was exhausted from the system, whereas the α -phase was evident when water was present in the system. Only α -cobalt hydroxide was formed from cobalt nitrate. This provided a relationship between the cobalt complex formed to the phase of cobalt hydroxide polymorph. A blue, tetrahedral orientated precursor complex, produced pink β -cobalt hydroxide particles, while a red, octahedral orientated precursor complex, produced α -cobalt

hydroxide. Cobalt oxide nanoparticles were formed from both α - and β -cobalt hydroxides.

Anion morphology-dependent changes were observed in the presence of alcohol only. Rods were formed in the presence of the nitrate anion, while rhombic shapes dominated in the presence of chloride anions. Only rods were produced in water.

An increase in the calcination temperature increased the crystallite size, which negatively affected the catalytic activity. It was also noted that a crystallite size between 8 and 11 nm resulted in highly active cobalt oxide particles for both anions explored. The catalytic ability of the cobalt oxide resulting from the β -phase was better than that of the α -phase. The best catalytic activity was produced by the cobalt oxide synthesised from cobalt chloride hexahydrate precursor salt in 100% methanol for which the ELNEFS analysis revealed a $\text{Co}^{3+}/\text{Co}^{2+}$ ratio of ten times that of its 50% counterpart.

Dedication

To my amazing parents,

Wendy and Claude Heuvel

Thank you for the love you show and for pushing me to be the best I can be.

I love you and I'm proud to be your daughter.

To my brother and sister,

Devin and Mishka Heuvel

I consider myself blessed and highly favoured for the siblings I have.

Thank you.

Thank You, Lord, for making me realise just how small I am, and how great Your love
for me is.

**'What is mankind that You are mindful of them, human beings that you care
for them?'**

Psalm 8:4

ACKNOWLEDGEMENTS

- First and foremost, I would like to give all glory to the most high God for this journey I've been on. I was faced with many trials throughout this research and had I not depended completely on my source of life, I would not have completed this Master's degree. This work is a testament to God's unfailing love and favour.
- To Professor Veruscha Fester, thank you so much for your role as my supervisor. I appreciate every guiding word and support. Thank you for always pushing me to do better. You've impacted my life more than you know.
- I thank the Eyethu Community Trust (administered by the Nedbank Foundation) for the bursary awarded to me. This provided the payment of my studies, as well as expenses I had throughout the completion time. I am very grateful.
- I would love to express my gratitude to Mr Siyasanga Makaluza for his assistance in chemical orders, as well as Ms Pamela Matshaya for their roles in the administrative side of the FPRC unit.
- A big thank you to Mr Richard du Toit, Mr Kwezi Xashimba and Mr S bongiseni Ntombela for all laboratory assistance, for always being available whenever I needed something lifted or fixed. Every task is appreciated.
- I would like to thank Mr Gunnar Visser for allowing me to use the results of his research as a tool in my research. It played a huge role in determining the catalytic value of the particles I produced.
- I would like to thank Mr Remy Bucher from iThemba Labs, Miss Natasha Peterson, Mr Adrian Josephs and Dr Subelia Botha from UWC; Mr Sandeeran Govender from UCT, as well as Mr Solly Motaung from CSIR, for their aid in the characterisation of my nanoparticles.

- To my friends/fellow students, Ms Jorika Theart, Ms Micaela Harry and Ms Zintle Ntshoko, thank you for always being an ear and an encouraging word. Your friendship is precious to me.
- A big thank you to Dr. Bertrand Sone for the review of my first draft and the valuable comments made for it to be improved.
- Finally, I would love to thank my loving boyfriend, Devan Visasie, for your continuous love and support. Thank you for always encouraging me and always covering me in prayer. I love and appreciate you.

TABLE OF CONTENTS

Declaration	ii
Abstract.....	iii
Dedication	v
ACKNOWLEDGEMENTS.....	vi
TABLE OF CONTENTS.....	viii
LIST OF FIGURES	xiii
LIST OF TABLES.....	xviii
TERMS AND CONCEPTS	xix
LIST OF ABBREVIATIONS	xx
CHAPTER 1 INTRODUCTION	1
1.1 Background and Motivation.....	1
1.2 Research problem.....	2
1.3 Research question	2
1.4 Aims and objectives	2
1.5 Significance.....	3
1.6 Delineation	3
1.7 Organisation of research.....	3

CHAPTER 2 LITERATURE REVIEW	5
2.1 Introduction.....	5
2.2 Nanoscale	6
2.3 Cobalt oxide.....	6
2.4 Particle morphology	7
2.4.1 <i>Particle shape</i>	7
2.4.2 <i>Particle size</i>	11
2.5 Co ₃ O ₄ precursors and synthesis methods.....	13
2.6 Cobalt oxide production methods.....	23
2.6.1 <i>Sol-gel synthesis</i>	24
2.6.2 <i>Hydrothermal/solvothermal decomposition</i>	24
2.6.3 <i>Thermal decomposition</i>	25
2.6.4 <i>Gamma irradiation</i>	25
2.7 The effect of alcohol on nanoparticle synthesis	26
2.8 Effect of calcination temperature	32
2.9 Effect of pH.....	32
2.10 Advanced Oxidation Processes (AOPs)	32
2.10.1 <i>Hydroxyl radicals vs. sulphate radicals</i>	33
2.10.2 <i>Factors influencing sulphate radical formation</i>	35
2.10.3 <i>Chloride effects on PMS- based degradation</i>	36

2.11	Conclusion	39
CHAPTER 3 RESEARCH METHODOLOGY		41
3.1	Research design	41
3.2	Experimental methods.....	41
3.2.1	<i>Cobalt hydroxide synthesis.....</i>	<i>42</i>
3.2.2	<i>Cobalt hydroxide calcination.....</i>	<i>43</i>
3.2.3	<i>Advanced oxidation process.....</i>	<i>43</i>
3.3	Characterisation methods.....	44
3.3.1	<i>Selected Area Electron Diffraction.....</i>	<i>45</i>
3.3.2	<i>Electron Diffraction Spectroscopy</i>	<i>45</i>
3.3.3	<i>Energy Loss Near-Edge Fine Structure</i>	<i>46</i>
3.3.4	<i>Fourier Transform Infrared Spectroscopy</i>	<i>46</i>
3.3.5	<i>Scanning Electron Microscopy and Transmission Electron Microscopy</i>	<i>46</i>
3.3.6	<i>X-Ray Diffraction.....</i>	<i>47</i>
3.3.7	<i>Brunauer-Emmett-Teller</i>	<i>47</i>
3.4	Data.....	47
3.4.1	<i>Cobalt hydroxide powders.....</i>	<i>47</i>
3.4.2	<i>Degradation vs. time.....</i>	<i>47</i>
3.4.3	<i>Particle size vs. surface tension</i>	<i>48</i>
3.4.4	<i>Particle shape vs. degradative quality</i>	<i>48</i>
3.4.5	<i>Calcination temperature vs. particle size</i>	<i>48</i>
3.4.6	<i>Calcination temperature vs. degradative efficiency</i>	<i>49</i>
3.5	Conclusion	49

CHAPTER 4 THE EFFECT OF Cl^- AND NO_3^- ANIONS IN WATER ON Co_3O_4 PARTICLES	50
4.1 Introduction.....	50
4.2 Hydroxide polymorphs obtained from hydrothermal synthesis in pure water	50
4.3 Cobalt oxide identification and purity	52
4.4 Particle morphology	54
4.5 Effect of calcination temperature	57
4.6 Conclusion	58
CHAPTER 5 THE EFFECT OF Cl^- AND NO_3^- ANIONS IN ALCOHOLS ON Co_3O_4 PARTICLES	59
5.1 Introduction.....	59
5.2 Hydroxide polymorphs obtained from hydro/solvothermal synthesis	59
5.3 Cobalt oxide identification and purity	64
5.4 Particle morphology	72
5.5 Conclusion	82
CHAPTER 6 EVALUATION OF THE CO_3O_4 PARTICLES SYNTHESISED during COLOUR DEGRADATION	84
6.1 Colour degradation studies.....	84
6.2 Comparative analysis	98
6.3 Optimisation of degradation studies	101
6.3.1 <i>Optimisation of catalyst load</i>	101

6.3.2	<i>Optimisation of Oxone® concentration</i>	103
6.3.3	<i>System optimisation for dye degradation</i>	103
6.4	Conclusion	107
CHAPTER 7 CONCLUSIONS AND RECOMMENDATIONS		109
7.1	Introduction.....	109
7.2	Conclusions.....	109
7.3	Contributions.....	111
7.4	Recommendations for future research	112
REFERENCES		113
APPENDICES.....		120
APPENDIX A XRD SPECTRA FOR THE SYNTHESISED PARTICLES		120
APPENDIX B FT-IR SPECTRA FOR THE SYNTHESISED PARTICLES.....		126
APPENDIX C EDS SPECTRA FOR THE SYNTHESISED PARTICLES.....		131
APPENDIX D PSD CURVES FOR THE SYNTHESISED PARTICLES.....		134
APPENDIX E SAED IMAGES FOR THE SYNTHESISED PARTICLES		140
APPENDIX F DEGRADATION CURVES		142

LIST OF FIGURES

Figure 2-1: Hydrothermal production of cobalt oxide using CoCl_2 and KCN only, or with the addition of Hydrazine or H_2O_2 in the synthesis route (Kim & Huh, 2011)	8
Figure 2-2: SEM images of $\alpha\text{-Mn}_2\text{O}_3$ catalysts a) truncated octahedra, b) octahedra, c) cubic (Saputra <i>et al.</i> , 2014)	9
Figure 2-3: Crystalline facets exhibited by various Mn_2O_3 shapes a) cubic, b) truncated octahedra and c) octahedra (Saputra <i>et al.</i> , 2014)	10
Figure 2-4: SEM images of Co_3O_4 catalysts a) cubic, b) spherical, c) truncated cube (Saputra <i>et al.</i> , 2017)	11
Figure 2-5: An illustration of the structure of layered double hydroxides (Mishra <i>et al.</i> , 2018)	14
Figure 2-6: XRD peaks for a) $\alpha\text{-Co(OH)}_2$ and b) $\beta\text{-Co(OH)}_2$ (Al-Ghoul <i>et al.</i> , 2009)	15
Figure 2-7: SEM images of a) $\alpha\text{-Co(OH)}_2$ and b) $\beta\text{-Co(OH)}_2$ (Al-Ghoul <i>et al.</i> , 2009)	15
Figure 2-8: Liesegang bands formed as hydroxide solution is added to the cobalt chloride solution at a) the initial interface as a blue $\alpha\text{-Co(OH)}_2$ band is formed, b) the formation of a pink $\beta\text{-Co(OH)}_2$ above the blue band c) two weeks after initial interface, d) enlargement of c. (El-Batlouni <i>et al.</i> , 2008)	16
Figure 2-9: XRD patterns exhibited by as prepared a) blue $\alpha\text{-Co(OH)}_2$ and b) pink $\beta\text{-Co(OH)}_2$ (El-Batlouni <i>et al.</i> , 2008)	17
Figure 2-10: Liesegang bands formed in 1% agar gel using 0.05 M cobalt chloride solution and 2 M ammonia, varying the pH to a) 2, b) 2.5, c) 3.5, d) 4.5 (Rajurkar & Ambekar 2015)	18
Figure 2-11: FESEM images of $\alpha\text{-Co(OH)}_2$ with varied interspatial anions a) as prepared Co(OH)_2 - chloride b) -nitrate c) - acetate, d) - sulphate (Hu <i>et al.</i> , 2009)	20
Figure 2-12: SEM images of $\alpha\text{-Co(OH)}_2$ with varied interspatial anions a) as prepared Co(OH)_2 - chloride b) -nitrate c) -acetate and d) -sulphate (Cheng <i>et al.</i> , 2014)	21
Figure 2-13: XRD patterns of as prepared $\alpha\text{-Co(OH)}_2$ (Cao & Wang, 2016)	21
Figure 2-14: XRD pattern exhibited by ultra-fine a) cobalt hydroxide nanowires and b) cobalt oxide nanowires (Mahmoud & Al-Agel, 2011)	22
Figure 2-15: a) XRD and b) FT-IR spectra of the as-prepared cobalt oxide nanopowders (Chani <i>et al.</i> , 2015)	24
Figure 2-16: a)XRD patterns, and b)FT-IR spectra for the Co(OH)_2 formed using different water/ethanol ratios and varying hydrothermal times at 220C. a-d) hydrothermal time: 24 h, and	

water/ ethanol ratios of a) 1:0, b) 2:1, c) 1:2, and d) 1:10. e-f) water/ ethanol ratio: 2:1, hydrothermal time for: e) 12 h, and f) 6 h (Wang <i>et al.</i> , 2011)	28
Figure 2-17: The effect of a) PMS concentration, b) cobalt ion concentration and c) pH on the rate of phthalic acid degradation in the Co/PMS system (Huang <i>et al.</i> , 2017).....	37
Figure 2-18: a) The effects of chloride ion addition to the Co/PMS system on the decomposition rates of PA and dyes, b) the dual effect exhibited in the Co/PMS/Cl system with increasing chloride ion concentration (Huang <i>et al.</i> , 2017).....	38
Figure 2-19: Adsorbable organic halides (AOX) formation during PA degradation in the Co/PMS/Cl system when increasing chloride ion concentration (Huang <i>et al.</i> , 2017)	39
Figure 3-1: Ring diffraction pattern observed for many crystallites (Egerton 2005)	45
Figure 3-2: Hydro/solvothermal reaction vessel with temperature controller.....	42
Figure 3-3: LABOFURN furnace used for calcination	43
Figure 3-4: In-house developed reactor used to evaluate the cobalt oxide particles in AOPs	44
Figure 4-1: Cobalt chloride hexahydrate and cobalt nitrate hexahydrate in pure water.....	50
Figure 4-2: Cobalt hydroxide particles synthesised from cobalt chloride hexahydrate and cobalt nitrate hexahydrate in pure water	51
Figure 4-3: EDS spectra for cobalt oxide particles produced with a cobalt chloride base salt in 50% alcohol/water solutions calcined at 300°C	53
Figure 4-4: FT-IR spectra for cobalt oxide particles produced with a cobalt chloride base salt in 50% alcohol/water solutions, calcined at 300°C	53
Figure 4-5: XRD spectra for the cobalt oxide particles produced with cobalt chloride hexahydrate and cobalt nitrate hexahydrate in pure water, calcined at 300°C.....	54
Figure 4-6: SAED images for the cobalt oxide particles synthesised from cobalt chloride hexahydrate and cobalt nitrate hexahydrate in pure water, calcined at 300°C.....	55
Figure 4-7: Transmission electron microscopy images for the cobalt oxide particles produced from a) cobalt chloride hexahydrate and b) cobalt nitrate hexahydrate in pure water	55
Figure 4-8: Scanning electron microscopy images for the cobalt oxide particles synthesised from a) cobalt chloride hexahydrate and b) cobalt nitrate hexahydrate in pure water	56
Figure 4-9: Particle size distribution curves as deduced from transmission electron microscopy images for the cobalt oxide particles synthesised from cobalt chloride hexahydrate in water	57
Figure 5-1: 100% octanol precursor after pH correction.....	61
Figure 5-2: Cobalt hydroxide precursors resulting from a) fully alcohol solutions (blue in colour), b) alcohol/water mixtures, c) cobalt chloride hexahydrate in 50% ethanol and 50% butanol respectively	

and d) all cobalt nitrate hexahydrate precursors.....	63
Figure 5-3: EDS spectra for the cobalt oxide synthesised from cobalt chloride hexahydrate in 100% alcohol solvents, calcined at 300°C.....	64
Figure 5-4: EDS spectra for the cobalt oxide synthesised from cobalt chloride hexahydrate in 50% alcohol/water solvents, calcined at 300°C.....	65
Figure 5-5: EDS spectra for the cobalt oxide synthesised from cobalt nitrate hexahydrate in 100% alcohol solvents, calcined at 300°C	65
Figure 5-6: EDS spectra for the cobalt oxide synthesised from cobalt nitrate hexahydrate in 50% alcohol solvents, calcined at 300°C	66
Figure 5-7: FT-IR spectra for the cobalt oxide particles synthesised from cobalt chloride hexahydrate precursor salt in 100% alcohol solvents, calcined at 300°C.....	67
Figure 5-8: FT-IR spectra for the cobalt oxide particles synthesised from cobalt chloride hexahydrate precursor salt in 50% alcohol solvents, calcined at 300°C	67
Figure 5-9: FT-IR spectra for the cobalt oxide particles synthesised from cobalt nitrate hexahydrate precursor salt in 100% alcohol solvents, calcined at 300°C	68
Figure 5-10: FT-IR spectra for the cobalt oxide particles synthesised from cobalt nitrate hexahydrate precursor salt in 50% alcohol solvents, calcined at 300°C	68
Figure 5-11: XRD spectra for the cobalt oxide particles synthesised from cobalt chloride hexahydrate precursor salt in 100% alcohol solvents, calcined at 300°C	70
Figure 5-12: XRD spectra for the cobalt oxide particles synthesised from cobalt chloride hexahydrate precursor salt in 50% alcohol solvents, calcined at 300°C	70
Figure 5-13: XRD spectra for the cobalt oxide particles synthesised from cobalt nitrate hexahydrate precursor salt in 100% alcohol solvents, calcined at 300°C	71
Figure 5-14: XRD spectra for the cobalt oxide particles synthesised from cobalt nitrate hexahydrate precursor salt in 50% alcohol/water solutions, calcined at 300°C.....	71
Figure 5-15: Transmission electron microscopy images for the cobalt oxide particles produced from cobalt chloride hexahydrate precursor salt in a) 100% methanol, b) 50% methanol as well as the c) scanning electron microscopy image of hierarchical hexagonal skeleton of Co ₃ O ₄ produced by Kim and Huh (2011).....	74
Figure 5-16: Crystallite size for the synthesised cobalt oxide particles calcined at 300°C versus alcohol/water solvent surface tension at 25°C	81
Figure 6-1: Degradation curves for the methylene blue solutions degraded using the cobalt oxide catalysts synthesised from cobalt chloride hexahydrate in 100% alcohol solutions, calcined at 300°C	

.....	85
Figure 6-2: Degradation curves for the methylene blue solutions degraded using the cobalt oxide catalysts synthesised from cobalt chloride hexahydrate in 50% alcohol/water solutions as well as 100% water, calcined at 300°C	85
Figure 6-3: Methylene blue samples a) before treatment, b) after treatment using the cobalt oxide catalysts synthesised in 100% alcohol solvents and c) after treatment using the cobalt oxide catalysts synthesised in 50% alcohol/water solutions, calcined at 300°C.....	86
Figure 6-4: Treated methylene blue samples after a 30-minute standing time	87
Figure 6-5: Degradation curves for the catalytic degradation of methylene blue using the cobalt oxide synthesised from cobalt nitrate hexahydrate in 100% alcohol solvents, calcined at 300°C.....	88
Figure 6-6: Degradation curves for the catalytic degradation of methylene blue using the cobalt oxide synthesised from cobalt nitrate hexahydrate in 50% alcohol/water solutions and 100% water, calcined at 300°C.....	88
Figure 6-7: Degradation curves for the methylene blue solutions degraded using commercially produced Sigma-Aldrich cobalt oxide samples, as well as the two synthesised cobalt oxide samples resembling the most rapid and slowest degradation rates	89
Figure 6-8: The degradation quality at 2 minutes vs. d50 particle size for the cobalt oxide particles synthesised from a) cobalt chloride hexahydrate and b) cobalt nitrate hexahydrate in 100% and 50% alcohols, calcined at 300°C, as well as the commercially available 50 nm cobalt oxide particles	91
Figure 6-9: The degradation quality at 2 minutes vs. crystallite size for the cobalt oxide particles synthesised from a) cobalt chloride hexahydrate and b) cobalt nitrate hexahydrate in 100% and 50% alcohols, calcined at 300°C, as well as the commercially available 50 nm cobalt oxide particles.....	91
Figure 6-10: The degradation quality at 2 minutes vs. BET surface area for the cobalt oxide particles synthesised from a) cobalt chloride hexahydrate and b) cobalt nitrate hexahydrate in 100% and 50% alcohols, calcined at 300°C, as well as the commercially available 50 nm cobalt oxide particles.....	92
Figure 6-11: Illustration of the interlamellar spacing measured for the cobalt oxide particles synthesised in 100% methanol	93
Figure 6-12: Degradation curves for the methylene blue solution degraded using the cobalt oxide catalysts synthesised from cobalt chloride hexahydrate in 100% alcohol solvents, calcined at 400°C	96
Figure 6-13: Degradation curves for the methylene blue solution degraded using the cobalt oxide catalysts synthesised from cobalt nitrate hexahydrate in 100% alcohol solvents, calcined at 500°C	96
Figure 6-14: Degradation curves for the treated methylene blue solution using the cobalt oxide	

catalysts which produced the fastest degradation rates	99
Figure 6-15: Degradation curved for the treated methylene blue solution using the cobalt oxide catalysts which produced the slowest degradation rates.....	99
Figure 6-16: ELNEFS spectra revealing the L3 and L2 peaks for the cobalt oxide particles showing the best catalytic degradation properties i.e. produced from cobalt chloride hexahydrate in 100% methanol, calcined at 300°C.....	100
Figure 6-17: ELNEFS spectra revealing the L3 and L2 peaks for the 50% counterpart of the 100% methanol cobalt chloride hexahydrate particles, calcined at 300°C	100
Figure 6-18: Methylene blue degradation with catalyst load variance	102
Figure 6-19: Methylene blue degradation with Oxone variance.....	103
Figure 6-20: Degradation of various concentrations of methylene blue at optimum conditions ..	104
Figure 6-21: Treated methylene blue solutions at concentrations of a) 50 mg/L, b) 75 mg/L and c) 100 mg/L.....	104
Figure 6-22: Degradation of methylene blue at various concentration at optimum conditions and increased filter bed	105
Figure 6-23: Degradation of various reactive dyes with the same molarity at the optimum conditions	106

LIST OF TABLES

Table 2-1: Properties of pure water, pure alcohol and alcohol/water mixtures	27
Table 2-2: Summary of various Co_3O_4 synthesis routes using alcohols	30
Table 4-1: Crystallite sizes for the synthesised cobalt oxide particles synthesised in pure water, calcined at 300, 400 and 500°C	58
Table 5-1: Cobalt chloride hexahydrate and cobalt nitrate hexahydrate in a) 100% and b) 50% alcohol/water solutions respectively	60
Table 5-2: SAED images for the cobalt oxide particles synthesised in methanol and ethanol at 50% and 100% alcohol/water ratios respectively, calcined at 300°C.....	73
Table 5-3: Transmission Electron Microscopy images at 50 nm and 0.2 m, and Scanning Electron Microscopy images for the selected cobalt oxide particles synthesised from cobalt nitrate hexahydrate, showing various particle morphologies	75
Table 5-4: Particle size distribution curves as deduced from transmission electron microscopy images for the cobalt oxide particles synthesised from cobalt chloride hexahydrate and cobalt nitrate hexahydrate in various alcohols at 100% or 50% concentrations	77
Table 5-5: d_{50} particle sizes for the cobalt oxide particles, adapted from the particle size distribution curves	80
Table 5-6: Crystallite sizes for the synthesised cobalt oxide particles calcined at 300, 400 and 500°C-	82
Table 6-1: The resulting d-spacing and main exposed facets of the cobalt oxide particles synthesised from cobalt chloride hexahydrate in 100% and 50% alcohol/water solvents	94
Table 6-2: Measured d-spacing and corresponding exposed facet for the cobalt oxide particles synthesised from cobalt nitrate in 100% and 50% alcohol solvents, calcined at 300°C.....	95
Table 6-3: Samples taken immediately after methylene blue colour degradation for the cobalt oxide catalysts synthesised from a cobalt nitrate hexahydrate precursor salt in 50% propanol, calcined at 300, 400 and 500°C.....	97
Table 6-4: Clarity of samples after a standing time for the samples taken immediately after the colour degradation of methylene blue using the cobalt oxide catalysts synthesised from cobalt nitrate hexahydrate precursor salt.....	97

TERMS AND CONCEPTS

100% alcohol: Only alcohol was used as a solvent in these solutions at its purity grade

Advanced oxidation processes: Processes which apply oxidation to remove organic waste in water through reactions with radicals.

Agglomeration: A mass or collection of particles which self-assemble.

Amorphous: A solid without a clearly defined shape or form.

Calcination: The thermal decomposition of solid materials as heat is applied in either a low-oxygen environment or in the absence of oxygen.

Catalytic degradation: The increased mineralisation of a substance as a result of the use of a catalyst.

Crystalline: Having the structure and form of a crystal - geometric in shape.

Facets: Flat faces on geometric shapes of crystallites differing in surface energies.

Hydro/solvothermal synthesis: The crystallisation of materials in a solution at elevated temperatures and pressure. Hydrothermal refers to a system specifically using water as a solvent, while solvothermal is a system using any other liquid as a solvent.

Hydroxylation: The introduction of a hydroxyl group into a molecule, especially by the replacement of a hydrogen atom.

Morphology: a form, shape, or structure of particles formed.

Nanoparticles: particles which hold sizes between 1 and 100 nm.

Oxidation: The combination of a substance with oxygen.

Precursor: A substance from which another is formed.

Radical: An atom, molecule or ion with an unpaired electron in its valence shell making it highly chemically reactive.

Reaction rate: The speed at which reactants are converted into products.

Solvent: A liquid able to dissolve other substances.

Surface tension: The tension of the surface of a liquid caused by the attraction of the atoms/molecules in the surface layer by the atoms/molecules in the bulk of the liquid.

LIST OF ABBREVIATIONS

AOP: Advanced Oxidation Processes

BET: Brunauer–Emmett–Teller

FESEM: Field Emission Scanning electron microscopy

FT-IR: Fourier Transform Infrared Radiation

HRTEM: High Resolution Transmission Electron Microscopy

ICP-OES: Inductively coupled plasma - optical emission spectrometry

JCPDS: Joint Committee on Powder Diffraction Standards

LDH: Layered Double Hydroxides

PMS: Peroxymonosulphate

SAED: Selected Area Electron Diffraction

SBA: Santa Barbara Amorphous

SEM: Scanning Electron Microscopy

XRD: X-ray Diffraction

CHAPTER 1 INTRODUCTION

1.1 Background and Motivation

Every aspect of life is at some point impacted by water – including food, power and commerce. Although most of the planet is made up of water, only about 3% is fresh drinking water, with only 0.3% of it accessible as surface waters, making less than 1% of the earth's waters usable by humans (National Geographic, 2019). It is therefore important for the utilisation of this resource to be carefully managed and for continuous education of its efficient usage to be encouraged. A method strongly being encouraged by researchers is the reuse of water, which allows for the demand on fresh drinking water to be diminished. One industry which could majorly benefit from this is the textile industry which is dependent on water for practically every step of textile manufacturing. However, several challenges exist in the water treatment processes within this industry.

The removal of organic toxic waste within textile wastewater has proven to be time-consuming, expensive and often a source of secondary pollution (Warang *et al.*, 2013). Advanced Oxidation Processes (AOPs) have shown promising results as an alternative for conventional wastewater treatment methods (Saputra *et al.*, 2013), with the conversion of harmful organic toxic waste to harmless H₂O and CO₂ (Warang *et al.*, 2013). The effectiveness of treatment using AOPs depends on the type of AOP used, physical/chemical properties of the target pollutants, operational conditions, as well as the oxidative strength (Deng & Zhao, 2015). With that in mind sulphate radicals have attracted attention because of higher reduction potentials when compared with hydroxyl radicals. The use of transition metals has therefore become popular in AOPs due to their ability to generate sulphate radicals by the activation of peroxymonosulphate (Saputra *et al.*, 2013; Chowdhury *et al.*, 2015).

Among various transition metals and their oxides, cobalt oxide (Co₃O₄) has become increasingly popular due to its widespread use in sensors, and energy storage devices (magnetic, electric, opto-electric), as well as its rapid catalytic activity (Athawale *et al.*, 2010; Gamonchuang *et al.*, 2016; Huang *et al.*, 2014; Yang *et al.*, 2004). These attractive properties are a result of its particle size (Yang *et al.*, 2004)

and morphology (Gamonchuang *et al.*, 2016; Huang *et al.*, 2014). Control of particle morphology has therefore been an important factor in Co_3O_4 synthesis (Gamonchuang *et al.*, 2016), and has been found to be complicated as small changes drastically affect the particles formed. This, however, provides a means of control, as the morphologies may purposefully be manipulated by simple, impactful changes as is the case with the hydrothermal route explored by Kim and Huh (2011).

1.2 Research problem

The effect of varying precursor anions in alcohol/water solutions at 100% and 50% concentrations on cobalt oxide morphology during hydro/solvothermal synthesis, as well as their resulting catalytic ability, has not yet been studied.

1.3 Research question

What is the effect of changing the precursor anion in various alcohols at 100% and 50% concentrations on the size and shape of cobalt oxide nanoparticles during hydro/solvothermal synthesis and the resulting effect it has on the particle's catalytic ability?

1.4 Aims and objectives

The aim of this research was to investigate the effect of precursor anion in various alcohol solvents, as well as varying calcination temperature, on the size and/or shape of cobalt oxide nanoparticles during hydro/solvothermal synthesis, and their resulting catalytic ability.

The objectives were as follows:

- to produce cobalt oxide nanoparticles from hydro/solvothermally synthesized cobalt hydroxide, using cobalt chloride hexahydrate and cobalt nitrate hexahydrate in methanol, ethanol, propanol, butanol and octanol at 100% and 50% concentrations;
- to characterize the synthesized particles using TEM, SEM, EDS, XRD, FT-IR, BET and ELNEFS;
- to evaluate the effect of precursor anion in water as well as alcohols at 100%

and 50% concentrations on the resulting cobalt hydroxide and cobalt oxide particles; and

- to evaluate the catalytic performance of cobalt oxide nanoparticles during cobalt oxide/peroxymonosulphate advanced oxidation processes.

1.5 Significance

Catalytic applications are highly dependent on surface structure of the catalysts used. Although strong catalytic activity of Co_3O_4 is noted, control of particle size and morphology has recently been a focus of researchers, especially for application purposes. Much focus has already been placed on varying methods to provide a fixed particle size and morphology, but the methods provided do not offer much opportunity for upscale synthesis. The work presented provides insight into the effects of precursor anion in combination with alcohol/water solutions for this specific hydro/solvothermal synthesis of Co_3O_4 particles. The significance provided is Co_3O_4 particles synthesised specifically from cobalt complexes, corresponding to the anion used in alcohol solutions at 100% and 50% concentrations, providing catalysts which could potentially be scaled up with ease.

1.6 Delineation

The research conducted does not include the synthesis of Co_3O_4 hybrids, containing other elements, for enhanced or varied results. Only 100% and 50% alcohol solutions were used during the synthesis in order to study the effect on cobalt complex formed. The effect of particle morphology and size on the quality of the produced particles were only tested catalytically in the colour degradation of the synthetic dye solutions prepared in the laboratory and not real textile wastewater.

1.7 Organisation of research

Chapter 2: Literature review

An in-depth review on the use, production, and importance of cobalt oxide, its precursors and the various effects on its morphology and catalytic ability. This chapter also focuses on its application in advanced oxidation procedures.

Chapter 3: Methodology

The hydro/solvothermal preparation methods of cobalt hydroxide precursors and its calcination to cobalt oxide is detailed. Further, the treatment methods of methylene blue using the in-house developed reactor are presented. In addition, the characterisation methods used are discussed.

Chapter 4: The effect of Cl^- and NO_3^- anions in water on Co_3O_4 particles

This chapter provides the discussion of the results obtained from using cobalt chloride hexahydrate and cobalt nitrate hexahydrate precursor salts in the hydrothermal synthesis of cobalt oxide.

Chapter 5: The effect of Cl^- and NO_3^- anions in alcohols on Co_3O_4 particles

This chapter provides results obtained from the use of various alcohols in 100% or 50% concentrations on the cobalt oxide particles formed in hydro/solvothermal synthesis.

Chapter 6: An evaluation of the Co_3O_4 particles synthesised in colour degradation

The performance of the various catalysts synthesised was evaluated in the degradation of methylene blue as a model dye and is described in this chapter.

Chapter 7: Conclusions

Presents the conclusions of the work and recommendations for future work.

CHAPTER 2 LITERATURE REVIEW

2.1 Introduction

An important function of engineering is the ability to control the output of a process. It is therefore an objective to produce size-controlled, monodispersed nanoparticles during nanomaterial synthesis (He *et al.*, 2004). Filipponi and Sutherland (2012) stated that nanotechnology is the design, characterisation, production and application of structures and systems at nanometre scale. Increasing attention has been drawn to nanostructured materials, due to the unique properties they possess as a result of their size and morphology (Ni *et al.*, 2001). These particles no longer follow Newtonian physics, but rather quantum mechanics (Filipponi & Sutherland, 2012).

An important feature of nanomaterials, widely exploited throughout research and application, is their large surface-to-volume ratio. These large ratios are important in processes such as catalysis and detection, in which the reactions occur at the surface of the material (Filipponi & Sutherland, 2012). In these reactions, the use of nanomaterials is economically as well as environmentally beneficial as it results in a drastic reduction of the required reactive material and provides an increase in active reaction sites in devices (Filipponi & Sutherland, 2012). The use of transition metal nanomaterials has recently gained momentum in this regard, as their unique magnetic and catalytic properties have been realised (Ni *et al.*, 2001). Among the transition metals, cobalt has become particularly popular in advanced oxidation processes (AOPs) for its ability to best activate sulphate radicals ($\bullet\text{SO}_4^-$) from Oxone (peroxymonosulphate) (Rivas *et al.*, 2009; Anipsitakis & Dionysiou, 2003).

Cobalt is a reactive transition metal that oxidises in air easily, especially at nanoscale (Ni *et al.*, 2001). Nanosized Co_3O_4 has been one of various cobalt oxides gaining interest in electrical, magnetic and catalytic applications, in which exceptional activity has been exhibited in contrast to bulk Co_3O_4 (Warang *et al.*, 2013). Co_3O_4 has also been reported to be useful in photocatalytic applications in the degradation of dyes under visible light and neutral pH (Warang *et al.*, 2013).

Moreover, its use in the activation of sulphate radicals ($\bullet\text{SO}_4^-$) from Oxone (peroxymonosulphate) has become popular in order to apply its high reduction

potential (2.5 – 3.1 V) (Neta *et al.*, 1988).

2.2 Nanoscale

Particles of a size measured in nanometres (nm) are particles which are typically between 1 and 100 nm in size. A nanometre (nm) is defined as one billionth of a metre. The three main reasons that the use of particles at nanoscale has become so popular lies in the properties of nanoparticles, which differ so strongly from their bulk counterparts, the fact that they are producible, and finally their large surface-to-volume ratio, which benefits processes that depend on surface reactions (Filipponi & Sutherland, 2012). The process of applying nanoscience to useful devices is termed nanotechnology. It entails the manufacturing and control of systems at nanoscale. All industrial sectors rely on materials made up of atoms and molecules and therefore, according to Filipponi and Sutherland (2012), may benefit from nanotechnologies.

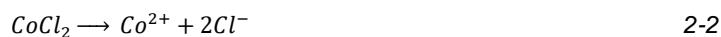
2.3 Cobalt oxide

Cobalt in its bulk form has been in use for decades in glass, glazes and pottery. It has been used as a blue dye in pottery from as early as 1450 BC (Yildiz, 2017). At the beginning of this century, the synthesis of cobalt compounds became popular, and much research has been carried out on cobalt catalysed reactions, which today have many different applications in industry. The salts and complexes of cobalt are commonly used as catalysts for the selective oxidation and selective epoxidation of alkanes and alkenes respectively, and therefore have gained interest in the areas of degradation of organic waste. Cobalt oxide (Co_3O_4) has been researched for application in wastewater treatment, as it shows thermodynamic stability and desirable catalyst properties, such as high surface-to-volume ratio, morphology-dependent properties and high concentration of active sites (Warang *et al.*, 2013). It may be synthesised using various methods utilising a cobalt salt along with a source of hydroxyl ions.

The use of ammonium hydroxide, also known as ammonia water, allows for the hydroxyl ions to be utilised. The following proceeds:



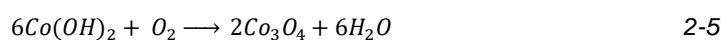
When using cobalt chloride solution:



When using cobalt nitrate solution:



Resulting in:



(Huang *et al.*, 2014)

2.4 Particle morphology

Reactions which are structure-sensitive depend on the morphology of the substances involved (Henry 2007). This is especially true for nanomaterials, as enhanced performance lies in their morphology (Huang *et al.*, 2014). Manipulating the size and morphology of nanoparticles is therefore important as they not only affect the properties of the materials themselves, but the performance of the devices they're used in (Huang *et al.*, 2014).

2.4.1 Particle shape

The development of nanoparticles is sensitive to many factors and may be manipulated by a simple change in production method. An example of this was shown in the work done by Kim and Huh (2011), demonstrated in Figure 2-1, in which three different morphologies of cobalt oxide were produced during hydrothermal synthesis by adjusting the amount of either hydrazine or H₂O₂ in the precursor solution.

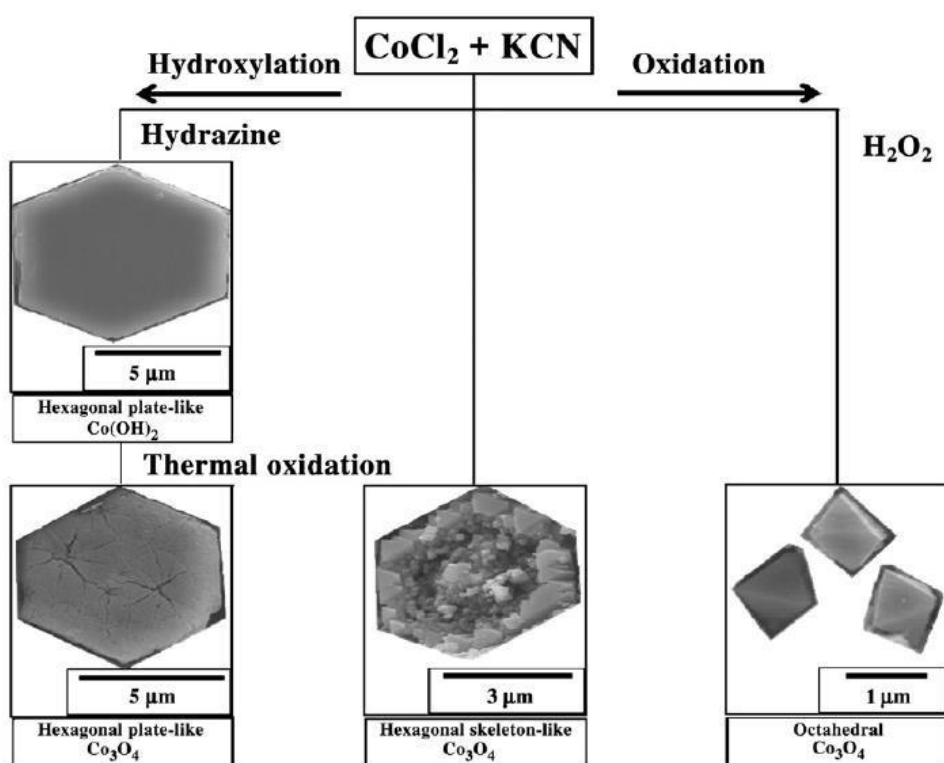


Figure 2-1: Hydrothermal production of cobalt oxide using CoCl_2 and KCN only, or with the addition of Hydrazine or H_2O_2 in the synthesis route (Kim & Huh, 2011) (Used with permission)

In this work, three methods are depicted: the first utilising CoCl_2 and KCN on its own, the second showing the effect of adding hydrazine and the third showing the effect of adding H_2O_2 to the hydrothermal system. This simple change ultimately resulted in three different morphologies, namely: hexagonal skeleton-like Co_3O_4 , hexagonal plate-like Co_3O_4 and octahedral Co_3O_4 . This is important, as it shows the delicate state of systems producing nanoparticles, and that simple changes could have major effects on the particles' shape and therefore the effectiveness of their use.

The general concept that higher surface area produces higher catalytic ability in solid catalysts was tested in a study performed by Saputra *et al.* (2014), whereby three different morphologies of $\alpha\text{-Mn}_2\text{O}_3$ catalysts, as shown in Figure 2-2, namely octahedral, truncated-octahedral and cube-shaped, were produced hydro/solvothermally. The first and second morphologies were obtained using ethanol and 2-butanol as solvents in similar production methods. The cubic morphology was obtained by adjusting the method to a two-step method by first producing MnCO_3 using KMnO_4 in a glucose

and water mixture and calcining to form Mn_2O_3 .

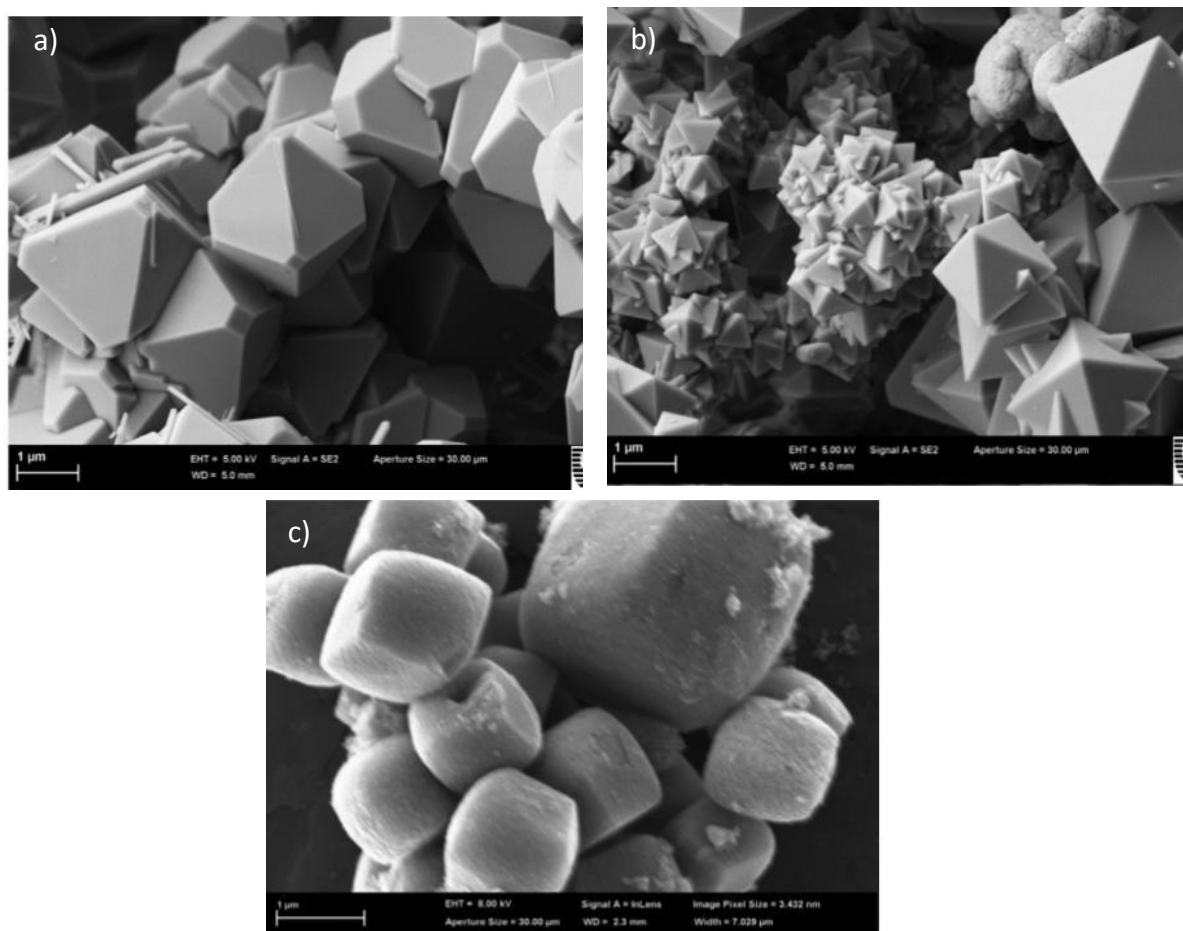


Figure 2-2: SEM images of $\alpha\text{-Mn}_2\text{O}_3$ catalysts a) truncated octahedra, b) octahedra, c) cubic (Saputra *et al.*, 2014) (Used with permission)

The surface area from Brunauer–Emmett–Teller (BET) characterisation was 4, 1.1 and 24.2 m^2/g for the truncated octahedra, octahedra and cubic samples respectively, with pore volumes of 0.011, 0.002 and 0.166, indicating that the high surface area exhibited by the cubic $\alpha\text{-Mn}_2\text{O}_3$ catalyst is due to the abundance of micropores in its structure.

Phenol mineralisation using these catalysts in combination with peroxymonosulphate revealed that the truncated octahedral particles provided the least phenol degradation, at 50% in 180 min; followed by the octahedral particles, which provided 100% phenol degradation in 180 min. The highest phenol degradation rate was exhibited by the cubic particles, which provided 100% degradation in 60 minutes. Overall, the catalytic ability followed the trend $\alpha\text{-Mn}_2\text{O}_3\text{-cubic} > \alpha\text{-Mn}_2\text{O}_3\text{-octahedral} > \alpha\text{-Mn}_2\text{O}_3\text{-truncated}$

octahedral, which provided a BET surface area of 24.2, 1.1, and 4 m²/g respectively, and pore volumes of 0.166, 0.002, and 0.011 respectively.

The general rule that higher surface area produces higher catalytic ability in solid catalysts was proven true in the case of α -Mn₂O₃-cubic particles. However, the remainder of the results indicated that surface area was not the only determining factor. Due to their non-porous structure, the α -Mn₂O₃-octahedral and α -Mn₂O₃-truncated octahedral particles presented far lower surface areas, and although the α -Mn₂O₃-octahedral particles had a lower BET surface area than that of the α -Mn₂O₃-truncated octahedral particles, it presented better degradation of phenol. It was therefore necessary to investigate the shape effects of the samples on the catalytic degradation. Previous work from Li *et al.* (2011) showed that the formation of M₂O₃ evolves from nanocubes to cuboctahedra and then octahedra, due to the growth rates exhibited by (001) and (111) facets. These facets are displayed in Figure 2-3. Taking this into account it was concluded that the α -Mn₂O₃-cubic particles were more active, as a combinative effect of their higher surface area, phenol adsorption and active surface facets.

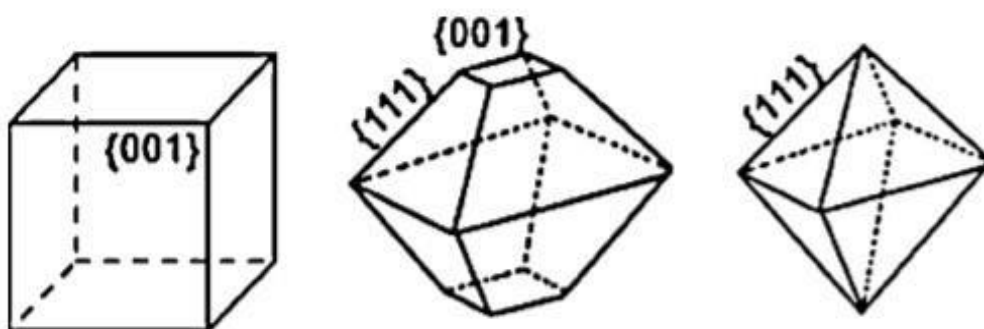


Figure 2-3: Crystalline facets exhibited by various Mn₂O₃ shapes a) cubic, b) truncated octahedra and c) octahedra (Saputra *et al.*, 2014) (Used with permission)

Work done by Saputra *et al.* (2017) supports this work during the production of Co₃O₄ of three different morphologies, shown in Figure 2-4, namely cubic, spherical and truncated cube, which were then used to mineralise phenol. From BET analysis, it was found that the surface area and pore volume of the produced particles decreased in order

of cube, truncated cube and sphere. However, in the degradation of phenol, the activity of the particles decreased in order of cube, sphere and finally truncated cube, once more indicating that catalytic activity is not dependent on surface area alone. The increased catalytic ability of cubic Co_3O_4 particles was attributed to the number of exposed (001) planes present, compared to that of the truncated cube (which had less) and the sphere (which had no specific facet). A test for cobalt leaching was done using an inductively coupled plasma-optical emission spectrometry (ICP-OES) spectrometer. Results revealed that the truncated cube Co_3O_4 presented the highest cobalt leaching while exhibiting the lowest catalytic ability, suggesting that exposed facets play a dominant role in peroxymonosulphate (PMS) activation.

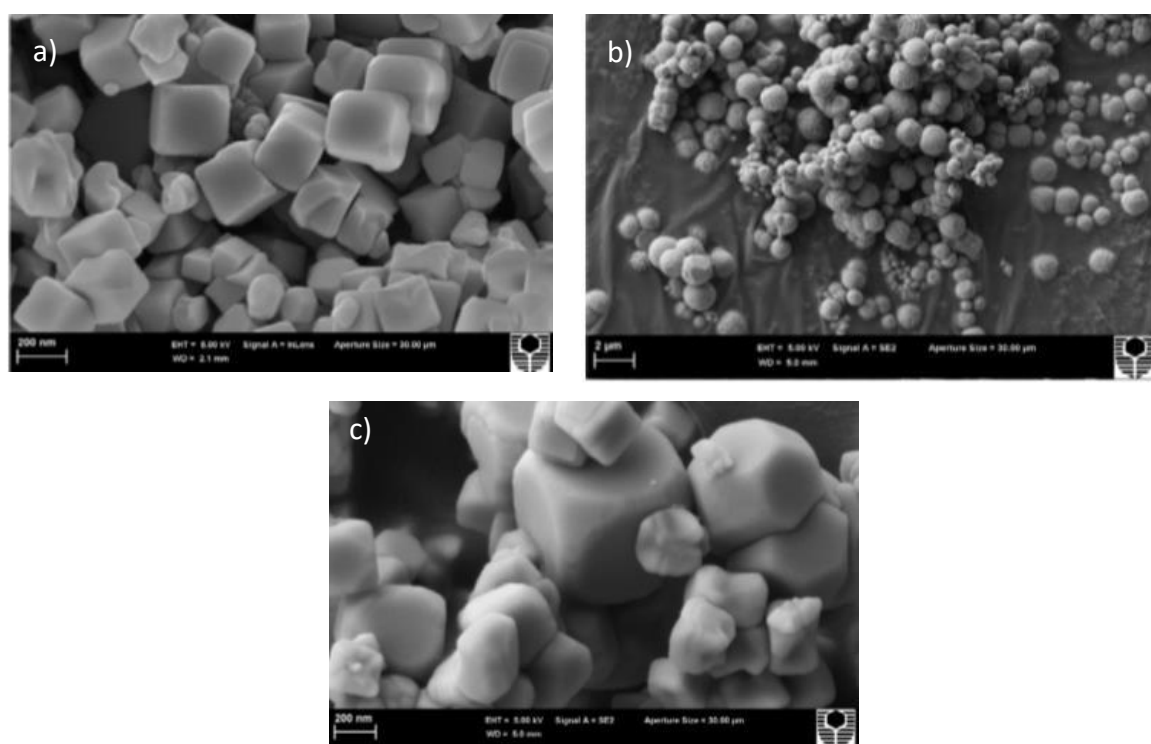


Figure 2-4: SEM images of Co_3O_4 catalysts a) cubic, b) spherical, c) truncated cube (Saputra *et al.*, 2017) (Used with permission)

2.4.2 Particle size

Although not the only determining factor, the surface area of the nanomaterial is important for catalytic performance, as the electron-hole pairs are generated at the surface (Li *et al.*, 2011). This is important, as the holes produced are responsible for the oxidative potential of the catalytic system. The electron holes may react either directly

with the organic waste or with the added oxidising agents, producing highly active radicals (Li *et al.*, 2011). The reduction of particle size increases the active surface area in catalysts (Vinod, 2010). In order to gain the advantage of an increased surface area, Choi *et al.* (2016) explored the synthesis of mesoporous Co_3O_4 . Previously, this was achieved using a hard template synthesis method. However, this gave rise to problems, mainly pertaining to cost. In order to eliminate this issue, two alternative methods were explored: a soft template synthesis method and a Santa Barbara Amorphous (SBA)-15 impregnation method.

The prepared catalysts were then used to decompose N_2O . Using the soft template method, it was noted that the surface area and porosity of the particles changed drastically as the particles lost their mesopores, therefore losing the purpose of the synthesis method. The SBA-15 impregnation method provided particles which maintained their structure and mesopores before and after N_2O decomposition. An interesting outcome of the studies showed that as the reaction temperature increased from 550 to 850°C, the N_2O conversions were impacted negatively (Choi *et al.*, 2016). This was attributed to the formation of Co_2SiO_4 , which was consequently inert for N_2O decomposition reactions. The reactions were then optimised to 550°C in order to avoid Co_2SiO_4 formation.

The fact that a reduced particle size increases the active surface area leads one to deduce that the smaller the particle, the more reactive. Li *et al.* (2011) demonstrate this in their production of urchin-like Co_3O_4 nanoparticles, as a larger specific surface area revealed a higher degradation efficiency in comparison to a lower specific area. However, nanocatalysts may be far more complex than this, as various other influences influence their reactivity.

An example of this has been reported in the use of cobalt catalysts in the Fischer-Tropsch process – in which no significance was attributed to catalyst size in the range of 6 to 200 nm. However, at a particle size lower than 6 nm, inferior reactivity was exhibited (Vinod, 2010). The key purpose of the Fischer-Tropsch process is to convert syngas to liquid hydrocarbon using a surface polymerisation reaction. The use of

cobalt catalysts in these processes are well known and widely used. Work done by Lu *et al.* (2015) explored the use of mesoporous SBA-15 particles as a support for cobalt, to achieve a higher density of active sites. Such studies have been explored using various porous substrates. In their experiments, it was found that smaller crystallite sizes were more beneficial in terms of cobalt dispersion in the 20% loaded SBA-15 samples in comparison to a SiO₂ substrate. Interplanar spacing, as investigated by high resolution transmission electron microscopy (HRTEM) was found to be 0.287 (220) and 0.208 (400) nm, showing that the cobalt used was Co₃O₄. Further, diffraction peaks from X-ray Diffraction (XRD) analysis of 19.0 (111), 31.3 (220), 36.9 (311), 44.8 (400), 59.4(511), and 65.2 (440) indicated that after calcination, the cobalt presented was in the form of Co₃O₄ spinel, according to the Joint Committee on Powder Diffraction Standards (JCPDS) card no. 42-1467. At Fischer-Tropsch conditions, CO conversion using the cobalt-loaded SBA-15 samples reached an optimum at 20% cobalt, and a minimum at 10%. The efficiency also dropped above 20% cobalt loading. Pore size of the SBA-15 substrate also played a major role in CO conversion, as the conversion increased with increases in pore volume in the range 4.9 to 9.7 nm. This was in agreement with work done by Xiong *et al.* (2008) as referenced by Lu *et al.* (2015), which indicated larger pores lead to larger cobalt cluster sizes, lower dispersion and higher reducibility. Overall, the smaller crystallite sizes of cobalt resulted in lower activity, as a result of lower reducibility from Co₃O₄ to CoO and finally to Co⁰.

2.5 Co₃O₄ precursors and synthesis methods

Cobalt hydroxide, a common precursor to Co₃O₄, exists as one of two polymorphs – alpha cobalt hydroxide - α -Co(OH)₂ and beta cobalt hydroxide - β -Co(OH)₂. The α -Co(OH)₂ has a hydrotalcite-like structure, as shown in Figure 2-5, with positively charged layers separated by anions occupying the interlayer spacing, ensuring neutrality. Such solids are often termed Layered Double Hydroxides (LDH) or anionic clays, as they store anions along with water molecules between their positively charged layers (Cheng *et al.*, 2014; Al-Ghoul *et al.*, 2009; Mishra *et al.*, 2018). Solids with this type of structure have been found to be useful as anion exchangers, catalysts, adsorbents, photo-functional materials and active electrode materials (Cheng *et al.*,

2014; Meng *et al.*, 2017). Also, α -Co(OH)₂ has a much larger interlayer spacing (>0.7 nm) versus β -Co(OH)₂ (0.46 nm), due to the anions occupying the layers. It has also been reported that the interlayer spacing may be varied, having a great effect on the electrochemical activity of the particles, by controlling the anions between its layers.

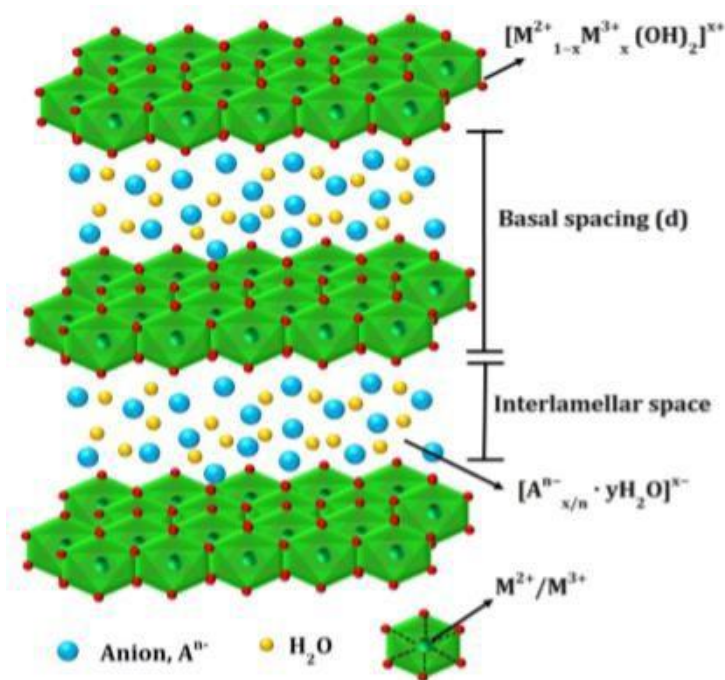


Figure 2-5: An illustration of the structure of layered double hydroxides (Mishra *et al.*, 2018) (Used with permission)

One of the major issues of α -Co(OH)₂ is the fact that it is thermodynamically metastable (Cheng *et al.*, 2014; Al-Ghoul *et al.*, 2009), and may rapidly transform to β -Co(OH)₂ during synthesis or in contact with a strong alkali. The XRD spectra of these polymorphs is found in Figure 2-6. This transformation was found to be the case in the transformation of α -Co(OH)₂ to cobalt compounds including β -Co(OH)₂, CoOOH and Co₃O₄ when exposed to an alkaline medium (KOH solution) for one to six days (Cheng *et al.*, 2014). This transformation drastically decreased the specific capacitance of the original α -Co(OH)₂. The α -Co(OH)₂ particles also exhibit low crystallinity and a disordered structure (Al-Ghoul *et al.*, 2009), as seen in Figure 2-7. Furthermore, the conversion of the α -form to the β -form is still unclear (Cheng *et al.*, 2014). The blue/green colour of the α -phase has been attributed to tetrahedral orientation of hydroxyl and intercalated anions bonded to Co(II), as well as some octahedral coordinated Co(II). The pink colour exhibited by the β -phase has been

attributed to the octahedral symmetry of the particles (Al-Ghoul *et al.*, 2009).

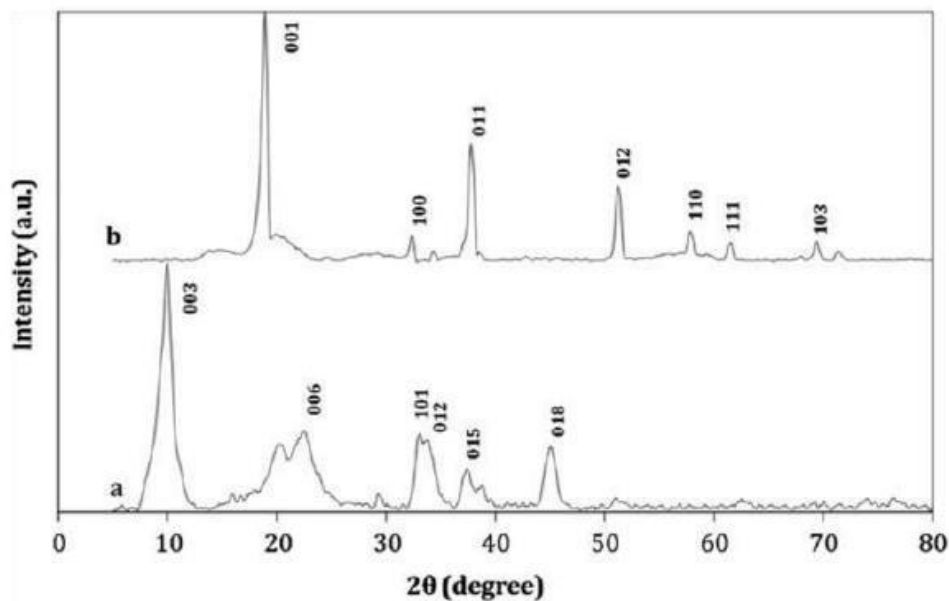


Figure 2-6: XRD peaks for a) α -Co(OH)₂ and b) β -Co(OH)₂ (Al-Ghoul *et al.*, 2009) (Used with permission)

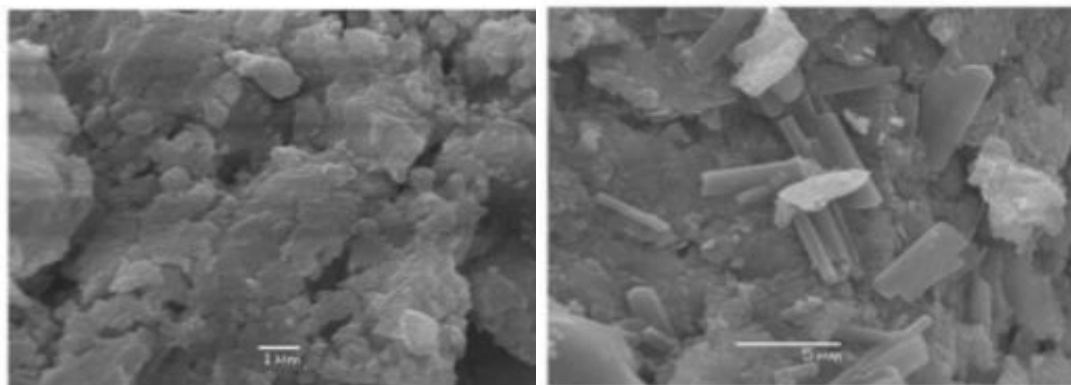


Figure 2-7: SEM images of a) α -Co(OH)₂ and b) β -Co(OH)₂ (Al-Ghoul *et al.*, 2009) (Used with permission)

The major drawbacks of α -Co(OH)₂ production showing some liquid crystalline properties lies in its thermodynamic instability, as well as its poor crystalline and disordered structure. El-Batlouni *et al.* (2008) presents a method in which the co-synthesis of α - and β -Co(OH)₂ can be studied, through a phenomenon known as Liesegang banding, as displayed in Figure 2-8. Liesegang banding may be defined as a periodic pattern which forms as two electrolytes interdiffuse, causing a precipitation reaction (Rajurkar & Ambekar, 2015). The resulting precipitates form bands parallel to the diffusion medium. In order to maintain these bands, the presence of a gel is

essential, for sedimentation prevention as well as to slow down nucleation and growth.

By using a cobalt-doped gel, sodium hydroxide was used to diffuse hydroxide ions into the gel medium. The cobalt gel was made up of a cobalt chloride solution containing agar or gelatine. The experiment was monitored for a number of weeks in which an immediate reaction was noted, as well as the gradual formation of Liesegang bands. First, a blue precipitate was formed at the point of initial reaction. After a while, a pink precipitate formed above the blue precipitate. As time progressed this pattern evolved down the tube, forming the Liesegang Bands. The pink precipitate above the initial blue precipitate did not, however, form Liesegang bands. This is of significance, as it displays the metastable nature of the α -form of the $\text{Co}(\text{OH})_2$ over that of the more stable β - $\text{Co}(\text{OH})_2$, and how easily the α - $\text{Co}(\text{OH})_2$ transforms to the β -phase, while the β -phase remains stable.

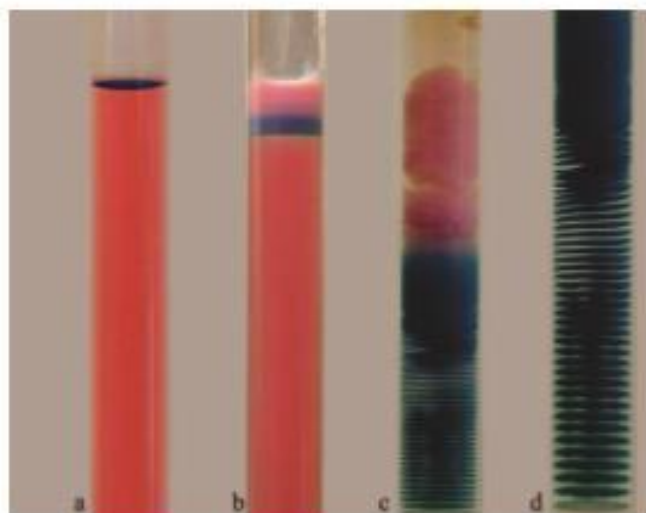


Figure 2-8: Liesegang bands formed as hydroxide solution is added to the cobalt chloride solution at a) the initial interface as a blue α - $\text{Co}(\text{OH})_2$ band is formed, b) the formation of a pink β - $\text{Co}(\text{OH})_2$ above the blue band c) two weeks after initial interface, d) enlargement of c. (El-Batlouni *et al.*, 2008) (Used with permission)

The XRD results of the pink and blue precipitates are shown in Figure 2-9. They exposed a higher crystallinity for the former in comparison to the latter. The broadness of the peaks in the blue sample was also attributed to the disoriented nature of the particles. The pink precipitates indicated clear brucite-like β -cobalt hydroxide with a hexagonal cell.

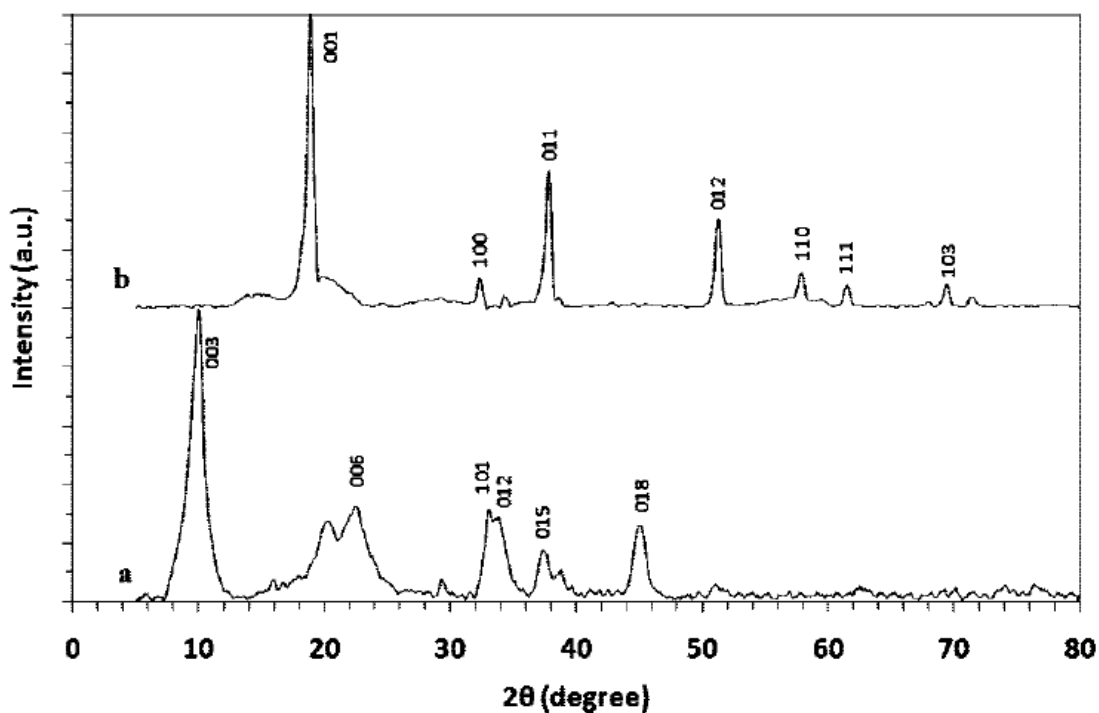


Figure 2-9: XRD patterns exhibited by as prepared a) blue α - $\text{Co}(\text{OH})_2$ and b) pink β - $\text{Co}(\text{OH})_2$ (El-Batlouni *et al.*, 2008) (Used with permission)

Similar studies conducted by Rajurkar & Ambekar (2015) used a 1% agar medium, as well as cobalt chloride and ammonium hydroxide solutions. In order for well-separated Liesegang bands to form at such a low concentration of agar, the pH had to be altered. At the initial point of interface, the bands are closely packed together. They become more dispersed as they move downwards, which may be seen in Figure 2-10. When examining the depths reached by the Liesegang banding at different concentrations, it was found that a higher distance was covered by a higher concentration of ammonium hydroxide solution, proving that the driving force of the phenomenon is diffusion.

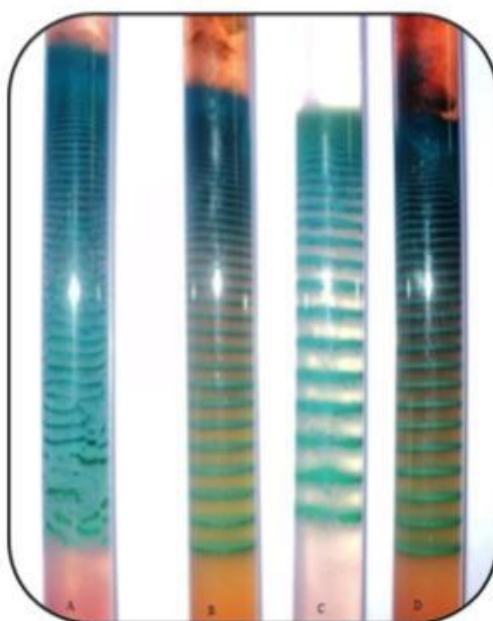


Figure 2-10: Liesegang bands formed in 1% agar gel using 0.05 M cobalt chloride solution and 2 M ammonia, varying the pH to a) 2, b) 2.5, c) 3.5, d) 4.5 (Rajurkar & Ambekar, 2015) (Used with permission)

Al-Ghoul *et al.* (2009) studied the co-synthesis of α - and β -Co(OH)₂ inspired by the phenomenon of Liesegang banding. Agar and gelatine was used to form the cobalt chloride gels studied. Sodium hydroxide solutions were added from the top (while the gel remained undisturbed) and, over time, Liesegang bands formed. XRD on the generated particles revealed that the pink compound had higher crystallinity. Furthermore, the crystallite sizes were determined using the Scherrer equation, as in Equation 2-6, and were found to be 8.4 nm and 13.2 nm for the α - and β -polymorphs respectively

$$\tau = \frac{K\lambda}{\beta \cos\theta} \quad 2-6$$

where:

- τ is the mean size of the crystallites
- K is a dimensionless shape factor
- λ is the X-ray wavelength;
- β is the Full Width at Half Maximum (FWHM)
- θ is the Bragg angle (in degrees).

The observed XRD patterns indicated hexagonal, brucite-like, structures for the β - $\text{Co}(\text{OH})_2$, while α - $\text{Co}(\text{OH})_2$ exhibited hydrotalcite structure, with rhombohedral symmetry. The Fourier transform infrared radiation (FT-IR) spectroscopy revealed an intense peak at 3631 cm^{-1} for the β -phase, with a less intense peak for the α -phase, attributed to the excess free OH ions in the interspatial layers. UV-vis diffuse reflectance measurements were used to examine the absorbance of the cobalt hydroxide phases. The α -phase exhibited a close relation to peaks reported for tetrahedral Co(II) complexes, at which these wavelengths are responsible for its green/blue colour.

Although metastable and structurally disordered, the use of α - $\text{Co}(\text{OH})_2$ is still widely researched, with much focus being placed on the intercalated ions they possess – one of the most prominent differences from its polymorph. A study conducted by Hu *et al.* (2009) focused on the production of α - $\text{Co}(\text{OH})_2$ with various intercalated anions, as well as their effect on morphology, basal plane spacing and capacitive property. The particles were prepared by chemical precipitation with cobalt salts of chloride, nitrate, sulphate and acetate anions. The XRD characterisation of these particles revealed a sawtooth-like peak in the case of the acetate sample, as a result of a sharp rise on the low angle side, and gradual reduction at the high angle side. This is an indication of layer stacking of the sample – a feature identified as the main difference between α - and β - $\text{Co}(\text{OH})_2$. β - $\text{Co}(\text{OH})_2$ forms perfectly stacked layers along the C-axis with an interlamellar distance of 4.6 Å, without any intercalated ions. The α -phase $\text{Co}(\text{OH})_2$, however, is made up of randomly-orientated layers which are separated by intercalated water molecules bonded to the hydroxyl groups by hydrogen bonds. The basal plane spacing, which is dependent on the intercalated species, exhibited by the Cl^- and NO_3^- anions, was found to be 7.797 and 7.852 Å respectively during these studies. Furthermore, the intercalated Cl^- anion sample produced sharp hkl reflection peaks, revealing a more crystalline nature than the other anions used. From field emission scanning electron microscopy (FESEM) images, displayed in Figure 2-11, it was noted that the intercalated Cl^- samples exhibited binary morphology with sheets and clusters assembled by solid rods, whereas the intercalated nitrate samples

produced a cluster with a thin-walled cell configuration.

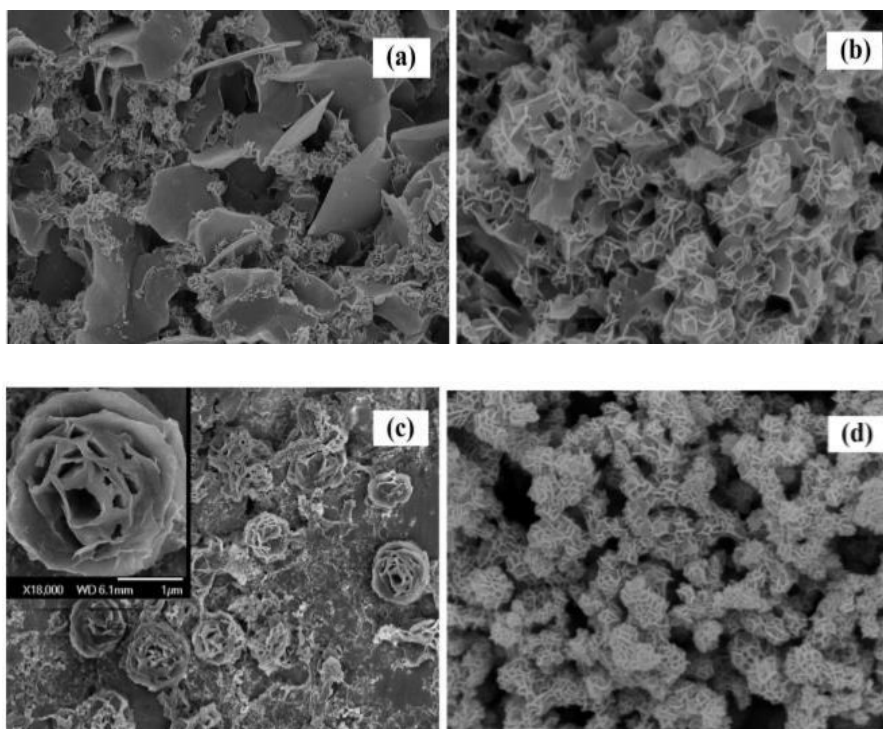


Figure 2-11: FESEM images of $\alpha\text{-Co(OH)}_2$ with varied interspatial anions a) as prepared Co(OH)_2 - chloride b) -nitrate c) - acetate, d) - sulphate (Hu *et al.*, 2009) (Used with permission)

The influence of anion exchange and phase transformation on the supercapacitive properties of $\alpha\text{-Co(OH)}_2$, synthesised via the precipitation method, was studied by Cheng *et al.* (2014). They were successful in producing $\alpha\text{-Co(OH)}_2$ with anion variances – chloride, nitrate, acetate, and sulphate. This was done adding the initially synthesised $\text{Co(OH)}_2\text{-Cl}$ particles into sodium salt solutions containing the various anions and purged with nitrogen gas for two hours. The XRD spectra revealed that similar peaks were observed for each anion, indicating that the crystal structure was not altered by change in anion. Differences between samples were identified by FT-IR in the region 800 to 1500 cm^{-1} . Scanning Electron Microscopy (SEM) analysis was done in order to evaluate the effect of anion exchange on morphology. No obvious changes in morphology were observed, as the original hexagonal plates remained as shown in Figure 2-12.

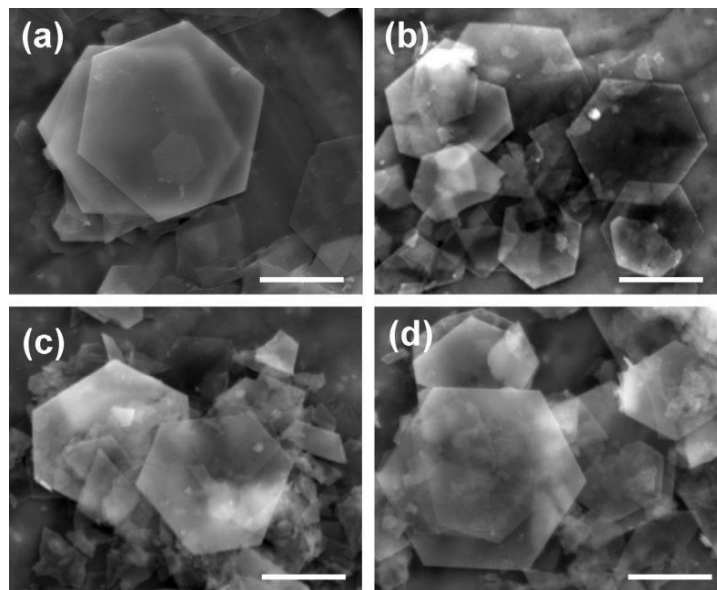


Figure 2-12: SEM images of α -Co(OH)₂ with varied interspatial anions a) as prepared Co(OH)-chloride b) -nitrate c) -acetate and d) -sulphate (Cheng *et al.*, 2014) (Used with permission)

Although widely studied, the application of α -cobalt hydroxide is still a relatively new concept. Cao and Wang (2016) studied α -cobalt hydroxide as an alternative to graphite, which has a theoretical capacity of 372 mA h/g, as an anode material. The particles were prepared using cobalt chloride hexahydrate, sodium chloride and hexamethylenetetramine dissolved in an ethanol and water solution. The green precipitates were collected and dried and used in the electrode preparation.

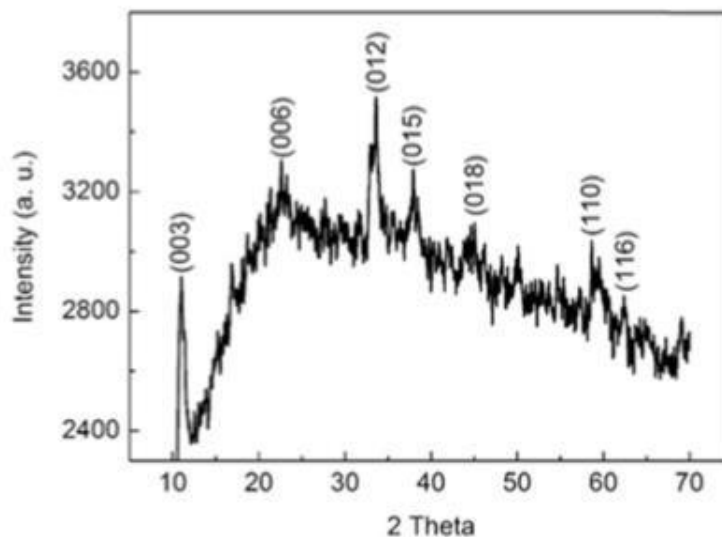


Figure 2-13: XRD patterns of as prepared α -Co(OH)₂ (Cao & Wang, 2016) (Used with permission)

The XRD pattern, shown in Figure 2-13, revealed the five main peaks which indicate that α -cobalt hydroxide has been formed – (003), (006), (012), (015) and (018). From cyclic voltammograms, the electrochemical activity of the produced particles was measured. At a current density of 100 mA/g, they expressed an initial capacity of 1765 mA h/g and, even after 50 cycles, maintained a higher capacity than that of graphite.

Mahmoud and Al-Agel (2011) explored the solvothermal synthesis of cobalt hydroxide nanowires, as well as their decomposition to Co_3O_4 . The cobalt phase explored was that of $\beta\text{-Co}(\text{OH})_2$, which was shown in the XRD results in Figure 2-14.

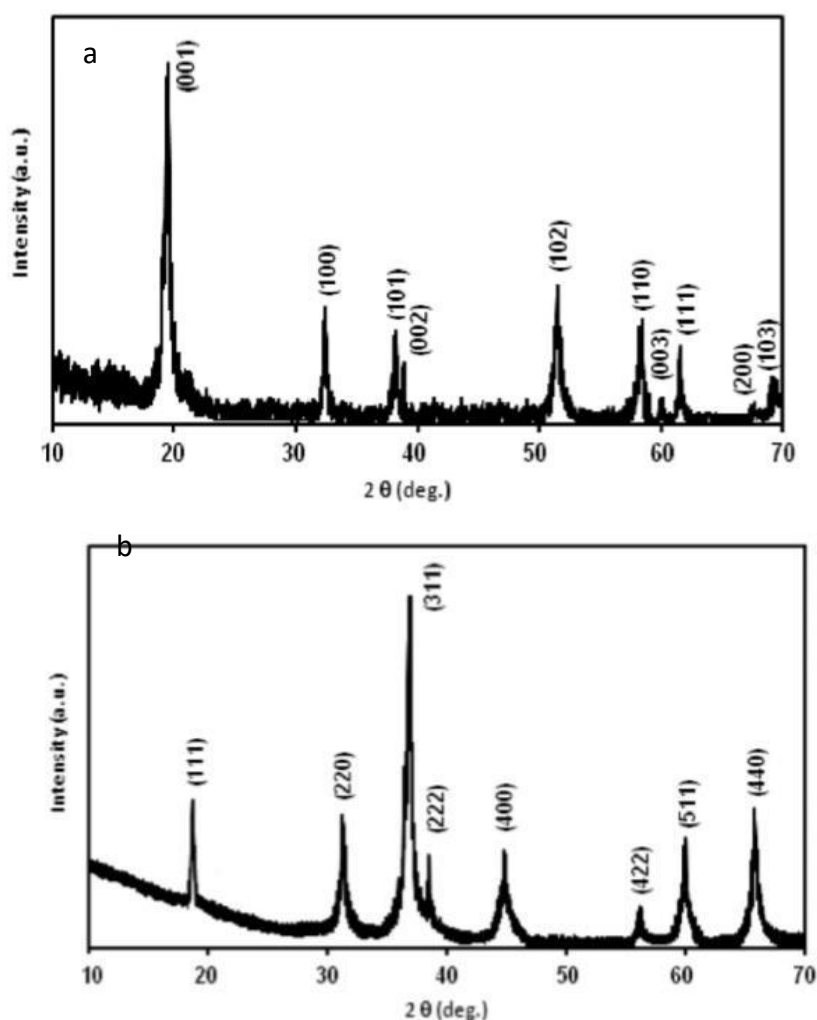


Figure 2-14: XRD pattern exhibited by ultra-fine a) cobalt hydroxide nanowires and b) cobalt oxide nanowires (Mahmoud & Al-Agel, 2011) (Used with permission)

Because the (001) peak was extremely sharp, it was noted that the oriented growth of

β -Co(OH)₂ nanowires was favoured, and also that impurities and the α -phase was not present. FT-IR spectra were also observed in which definite peaks of 3630, and 496- 540 cm^{-1} were assigned to the hydroxyl group and metal-oxygen and metal-hydroxyl bending vibrations respectively. According to the HRTEM images of the hydroxide phase, the lattice spacing was found to be 0.46 nm, in accordance with the (001) plane. After calcination, the HRTEM image of the oxide phase of the material revealed lattice spacing of 0.81 nm, in accordance with the (111) plane.

2.6 Cobalt oxide production methods

Nanoparticles are synthesised using two main methods: top-down or bottom-up. The first method describes the formation of nanomaterials from their bulk counterparts, which is obtained by the breakdown of these materials until nano size is achieved. The bottom-up method produces nanoparticles starting from atomic or molecular precursors, using various techniques to gradually build up nanomaterial (Filipponi & Sutherland, 2012). The bottom-up techniques are usually preferred, as they provide control of the nanoparticle synthesis as they begin with the atoms and molecules used in the desired product.

Such is the case for cobalt oxide synthesis in which various methods have been employed in the production of Co₃O₄ in their various forms (Huang *et al.*, 2014). Popular metal oxide synthesis routes include sol-gel, hydrothermal /solvothetmal decomposition, thermal decomposition, and gamma irradiation. Many other synthesis routes exist, such as the co-precipitation method explored by Chani *et al.* (2015), which resulted in pristine cobalt oxide (Co₃O₄) nanopowder used for pressure testing. The XRD and FT-IR spectra of the resulting cobalt oxide is shown in Figure 2-15, with the XRD spectra showing excellent correspondence to the JCPDS card 42-1467. The FT-IR spectra reveals peaks at 660 cm^{-1} and 550 cm^{-1} , which provides evidence of the existence of Co₃O₄, with the addition of a strong peak at 1339 cm^{-1} , which is accredited to the presence of an NO₃ group (Chani *et al.*, 2015).

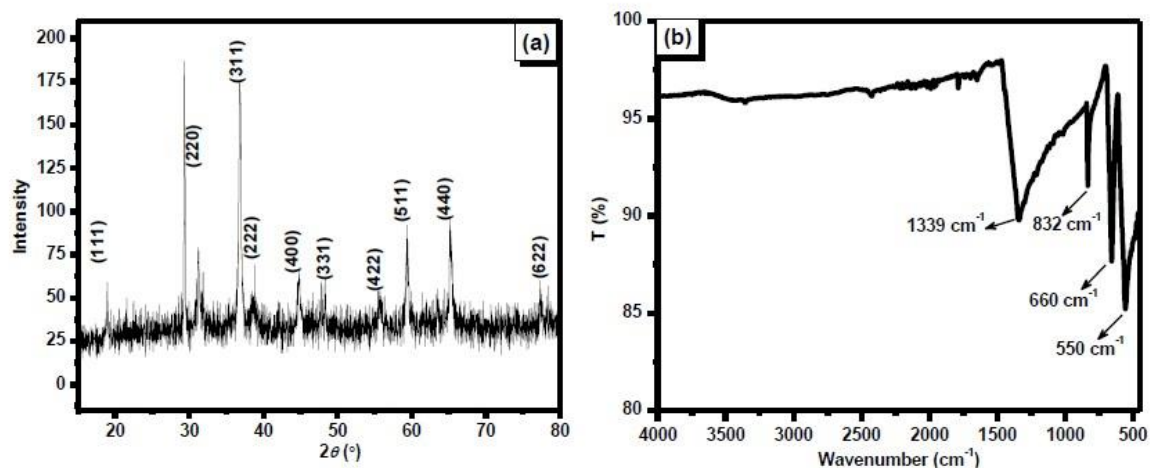


Figure 2-15: a) XRD and b) FT-IR spectra of the as-prepared cobalt oxide nanoparticles (Chani *et al.*, 2015)

2.6.1 Sol-gel synthesis

During sol-gel synthesis, cobalt salts and solvents are used to form cobalt solutions. The solution is then refluxed in order to obtain the sol (Guo *et al.*, 2014). The sol is then further treated by an addition of a chelating agent (Thota *et al.*, 2009) (no refluxing required) or refluxed and aged to form a thicker consistency gel (Thota *et al.*, 2009; Guo *et al.*, 2014). When the chelating agent is added, the resulting gel is dried and then calcined to form Co_3O_4 nanoparticles (Thota *et al.*, 2009). When using the reflux method, the gel is aged and calcined to form Co_3O_4 nanoparticles (Guo *et al.*, 2014). The main advantages of the sol-gel synthesis technique is that it's a simple method, and particle size and morphology may be controlled by the systematic monitoring of the system's parameters (Jamkhande *et al.*, 2019). One of the main disadvantages of this method is that it requires an aging time, ranging from 24 hours to numerous days, to obtain the final products.

2.6.2 Hydrothermal/solvothermal decomposition

The primary principle of hydro/solvothermal synthesis is its use of solvents at their critical states (Cushing *et al.*, 2004). This is done in an enclosed vessel, which allows for solvents to reach temperatures far beyond their boiling points with the increase in pressure (Cushing *et al.*, 2004). Hydrothermal and solvothermal synthesis of Co_3O_4 both make use of dissolving a cobalt salt in a solvent. The prefix

used describes the solvent in which the process is carried out – hydro, for water-based solutions, and solvo, for solvent-based solutions. Popular solvents used include ethylene glycol, pure alcohols and alcohol/water mixtures (Beach *et al.*, 2008; Jamil *et al.*, 2014; Jing *et al.*, 2012). Once a solution of the cobalt salt has been made, a precipitating agent, as well as a surfactant (depending on the process) is added. The solution is then transferred to the enclosed pressure vessel, where it is heated to the required temperature for a specified time period. The resulting precipitates are collected and calcined to obtain the final Co_3O_4 nanoparticles. The advantages of the hydro/solvothermal synthesis route include the ability to synthesise the desired size and shape of nanoparticles, and that well-crystallized powders may be formed containing monodispersed particles with a high crystallinity. It also provides a narrow size distribution. An additional advantage is that much research has been done on the upscaling of this method to a continuous form. The disadvantages are that the processes are difficult to control, and a limitation of the reliability and reproducibility exists (Jamkhande *et al.*, 2019).

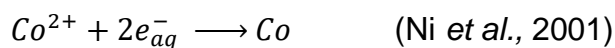
2.6.3 Thermal decomposition

Thermal decomposition relies on the breakdown of chemical substances by heat. In the production of cobalt oxide, this is usually brought about by refluxing of a cobalt salt dissolved in solvent at temperatures exceeding 200°C . It has been reported to be one of the easiest methods to synthesise monodispersed nanoparticles (Odularu, 2018). However, it entails the disadvantage that uneven heating of the processed material exists at the source of heat, and it has a limited scaling up potential.

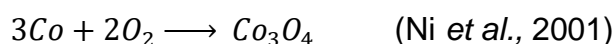
2.6.4 Gamma irradiation

Gamma irradiation utilises microwaves for the breakdown of water molecules within nanomaterial applications. As there is no need for toxic materials in this synthesis, it has been reported to be a ‘green’ approach to nanomaterial synthesis. It provides control of the nucleation process, depending on the radiation dose rate. The limitations of this process exist in the low accessibility of the technology worldwide, in comparison to other synthesis techniques. It also has limitations in the capping and stabilising materials, depending on their sensitivity to the irradiation used (Freitas *et al.*, 2018).

It has been reported that many electronegative metals, along with all noble metals may be reduced in water when exposed to gamma irradiation (Cushing *et al.*, 2004) as the water is broken down to H₂, H₂O₂, OH[•] and H[•] radicals (Cushing *et al.*, 2004), etc., i.e. active particles in reducing cobalt ions in solution to cobalt, which then allows for these reactions to follow:



2-7



2-8

2.7 The effect of alcohol on nanoparticle synthesis

The effect of alcohols in nanoparticle synthesis provides a means of control, as the properties of alcohols change with increasing alkyl chain lengths, as seen in Table 2-1. Due to this change in properties, it provides noticeable differences in systems using alcohol/water mixtures. This was noted in a study by Petkova and Nedkov (2013) in which the optical properties of Co²⁺ cations were explored in aqueous and alcoholic solutions using CoCl₂·6H₂O at room temperature. In an aqueous or alcohol medium, metals from the 3d group form complexes. This was noted in these experiments, as the colour of the aqueous solution was pink, whereas the alcohol solution was blue (Petkova & Nedkov, 2013). The cobalt complexes formed were therefore octahedral and tetrahedral. It was concluded that the reason for a difference of colour lies in the spectral positioning of the 3d electrons, leading to a difference in optical properties (Petkova & Nedkov, 2013).

Table 2-1: Properties of pure water, pure alcohol and alcohol/water mixtures

	Surface tension at 25°C σ , mN/m (Vazques <i>et al.</i> , 1995 and Demond & Lindner, 1993)		Interfacial tension at 25°C (Demond and Lindner) 1993)	Solubility in water at 25°C, g/L	Boiling point, °C at 101,3 kPa
	100%	50%			
Water	72.01				100
Methanol	22.51	32.86		1000	64.7
Ethanol	21.82	27.96		1000	78.37
Propanol	23.28	24.8		1000	97
Butanol	24.95		1.8	73	117.7
Octanol	27.5		8.52	0.3	188

Nanoparticle synthesis using metal alkoxides allows for the nucleation and growth of the particles to be controlled by adjusting the reaction conditions (He *et al.*, 2004). This control results in monodispersed nanoparticles (He *et al.*, 2004). However, the nucleation process of oxides often occurs too quickly, and the primary control is therefore set within the growth step (He *et al.*, 2004). The growth step may occur in one of two methods: aggregation or coarsening. Coarsening may be defined as the growth of larger crystals over smaller crystals, whereas aggregation forms polycrystalline solids (He *et al.*, 2004).

He *et al.* (2004) present a method for the controlled aggregation of nanocrystals in solvents. In their study, long carbon chain alcohols were used to produce Co_3O_4 nanoparticles by thermal decomposition and aggregated using small quantities of water to form monodispersed particles with a controlled size (He *et al.*, 2004). From these studies it was found that the particle size increases with the increase in reaction temperature and reaction time, along with a larger size distribution. However, varying the water content only in a solvent system provides an increase in particle size due, to aggregation with a narrow size distribution (He *et al.*, 2004).

The hydro/solvothermal route for β -cobalt hydroxide was employed using cobalt nitrate and dimethylglyoxime in water/ethanol solutions, with the addition of sodium hydroxide. The ratios of water to ethanol were varied, and it was found that lower

concentrations of ethanol produced more crystalline particles, as noted in the (011) peak in the XRD patterns (Figure 2-16). Results from FT-IR analysis, shown in Figure 2-16, also indicated that the particles formed from pure water contained fewer impurities than that of the water/ethanol mixtures, which provided aldehydes usually found in alcohols as impurities.

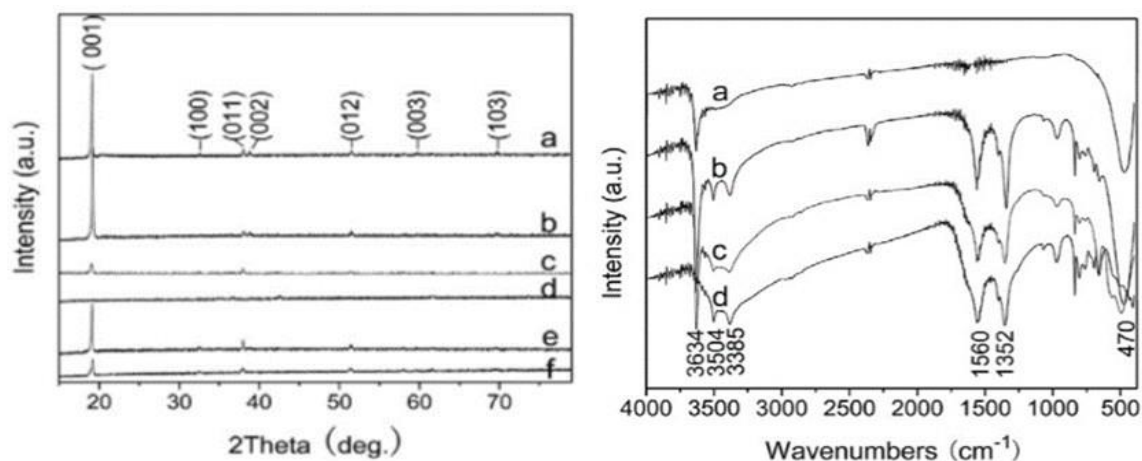


Figure 2-16: a) XRD patterns, and b) FT-IR spectra for the -Co(OH)_2 formed using different water/ethanol ratios and varying hydrothermal times at 220C. a-d) hydrothermal time: 24 h, and water/ ethanol ratios of a) 1:0, b) 2:1, c) 1:2, and d) 1:10. e-f) water/ ethanol ratio: 2:1, hydrothermal time for: e) 12 h, and f) 6 h (Wang *et al.*, 2011) (Used with permission)

The morphology was greatly affected by the change in water/ethanol ratio. Pure water produced hexagonal plates, while increasing ethanol produced broom-like, straw-like and grass-like cobalt hydroxide structures (Wang *et al.*, 2011). It was found that the major contributing factors to the reaction, self-assembly and crystallisation of the particles was alkalinity and polarity, as the alkalinity as well as the polarity of the water/ethanol mixtures decreased as ethanol increased (Wang *et al.*, 2011).

The use of various alcohol media during cobalt oxide nanoparticle synthesis was explored by Athawale *et al.* (2010). The studies focused on the use of gamma-ray techniques. Although cobalt nitrate, cobalt chloride and cobalt acetate salts were used during this investigation, only cobalt nitrate proved effective in the conversion to cobalt oxide. The alcohols explored included methanol, ethanol, n-propanol, iso-propanol, n-butanol and n-hexanol, with the addition of aniline and ammonium persulphate. The results obtained showed that shorter carbon chained alcohols produced spherical particles, while alcohols with longer carbon chains produced fibres, with the best alcohol for the purpose being isopropanol, owing to its stability and homogeneous fibre

synthesis (Athawale *et al.*, 2010).

Gamonchuang *et al.* (2016) studied the effect of alcohol type on the thickness of the silica shell when coating Co_3O_4 nanoparticles. A component of this study focused on the formation of Co_3O_4 nanoparticles using cobalt nitrate and octanol as the raw materials (Gamonchuang *et al.*, 2016). Spherical Co_3O_4 nanoparticles were formed during thermal decomposition, with strong morphology which remained unchanged with the increase in reflux time (Gamonchuang *et al.*, 2016). The increase in reflux time did, however, lead to a broader size distribution, owing to an increase in agglomeration time (Gamonchuang *et al.*, 2016).

A summary of the techniques used to synthesise cobalt oxide using alcohol in the synthesis method is displayed in Table 2-2. From these studies, it is noted that the most common cobalt precursor salts used are cobalt chloride and cobalt nitrate. Although different synthesis methods are shown, it is noted that they differ in the system conditions and components used. Most importantly, it is noted that the combination of variances provides completely different results. Such is the case for Athawale *et al.* (2010) and Gamonchuang *et al.* (2016) who used the same precursor salt, but two different methods. Athawale *et al.* (2010) used the Gamma-ray technique, in which shorter alcohol chain lengths produced spherical particles and longer carbon chain lengths provided longer fibre particles. This was significant, as Gamonchuang *et al.* (2016) used octanol (a longer carbon chained alcohol) and produced spherical particles, contrary to the aforementioned trend. From the table provided, it is noted that not much focus has been placed on comparing various alcohol chain lengths to the particles synthesised. Neither has the solvothermal synthesis of cobalt oxide in alcohols been a focus.

Table 2-2: Summary of various Co₃O₄ synthesis routes using alcohols

Author	Synthesis method	Alcohols used	Precursor salt used	Additional agents	Reaction conditions	Reaction time	Summarised result
Ni <i>et al.</i> (2001)	Gamma irradiation	Isopropanol	Cobalt chloride	Sodium acetate	50 Gy/min precipitates were collected	Precipitates were dried for 24 hours	Particles approximately 5 nm in size were synthesised
He <i>et al.</i> (2004)	Thermal decomposition	1) n-hexanol 2) n-octanol 3) n-octanol	1) Cobalt nitrate 2) intermediate salt 3) Initial cobalt oxide	Water	1) Refluxed between 90°C and 100°C, depending on changing boiling point 2) Refluxed again, increasing to 150°C 3) Refluxed at 180°C	1) 10 hours 2) 3 hours 3) 4 hours	Monodispersed particles primarily 5 nm in size were aggregated by the addition of water into the system in the final step
Beach <i>et al.</i> (2007)	Solvothermal	Ethanol and water (ratio 1:1)	Cobalt nitrate	Urea & sodium dodecyl sulphate	Reaction at 110°C Calcination at 250°C	Reaction for 15 hours Calcination for 2 hours	Microspherical particles composed of platelets with bundles of nanofibers on some platelet corners
Thota <i>et al.</i> (2009)	Sol-gel	Ethanol	Cobalt acetate	Oxalic acid	1) Sol is heated to 35-40 2) Gel is dried at 80 3) Calcination at various temperatures above 400	Gel is dried for 24 hours	Matchstick-shaped particles synthesised. Calcination temperature played a huge part in particle morphology. Agglomeration was noted with

							increasing temperature
Athawale <i>et al.</i> (2010)	Gamma-ray	Methanol, ethanol, n-propanol, isopropanol, n-butanol & n-hexanol	Cobalt nitrate	Aniline and ammonium persulphate	Irradiation at 5,1 Gy.min ⁻¹	0 – 72 hours	Shorter alcohols produced spherical particles, while longer particles produced fibres
Guo <i>et al.</i> (2014)	Sol-gel	Ethanol	Cobalt chloride	Triblock copolymer F127 soft template	1) Refluxed at 100°C 2) Sol is aged at 40°C 3) Gel is heated at 130°C 4) Black product calcined at 400°C	1) Refluxed for 8 hours 2) Sol was aged for 2-3 days 3) Gel was heated for 15 minutes 4) Product calcined for 3 hours	Mesoporous octahedral particles were successfully prepared
Gamonchuang <i>et al.</i> (2016)	Thermal decomposition	Octanol	Cobalt nitrate	-	1) Refluxed at 170°C 2) Dried at 80°C 3) Calcined at 400°C	1) Refluxed for 1, 1.5, 2 and 4 hours 2) Dried for 24 hours 3) Calcined for 6 h	Monodispersed spherical particles synthesised. Increasing reflux time resulted in increased particle sizes and wider size distributions

2.8 Effect of calcination temperature

The mechanochemical synthesis of cobalt oxide, as studied by Yang *et al.* (2004) focused on the thermal treatment (calcining) of a milled precursor consisting of $\text{Co}(\text{NO}_3)_2 \cdot 6\text{H}_2\text{O}$ and NH_4HCO_3 in order to obtain cobalt oxide nanoparticles (Yang *et al.*, 2004). The production method provided monodispersed nanoparticles which, by varying the calcination temperature, were found to increase in size with increasing calcination temperature, obeying Scott's equation, shown in Equation 2-9, of homogeneous nanocrystal growth (Yang *et al.*, 2004).

$$D = C \exp\left(-\frac{E}{RT}\right) \quad 2-9$$

Jing *et al.* (2012) however, provided a solvothermal method for Co_3O_4 production by calcining a CoCO_3 precursor. Their statistical findings contradicted the above, in that the average particle sizes decreased with increased calcination temperature (Jing *et al.*, 2012).

2.9 Effect of pH

Yang *et al.* (2007) provided a method in which the effect of pH on shape-controlled nanocubic Co_3O_4 particles was monitored. During their investigation, various agents were used to maintain the pH either between 8 and 9 or between 11 and 12. Their findings exhibited that controlled nanocubes are formed when the pH is between 8 to 9, but irregular shapes formed at an increased pH. This was attributed to the ease in condensation of the $\text{Co}(\text{OH})_2$ precursor at higher pH values, leading to agglomeration. The results obtained by Yang *et al.* (2007) were reiterated in an independent study by Allawdini *et al.* (2014), who studied the effect of pH on cobalt oxide produced during the co-precipitation method.

2.10 Advanced Oxidation Processes (AOPs)

One of the major drawbacks in the treatment of wastewater from industries such as the textile industry, tanneries, pharmaceutical industries, etc. is that the production processes vary, not only industrially, but between companies as well. This results in effluents of an unpredictable nature, which makes the treatment process complicated.

2.10.1 Hydroxyl radicals vs. sulphate radicals

Deng and Zhao (2015) wrote a review paper comparing all the current methods using AOPs for wastewater treatment. They reported on hydroxyl radical-based as well as sulphate radical-based systems. According to Deng and Zhao (2015), hydroxyl radicals are the most reactive oxidising agents in water, with oxidation potentials ranging between 1.95 – 2.8 V (depending on pH). However, due to their short lifespan they are only produced in combination with oxidising agents, irradiation, and catalysts. They further state the oxidation potentials of both the peroxydisulphate anion as well as sulphate radicals, as 2.01 V and 2.6 V respectively. It should however, be noted that no pH was specified for these species, and according to Neta *et al.* (1988), the reduction potential of sulphate radicals may range between 2.5- 3.1 V.

Work done by Anipsitakis and Dionysiou (2003) studied the degradation of organic contaminants in water using sulphate radicals produced from peroxymonosulphate, activated by cobalt. The results obtained were compared to a similar test done, using the Fenton reagent (Fe(II)/H₂O₂)-hydroxyl radical based. During their investigations, transition metals, pH, as well as organic contaminants were varied. pH played a major role in the comparison between the two treatment methods. A limitation of the need for an acidic pH was highlighted for the Fenton reagent. The degradation of 2,4-dichlorophenol was observed for both degradation methods, at a pH range of 3-8. At high pH values, the cobalt/ peroxymonosulphate (Co/PMS) reagent maintained its degradation quality, while the Fenton reagent significantly decreased. Similar results were obtained for the degradation of atrazine, although the initial degradation using Co/PMS was slower than that of Fenton reagent. It was deduced that, given sufficient reaction time, the Co/PMS system provides better degradation, even at a pH which favours Fenton reagent reactions. It should be noted, however, that for the third contaminant tested (naphthalene) at a pH of 3, the Fenton reagent was favoured over the Co/PMS system. This shows that sulphate radicals are not universally more effective than hydroxyl radicals, and that the structure of the contaminant impacts the reactivity of the sulphate radical to a greater extent than the hydroxyl radicals.

Azo dyes discharged into municipal wastewater streams is undesirable, due to their toxic nature, as well as for aesthetic reasons. These dyes, as well as their aromatic amine intermediates, are not biodegradable under aerobic conditions. The Fenton oxidation (FO) process was exploited in the research by Meriç et al. (2004) in which the removal of colour, COD, and toxicity from wastewater containing Reactive Black 5 was monitored. The Fenton oxidation process is dependent on the release of hydroxyl radicals, and therefore employs an acidic pH which favours hydroxyl radical release. The experiments were conducted at various temperatures typically encountered within the textile industry: 30, 40, 50 and 60°C. In the experiments conducted, it was found that the optimum pH varies between 3.0 and 3.5 for colour and COD removal. The optimum temperature was found to be 40°C. Temperatures above this caused an increase in ferrous ions, which scavenged OH radicals, therefore reducing the effectiveness of the Fenton reaction.

Ozone (O₃) is an oxidant which has been widely studied in the mineralisation of undesired organic compounds by exploiting its ability to react with electron-rich organic compounds. During the peroxone process, ozone reacts with H₂O₂ to form $\cdot\text{OH}$ for pollutant mineralisation. Much research has been done on the mineralisation of organic wastes by AOPs exploiting $\cdot\text{OH}$, though the use of sulphate radicals ($\cdot\text{SO}_4^-$) has become increasingly popular due to their higher reduction potential (2.5-3.1 V). Sulphate radicals have since been preferred, as they are less influenced by competing factors, such as alkalinity and organic matter in water, than that of the hydroxyl radicals.

Yang *et al.* (2015) studied the interactions in a system exploiting both hydroxide and sulphate radicals by using both ozone and PMS as oxidants in a system for contaminant degradation. Atrazine (ATZ) was the contaminant monitored in these studies. The results revealed that the O₃/PMS system provided 81% degradation within 10 minutes, in comparison to 27% degradation achieved by O₃ on its own, in a timeframe of 20 minutes. The reaction rate constant was improved by a factor of 2 with the addition of PMS.

2.10.2 Factors influencing sulphate radical formation

Rivas *et al.* (2009) studied the effects of variables on the decomposition of Oxone (potassium monopersulphate). They report that the monopersulphate molecule may be broken down by influences of transition metals, heterogeneous catalysis by oxides, and by the application of thermal or radiant energy. Deng and Zhao (2015) also report that the peroxydisulphate anion may be activated to form sulphate radicals with heat, transition metals, or an elevated pH (not specified).

During the tests carried out by Rivas *et al.* (2009) both homogenous and heterogeneous catalysts were used, though heterogeneous catalysts were recommended for their ease in catalyst removal, as well as a wider range of working pH. They tested several transition metals, including Co(II), Fe(II), Mn(II) and Ti(II), but only Co(II) showed considerable reactivity with Oxone. Similar results were reported for a simple test by Anipsitakis and Dionysiou (2003) using cobalt, nickel and iron.

Rivas *et al.* (2009) further studied the effect of catalyst concentration, monopersulphate concentration, initial pH, and temperature. When studying the effect of catalyst concentration, the temperature, pH, Oxone concentration and volume were kept constant. The results obtained showed that Oxone decomposed faster with an increase in catalyst load. The same study was done for the effect of Oxone concentration, in which the temperature, catalyst load were kept constant. The pH varied based on Oxone concentration. The results obtained revealed that pH is an important factor that may not be neglected, since proton concentration plays a key role in monopersulphate decomposition, and small changes may significantly alter the reaction rate. In a study focused on pH, it was found that in a range of 1.0-3.1, the rate of decomposition increased with increase in pH. The temperature study exhibited expected results, as an increase in temperature led to an increase in decomposition rate. It was, however, noted that although an increase in rate was observed, this does not imply that more sulphate radicals are available, since excessive heat may result in the formation of inactive sulphate and oxygen molecules. The same tests were done heterogeneously, with significant findings for the pH study. It was also noted that a high

pH is beneficial in terms of metal leaching. Thus, release of active metallic species from solid catalysts is normally associated with low pH values (Rivas *et al.*, 2009). It is therefore beneficial to note that most contaminated natural waters exist in the pH range of 6-8 (Anipsitakis & Dionysiou, 2003).

2.10.3 Chloride effects on PMS- based degradation

Huang *et al.* (2017) investigated the effects of chloride on PMS-based pollutant degradation, specifically the intermediates formed and how the presence of chloride affects the complete mineralisation of the pollutants. Their investigation was based on phthalic acid (PA), a common and dominant dye degradation intermediate. Chloride ion is one of the major constituents within the dye industry's wastewater, and has previously been deemed to have an inhibitory effect on AOP performance. However, recently a dual effect has been reported (inhibitory then accelerating effect) during dye decolouration AOPs. The initial inhibitory effect at low chloride concentrations (<5 mM) has been attributed to the consumption of sulphate radicals by chloride ions, resulting in the formation of less reactive chloride radicals. However, at higher concentrations (>50 mM), an increased bleaching effect was experienced in response to the generation of HOCl and Cl₂ at high chloride ion concentrations.

In addition, the concentrations of PMS, Co²⁺ and pH were varied in order to monitor the impact on PA degradation as shown in Figure 2-17. Increased degradation rates were experienced for the three variables. With an increase in PMS concentration, more free radicals were available for reaction. An increase in Co²⁺ concentration provided an enhanced radical production from the available PMS. A significant increase in degradation rate was also experienced when increasing the pH above 4. pH was highlighted as a *critical variable in dye degradation, due to pH-dependency of the concentration and speciation of free radicals. A significant increase in degradation rate was displayed as the pH was increased from 2 to 7. Ultimately, the pH controls the PMS system, as it controls the formation of radicals which drive it.

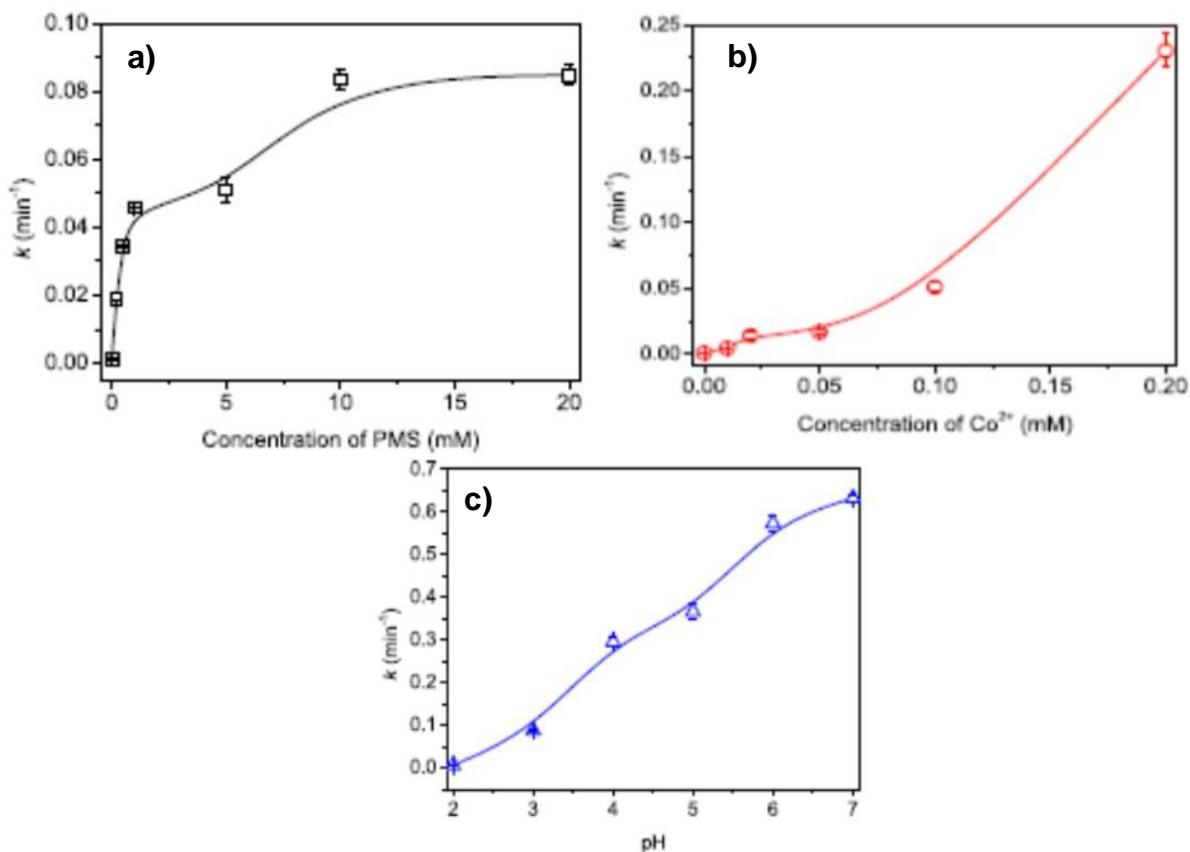


Figure 2-17: The effect of a) PMS concentration, b) cobalt ion concentration and c) pH on the rate of phthalic acid degradation in the Co/PMS system (Huang *et al.*, 2017) (Used with permission)

Upon investigating the presence of chloride ions on the degradation efficiency of PA as indicated in Figure 2-18, it was found that a significant drop in degradation rate was experienced with the mere presence of chloride ions. The investigation was expanded to the degradation of Acid Orange 7 and Rhodamine B, in which a dual effect (first decrease then increase in degradation rate) was experienced. It was also noted that the degradation rate constants were far higher for that of the intermediate (PA) than that of the initial PA.

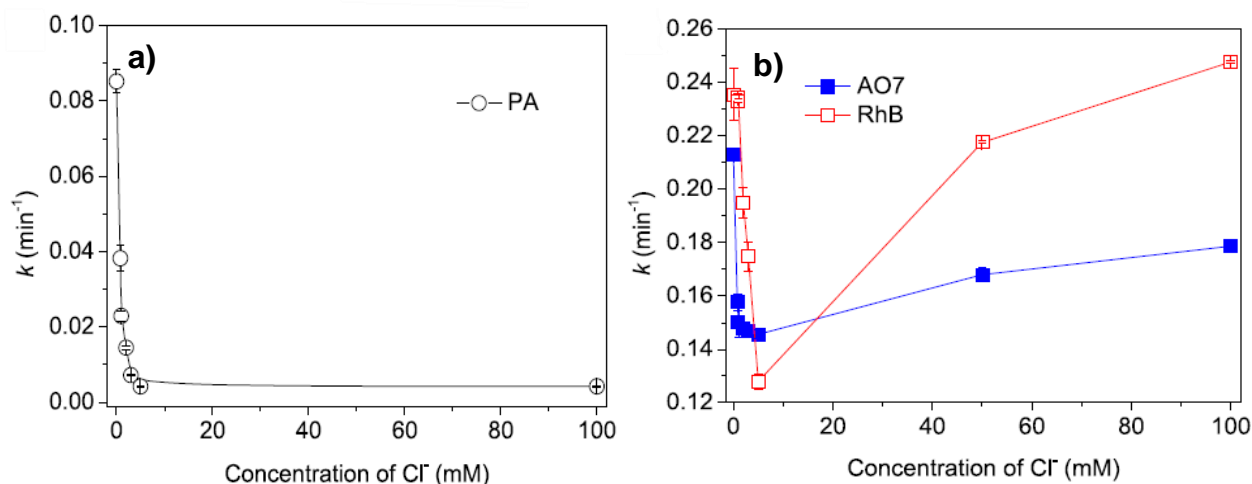


Figure 2-18: a) The effects of chloride ion addition to the Co/PMS system on the decomposition rates of PA and dyes, b) the dual effect exhibited in the Co/PMS/Cl system with increasing chloride ion concentration (Huang *et al.*, 2017) (Used with permission)

The intermediates formed from degrading PA in the presence of chloride ions at varied concentrations were determined using LC/TOF-MS. It was found that at low concentrations of chloride, up to ten different intermediates were formed, while increased chloride concentration reduced the number of by-products formed. However, at 1 mM chloride, 41.4% PA degradation was achieved and at 100 mM chloride, only 14.5% PA degradation was achieved.

A test for adsorbable organic halide (AOX) formation was performed, as AOX forms an important parameter in industrial wastewater treatment. The results obtained are displayed in Figure 2-19. It was found that AOX only formed when the system was introduced to a chloride addition. Findings indicated that the formation of AOX is not necessarily chloride concentration related, contradicting the conclusion of Yuan *et al.* (2011). An increase in AOX at low chloride concentrations was attributed to the large number of chlorinated by-products formed at low chloride levels.

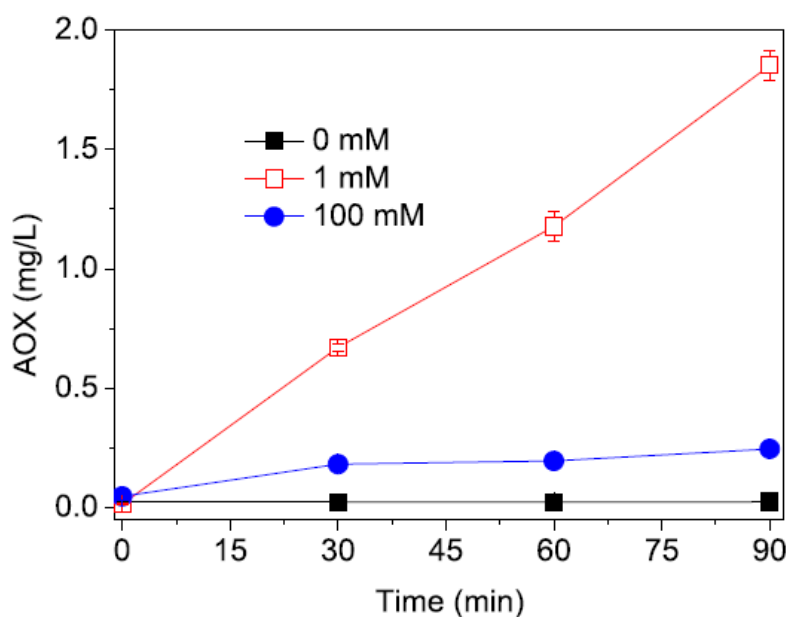


Figure 2-19: Adsorbable organic halides (AOX) formation during PA degradation in the Co/PMS/Cl system when increasing chloride ion concentration (Huang *et al.*, 2017) (Used with permission)

From their investigations it was concluded that the inhibitory effect that chloride ions have on PA degradation may negatively affect the overall degradation of dye-containing wastewater.

2.11 Conclusion

Cobalt oxide (Co_3O_4) has been proposed for use in wastewater treatment, in preference to other transition metals, for its ability to best activate sulphate radicals ($\cdot\text{SO}_4$) from Oxone (peroxymonosulphate).

Kim and Huh (2011) demonstrate that minor changes within the hydrothermal synthesis of cobalt oxide may result in different morphologies with the simple adjustment of the amount of either hydrazine or H_2O_2 in the precursor solution. Since reactions which are structure-sensitive are dependent on morphology, these simple changes not only affect the particles synthesised but also the effectiveness of their use.

Saputra *et al.* (2014) and Saputra *et al.* (2017) demonstrate that BET surface area is not the only factor affecting the catalytic activity of the particles, but that its activity lies in the combinative effect of high surface area and active surface facets, opposing the general concept that higher surface area produces higher catalytic ability. Additionally,

they report that no significance was attributed to cobalt oxide size in the range of 6 to 200 nm in the Fischer-Tropsch process. However, at a particle size lower than 6 nm, inferior reactivity is exhibited (Vinod, 2010).

Various precursors to the final product may vary the structure of the particles synthesised. Cobalt hydroxide, as the precursor to cobalt oxide exists as either α -cobalt hydroxide or β -cobalt hydroxide. The most obvious difference between these phases lies in their colour. The α -phase is blue/green in colour while the β -phase is pink in colour. The major issues reported for α -Co(OH)₂ is its thermodynamic metastability, as well as poor crystalline and disordered structure, causing the rapid transformation to the β -phase, while the β -phase remains stable. The transformation to cobalt oxide usually occurs in literature concerning the β -phase. However, a comparison of the catalytic properties of cobalt oxide from both polymorphs has not been studied.

Athawale *et al.* (2010) and Gamonchuang *et al.* (2016) used the same precursor salt in alcohols, using the gamma-ray technique and thermal decomposition respectively. The gamma-ray technique provided spherical particles in alcohols with shorter alcohol chain lengths and fibres in alcohols with longer carbon chain lengths, in which the longest chain length explored was hexanol. The thermal decomposition also provided spherical particles in octanol, an alcohol with a carbon chain longer than that of hexanol. However, the systematic study of the effect of alcohols at various alcohol chain lengths in hydro/solvothermal synthesis of cobalt oxide nanoparticles has not been undertaken.

Studies on the effect of calcination temperature have contradicting outcomes, as Yang *et al.* (2004) found an increase in size with increase in calcination temperature for the cobalt oxide particles synthesised mechanochemically, while Jing *et al.* (2012) found the particle size decreased in their solvothermal synthesis of Co₃O₄ when calcining a CoCO₃ precursor.

This study therefore focuses on the evaluation of the effects of the precursor anion and alcohols on the cobalt hydroxide phase achieved, the effect of calcination temperature on the resulting cobalt oxide particles, and finally the effects on catalytic ability in colour degradation of synthetic textile dye solutions.

CHAPTER 3 RESEARCH METHODOLOGY

In this chapter, the experimental methods used will be provided, highlighting the hydro/solvothermal synthesis route used in producing the particles. The equipment used will also be presented and explained, as well as the data extraction and analysis methods used in the characterisation methods used.

3.1 Research design

The experiments were arranged threefold: firstly, the hydro/solvothermal synthesis of cobalt hydroxide, secondly, the calcination at various temperatures, and lastly, the advanced oxidation processes. The first step involved the hydro/solvothermal synthesis of cobalt hydroxide, by varying the anion of the cobalt salt used, as well as the alcohol solvents used. Cobalt chloride hexahydrate and cobalt nitrate hexahydrate were selected as the base salts for these experiments. Methanol, ethanol, propanol, butanol and octanol were selected as the alcohols, and mixed in ratios 1:0 (referred to as 100% alcohol) and 1:1 (referred to as 50% alcohol) with water. The second part evaluated the conversion from the precursor powders α - and β -Co(OH)₂ to Co₃O₄ via calcination, which occurred at 300, 400 and 500°C. Lastly, the advanced oxidation processes were carried out by degrading a standard methylene blue solution, with a concentration of 10 mg/L, using the produced catalyst to activate Oxone[®] (peroxymonosulphate). The results obtained were compared with the characterisation results obtained.

3.2 Experimental methods

The following sections describe the methods used in the synthesis of cobalt oxide, as well as their application in advanced oxidation processes. Sections 3.3.1 and 3.3.3 were completed in the nanotechnology laboratory and section 3.3.2 completed in the chemical engineering laboratory, both located at CPUT, District Six campus. Further, the methods used to characterise the resulting particles are briefly detailed.

3.2.1 Cobalt hydroxide synthesis

All chemicals used were at analytical grade and used without further purification. They were sourced from the Associated Chemical Enterprises (98% purity grade) and Sigma-Aldrich for the salts and solutes respectively. For these experiments, two cobalt salts were used, namely, cobalt chloride hexahydrate and cobalt nitrate hexahydrate. These salts were dissolved in the solvent, which was either deionised water, methanol (99.9% purity grade), ethanol (96% purity grade), propanol (99.5% purity grade), butanol (99% purity grade) or octanol (99% purity grade), or in alcohol/deionised water solutions in the ratio 1:1. This was done in order to study the effects of alcohol surface tension. A molarity of 0.23 M was maintained for both salts. Once dissolved, the pH of the solution was adjusted to 8.10 by adding ammonium hydroxide solution dropwise. The resulting mixture was then inserted into the 0.99 L Teflon-lined pressure reactor fitted with a thermocouple and a self-regulating heating jacket, as shown in Figure 3-1. The reaction temperature was maintained at $105 \pm 5^\circ\text{C}$ for 6 hours after a ramp up time of 1 hour. The pressure reactor was then allowed to cool down naturally overnight.

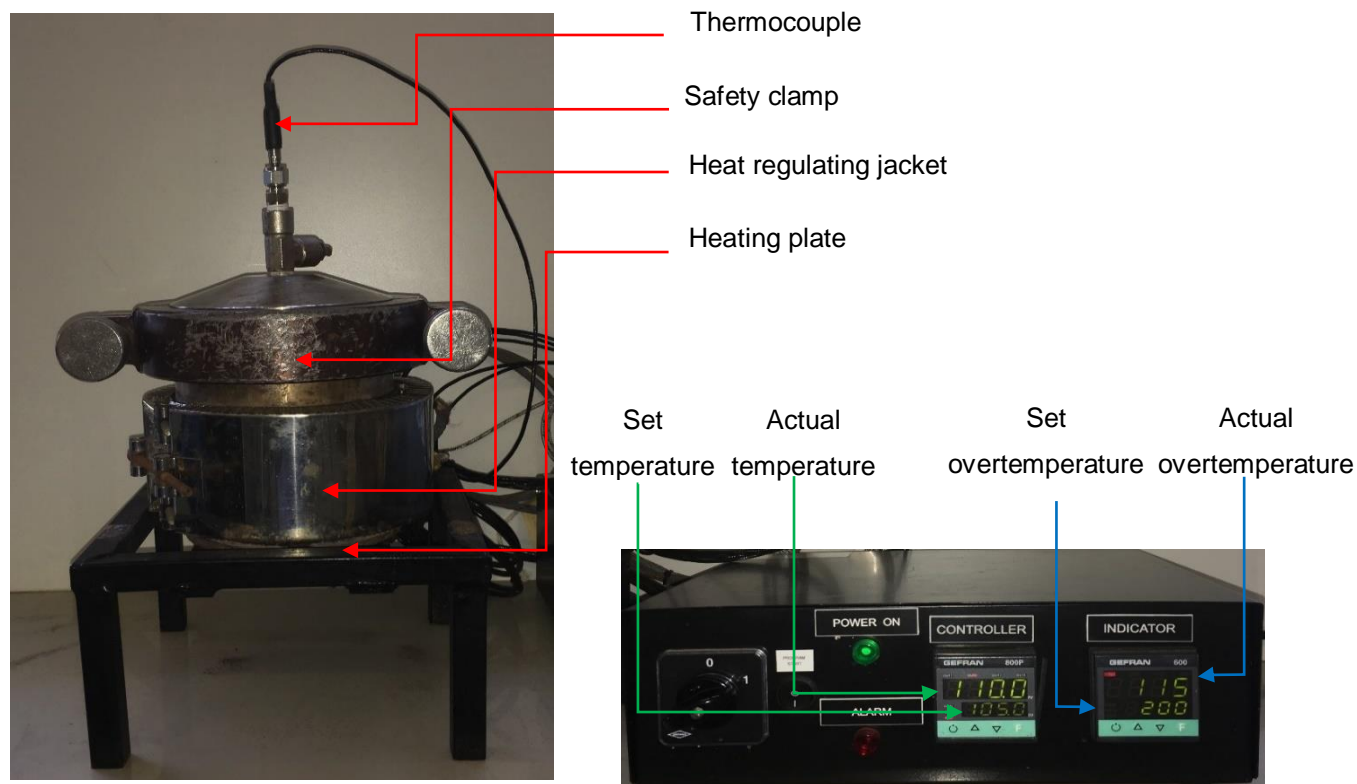


Figure 3-1: Hydro/solvothermal reaction vessel with temperature controller

3.2.2 Cobalt hydroxide calcination

The resulting cobalt hydroxide particles were centrifuged and rinsed several times with deionised water and finally with ethanol, and dried overnight in an oven at 60°C. Porcelain crucibles were used to store the powders, which were then annealed in a LABOFURN furnace, as presented in Figure 3-2, at temperatures of 300, 400 and 500°C. A standard ramp time of 1 hour was employed, and the set temperature was maintained for 3 hours. The samples were removed immediately and stored in airtight sample vials for further analysis and application in the AOP reactor.



Figure 3-2: LABOFURN furnace used for calcination

3.2.3 Advanced oxidation process

The catalytic efficiency was evaluated in the sulphate radical-based advanced oxidation process using an in-house developed continuous reactor, shown in Figure 3-3. A stock solution of 10 mg/L methylene blue solution was prepared and kept for test work. Peroxymonosulphate (Oxone[®]) powder of 0.184 g was added to 500 mL methylene blue solution and stirred for five minutes. An initial sample of the dye solution, along with 4 mL aliquots every 2 minutes at the exit of the reactor was then taken, and analysed using a handheld Lovibond[®] spectrophotometer. The spectrophotometer provides a numerical output (ΔE), quantifying the colour variance to a selected standard. In this case deionised water was selected as the standard as the objective was to get the water as clear as possible. The percentage degradation was calculated according to Equation 3-1

$$\% \text{ Degradation} = \left(1 - \frac{\Delta E_{(sample)}}{\Delta E_{(deionised\ water)}} \right) \times 100 \quad 3-1$$

The solution was then pumped through filters embedded in the reactor with 0.3 g catalyst at a flowrate of 40 mL/min using a peristaltic pump. The preparation of these filters may not be disclosed as it is protected intellectual property. Further, samples were taken every two minutes from the initial point of reaction.

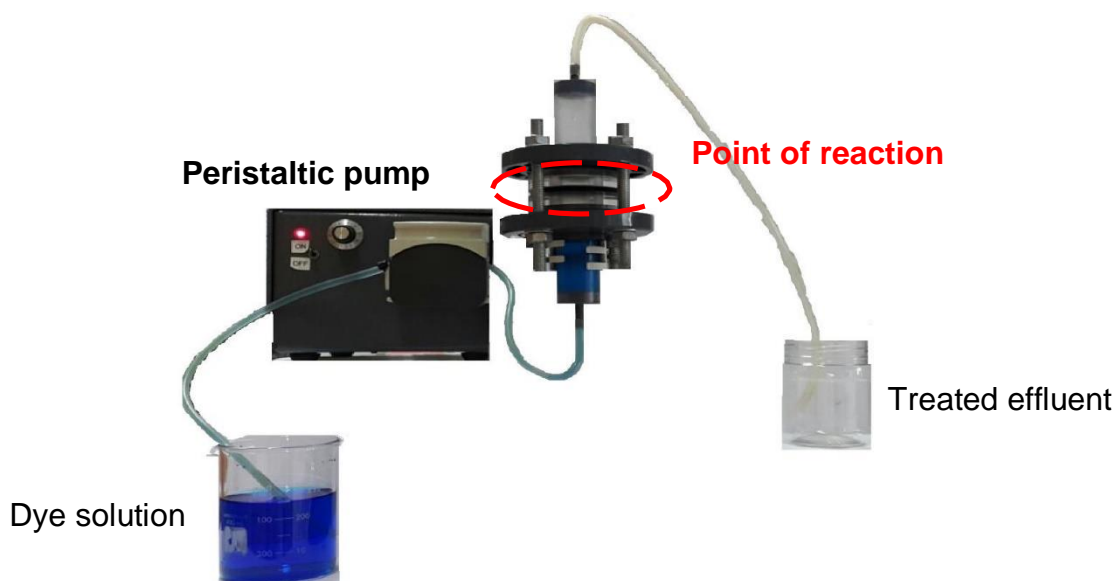


Figure 3-3: In-house developed reactor used to evaluate the cobalt oxide particles in AOPs

3.3 Characterisation methods

Various characterisation techniques were employed to study the structure, morphology and purity of the cobalt hydroxide and cobalt oxide nanopowders synthesised, as described in the sections 3.3.1 to 3.3.7. All the generated nanoparticles were sampled after calcination and some before calcination for analysis. EDS along with TEM, SEM, SAED and electron energy-loss near-edge structure (ELNEFS) were performed at the Electron Microscopy Unit located at the University of the Western Cape. Particle size distributions (PSD) and interlayer spacing (or D-spacing) were determined from TEM using Image J software, as well as GATAN micrograph software respectively, in which 200 individual particles were measured to determine the PSD. The composition, phase and degree of crystallinity were further determined using XRD analysis performed at the Materials Research Department located at iThemba LABS. In addition, FT-IR was done on a selection of particles in the Chemistry Department of

CPUT (District 6 campus). BET analysis was performed either at the National Centre for Nanostructured Materials, located at the Council for Scientific and Industrial Research, or the department of Chemical Engineering at the University of Cape Town using the same method.

3.3.1 Selected Area Electron Diffraction

SAED may be used to identify the lattice structure and crystal make-up of a substance. Figure 3-4 represents a typical polycrystalline substance in which concentric rings are formed. This occurs as the grains of polycrystalline material are randomly orientated, providing diffraction at the same length from the centre, producing continuous rings (Egerton 2005).

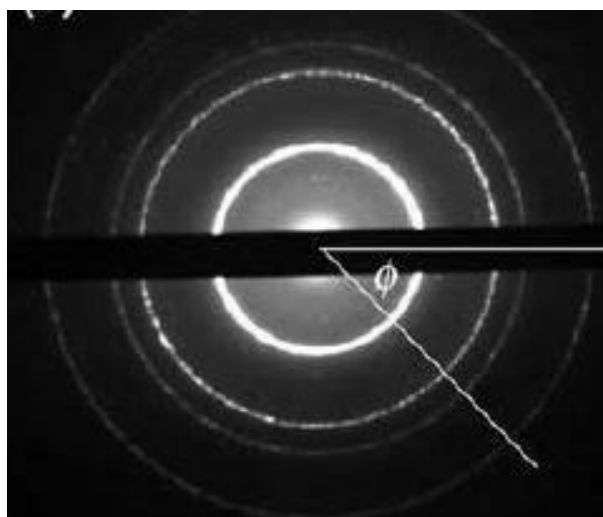


Figure 3-4: Ring diffraction pattern observed for many crystallites (Egerton 2005)

3.3.2 Electron Diffraction Spectroscopy

EDS provides an overview of the elemental make-up within a sample. The results obtained are plotted as intensity versus x-ray wavelength, showing the various elements within the sample. EDS has the limitation that it is not normally quantitative, but may be semi-quantitative. Trace elements are also not detected, as detection limits of 1% or higher exists.

3.3.3 Energy Loss Near-Edge Fine Structure

ELNEFS studies the ratio of valence states within transitional metal samples, in which various valence states within a sample may exist. It allows for the more dominant species to be determined. This may provide insight into the activity in metal oxide catalysts, depending on the more active species.

3.3.4 Fourier Transform Infrared Spectroscopy

FT-IR analysis is used to identify various samples using infrared light to scan test the samples and observe their chemical properties. It may be used as a means of quality control within industry, and often serves as the initial analysis of synthesised materials, as changes and variances in the product are clearly seen.

3.3.5 Scanning Electron Microscopy and Transmission Electron Microscopy

SEM is a characterisation method which provides use of electrons for image development, therefore resulting in black and white images of the sample studied. Similarly, TEM is a microscopy technique in which a beam of electrons is used. Here it is transmitted through the specimen, therefore forming an image.

The main exposed facets present within inorganic particles can be determined using TEM, by examining the d-spacing of the as-prepared particles, which may then be indexed using Equation 3-2 for face-centred cubic (FCC) unit cells (Egerton 2005).

$$d = a/(h^2 + k^2 + l^2)^{1/2} \quad 3-2$$

For this calculation, it is necessary to know the lattice parameter (a), which is a constant for the particles worked with, and either the d-spacing value (d) or the h, k, and l, known as Miller indices, values which represent the orientation of the planes of the particles. According to this equation, larger Miller indices correspond to smaller d-spacing (Egerton 2005). It is also to be noted that for FCC particle orientation, the h, k and l values must all be positive or negative. Using this rule, the first few rings of polycrystalline FCC metals may therefore be indexed to Equation 3-3 (Egerton 2005).

$$(hkl) = (111), (200), (220), (311), (222), \dots$$

3.3.6 X-Ray Diffraction

XRD is a rapid analytical technique used for the identification of an unknown crystalline material. It provides results which are accurate and unambiguous in terms of phase identification. However, the standard reference files (JCPDS cards) are required for inorganic compounds.

3.3.7 Brunauer-Emmett-Teller

BET surface area measurements are used to determine the surface area of particles. It is especially important in catalysis, as it may be a direct indication of the catalytic efficiency displayed. The samples synthesised within this study were degassed at 150°C for two hours and analysed using a Micromeritics TRISTAR II 3020 system.

3.4 Data

3.4.1 Cobalt hydroxide powders

During the synthesis process, various precursor powders were formed based on the type of alcohol used. The different powders were also characterised by X-ray diffraction (XRD) and Fourier-transform infrared spectroscopy (FT-IR) to confirm their phase and to compare them to the annealed cobalt oxide particles. Their undisputable differences were presented in their colours. The colour of precursor powder was therefore recorded in order to draw correlations between the resulting cobalt oxide particles and their catalytic ability, i.e. which 'colour' produced the better catalyst.

3.4.2 Degradation vs. time

The rapid rate of reaction presented by the peroxymonosulphate/ AOP, specifically for cobalt oxide, was the spark of interest in this metal oxide research. Determining the rate of reaction for this process, and drawing correlations to the particle sizes, as well as the differences in production, was therefore important. Produced cobalt oxide particles were used to degrade methylene blue solutions in order to monitor the

catalytic effectiveness. Degradation curves were plotted versus time to evaluate which of the produced particles provided the most rapid degradation.

3.4.3 Particle size vs. surface tension

The most important change occurring in this research is the change in alcohols and therefore the change in surface tension of the precursor solutions. The surface tensions of the alcohols at room temperature (25°C) is known and has been measured in literature, as well as water/alcohol solvents, except for those experiencing an interface. One of the problems encountered is that this information is difficult to obtain at elevated temperatures and pressures, emulating the environment experienced inside of the pressure reactor. However, since input variables were available, it allows for control at the input to be monitored in order to draw correlations to the output. Transmission electron microscopy (TEM) was used to visually examine and measure the particle sizes. An average of 200 particles were measured in order to determine the particle size distribution curves. In addition, the crystallite sizes were also determined from XRD analysis. This information was plotted against the surface tension to determine the effect it had.

3.4.4 Particle shape vs. degradative quality

Just as particle size is important in catalyst-dependent reactions, so is the particle shape. Literature has revealed that particles with exposed facets have enhanced catalytic ability. Saputra *et al.* (2014) has specifically noted that exposed facets play a significant role in peroxymonosulphate activation. The shape of the particles was determined in scanning electron microscopy (SEM) analysis and compared to the degradative quality achieved.

3.4.5 Calcination temperature vs. particle size

Due to the contradicting findings by Yang *et al.* (2004) and Jing *et al.* (2012) regarding the calcination temperature effect on particle size, it was important to study its effect on the particles produced in this study. This provided even more insight, as the particles after hydro/solvothermal synthesis is cobalt hydroxide which requires calcination to form cobalt oxide for use as a catalyst. The particle and crystallite sizes as determined by TEM and XRD were therefore compared with increasing calcination temperature.

3.4.6 Calcination temperature vs. degradative efficiency

In addition to the above, it was important to determine the effect the calcination temperature has on the degradative efficiency. Common knowledge about catalysts says that the larger the surface area, the more active it is due to the higher density of active sites. However, Vinod (2010) reported an instance contradicting this when using cobalt catalyst in the Fischer-Tropsch process. In addition, it was important to note changes in crystallinity, as well as morphology and the resulting effect on degradative efficiency.

3.5 Conclusion

The hydro/solvothermal method used for the cobalt hydroxide synthesis and the calcination method used to obtain cobalt oxide has been detailed, along with the catalytic degradation of methylene blue in an advanced oxidation process. The characterisation techniques (TEM, SEM, XRD, FT-IR, EDS, ELNEFS and BET) used to analyse the resulting particles were described, along with the motivation for using these.

CHAPTER 4 THE EFFECT OF Cl^- AND NO_3^- ANIONS IN WATER ON Co_3O_4 PARTICLES

4.1 Introduction

In this chapter, the effect of changing the precursor salt to either cobalt chloride hexahydrate or cobalt nitrate hexahydrate in the absence of alcohols during hydrothermal synthesis of Co_3O_4 was evaluated. The precursor solutions are discussed, as is the phase of resulting precursor powders, as well as the morphology and particle size distributions for the resulting particles.

4.2 Hydroxide polymorphs obtained from hydrothermal synthesis in pure water

In order to determine the effect of anion only, pure water solutions had to be made up using the cobalt chloride hexahydrate and cobalt nitrate hexahydrate. Both resulting solutions were red in colour, as shown in Figure 4-1. This was expected, as both salts used were in the hydrous form, as red coloured salts. The anhydrous forms of cobalt complexes are blue in colour and obtain a reddish colour from the presence of water molecules alone. At the point of solution, the cobalt salts follow the reaction Equations 4-1 and 4-2, for cobalt chloride and cobalt nitrate respectively.

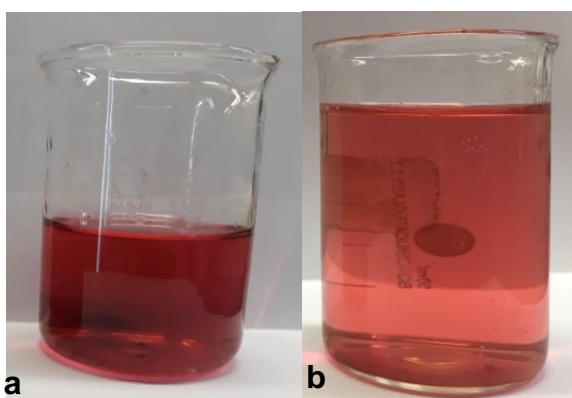
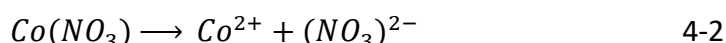
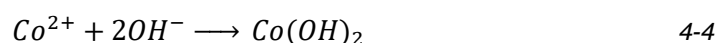


Figure 4-1: a) Cobalt chloride hexahydrate and b) cobalt nitrate hexahydrate in pure water

The pH of the solution was then adjusted to approximately 8.10, using an ammonium hydroxide solution, for precipitation of the cobalt hydroxide particles, as shown in

reaction Equation 4-4. After the pH was adjusted, the solutions were hydrothermally treated to form the cobalt hydroxide particles.



Cobalt hydroxide, the precursor to cobalt oxide, exists as polymorphs alpha (α) and beta (β) cobalt hydroxide ($Co(OH)_2$) most obviously recognised by their colours green/blue and pink respectively (Al-Ghoul *et al.*, 2010). As presented in literature, the two phases of cobalt hydroxide vary in their structure, which ultimately leads to the colour they exude. The α - $Co(OH)_2$ phase has a layered double hydroxide structure, with positively charged layers separated by anions and water molecules (Cheng *et al.*, 2014; Al-Ghoul *et al.*, 2009; Mishra *et al.*, 2018; Hu *et al.*, 2009). The tetrahedral structure, along with the intercalated anions and water molecules, provides a large interlaminar spacing of >0.7 nm and disordered structure, which cause the green/blue colour. Figure 4-2 displays the cobalt hydroxide powders obtained for the chloride and nitrate precursor anions respectively. The green colour indicated that the polymorph synthesised hydrothermally was the α -phased $Co(OH)_2$, which was further validated through XRD, showing the characteristic peak (003), as given in Figure 4-3. Therefore, in water only, the role of the anion on the hydroxide polymorph is negligible.

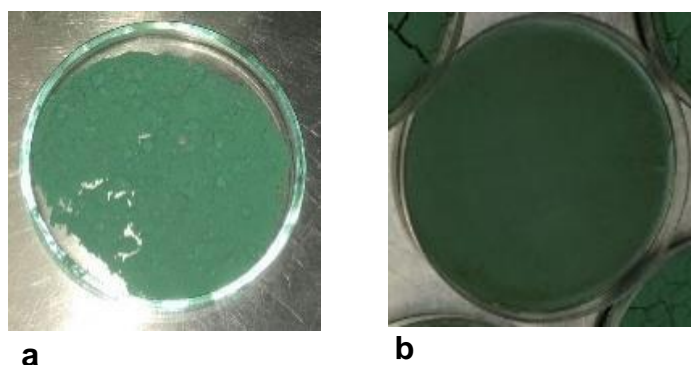


Figure 4-2: Cobalt hydroxide particles synthesised from a) cobalt chloride hexahydrate and b) cobalt nitrate hexahydrate in pure water

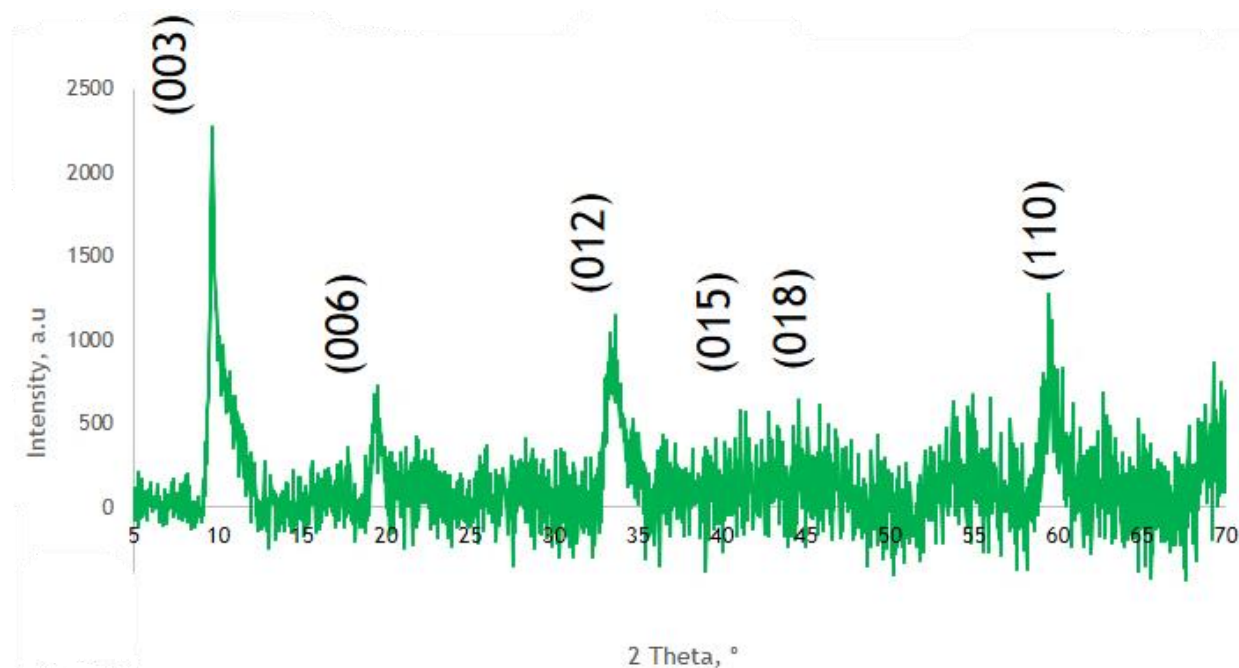
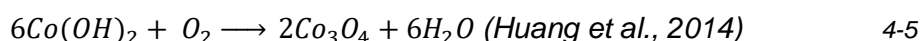


Figure 4-3: XRD spectra obtained for the green α -phased cobalt hydroxide

4.3 Cobalt oxide identification and purity

The cobalt oxide (Co_3O_4) nanopowders were produced by the calcination of the hydrothermally synthesised cobalt hydroxide particles at 300, 400 and 500°C, according to the reaction in Equation 4-5. They were identified and tested for purity by means of electron diffraction spectroscopy (EDS), Fourier-transform infrared spectroscopy (FT-IR) and X-ray diffraction (XRD).



Electron diffraction spectroscopy (EDS) was used to identify the elements which were present in the samples synthesised. The EDS spectra for the resulting cobalt oxide particles are therefore shown in Figure 4-4. The peaks exhibited show the presence of cobalt and oxygen; the constituents of the Co_3O_4 analysed. It also presented peaks for carbon, which will always be present in this analysis, and copper for the copper grid used in the analysis process. Besides these peaks, additional peaks at ± 2260 eV were evident, showing evidence of the presence of chloride ions. This was expected for the cobalt chloride precursor, but not for the cobalt nitrate precursor, and was therefore attributed to the trace amounts of chloride ions present in the cobalt nitrate salt. The major limitations of EDS lie in its inability to differentiate between compounds of a similar chemical make-up, and the fact that it is normally not quantitative. It was therefore

necessary for further characterisation to be done. The FT-IR spectra, as seen in Figure 4-5, for the same particles provided major peaks at 550 and 660 cm^{-1} , provides additional evidence of Co_3O_4 , according to Chani *et al.* (2015).

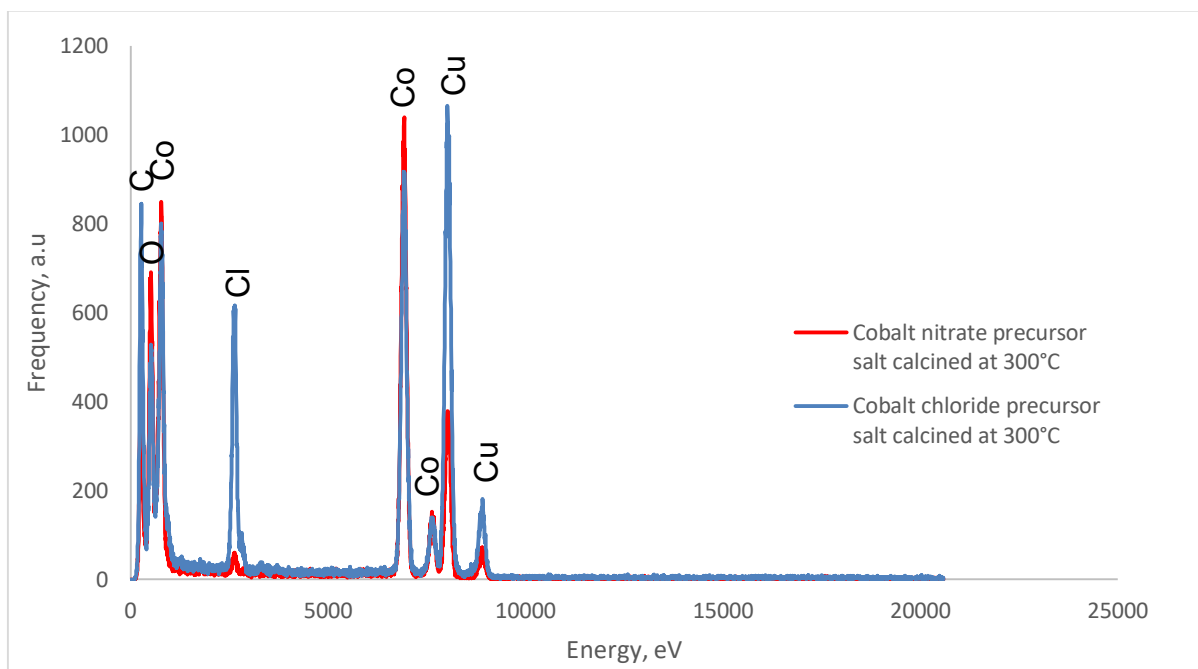


Figure 4-4: EDS spectra for cobalt oxide particles produced with a cobalt chloride precursor salt in pure water calcined at 300°C

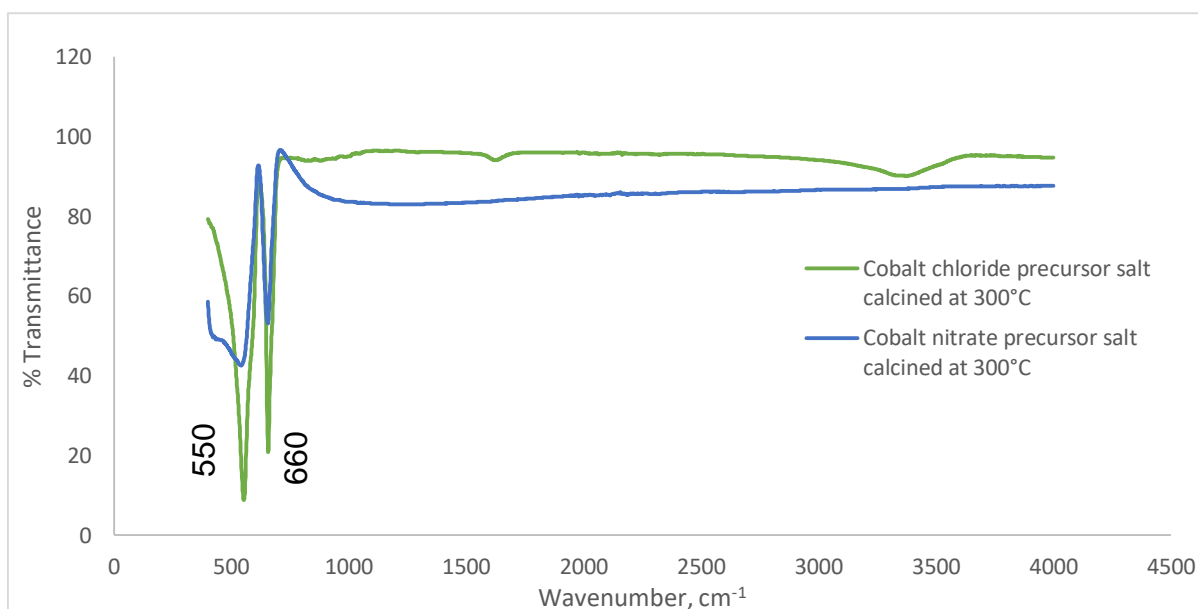


Figure 4-5: FT-IR spectra for cobalt oxide particles produced with a cobalt chloride precursor salt in pure water, calcined at 300°C

Finally, X-ray diffraction was performed on Co_3O_4 particles to identify the purity of the

samples synthesised. The XRD patterns shown in Figure 4-6 reveal a high purity level, as the peaks represented are in accordance with the JCPDS card 42- 1467, which exhibits diffraction peaks at 19°, 31.3°, 36.9°, 38.6°, 44.8°, 55.7°, 59.4° and 65.2°, indexed to (111), (220), (311), (222), (400), (422), (511) and (440). The unreacted chloride ions as noted in Figure 4-3 would have revealed an additional peak at 16° in accordance to JCPDS cards 29- 0466, 25- 0242, and 73- 2134. However, no prominent peak exists, indicating insignificant volumes in the sample.

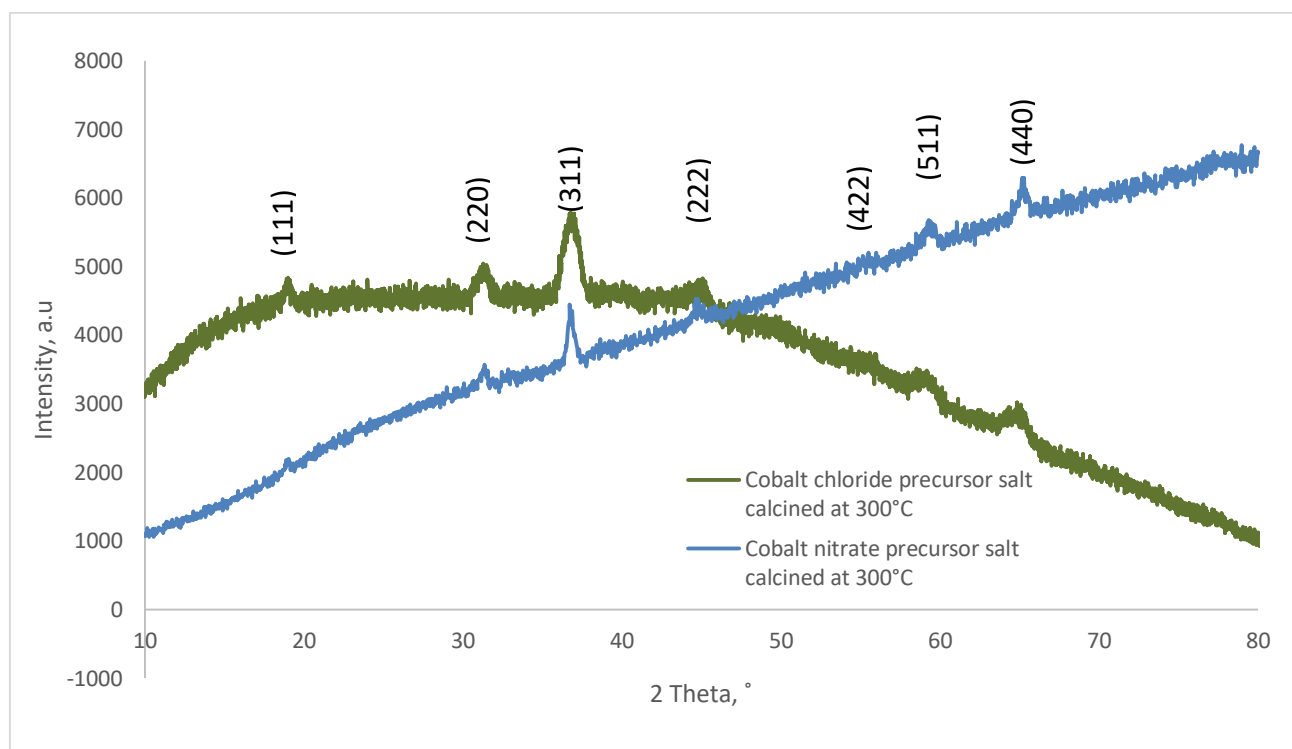


Figure 4-6: XRD spectra for the cobalt oxide particles produced with cobalt chloride hexahydrate and cobalt nitrate hexahydrate in pure water, calcined at 300°C

4.4 Particle morphology

Metal oxides are of polycrystalline nature, and their lattice structure may therefore be identified using selected area electron diffraction (SAED) (Egerton, 2005), in which they may be identified by concentric rings. Non-crystalline particles may also easily be identified by their SAED images, as no bright spots will be evident. Polycrystalline particles were evident in the cobalt chloride precursor sample, as seen in the SAED image presented in Figure 4-7. However, the cobalt nitrate hexahydrate sample produced an amorphous state, as no bright spots were evident.

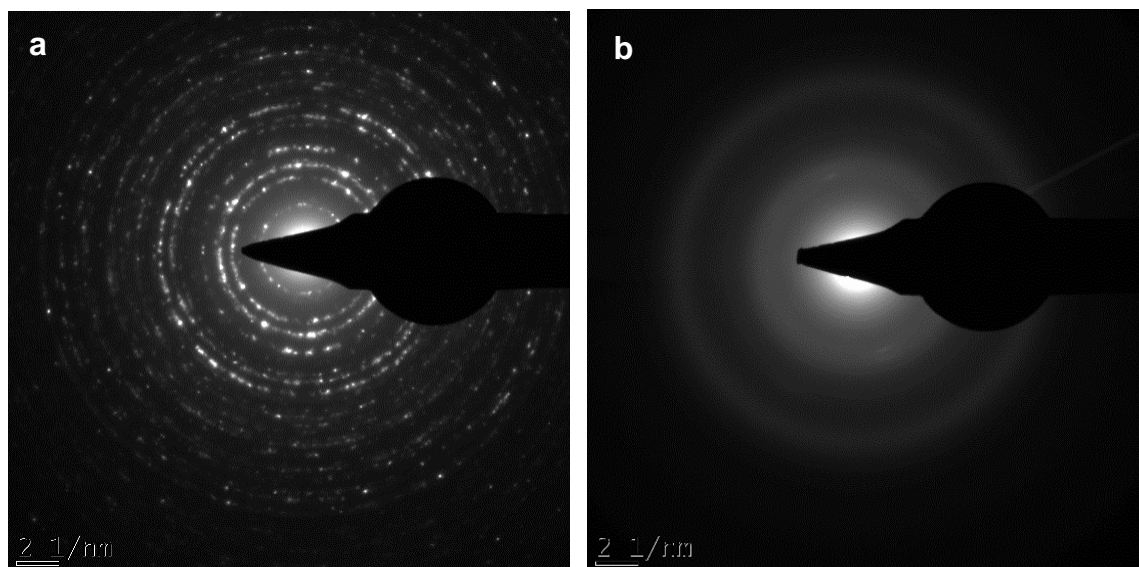


Figure 4-7: SAED images for the cobalt oxide particles synthesised from a) cobalt chloride hexahydrate and b) cobalt nitrate hexahydrate in pure water, calcined at 300°C

This was further reiterated by the transmission electron microscopy (TEM) images of the cobalt oxide samples, as shown in Figure 4-8. The cobalt chloride hexahydrate precursor salt resulted in rod-shaped particles, approximately 30 nm in size, while the cobalt nitrate hexahydrate salt provided particles which were hard to identify, therefore resembling an amorphous nature. However, upon further investigation using scanning electron microscopy (SEM), it was noted that the particles synthesised from the nitrate precursor salt showed a tendency to agglomerate, forming larger particles approximately 20 µm in size, as seen in Figure 4-9.

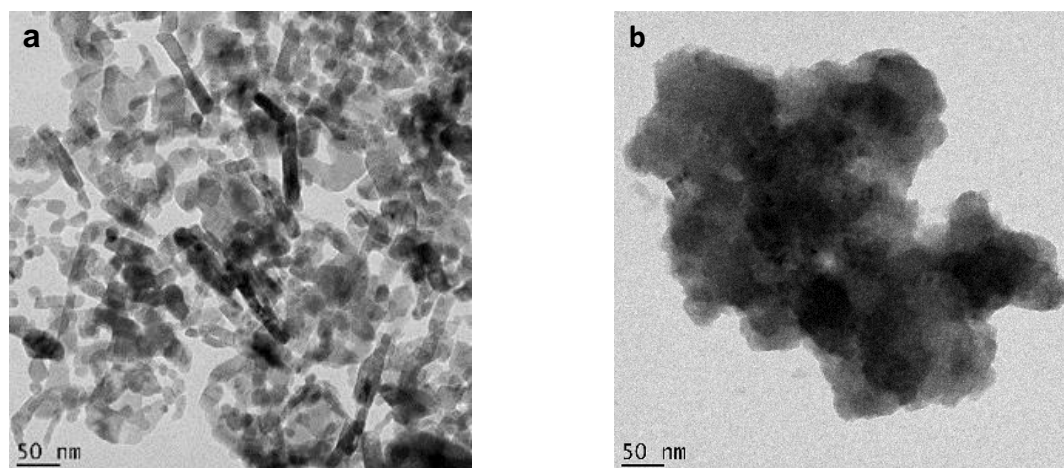


Figure 4-8: Transmission electron microscopy images for the cobalt oxide particles produced from a) cobalt chloride hexahydrate and b) cobalt nitrate hexahydrate in pure water

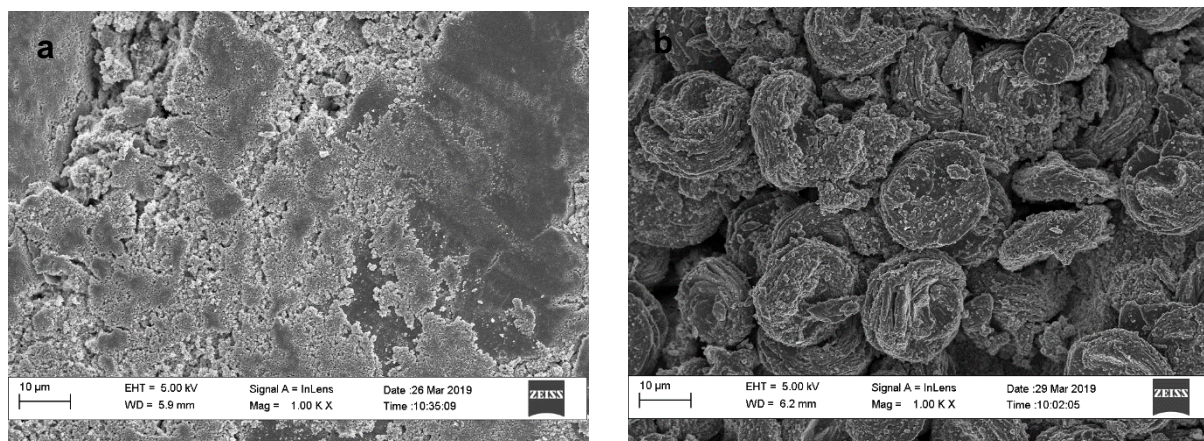


Figure 4-9: Scanning electron microscopy images for the cobalt oxide particles synthesised from a) cobalt chloride hexahydrate and b) cobalt nitrate hexahydrate in pure water

The size distribution curves were based on the particles as presented in the TEM images at various magnifications, which therefore were the initial/smaller particles before taking agglomeration into consideration. The particle size distribution (PSD) in Figure 4-9 is therefore only that of the cobalt oxide particles synthesised from the cobalt chloride precursor. Bin limits of 10 nm were used, which provided a smooth and narrow PSD for the remaining samples, as displayed in Appendix D. From the PSD in Figure 4-10, an average particle size of 30 nm was noted for the sample studied. The cumulative frequency of the measured particles provided the d_{50} particle size within each batch. Since the d_{50} particle size provides that point at which half the particles are accounted for, it provides an overview of the majority of the particles represented in a batch. Using this principle, the d_{50} particle size of the cobalt oxide particles synthesised from cobalt oxide was found to be 28,69 nm, which was in close proximity to the particle size estimated from the PSD.

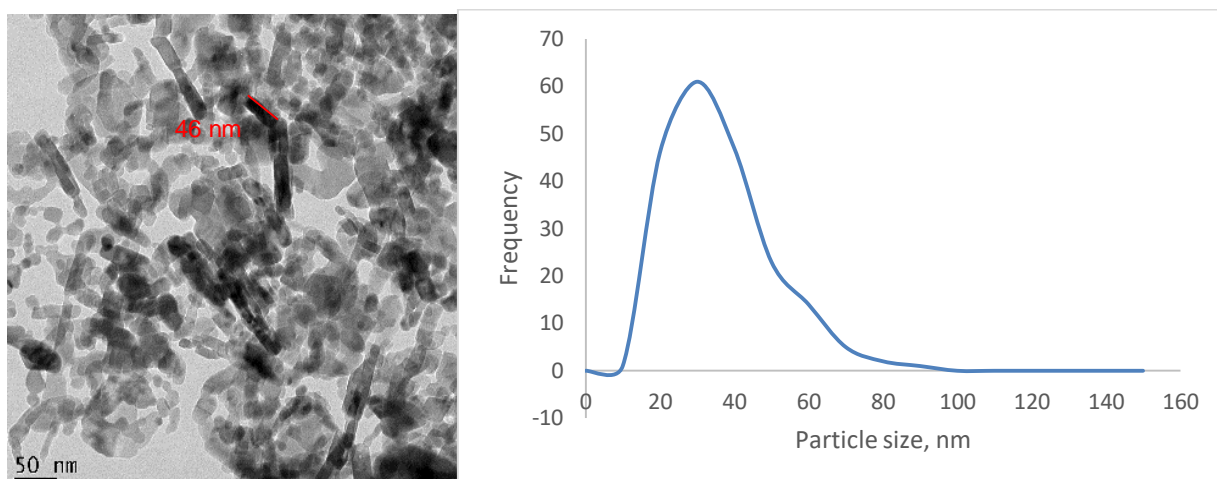


Figure 4-10: Particle size distribution curves for the cobalt oxide particles synthesised from cobalt chloride hexahydrate in water

4.5 Effect of calcination temperature

Contradicting findings in literature led to the investigation of the effect of the calcination temperature on the particle characteristics. Yang *et al.* (2004) used milled cobalt precursors and reported that an increase in size was attributed to an increase in calcination temperature, obeying Scott's equation, which shows a direct relation between temperature and particle diameter. However, Jing *et al.* (2012) found the opposite in their solvothermal synthesis of Co_3O_4 when calcining a CoCO_3 precursor. Appendix A provides all the analysed cobalt oxide particles synthesised, calcined at 300, 400 and 500°C. It was noted that the sharpness of the peaks increased with increasing temperature. Since the full width at half maximum (FWHM) is derived from these peaks, it is noted that with increasing temperature, the FWHM decreases. The Scherrer equation relates crystallite size to the FWHM. It was therefore used to confirm that the crystallinity of the particles increases with increasing temperature.

The FWHM was extracted from the major peak presented within the XRD spectra, at 36.9°. Table 4-1 presents the crystallite sizes calculated from the Scherrer equation, as shown in Equation 4-6, relating them to the FWHM as well as the calcination temperature. The results show that with an increase in calcination temperature, there is a definite increase in crystallite size, in agreement with Yang *et al.* (2004).

$$\tau = \frac{K\lambda}{\beta \cos\theta} \quad 4-6$$

Where:

- τ is the average size of the ordered crystallite, which may be smaller/equal to the grain size.
- K is the dimensionless shape factor, which varies around 0.9, depending on shape.
- λ is the X-ray wavelength.
- β is the Full Width at Half Maximum, in radians.
- θ is the Bragg angle.

Table 4-1: Crystallite sizes for the synthesised cobalt oxide particles synthesised in pure water, calcined at 300, 400 and 500°C

Cobalt oxide sample	Crystallite sizes, nm		
	300°C	400°C	500°C
Cobalt chloride precursor	7.09	28.87	34.89
Cobalt nitrate precursor	17.08	19.47	27.91

4.6 Conclusion

Cobalt oxide nanoparticles, with a high level of purity, were produced hydrothermally, using cobalt chloride hexahydrate and cobalt nitrate hexahydrate precursor salts in pure water. Of the cobalt hydroxide polymorphs encountered in literature, only α -cobalt hydroxide was encountered during synthesis, for both anions explored. The cobalt chloride precursor salt provided rod-shaped particles approximately 30 nm in length measured from the TEM images. This differed substantially from the cobalt nitrate precursor salt, which according to the SAED images, and confirmed from the TEM images, revealed an amorphous nature, as the particle size and shape were hard to identify. Upon further investigation it was noted that agglomeration had taken place, as the SEM images showed larger agglomerates approximately 20 μm in size. From these results, it is important to note that one change, such as altering the precursor salt, can completely alter the cobalt oxide nanoparticles obtained, even though the cobalt hydroxide phase remains unchanged.

CHAPTER 5 THE EFFECT OF Cl⁻ AND NO₃⁻ ANIONS IN ALCOHOLS ON Co₃O₄ PARTICLES

5.1 Introduction

This chapter presents the effects various alcohols at 100% and 50% concentrations have on the Co₃O₄ particles formed from the precursor salts, cobalt chloride hexahydrate and cobalt nitrate hexahydrate, during hydro/solvothermal synthesis. It highlights the changes experienced in the precursor solutions, resulting hydroxide precursor powders, and the size and shape differences of the final cobalt oxide in comparison to the pure water batches.

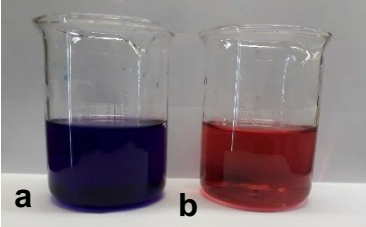
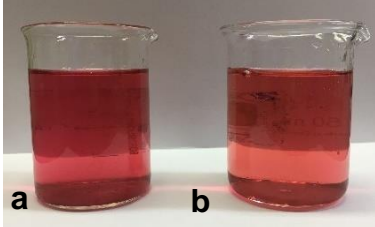
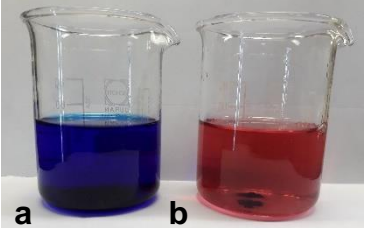
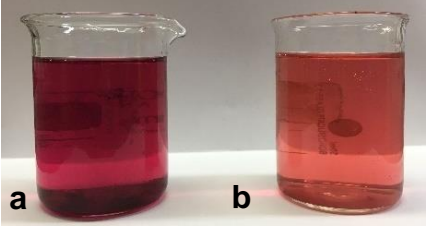
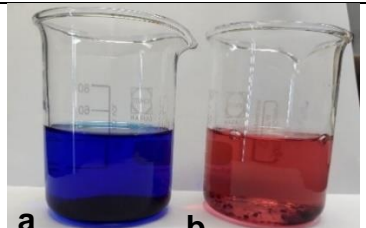
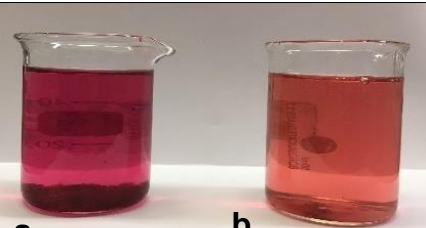
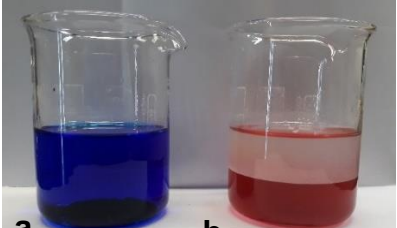
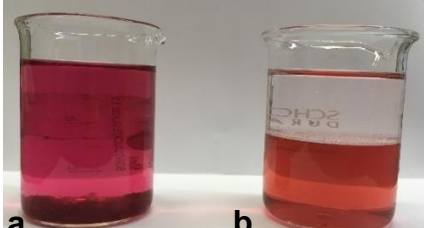

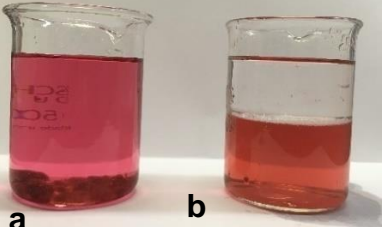
5.2 Hydroxide polymorphs obtained from hydro/solvothermal synthesis

The hydrothermal synthesis explored in Chapter 4 was converted to hydro/solvothermal synthesis with the replacement of pure water with various alcohols at 100% and 50% concentrations. Table 5-1 shows the cobalt chloride hexahydrate and cobalt nitrate hexahydrate salts dissolved in 100% and 50% alcohol solutions. Anhydrous cobalt salts without the presence of water are blue in colour. Cobalt chloride hexahydrate and cobalt nitrate hexahydrate therefore naturally obtains its reddish colour from the presence of water molecules. It was therefore easy to monitor the exhaustion of water with the increase in alcohol, as the solution should become blue. However, this was found for the cobalt chloride precursor salts only, and not for the cobalt nitrate precursor salts, as displayed in Table 5-1.

Table 5-1 also reveals that the water present within the sample was only exhausted for the cobalt chloride hexahydrate precursor salt solutions, as the addition of 100% alcohol resulted in a blue solution. The cobalt nitrate hexahydrate precursors presented for each alcohol were expected to perform the same as the chloride anion. However, a noticeable difference in the colour of the precursor solutions used occurred at both 100% alcohol solutions and 50% alcohol/water solutions, provided a reddish colour, indicating that the cobalt complex orientation remains unchanged. The

100% alcohol samples do, however, display a darker shade of red. It is worth noting that the molarity was kept the same for both anions used.

Table 5-1: Cobalt chloride hexahydrate and cobalt nitrate hexahydrate in a) 100% and b) 50% alcohol/water solutions respectively

	Cobalt chloride hexahydrate	Cobalt nitrate hexahydrate
Methanol		
Ethanol		
Propanol		
Butanol		
Octanol		

During the production of cobalt oxide using cobalt chloride hexahydrate in 100%

octanol, the precipitation step occurred much more rapidly than the other alcohols. While correcting the pH, the particles (resembling β -Co(OH)₂) began to cake at the bottom of the beaker, as shown in Figure 5-1. At the prescribed pH (8.10), the stirrer was stopped and the clear liquid immediately separated from the precipitates (without centrifuging), which formed a porridge-like layer at the bottom of the beaker. During the addition of the ammonia solution, water was added back to the system with the precipitating agent. The separation of the particles and consequent caking may therefore be attributed to the immiscibility of octanol in water. Similar, though less clear, findings occurred when using 100% butanol as the solvent, as butanol is only partly miscible with water, as seen in Table 5-1.



Figure 5-1: 100% octanol precursor after pH correction

A relationship may also be drawn between the presence of water and the cobalt hydroxide phase synthesised. As presented in literature, the two phases of cobalt hydroxide vary in their structure, which ultimately affects the colour they exude. The α -Co(OH)₂ phase has a layered double hydroxide structure, with positively charged layers separated by anions and water molecules (Cheng *et al.*, 2014; Al-Ghoul *et al.*, 2009; Mishra *et al.*, 2018; Hu *et al.*, 2009). The tetrahedral structure, along with the intercalated anions and water molecules, providing a large interlaminar spacing of >0.7 nm and disordered structure, are responsible for the green/blue colour. The octahedral symmetry and perfectly ordered stacking along the C-axis, with interlaminar spacing of 0.46 nm, exhibited by the β -phase is responsible for its pink colour (Al-Ghoul *et al.*, 2009). This is in line with Petkova and Nedkov (2013) who concluded that the optical differences lie in spectral positioning of the 3d electrons present in the cobalt complexes formed: both octahedral and tetrahedral.

Some of the cobalt hydroxide polymorphs synthesised are provided in Figure 5-2. Interestingly, when using cobalt chloride hexahydrate as a precursor salt in 100% alcohols, pink β -Co(OH)₂ powders were produced. The remainder of the cobalt chloride hexahydrate and cobalt nitrate hexahydrate salts mostly produced green α -Co(OH)₂ powders, with the exception of cobalt chloride hexahydrate in 50% ethanol and 50% butanol, which produced brown powders. However, the formation of these phases, as well as the transformation between one another, are still not well understood in literature, and a lot of the focus has been placed on synthesising them in order to gain better understanding of the chemistry. It has also been reported that α -Co(OH)₂ is thermodynamically metastable and may therefore rapidly transform to β -Co(OH)₂ during synthesis or in contact with a strong alkali (Cheng *et al.*, 2014). From this, one may deduce that the 50% ethanol and 50% butanol samples shown in Figure 5-2 contain both α -Co(OH)₂ and transformed β -Co(OH)₂ mixing their pink and green colours to form the brown powders, but this was not confirmed by XRD, which only indicated the presence of the β -phase.

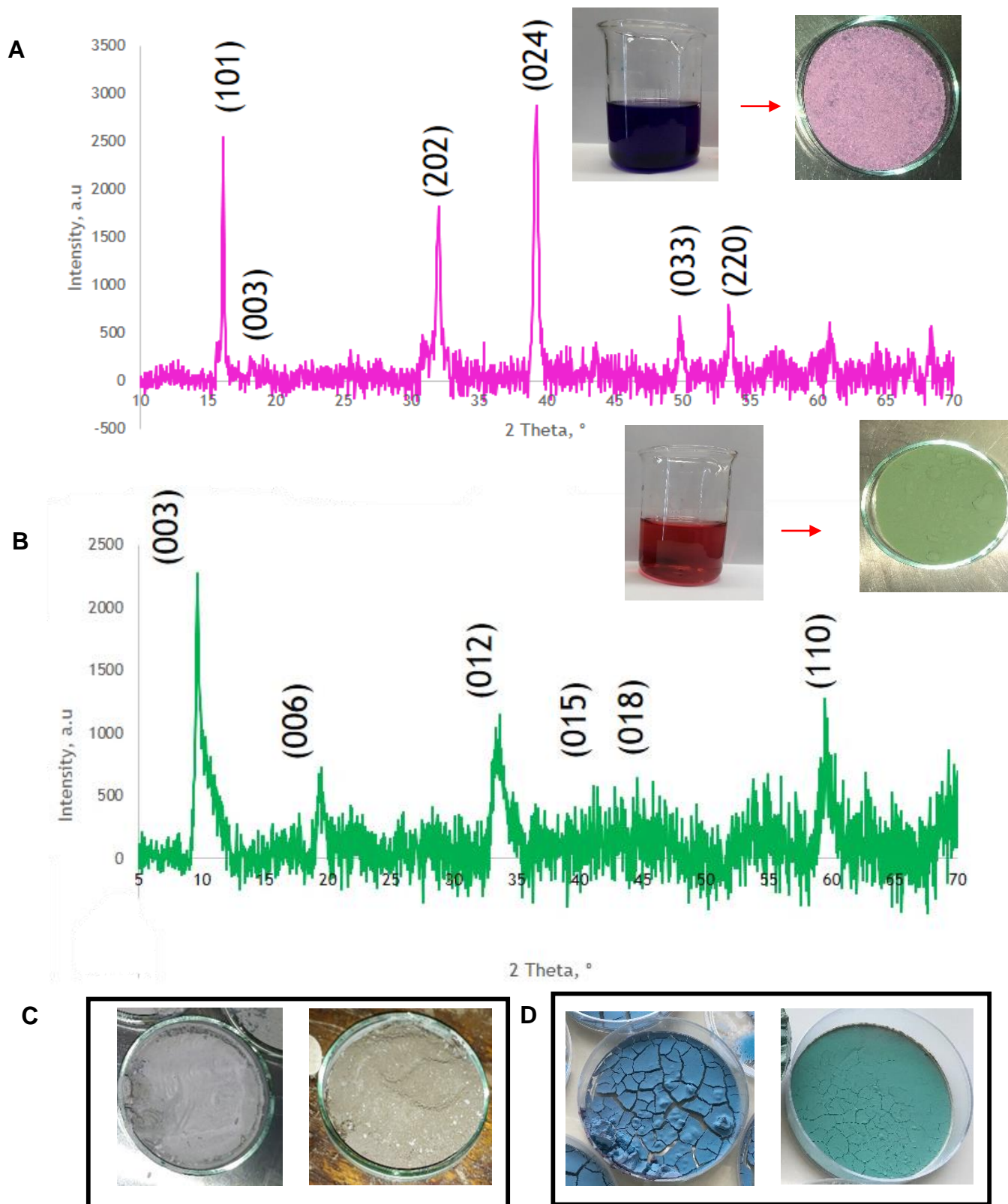


Figure 5-2: Cobalt hydroxide precursors resulting from A) cobalt chloride hexahydrate in 100% alcohols (blue in colour), B) cobalt nitrate in 100% alcohol and 50% alcohol/water mixtures for both precursor salts, C) cobalt chloride hexahydrate in 50% ethanol and 50% butanol respectively and D) cobalt nitrate hexahydrate in 100% methanol and 100% octanol respectively

5.3 Cobalt oxide identification and purity

The identification and purity of the synthesised cobalt oxide particles was determined using EDS, FT-IR and XRD analysis. As in Chapter 4, EDS was used to identify the elements which were present in the samples synthesised. The results are found in Figures 5-3 to 5-6. Figures 5-3 and 5-4 represent the EDS spectra for the cobalt oxide particles resulting from cobalt chloride hexahydrate in 100% and 50% alcohol respectively, revealing similar results to that of the water batches. Again, the peaks exhibited provided evidence of cobalt and oxygen with the addition of carbon and copper, as well as unreacted chloride ions shown at ± 2260 eV. Figures 5-5 and 5-6 represent the EDS spectra for the cobalt oxide particles resulting from cobalt nitrate hexahydrate in 100% and 50% alcohol respectively. While Figure 5-5 presents no impurity formed, Figure 5-6 reveals an impurity between 2500 and 2700 eV, which was attributed to the presence of sulphur.

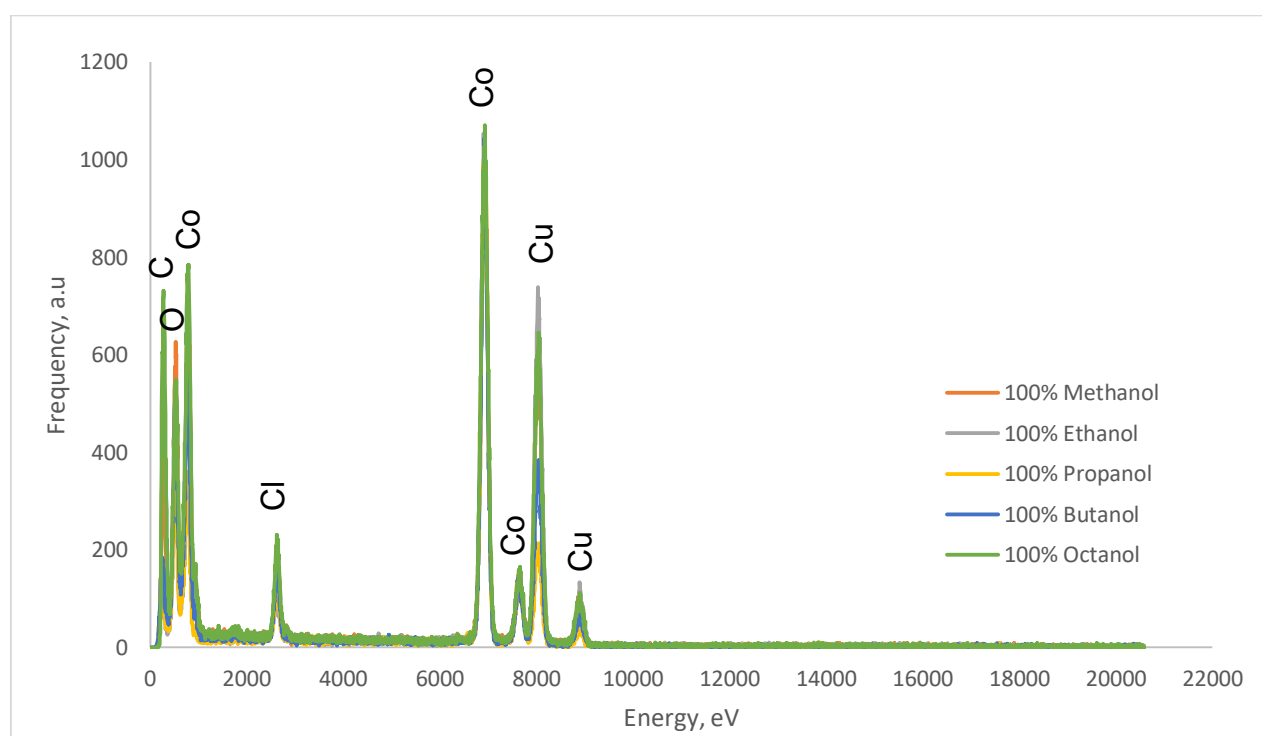


Figure 5-3: EDS spectra for the cobalt oxide synthesised from cobalt chloride hexahydrate in 100% alcohol solvents, calcined at 300°C

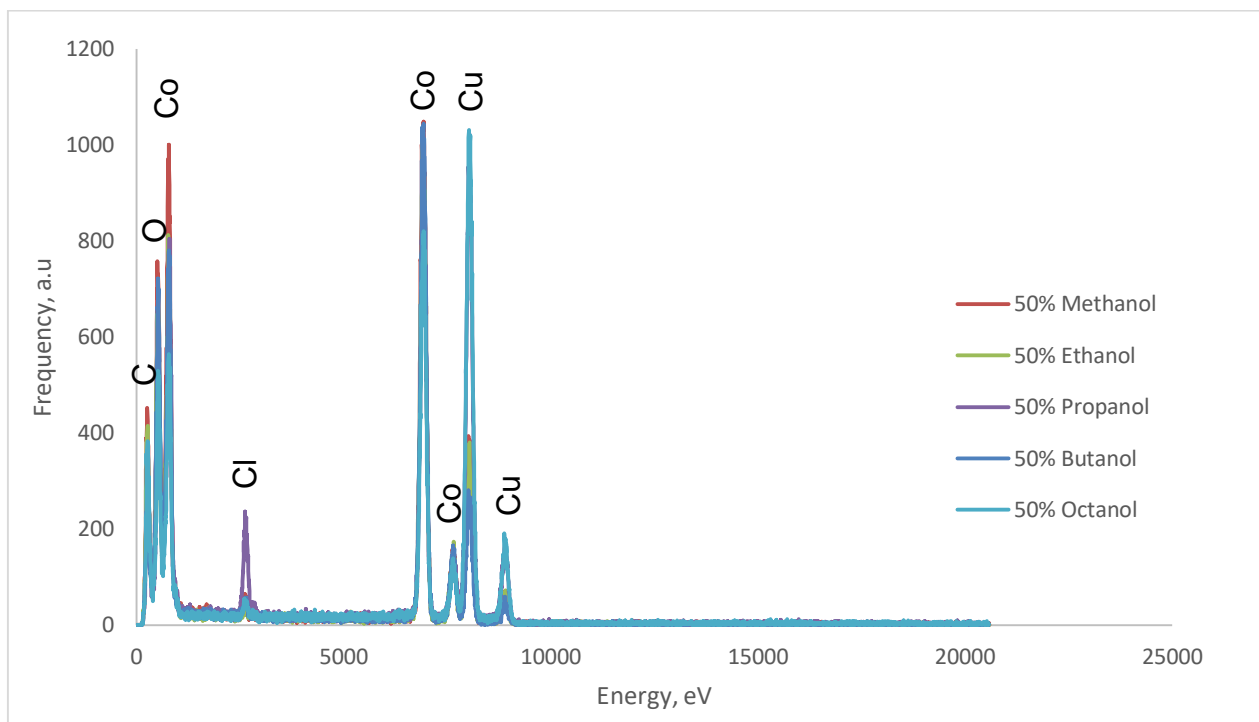


Figure 5-4: EDS spectra for the cobalt oxide synthesised from cobalt chloride hexahydrate in 50% alcohol/water solvents, calcined at 300°C

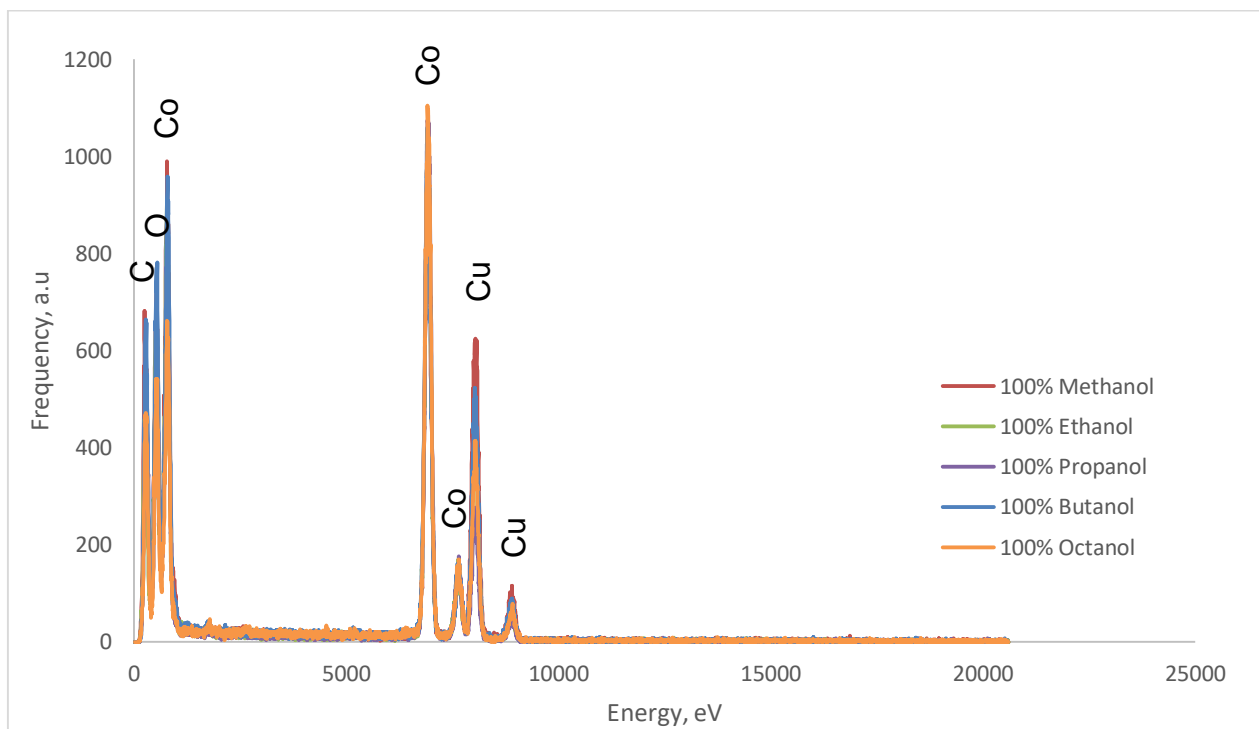


Figure 5-5: EDS spectra for the cobalt oxide synthesised from cobalt nitrate hexahydrate in 100% alcohol solvents, calcined at 300°C

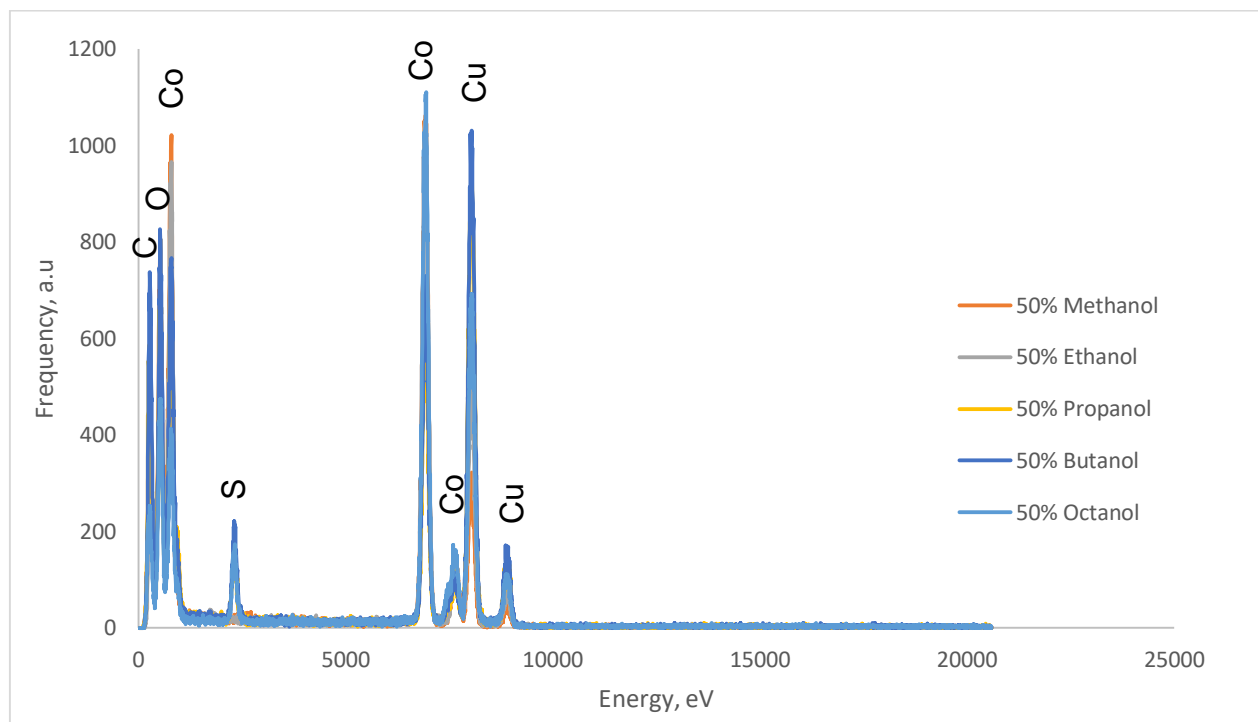


Figure 5-6: EDS spectra for the cobalt oxide synthesised from cobalt nitrate hexahydrate in 50% alcohol solvents, calcined at 300°C

The FT-IR spectra, shown in Figures 5-7 to 5-10, provided major peaks at 550 and 660 cm^{-1} for all the synthesised particles, which provides additional evidence of Co_3O_4 , according to Chani *et al.* (2015), with additional peaks at 1600 cm^{-1} and 3460 cm^{-1} , attributed to the broad peak of OH stretching bonds in water, for the cobalt oxide particles synthesised from cobalt chloride hexahydrate in 100% and 50% alcohols respectively. Figures 5-9 and 5-10 present the FT-IR spectra for the cobalt oxide particles synthesised from cobalt nitrate hexahydrate in 100% and 50% alcohols respectively. An additional peak was noted for the 50% alcohol batches at 1100 cm^{-1} , for the propanol, butanol and octanol, which was therefore attributed to the presence of sulphur, as noted in the EDS spectra.

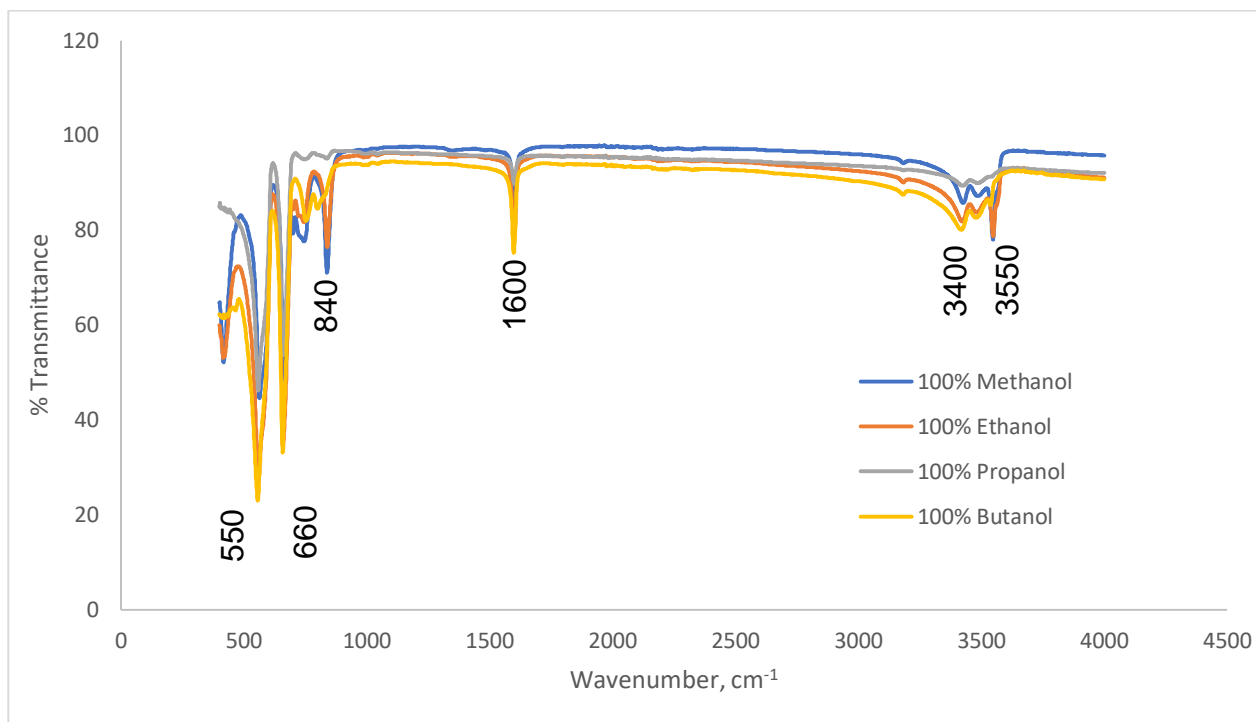


Figure 5-7: FT-IR spectra for the cobalt oxide particles synthesised from cobalt chloride hexahydrate precursor salt in 100% alcohol solvents, calcined at 300°C

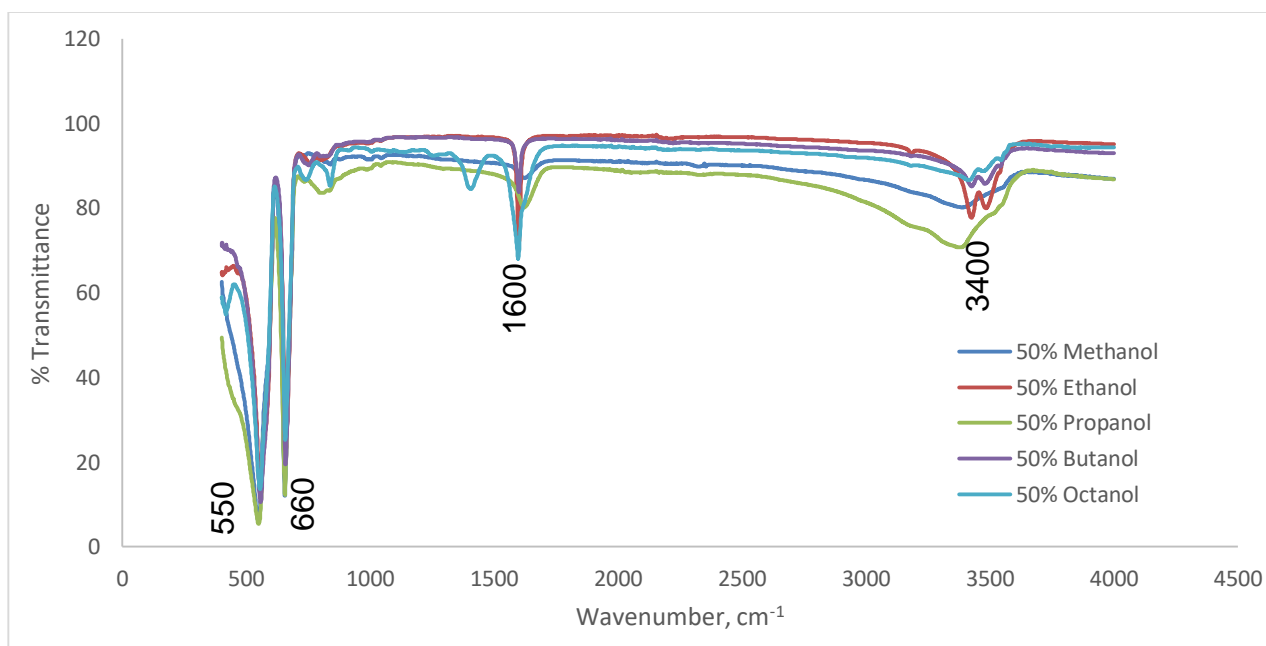


Figure 5-8: FT-IR spectra for the cobalt oxide particles synthesised from cobalt chloride hexahydrate precursor salt in 50% alcohol solvents, calcined at 300°C

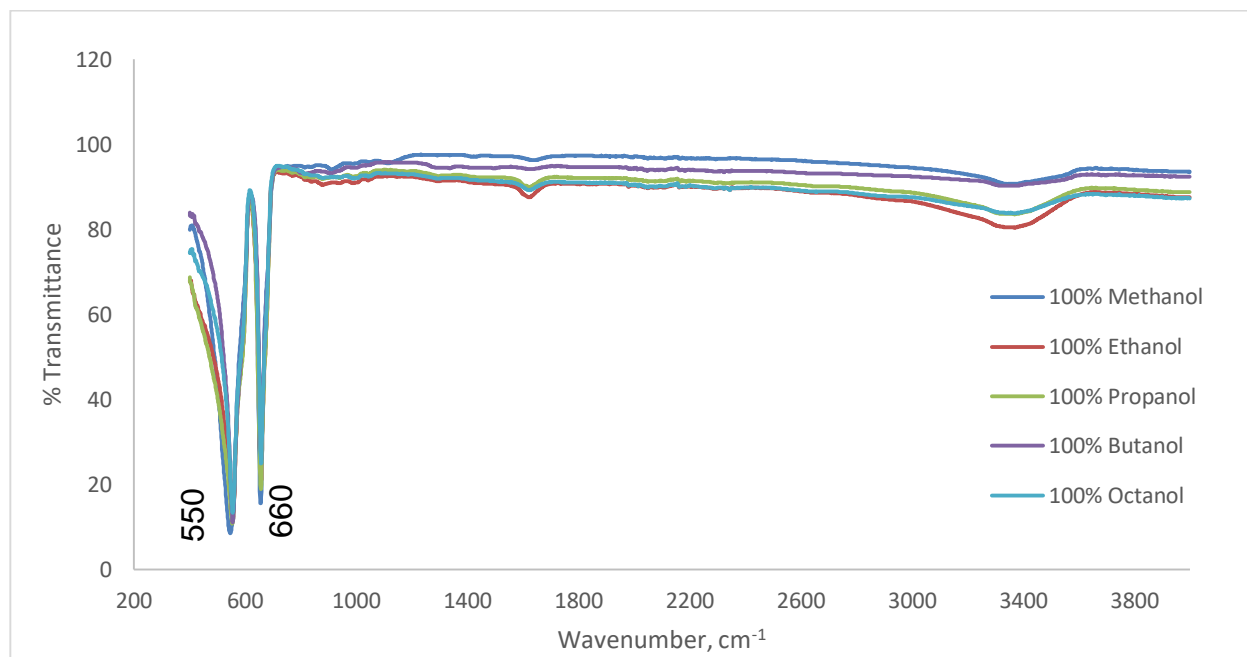


Figure 5-9: FT-IR spectra for the cobalt oxide particles synthesised from cobalt nitrate hexahydrate precursor salt in 100% alcohol solvents, calcined at 300°C

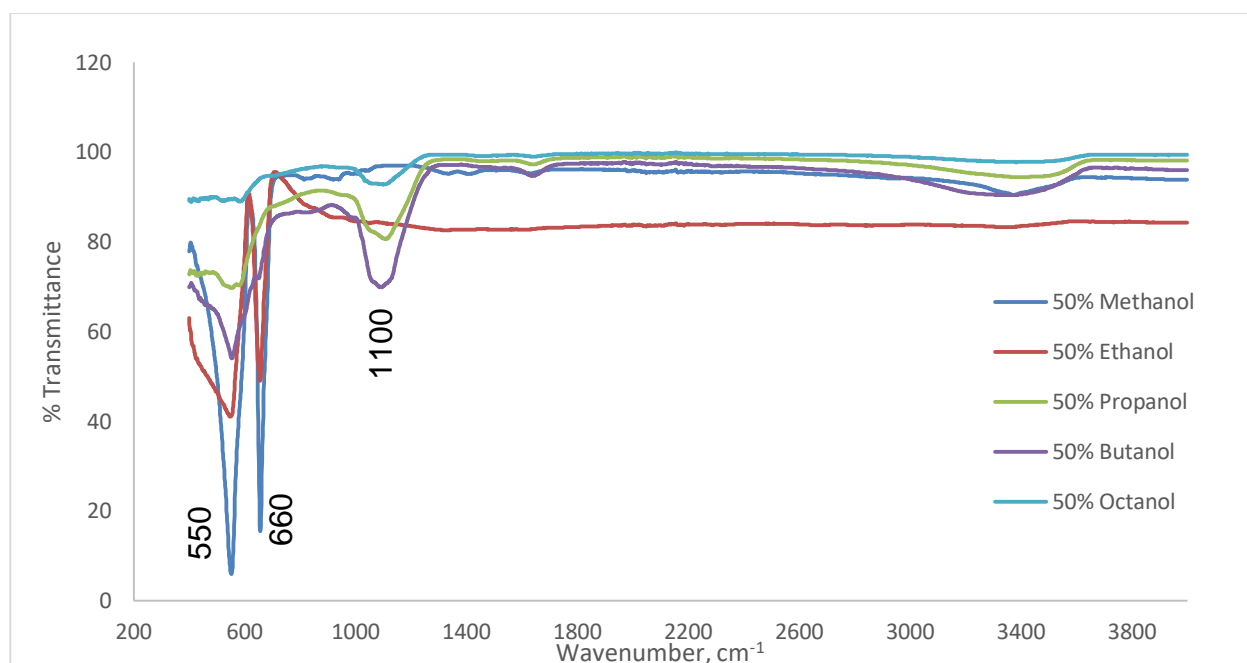


Figure 5-10: FT-IR spectra for the cobalt oxide particles synthesised from cobalt nitrate hexahydrate precursor salt in 50% alcohol solvents, calcined at 300°C

Final identification and purity analysis was achieved by XRD analysis, as shown in Figures 5-11 to 5-14. The XRD spectra shown in Figures 5-11 and 5-12 show the cobalt oxide particles synthesised from cobalt chloride hexahydrate in 100% and 50% alcohol solvents respectively. Figures 5-13 and 5-14 show the XRD spectra for the cobalt oxide particles synthesised from cobalt nitrate hexahydrate in 100% and 50%

alcohol solvents respectively. The chloride precursor samples in Figure 5-11, produced in 100% alcohol solvents, all provided pink β -Co(OH)₂ precursors. Although optically and structurally different precursors were produced, both cases provided similar cobalt oxide results in terms of diffraction and purity, when comparing Figures 5-11 and 5-12.

As with Figure 4-11, the same major peaks are exhibited, showing clear evidence of developed Co₃O₄. However, besides a peak at 16°, additional peaks exist in the 100% butanol and 100% octanol samples. These peaks exist at 17.8, 18.3, 19.3 and 20.7, showing traces of unreacted chlorides in CoCl₂•6H₂O (the precursor salt used), CoCl₂•2H₂O and Co₂(OH)₃Cl, as indicated from the JCPDS cards 29- 0466, 25- 0242, and 73- 2134.

The XRD spectra shown in Figures 5-13 and 5-14 represent the particles synthesised from cobalt nitrate hexahydrate in 100% and 50% alcohol solvents respectively. Most of the peaks represented are in accordance with the JCPDS card 42- 1467, with the addition of a peak at 59,5° for all the samples. From the graphs it is noted that with the increase in alkyl carbon chain length came a decrease in crystallinity of the particles synthesised. The 50% propanol to 50% octanol batches barely provided any peaks, showing the amorphous state of the samples.

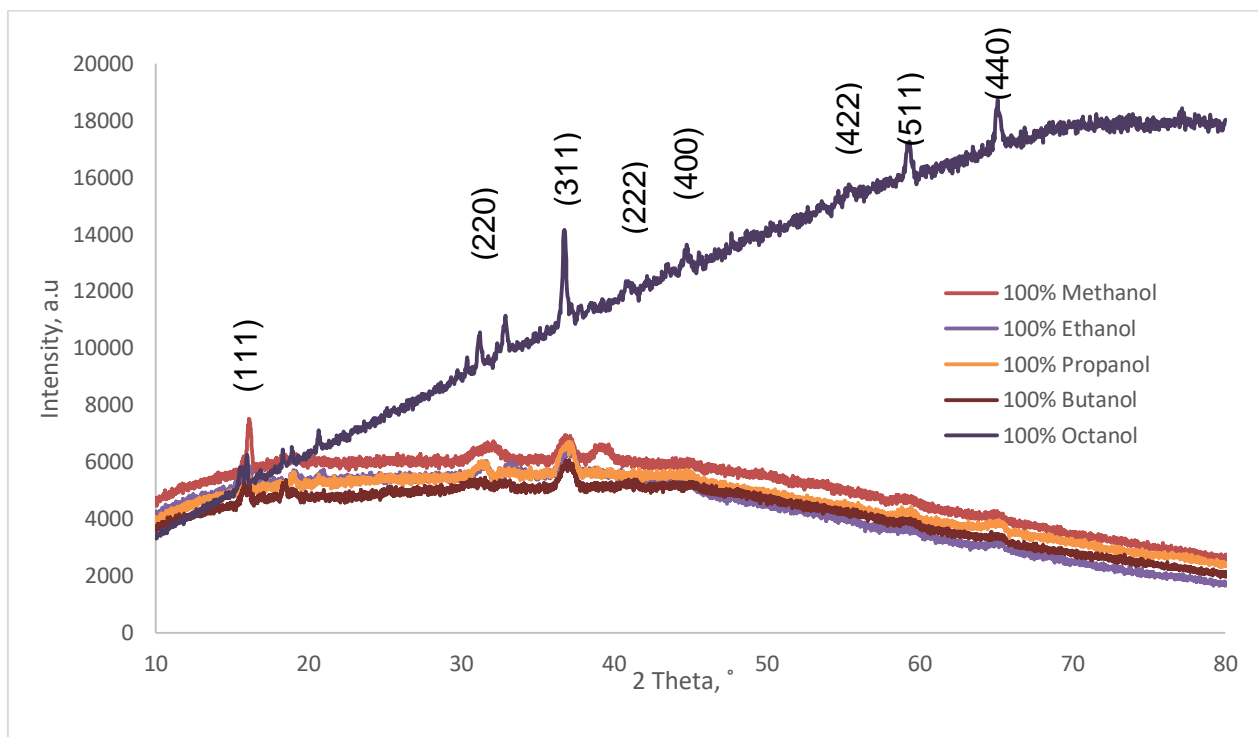


Figure 5-11: XRD spectra for the cobalt oxide particles synthesised from cobalt chloride hexahydrate precursor salt in 100% alcohol solvents, calcined at 300°C

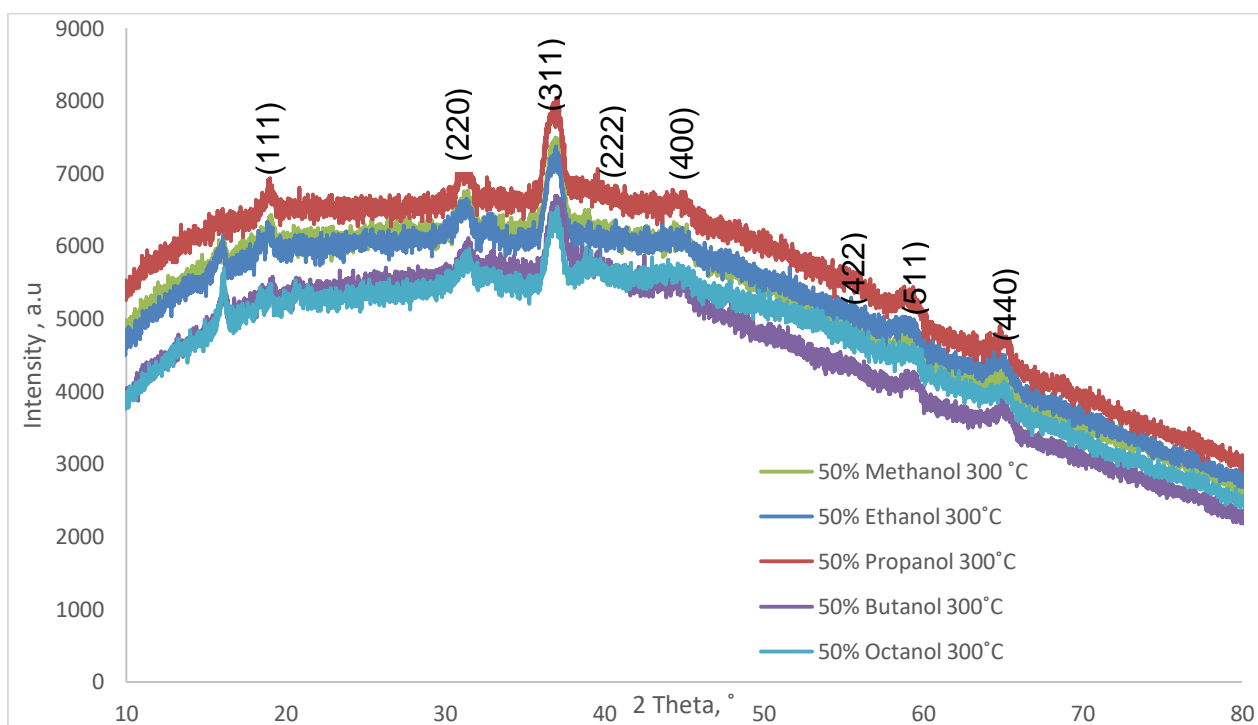


Figure 5-12: XRD spectra for the cobalt oxide particles synthesised from cobalt chloride hexahydrate precursor salt in 50% alcohol solvents, calcined at 300°C

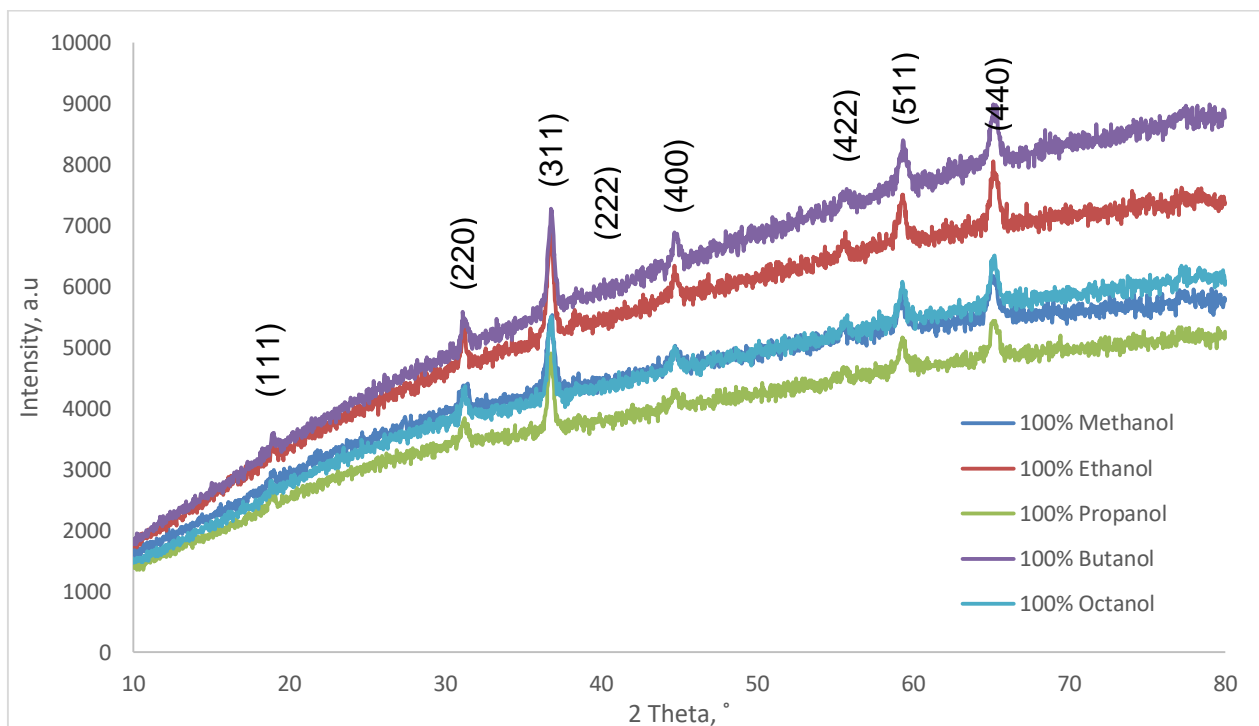


Figure 5-13: XRD spectra for the cobalt oxide particles synthesised from cobalt nitrate hexahydrate precursor salt in 100% alcohol solvents, calcined at 300°C

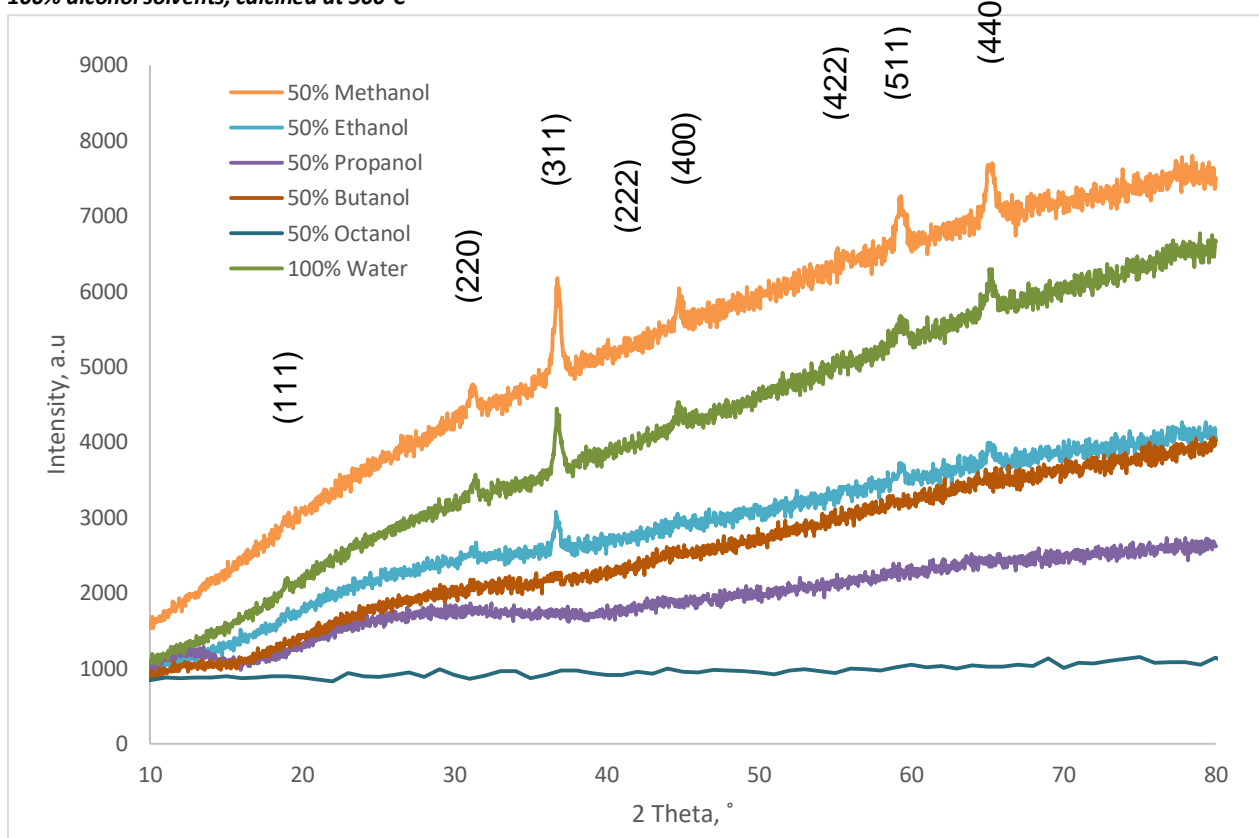


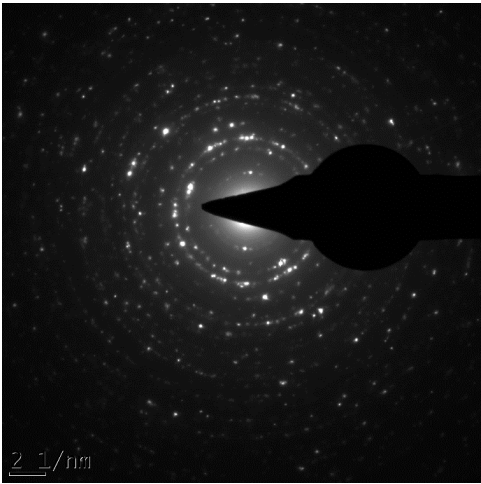
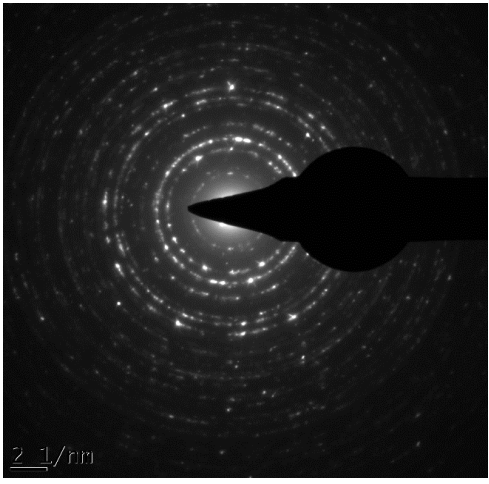
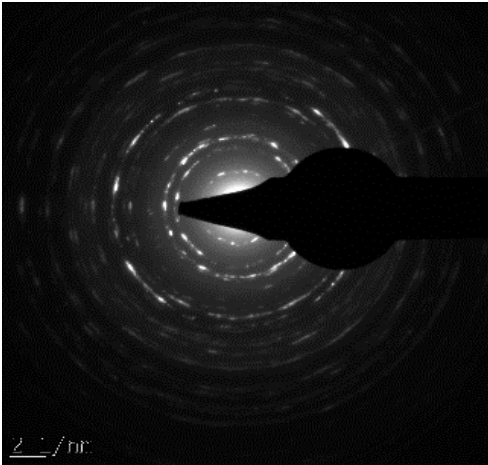
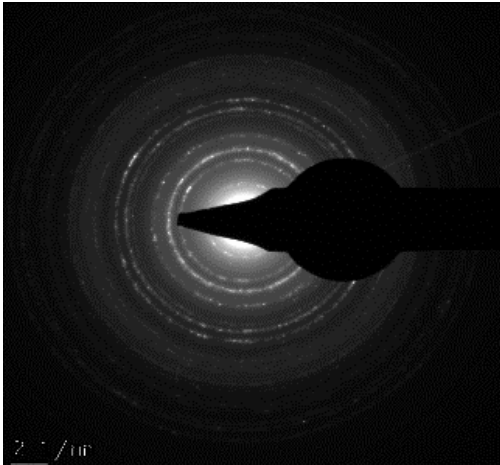
Figure 5-14: XRD spectra for the cobalt oxide particles synthesised from cobalt nitrate hexahydrate precursor salt in 50% alcohol/water solutions, calcined at 300°C

5.4 Particle morphology

The effect of varying alcohols in 100% and 50% concentrations on particle morphology was studied using transmission electron microscopy (TEM), scanning electron microscopy (SEM), selected area electron diffraction (SAED) and XRD (for crystallite sizes). According to He *et al.* (2004) the nucleation and growth of nanoparticles may be controlled using metal alkoxides in their synthesis by adjusting the reaction conditions, with the primary control occurring in the growth stage. This may occur by either aggregation, which leads to polycrystalline solids, or coarsening (He *et al.*, 2004). As previously noted, metal oxides are of polycrystalline nature, and may therefore be identified by concentric rings in SAED.

Polycrystalline particles were evident in all the cobalt oxide samples synthesised in alcohols at either 100% or 50% concentrations, as seen in the SAED images presented in Appendix E. The SAED patterns provided continuous/more frequent bright spots when finer grains were present within the sample. Vague and undefined areas presented amorphous material, while bright spots show larger grains. From the images, it may be noted that the bright spots within the concentric rings are more frequent for the samples containing water molecules when synthesised with a cobalt chloride precursor, creating nearly complete circles, whereas the samples synthesised using 100% alcohol solvents show less frequent bright spots. This gives reference to the grain sizes within the sample studied, showing that finer particles were synthesised for the samples containing water. The SAED images showing cobalt oxide particles produced in methanol at 100% and 50% are presented in Table 5-2. Although this was evident in all the cobalt chloride samples, the trend was only shown for the cobalt nitrate precursor in methanol, while the rest of the alcohols revealed the opposite, as seen in Appendix E. Appendix E also further emphasised the amorphous state of the cobalt oxide particles synthesised from cobalt nitrate precursor in 50% propanol; 50% butanol and 50% octanol batches, as hazy areas were noted in their SAED images, with few bright spots showing larger developed crystals. The TEM image provided in Table 5-3 further supports this, as unclear particles were formed.

Table 5-2: SAED images for the cobalt oxide particles synthesised in methanol and ethanol at 50% and 100% alcohol/water ratios respectively, calcined at 300°C

	100% alcohol	50% alcohol
Cobalt chloride precursor		
Cobalt nitrate precursor		

Distinct morphology changes occurred for the change in cobalt precursor salt in alcohols. Using a cobalt chloride hexahydrate precursor salt in alcohols at 100% and 50% provided a very distinct rhombic shape for most of the particles, apart from the hexagonal skeleton shapes, which were noted in the 50% methanol batch, which mainly contained rhombic-shaped particles orientated in hexagonal skeletons. These hexagonal skeletons were attached at the ends of longitudinal rhombic particles, as shown in Figure 5-15. Particles similar in shape were also reported Kim and Huh (2011). Cobalt nitrate hexahydrate precursor salt in the cobalt oxide synthesis

produced mostly nanorods shapes, except for the instances in which an amorphous state was observed. The particles synthesized by changing the anion to cobalt nitrate hexahydrate also showed a tendency to agglomerate forming larger particles approximately 40 μm in size with interesting shapes most obviously noticed at higher magnification of the TEM images as well as the SEM images provided in Table 5-3.

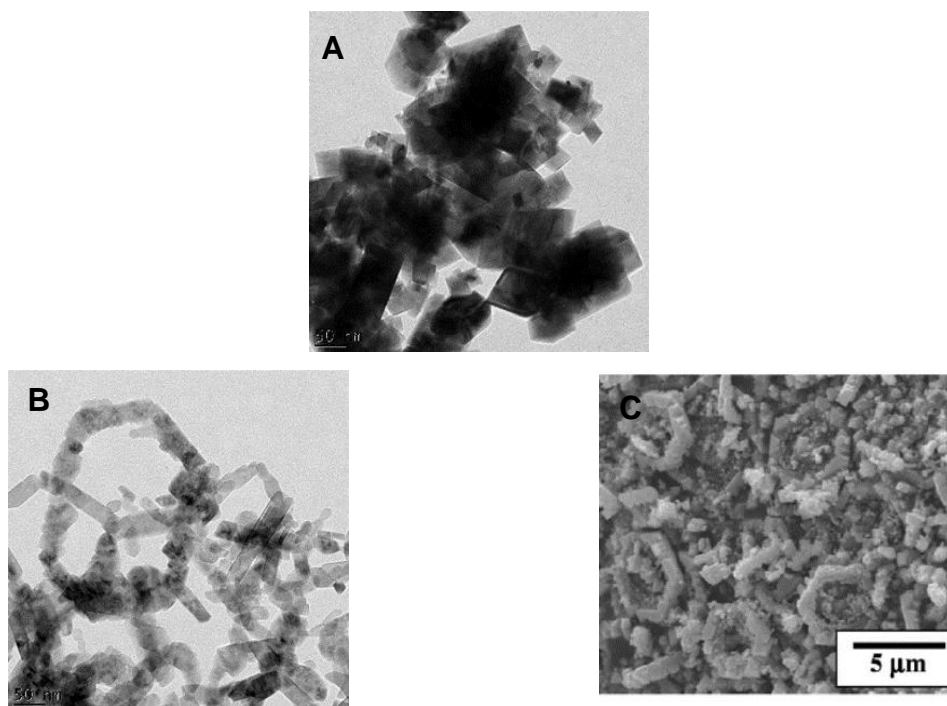
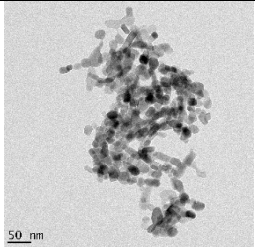
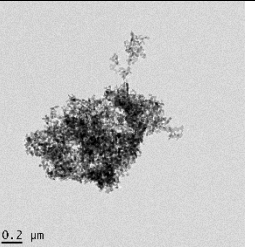
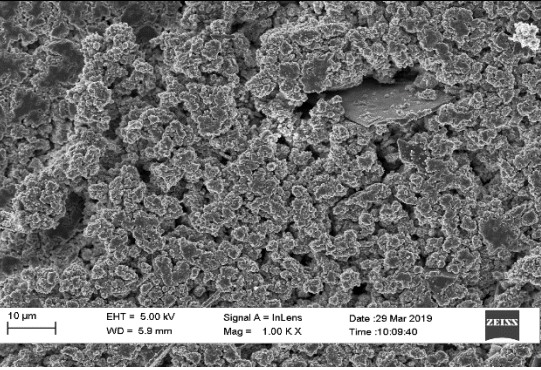
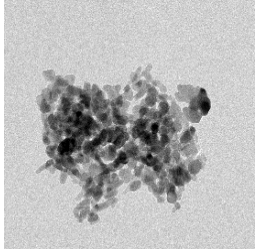
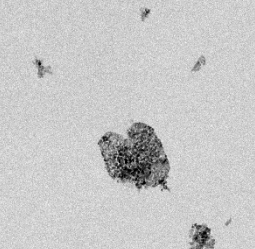
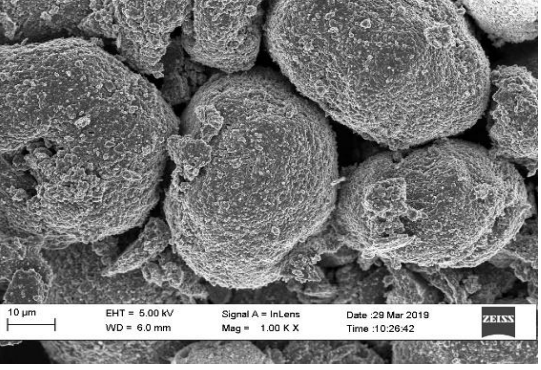
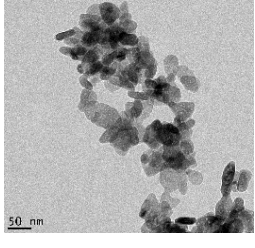
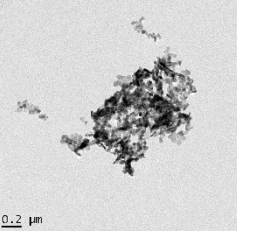
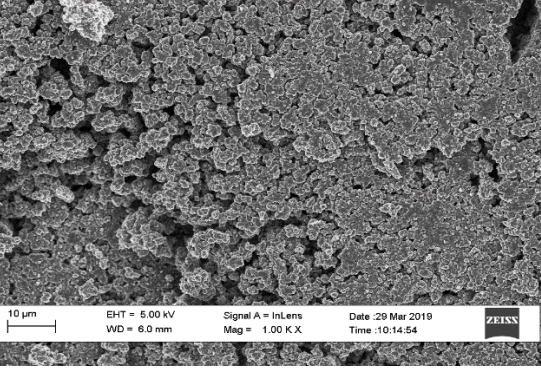
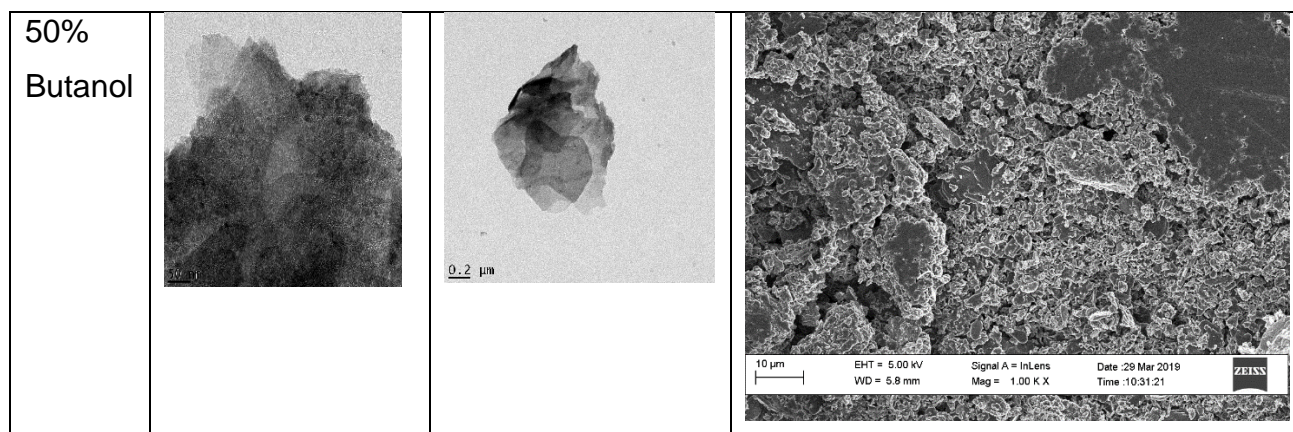


Figure 5-15: Transmission electron microscopy images for the cobalt oxide particles produced from cobalt chloride hexahydrate precursor salt in a) 100% methanol, b) 50% methanol as well as the c) scanning electron microscopy image of hierarchical hexagonal skeleton of Co_3O_4 produced by Kim and Huh (2011)

THE EFFECT OF Cl- AND NO3- ANIONS IN WATER ON Co3O4 PARTICLES

Table 5-3: Transmission Electron Microscopy images at 50 nm and 0.2 m, and Scanning Electron Microscopy images for the selected cobalt oxide particles synthesised from cobalt nitrate hexahydrate, showing various particle morphologies

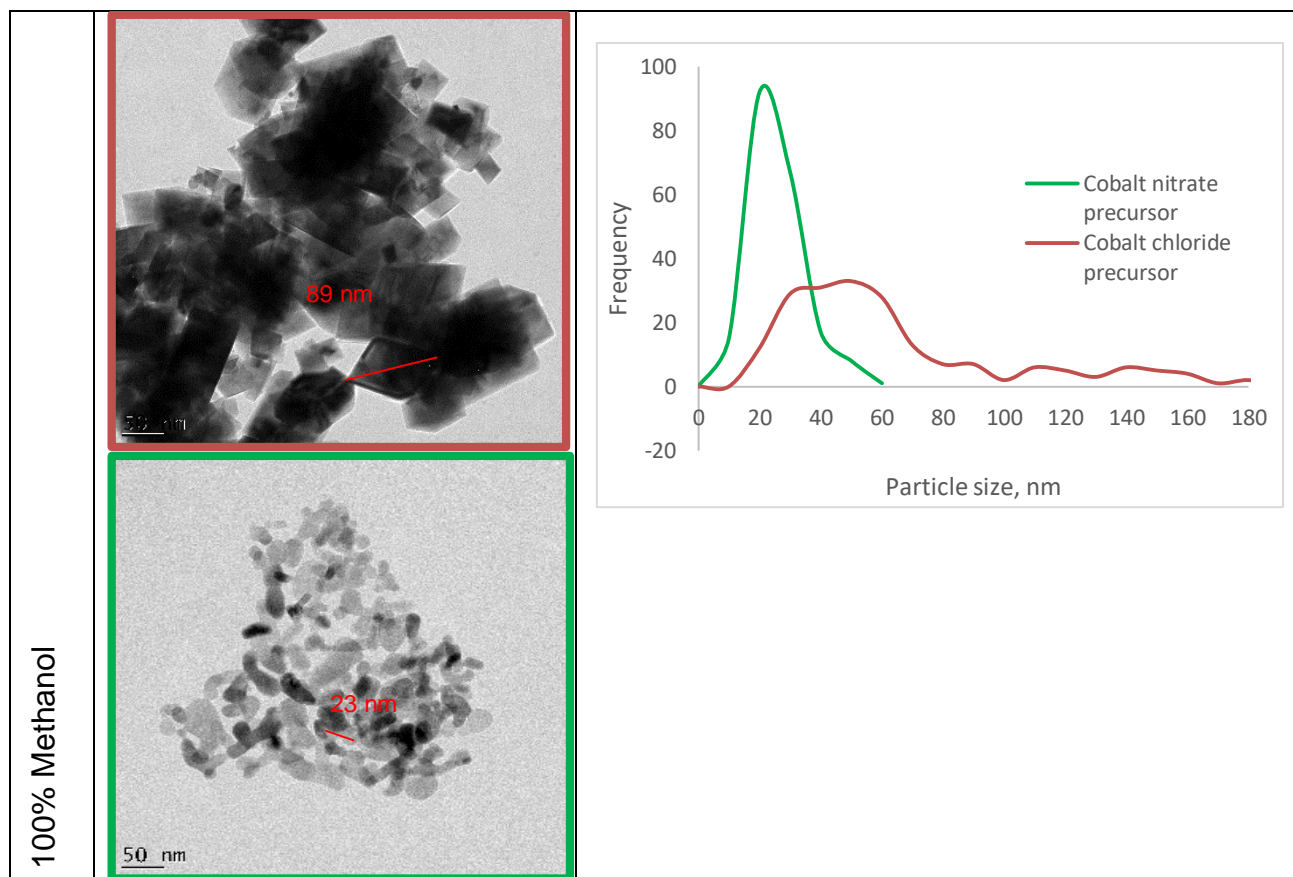
Sample	TEM magnification		SEM
	50 nm	0.2 μm	
100% Ethanol			 10 μm EHT = 5.00 kV Signal A = InLens Date :29 Mar 2019 WD = 5.9 mm Mag = 1.00 K X Time :10:08:40 ZEISS
50% Ethanol			 10 μm EHT = 5.00 kV Signal A = InLens Date :29 Mar 2019 WD = 6.0 mm Mag = 1.00 K X Time :10:26:42 ZEISS
100% Butanol			 10 μm EHT = 5.00 kV Signal A = InLens Date :29 Mar 2019 WD = 6.0 mm Mag = 1.00 K X Time :10:14:54 ZEISS



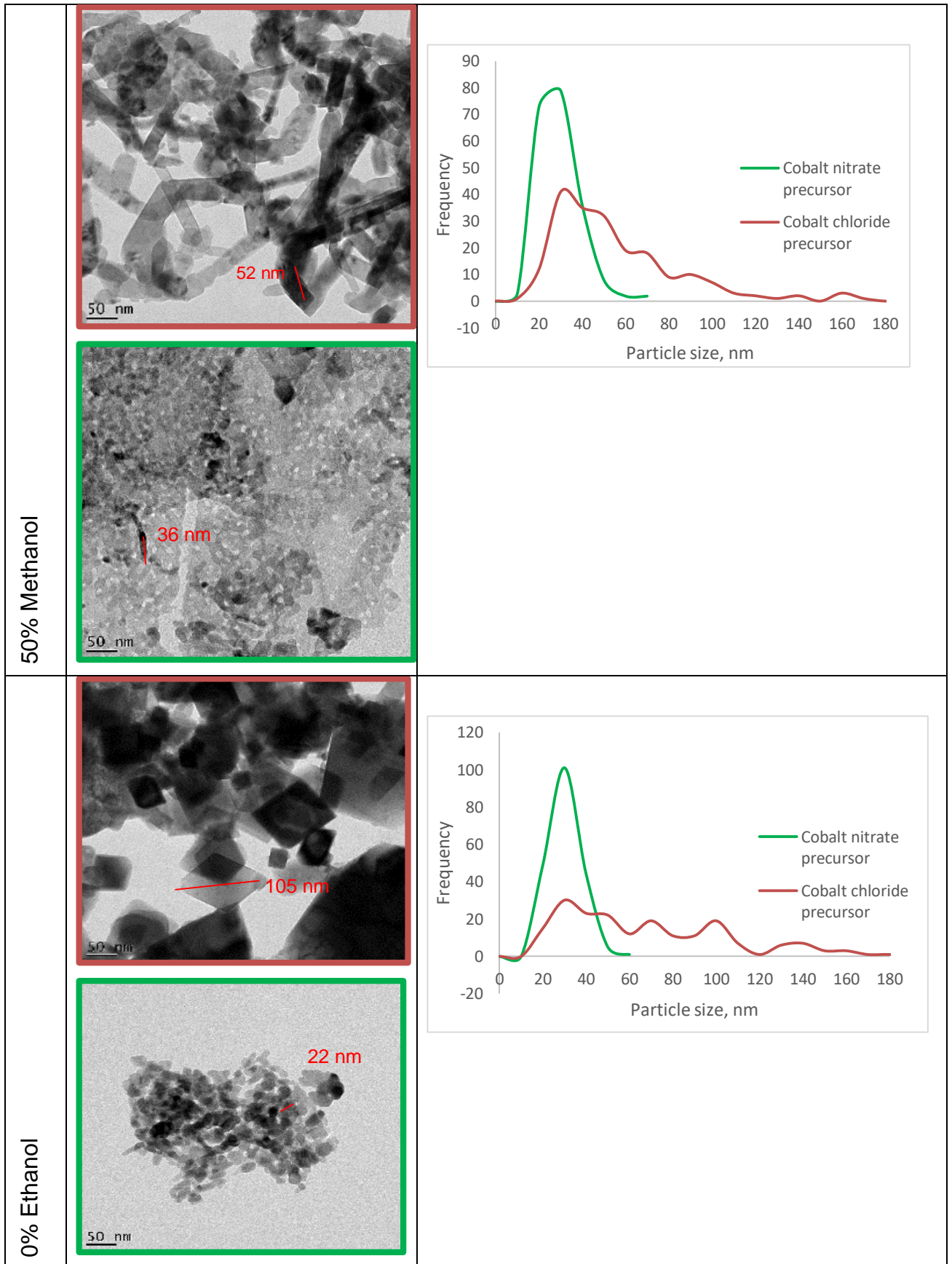
The rhombic-shaped particles, as shown by the TEM images in Table 5-4, were all synthesised from cobalt chloride hexahydrate in an alcohol medium, at either 100% concentration or 50% concentration, while the cobalt nitrate particles were made up of nanorods, agglomerated into larger particles. The particle size distribution curves presented in Appendix D were developed from the data collected in the TEM images, at various magnifications, as 200 particles were individually measured using Image J software. These curves were based on the diagonal length of rhombic shapes and length of the rod shapes, as demonstrated in Table 5-4, before taking agglomeration into consideration. Originally, bin limits of 25 nm were used, which allowed for an average and smooth representation of the particle sizes presented in each sample. However, because most variances occurred in the range 25 to 60 nm, the graphs presented all assumed a peak at ± 50 nm and therefore an inaccurate representation of the particles was presented. By reducing the bin limits to 10 nm a more accurate size distribution was obtained, but the smooth curve was lost in the process. From the general appearance of the size distribution curves, it is noticed that with increasing carbon chain on the alcohol chain, the wider the size distribution. The widest size distribution was for the particles synthesised from cobalt chloride hexahydrate in 50% octanol, with the narrowest size distribution occurring in the particles synthesised in propanol. These curves were not available for the cobalt nitrate precursor, due to their semi-amorphous nature. The PSD taken from the cobalt nitrate precursor salt shows that with increased water content, wider size distributions occur. However, no trend was noted for the increase in alkyl chain length. Generally, these particles were smaller than the average particles synthesised using

the chloride base salt, but not taking agglomerates into consideration.

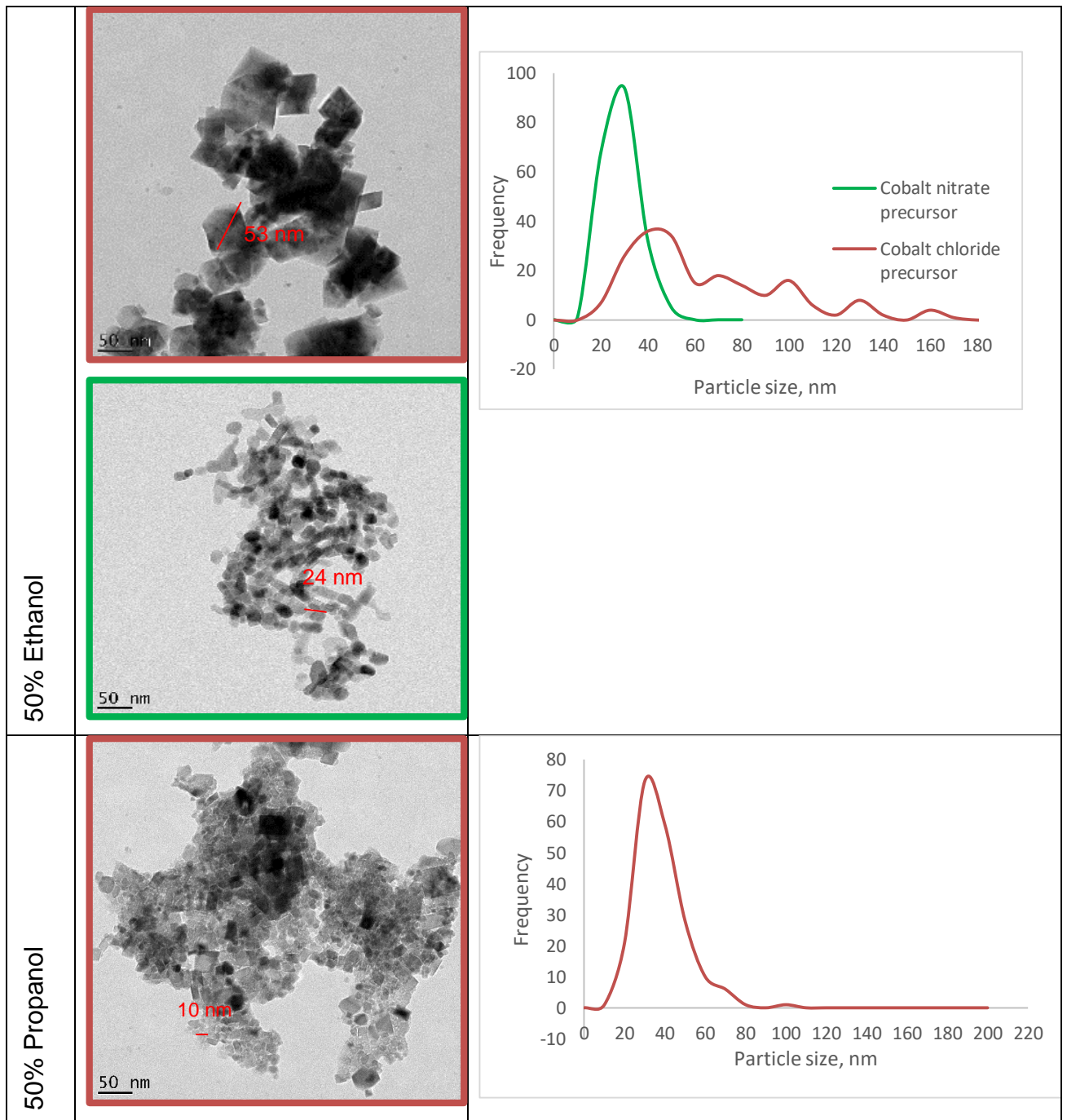
Table 5-4: Particle size distribution curves as deduced from transmission electron microscopy images for the cobalt oxide particles synthesised from cobalt chloride hexahydrate and cobalt nitrate hexahydrate in various alcohols at 100% or 50% concentrations

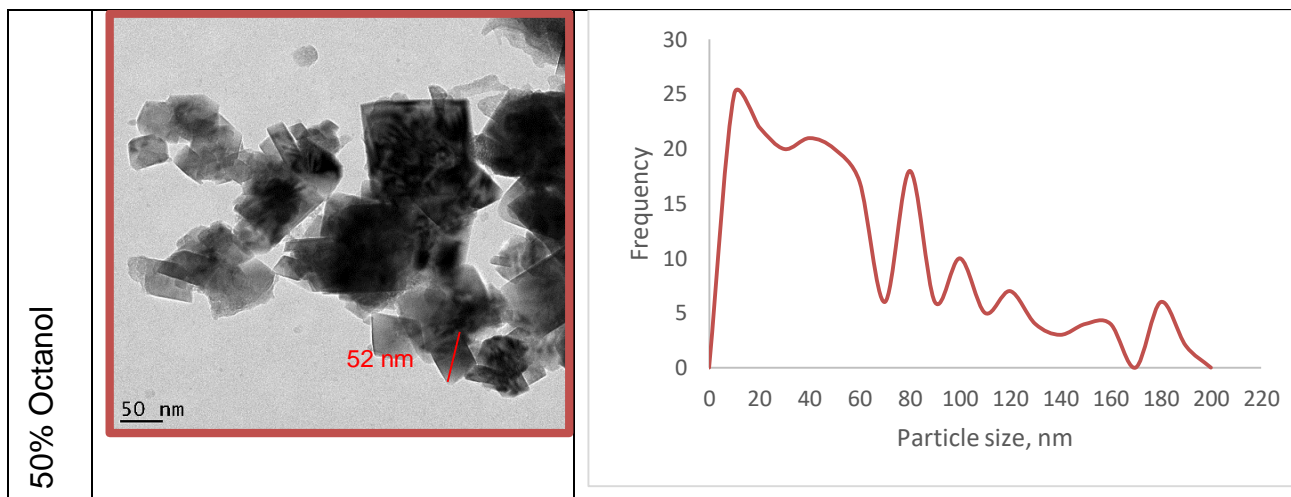


THE EFFECT OF Cl- AND NO3- ANIONS IN WATER ON Co3O4 PARTICLES



THE EFFECT OF Cl- AND NO3- ANIONS IN WATER ON Co3O4 PARTICLES





The cumulative frequency of the measured particles provided the d_{50} particle size within each batch. Since the d_{50} particle size provides that point at which half the particles are accounted for, it provides an overview of the majority of the particles represented in a batch. The d_{50} particle sizes are dependent on the particle size distribution curves, and therefore are not shown for particles of a semi-amorphous particle composition. The d_{50} particle sizes of the polycrystalline particles are presented in Table 5-5.

Table 5-5: d_{50} particle sizes for the cobalt oxide particles, adapted from the particle size distribution curves

	Solvent	100% alcohol	50% alcohol
Cobalt chloride precursor	Methanol	46.79 nm	41.76 nm
	Ethanol	56 nm	46.07 nm
	Propanol	66.5 nm	33.96 nm
	Butanol	67.14 nm	54.67 nm
	Octanol	62.27 nm	22 nm
Cobalt nitrate precursor	Methanol	19.19 nm	22.67 nm
	Ethanol	24.18 nm	23.23 nm
	Propanol	34.61 nm	Semi-amorphous
	Butanol	37.03 nm	
	Octanol	28.65 nm	

In comparing the crystallite sizes as well as the d_{50} particle sizes of the resulting particles, it may be noted that there is a decrease in both the crystallite size and d_{50} particle size for each of the alcohols used, when decreasing the alcohol concentration. This is the general trend, with the exception of the particles synthesised with cobalt nitrate hexahydrate in methanol. This is a very interesting finding, as the surface tension increases with increasing water content, i.e. decreasing alcohol concentration. This is visually expressed in Figure 5-16 below.

The effect of temperature on the crystallite sizes of the various particles were calculated using the Scherrer equation, which relates the crystallite size to the full width at half maximum (FWHM) within the diffraction pattern, and the results are displayed in Table 5-6. The results obtained mirror those of the pure water batches, as the crystallite size generally increased with increasing calcination temperature, with the exception of the cobalt oxide particles synthesised from cobalt nitrate hexahydrate* in 50% ethanol and 50% octanol, which revealed a decrease from 400 to 500°C. It may therefore be noted that small changes do affect the outcome in nanocrystal synthesis, and although variances existed in literature on the effect of calcination temperature on the size of nanoparticles, it may vary with regard to type as well as process. Using the synthesis method described within this study, however, provides an increase in crystallite size with the increase in calcination temperature.

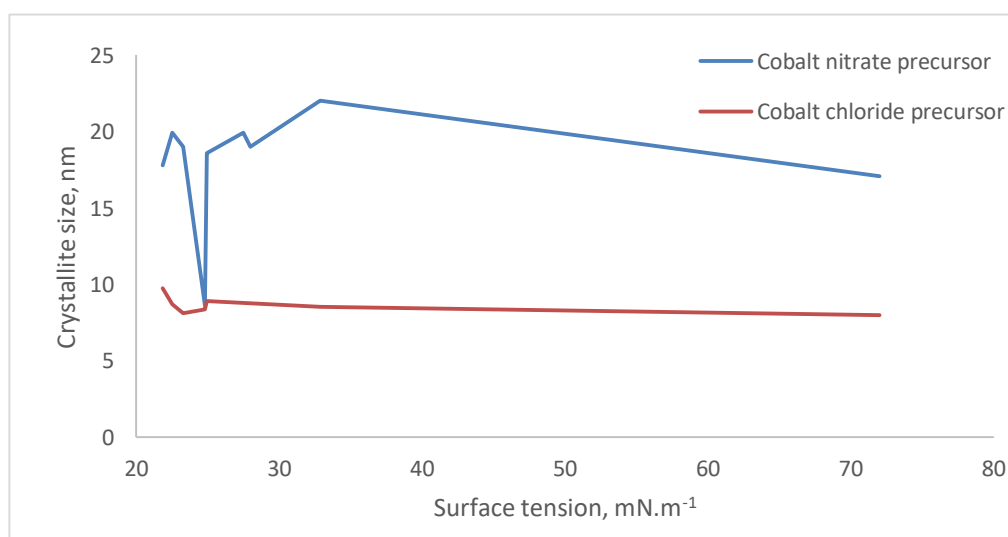


Figure 5-16: Crystallite size for the synthesised cobalt oxide particles calcined at 300°C versus alcohol/water solvent surface tension at 25°C

Table 5-6: Crystallite sizes for the synthesised cobalt oxide particles calcined at 300, 400 and 500°C

Cobalt oxide sample		Crystallite sizes from FWHM, nm		
		300°C	400°C	500°C
Cobalt chloride hexahydrate precursor	50% Methanol	7.98	31.00	34.88
	50% Ethanol	8.55	27.91	32.2
	50% Propanol	8.38	22.03	31.01
	50% Butanol	8.05	27.01	32.20
	50% Octanol	10.74	27.01	33.49
	100% Methanol	8.72	31.01	36.40
	100% Ethanol	9.74	29.90	32.20
	100% Propanol	8.14	29.90	32.20
	100% Butanol	8.91	31.01	32.21
	100% Octanol	29.90	28.87	34.88
Cobalt nitrate hexahydrate precursor	50% Methanol	22.03	31.01	34.88
	50% Ethanol	19.02	26.16	19.93
	50% Propanol	8.64	20.93	26.17
	50% Butanol	11.01	11.63	18.21
	50% Octanol	11.31	13.08	9.73
	100% Methanol	19.94	22.03	24.62
	100% Ethanol	17.81	18.20	27.00
	100% Propanol	19.03	23.26	27.00
	100% Butanol	18.60	20.42	26.16
	100% Octanol	19.94	25.37	32.20

5.5 Conclusion

This chapter focused on the effect of alcohols in 100% and 50% concentrations during hydro/solvothermal synthesis on cobalt oxide. The precursor solutions revealed that the choice of anion has an effect on the precursor complex solution. When using cobalt chloride hexahydrate in 100% alcohols, blue precursor solutions occurred.

The remainder of the precursor solutions, i.e. cobalt chloride hexahydrate in 50% alcohol as well as cobalt nitrate hexahydrate in 100% and 50% alcohol, provided precursor solutions which were red in colour. The hydro/solvothermal treatment of these precursor solutions resulted in both α - and β - cobalt hydroxide powders which were recognised by their colours green/blue and pink respectively. A direct relationship between the precursor solution colour and cobalt hydroxide polymorph was therefore determined. The blue precursor solutions resulted in pink β -cobalt hydroxide, while the red precursor solutions provided green α - cobalt hydroxide. It was noted that the

α -phase is thermodynamically metastable, allowing it to rapidly transform to the β -phase depending on its environment. This was found for the cobalt hydroxide formed from cobalt chloride hexahydrate in 50% ethanol and 50% butanol, which was initially the α -phase.

Upon calcination, the cobalt oxide particles obtained were characterised using EDS, FT-IR and XRD for identification and purity. The results revealed that cobalt oxide was successfully synthesized with a common impurity for the cobalt chloride hexahydrate precursor samples. These included samples containing chloride ions for the partial conversion of the cobalt chloride salt. The cobalt nitrate hexahydrate revealed cobalt oxide was formed with an impurity of sulphur in the 50% propanol, butanol and octanol batches. Furthermore, the XRD spectra of these samples revealed no specific peaks, showing its lack of crystallinity and amorphous nature. This was further noted in the TEM and SAED images discussed.

The morphology of the particles was generally affected by the change in anion rather than that of the change in alcohol. However, the change in alcohol concentration, i.e. the presence of water, played a role in the polymorph formation, and consequently the cobalt oxide particles formed. This, however, did not change the shape of the particles encountered, as rhombic shaped particles were produced from the cobalt chloride hexahydrate precursor in 100% as well as in 50% alcohols. Similarly, rod like particles were synthesized from cobalt nitrate hexahydrate in 100% and 50% alcohols. Three of the samples were semi-amorphous while the SEM images provided insight into the formation of larger agglomerates. Generally, it was found that the d_{50} particle size increases with carbon on the alkyl chain for the particles calcined at 300°C, and decreases with a decrease in alcohol concentration. The particle size distribution curves revealed that the cobalt nitrate hexahydrate precursor salt resulted in monodispersed particles, while the cobalt chloride precursor had wider size distributions.

CHAPTER 6 EVALUATION OF THE Co_3O_4 PARTICLES SYNTHESISED DURING COLOUR DEGRADATION

The objective of this chapter was to evaluate the cobalt oxide particles synthesised in Chapters 4 and 5, specifically as catalysts in colour degradation. It entails the catalytic degradation of methylene blue, using the as-prepared cobalt oxide particles in combination with peroxymonosulphate. The catalytic efficiency of the cobalt oxide synthesised from cobalt chloride hexahydrate and cobalt nitrate hexahydrate precursors in pure water, as well as 100% and 50% alcohols, were shown, and the most active catalyst determined. The advanced oxidation process in place was then optimised for the most active catalyst. This included Co^{3+} to Co^{2+} ratio of the best performing catalyst. The optimisation studies revealed an aptitude for further enhancement, specifically for the application in actual textile wastewater treatment, as well as scrutiny of the current methods used.

6.1 Colour degradation studies

An inhouse developed reactor, was used to treat a 10 mg/L methylene blue dye in water for this study. The reactor makes use of an AOP, using cobalt oxide as its catalyst, and Oxone[®] (peroxymonosulphate) as its active ingredient. As the cobalt oxide nanoparticles are immobilised in its system, it provides a product with practically no cobalt, besides instances where leaching occurs. This approach is beneficial to the reuse of the treated water, as it eliminates difficulties associated with the removal of the catalyst from the treated effluent.

The produced particles were inserted into the reactor for the purpose of testing their catalytic ability. They were used in conjunction with Oxone in order to generate sulphate radicals. The sulphate radicals were responsible for the mineralisation of the dye particles, resulting in colour removal of the wastewater.

The particles synthesised and calcined at the various temperatures were tested in order to study the effect of calcination temperature on the particle's catalytic ability. A blank test was also performed, without catalyst and Oxone, in order to accurately

study the effects the components had.

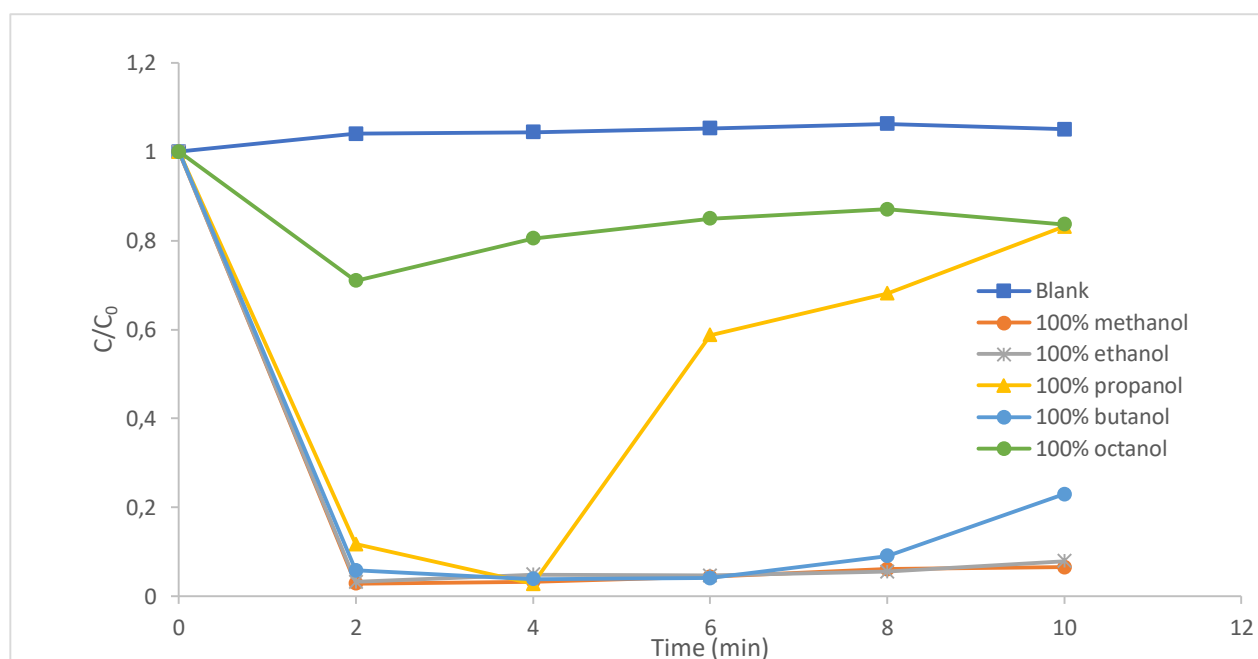


Figure 6-1: Degradation curves for the methylene blue solutions degraded using the cobalt oxide catalysts synthesised from cobalt chloride hexahydrate in 100% alcohol solutions, calcined at 300°C

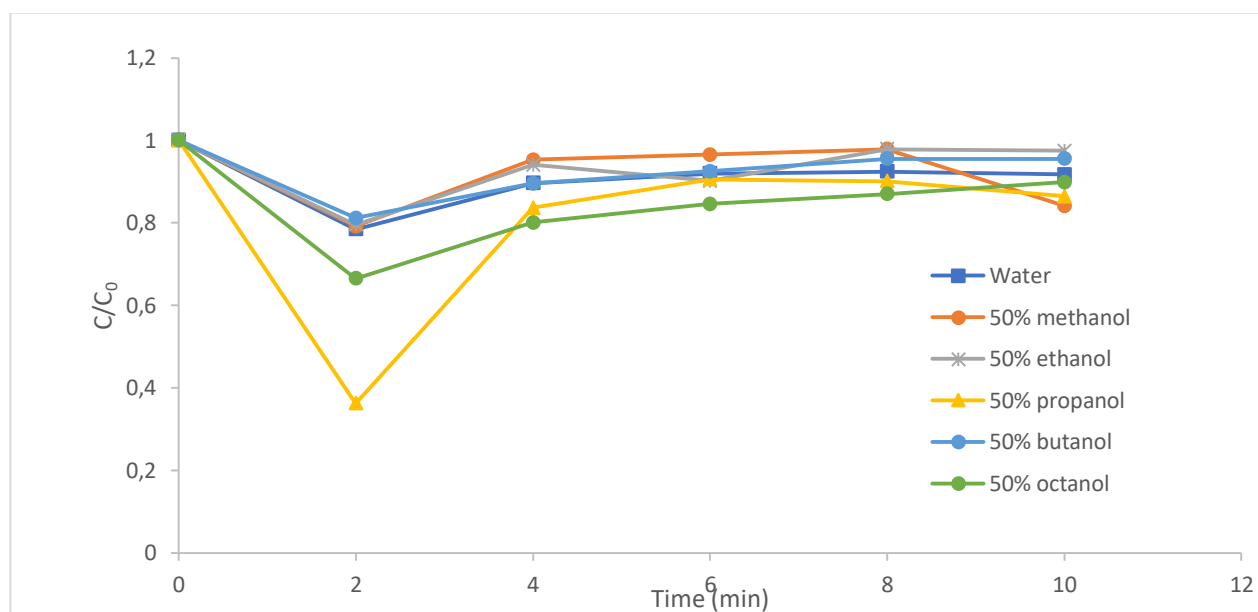


Figure 6-2: Degradation curves for the methylene blue solutions degraded using the cobalt oxide catalysts synthesised from cobalt chloride hexahydrate in 50% alcohol/water solutions as well as 100% water, calcined at 300°C

The degradation curves presented in Figures 6-1 and 6-2 show the treatment of a 500 mL sample of methylene blue over a period of 10 minutes, using the cobalt oxide particles synthesised from cobalt chloride hexahydrate in 100% and 50% alcohols respectively, as well as pure water. An initial sample was taken, along with 4 mL aliquots every 2 minutes at the exit of the reactor for analysis. From the results, it may

be seen that the particles produced from 100% alcohols have a higher degradation rate than that of the particles synthesised in the 50% alcohol solutions. This was evident in all cases, as displayed in Appendix F, as the 100% batches provided instant degradation, with the exception of 100% propanol which became increasingly inactive after 4 minutes, while the 50% batches, along with the water batch, provided degradation initially, but rapidly became less active with time. This is evidently seen in the products they produce; i.e. while the 100% batches produced treated methylene blue solution with no visible colour, the 50% batches provided a product which remained blue at the 10-minute mark, as displayed in Figure 6-3. It should be noted that all the treated methylene samples became visibly clear within a standing time of 30 minutes, as shown in Figure 6-4. From the degradation curves, it is deduced that the most rapid degradation rate was found when using the cobalt oxide particles synthesised in 100% methanol, while the slowest degradation rate was found for the cobalt oxide particles synthesised in 50% ethanol. Interestingly, the water and 50% alcohol cobalt oxide particles resulted from $\alpha\text{-Co}(\text{OH})_2$, while the 100% alcohol particles from $\beta\text{-Co}(\text{OH})_2$. From Figure 6-4, it is evident that all the particles produced from cobalt chloride hexahydrate are indeed active, though some of the catalysts require a residence time within a holding vessel to become fully transparent.

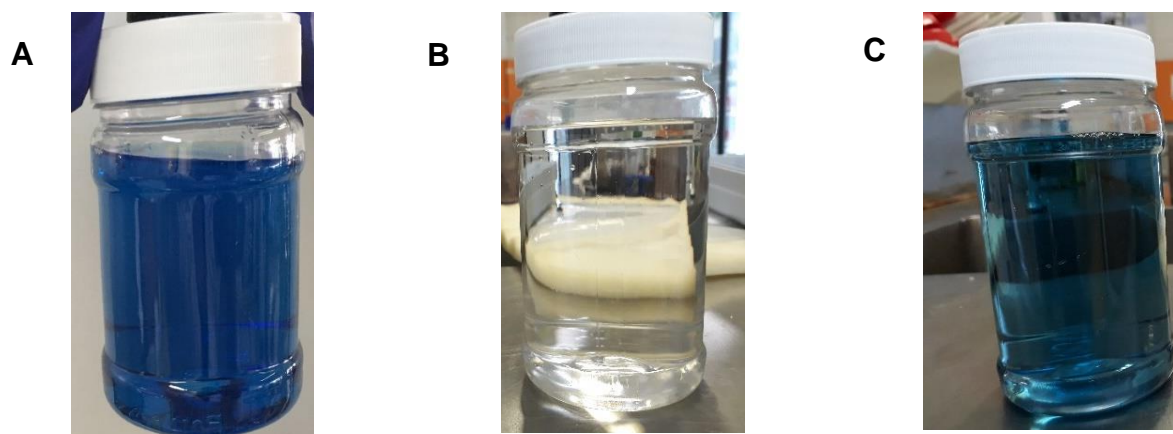


Figure 6-3: Methylene blue samples a) before treatment, b) after treatment using the cobalt oxide catalysts synthesised in 100% alcohol solvents and c) after treatment using the cobalt oxide catalysts synthesised in 50% alcohol/water solutions, calcined at 300°C

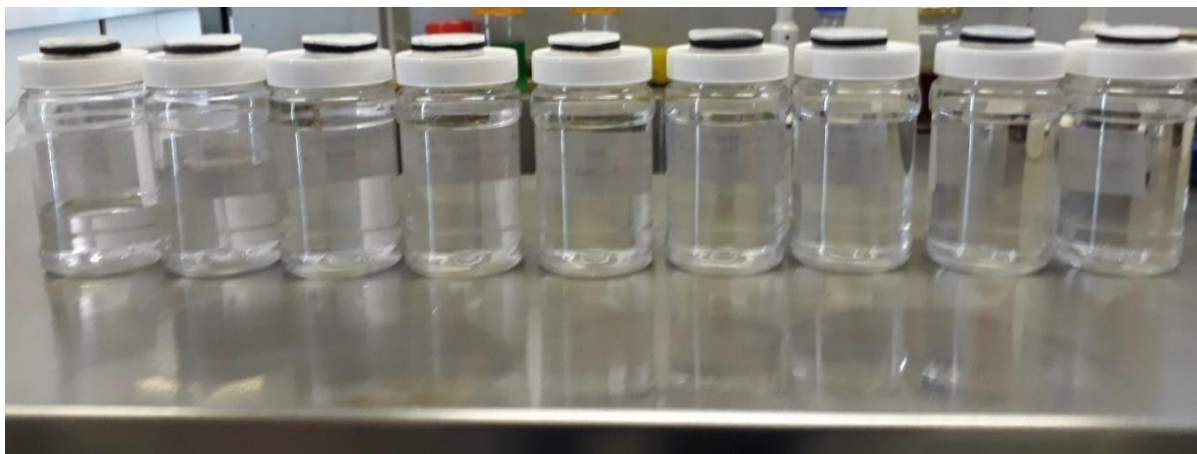


Figure 6-4: Treated methylene blue samples after a 30-minute standing time

As with the chloride precursor samples, the particles synthesised from cobalt nitrate hexahydrate in 100% and 50% alcohols, as well as pure water, were inserted into the in-house developed reactor for the purpose of testing their catalytic ability. They too were used in conjunction with Oxone[®] (peroxymonosulphate) to treat a methylene blue solution of the same concentration. Figures 6-5 and 6-6 present the degradation data received when testing the cobalt oxide synthesised in 100% and 50% alcohol respectively. It is noted that within 10 minutes of treating the methylene blue solutions, less than 10% degradation occurred for all the samples. The cobalt oxide particles that were synthesised in 50% alcohol performed at better degradation rates, with the lowest degradation being 4.2% for the pure water sample. The highest degradation was found to be 91.3% for the cobalt oxide particles synthesised in a 50% propanol sample. This was highly unexpected, taking the results obtained from the cobalt oxide particles synthesised from the cobalt chloride precursor into consideration, as the degradation results had been inverted. The cobalt chloride precursor provided particles which performed better when synthesised in 100% alcohol, while the cobalt nitrate precursor provided particles which performed better when synthesised in 50% alcohol. However, taking all factors into account, it is noted that the three catalysts formed from cobalt nitrate hexahydrate producing the highest degradation rates, namely 50% propanol, 50% butanol and 50% octanol batches, all had an impurity of sulphur, as noted in their EDS results. These were the only samples with this specific impurity, and this may therefore have altered the results in the formation of additional sulphate radicals, thus aiding the degradation process.

EVALUATION OF THE Co_3O_4 PARTICLES SYNTHESISED during COLOUR DEGRADATION

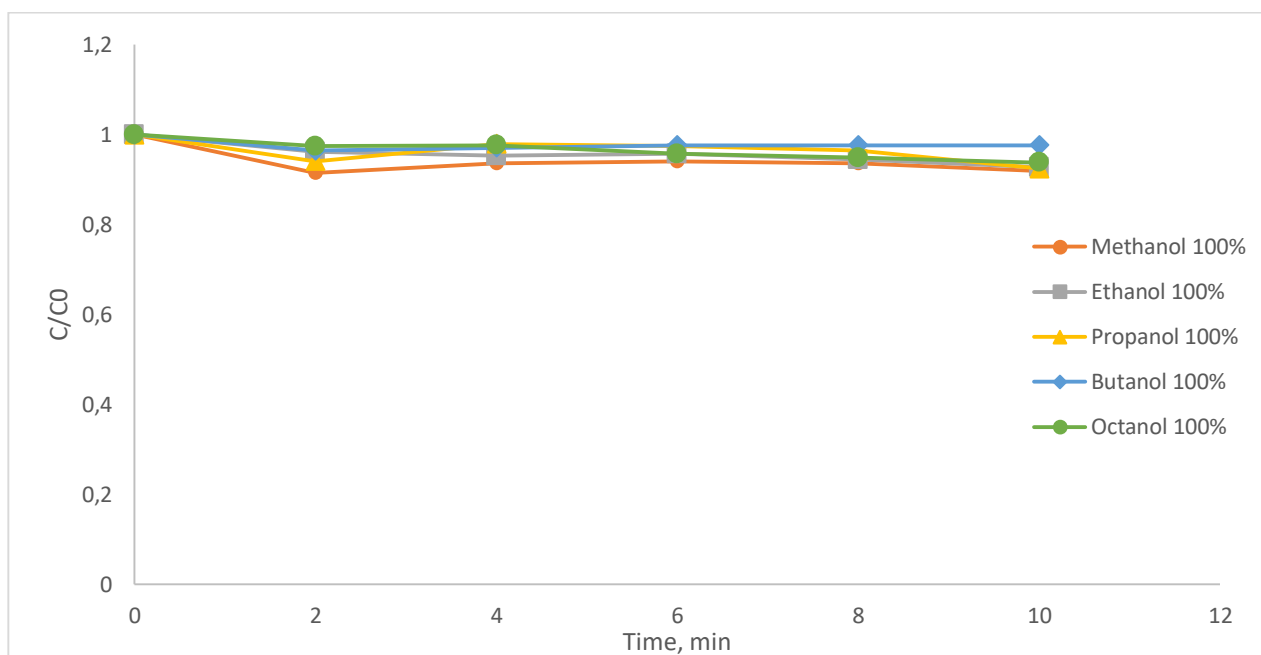


Figure 6-5: Degradation curves for the catalytic degradation of methylene blue using the cobalt oxide synthesised from cobalt nitrate hexahydrate in 100% alcohol solvents, calcined at 300°C

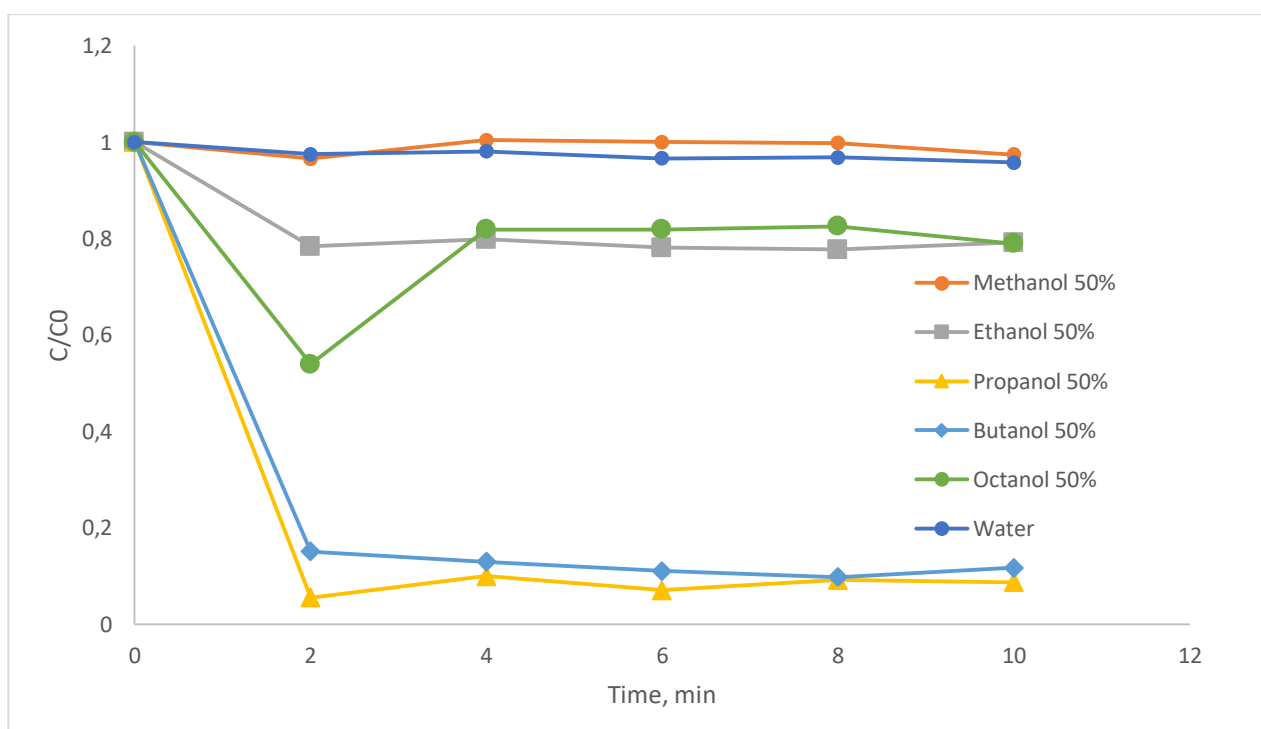


Figure 6-6: Degradation curves for the catalytic degradation of methylene blue using the cobalt oxide synthesised from cobalt nitrate hexahydrate in 50% alcohol/water solutions and 100% water, calcined at 300°C

As cobalt oxide is already commercially available in various quantities for laboratory work, it was necessary for the viability of the synthesised cobalt oxide particles as a catalyst to be tested. Commercially produced Sigma-Aldrich cobalt oxide samples; one at 50 nm resembling the size of the particles synthesised in this study, and one at 10

μm , were selected to comparatively assess the cobalt oxide particles synthesised. Using the same degradation method, methylene blue was treated, and the results displayed in Figure 6-7. The Sigma-Aldrich sample at 50 nm initially provided a more rapid degradation than the 10 μm sample, as expected due to the high exposed surface area. However, both the Sigma-Aldrich samples provided a degradation quality similar to the cobalt oxide synthesised from cobalt chloride precursor in 50% and cobalt nitrate precursor in 100% butanol. The aforementioned in-house synthesised particles provided the worst degradation of the synthesised cobalt oxide particles, while the cobalt chloride and cobalt nitrate precursors in 100% methanol and 50% propanol respectively, far exceeded the degradation quality of the commercially available cobalt oxide, providing up to 85% more degradation.

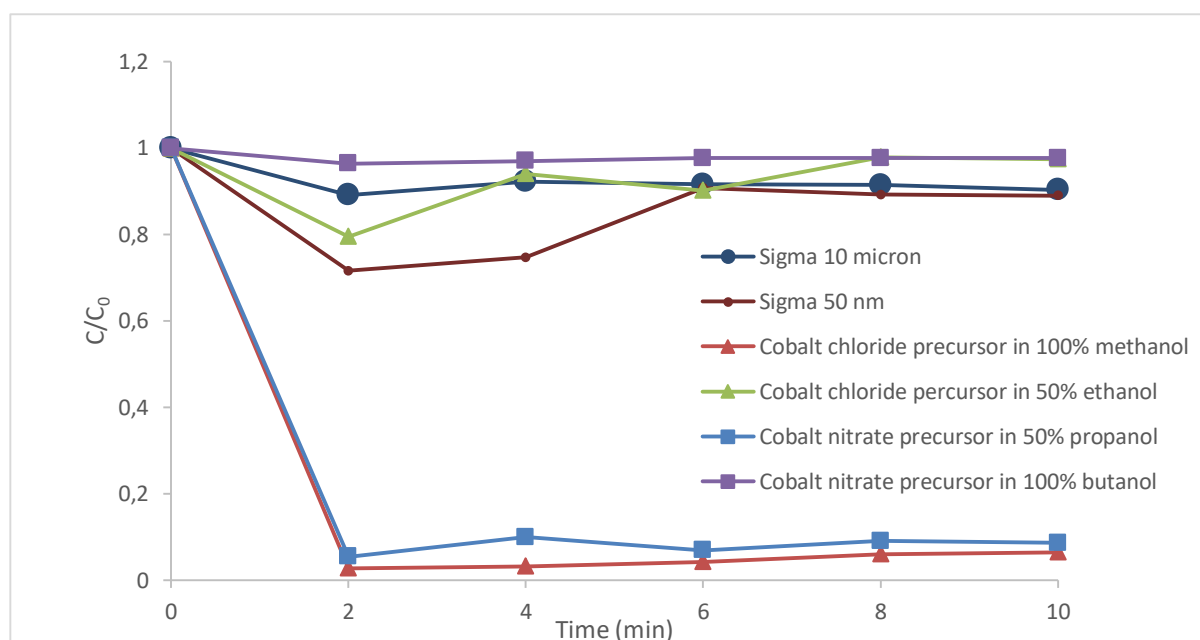


Figure 6-7: Degradation curves for the methylene blue solutions degraded using commercially produced Sigma-Aldrich cobalt oxide samples, as well as the two synthesised cobalt oxide samples resembling the most rapid and slowest degradation rates

Figure 6-8 provides the degradation quality at 2 minutes from the point of reaction within the in-house developed reactor, in order to monitor the effectiveness of each produced cobalt oxide type as a rapid catalyst. The figure confirms that the particles synthesised from cobalt chloride hexahydrate in 100% alcohol are more active than the particles synthesised in 50% alcohol within the first 2 minutes. Additionally, the degradation is plotted against the d_{50} particle size. From it, it may be noted that there is

a slight trend; as the particle size increases, the degradation rate increases. This is contrary to the notion that with an increase in surface area, an increase in activity occurs. Additionally, it is noted that the degradation quality for the cobalt oxide particles synthesised from cobalt nitrate hexahydrate barely changes for the particles represented (excluding semi-amorphous particles), showing degradation of approximately 20%. In the graph it may be noted that the Sigma-Aldrich particles previously discussed provided better degradation than the synthesised particles. It may also be noted that the particle sizes for both the cobalt oxide synthesised from cobalt chloride hexahydrate and from cobalt nitrate hexahydrate, fall within the range 20 to 70 nm.

When taking the crystallite sizes into account, as seen in Figure 6-9, it may be noted that the crystallite sizes for the particles synthesised from the cobalt chloride precursor are generally smaller than that of the particles synthesised from the cobalt nitrate precursor. The crystallite sizes vary from approximately 8 nm to 10 nm, taking the particles synthesised from the cobalt chloride precursor in alcohols into consideration, while the particles synthesised from the cobalt nitrate precursor provided crystallite size variance between approximately 9 and 23 nm. Additionally, it may be noted that for the cobalt chloride precursor, the degradation quality increased with increasing crystallite size, while for the cobalt nitrate precursor the degradation quality decreased with increasing crystallite size. It must, however, be noted that the crystallite ranges between approximately 8.5 and 11 nm provided the best degradation for both cases.

The surface dependency of catalytic reactions places a demand on the active surface area exhibited within a sample. The contradictory findings when taking the particle sizes into account necessitated the study of the active surface area on the synthesised particles. BET analysis was done on selected cobalt oxide particles in order to gauge the effect on the degradation rate. The catalysts which provided the fastest and slowest degradation are indicated in Figure 6-10. From the cobalt chloride precursor results, it is noted that there is not much difference between the BET surface areas achieved, while the cobalt nitrate precursor results revealed that faster degradation rates were found for particles with lower BET surface areas, contrary to the notion that the increase in surface area leads to a concomitant increase in catalytic activity.

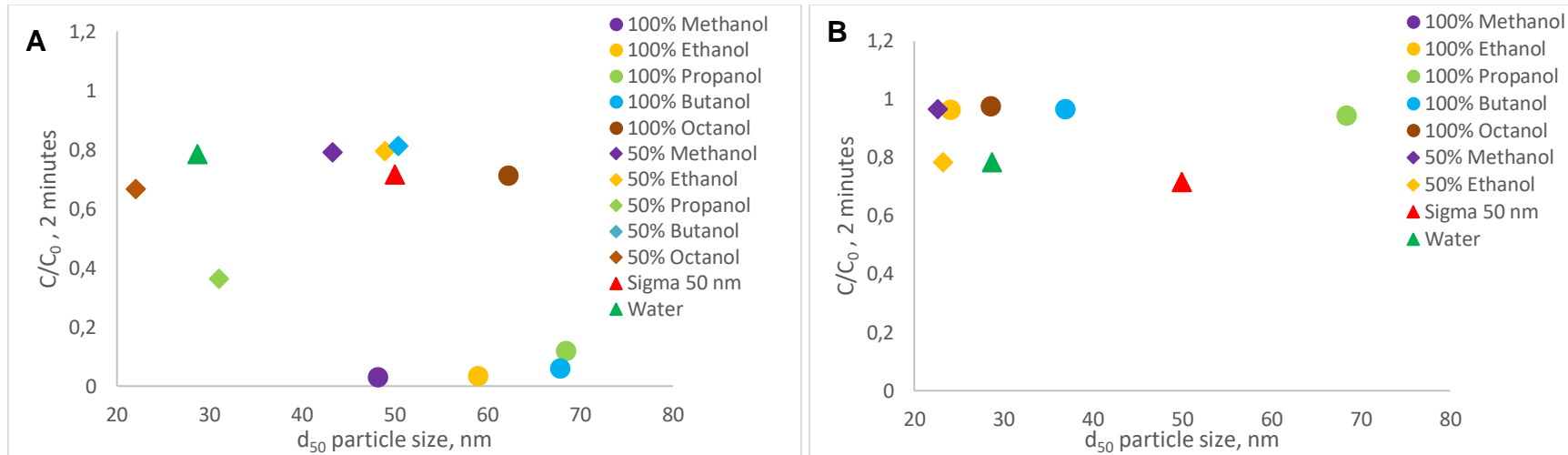


Figure 6-8: The degradation quality at 2 minutes vs. d_{50} particle size for the cobalt oxide particles synthesised from a) cobalt chloride hexahydrate and b) cobalt nitrate hexahydrate in 100% and 50% alcohols, calcined at 300°C, as well as the commercially available 50 nm cobalt oxide particles

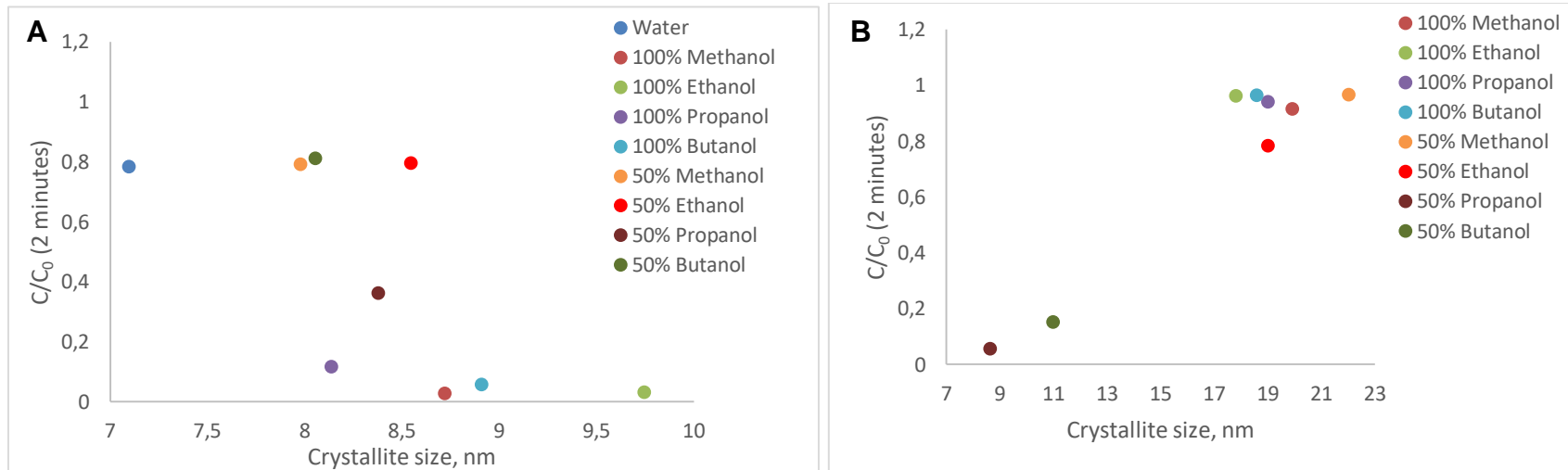


Figure 6-9: The degradation quality at 2 minutes vs. crystallite size for the cobalt oxide particles synthesised from a) cobalt chloride hexahydrate and b) cobalt nitrate hexahydrate in 100% and 50% alcohols, calcined at 300°C, as well as the commercially available 50 nm cobalt oxide particles

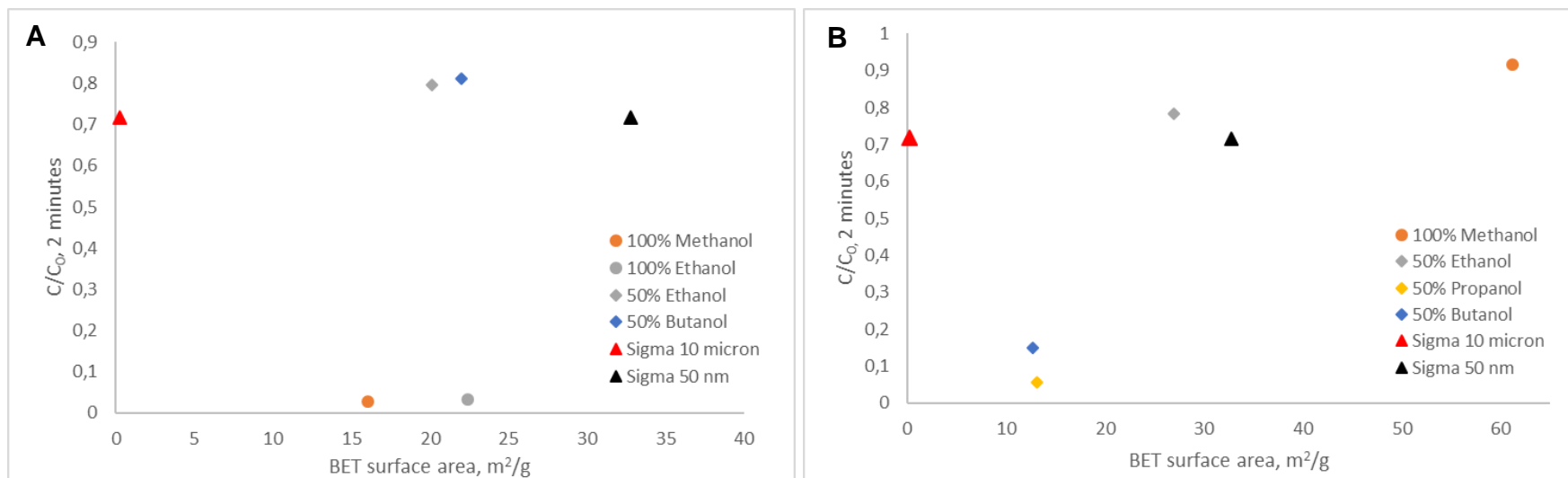


Figure 6-10: The degradation quality at 2 minutes vs. BET surface area for the cobalt oxide particles synthesised from A) cobalt chloride hexahydrate and B) cobalt nitrate hexahydrate in 100% and 50% alcohols, calcined at 300°C , as well as the commercially available 50 nm cobalt oxide particles

The particles were further analysed by determining the interlamellar d-spacing. This was accurately achieved using the TEM images received and applying GATAN digital micrograph software. This allowed for the main exposed facets of the samples to be determined. The d-spacing for all the samples were determined in the same way and indexed using Equation 3-1. The majority of the particles synthesised from cobalt chloride hexahydrate exhibited that the main exposed facet of the particles is [111] of nature, with the exception of the particles synthesised in 100% octanol, which provided particles with the main exposed facet of [311], as shown in Table 6-1. In the rapid and large-scale synthesis of cobalt oxide particles studied by Chowdhury *et al.* (2015), octahedral particles enclosed by [111] facets were produced and tested in the degradation of methylene orange. One of the reasons for the rapid degradation was attributed to the [111] exposed facets, as water molecules were dissociated at its surface, forming Co-OH complexes which were responsible for peroxymonosulphate activation. The main exposed facets of the particles synthesised from cobalt nitrate hexahydrate are presented in Table 6-2. The variation of exposed facets found in the samples is because of the variation of particle shapes and sizes formed. It also provides insight into the lower degradation efficiency achieved in comparison to its cobalt chloride counterpart.

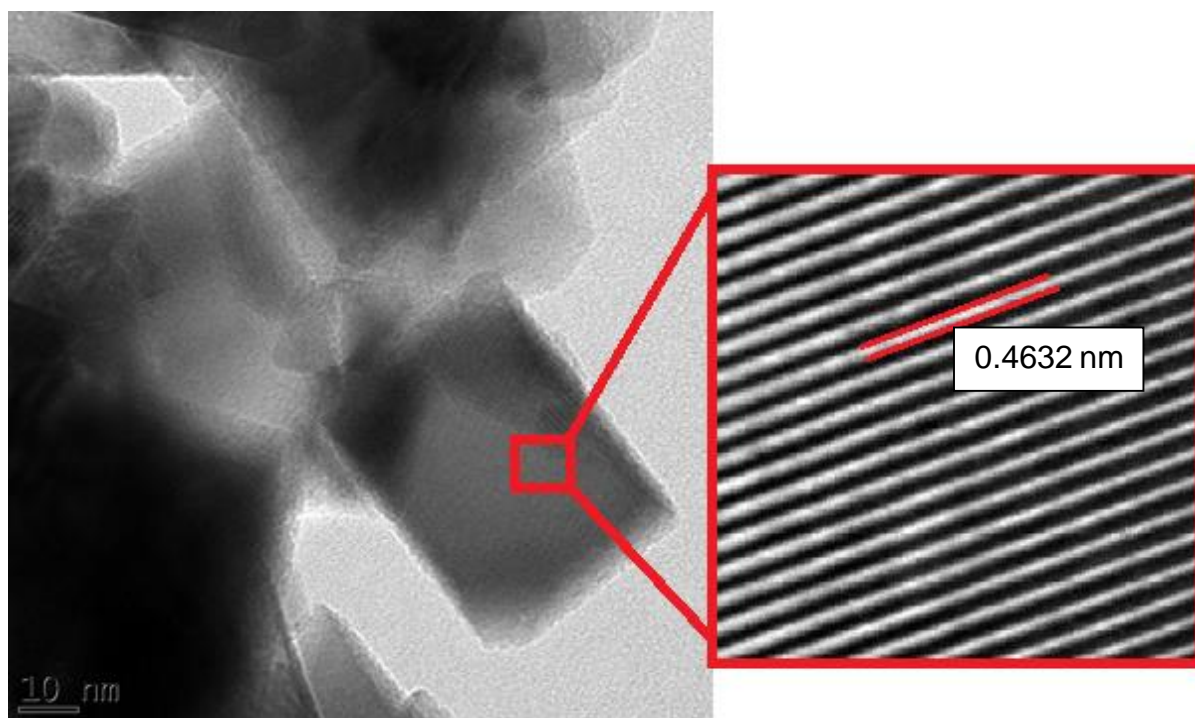


Figure 6-11: Illustration of the interlamellar spacing measured for the cobalt oxide particles synthesised in 100% methanol

Table 6-1: The resulting d-spacing and main exposed facets of the cobalt oxide particles synthesised from cobalt chloride hexahydrate in 100% and 50% alcohol/water solvents

Solvent	d-spacing	Main exposed facet
Water	0.468	111
100% methanol	0.463	111
100% ethanol	0.465	111
100% propanol	0.472	111
100% butanol	0.469	111
100% octanol	0.246	311
50% methanol	0.471	111
50% ethanol	0.460	111
50% propanol	0.467	111
50% butanol	0.466	111
50% octanol	0.462	111

Table 6-2: Measured d-spacing and corresponding exposed facet for the cobalt oxide particles synthesised from cobalt nitrate in 100% and 50% alcohol solvents, calcined at 300°C

Sample	Measured d-spacing	Main exposed facet
50% methanol	0.286	220
50% ethanol	0.243	311
50% propanol	0.253	301
50% butanol	0.280	220
50% octanol	0.255	301
Water	0.253	301
100% methanol	0.247	311
100% ethanol	0.246	311
100% propanol	0.283	220
100% butanol	0.243	311
100% octanol	0.245	311

The effect of calcination temperature on the catalytic performance of the cobalt oxide particles was also tested in the in-house developed reactor. As the particles synthesised from cobalt chloride hexahydrate in 100% alcohol provided better results initially, they are presented in Figures 6-12 and 6-13 as the temperature study, while the remaining results are found in Appendix F. The Co(OH)₂ particles were initially calcined at 300°C, and therefore the calcination temperatures studied were at 400 and 500°C respectively. The effect of calcination temperature on crystallite size was discussed in Chapters 4 and 5. It was found that with increasing temperature, the crystallite sizes increased. This was reflected in the catalytic degradation, as the particles became noticeably less active with the increase in calcination temperature. It is additionally noted in Appendix F, specifically for the cobalt oxide particles synthesised from cobalt nitrate hexahydrate in 50% octanol, when calcined at 500°C. This was one of the cases in which a crystallite size drop occurred, and it directly affected the catalytic ability, as shown in Appendix F.

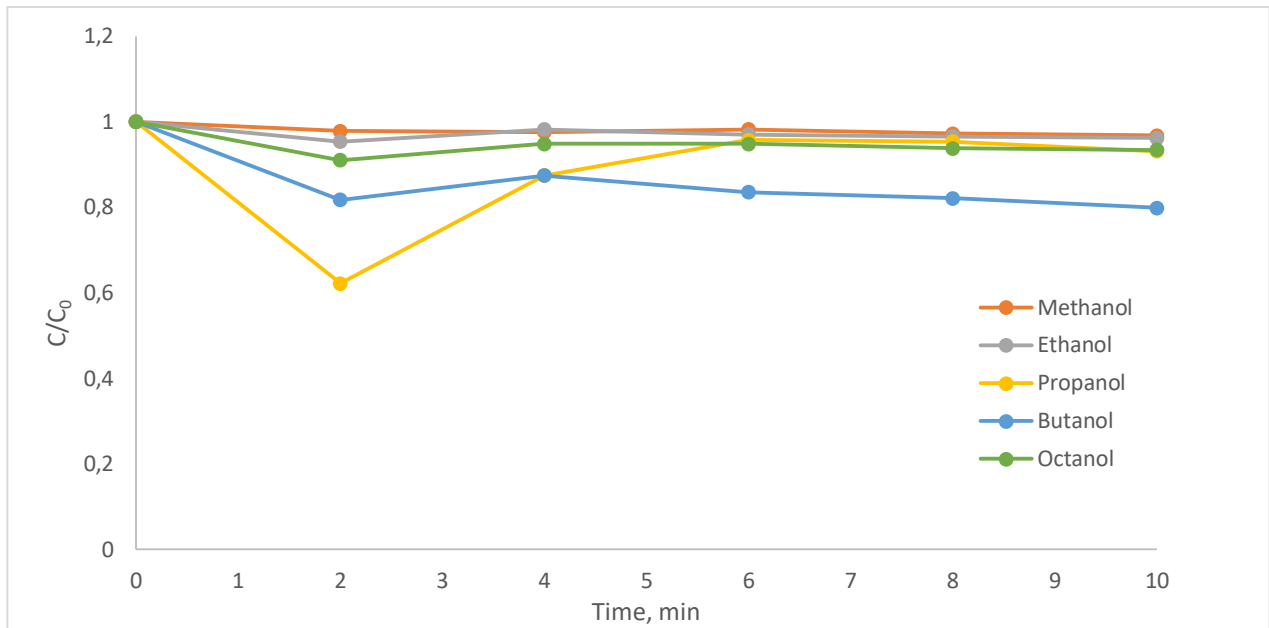


Figure 6-12: Degradation curves for the methylene blue solution degraded using the cobalt oxide catalysts synthesised from cobalt chloride hexahydrate in 100% alcohol solvents, calcined at 400°C

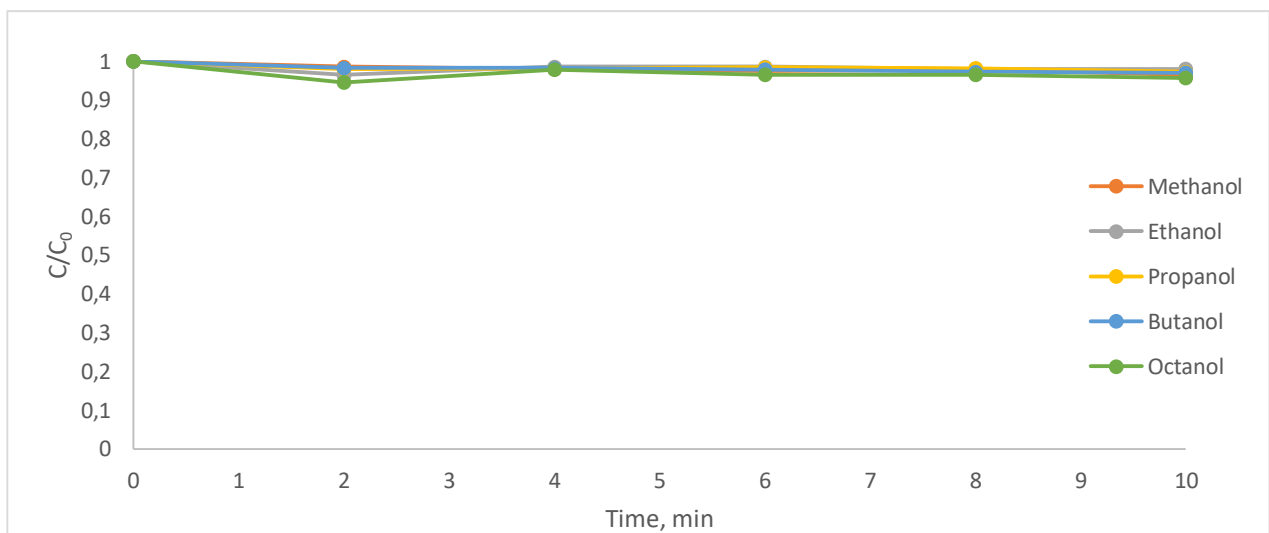


Figure 6-13: Degradation curves for the methylene blue solution degraded using the cobalt oxide catalysts synthesised from cobalt nitrate hexahydrate in 100% alcohol solvents, calcined at 500°C

Increased calcination temperature had a negative effect on the degradative quality of the particles synthesised from the cobalt nitrate precursor, as was the case with the cobalt chloride precursor samples. However, whether degradation was shown within the first 10 minutes or not, the colour was removed within a standing time. This is displayed in Table 6-3 and 6-4. As seen from the images, a standing time of an hour was required to remove the colour. Although the synthesised catalysts were active, the increased time required to remove the colour defeats the purpose of the use of a catalyst, which is to increase the reaction rate.

Table 6-3: Samples taken immediately after methylene blue colour degradation for the cobalt oxide catalysts synthesised from a cobalt nitrate hexahydrate precursor salt in 50% propanol, calcined at 300, 400 and 500°C

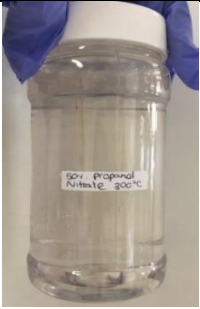





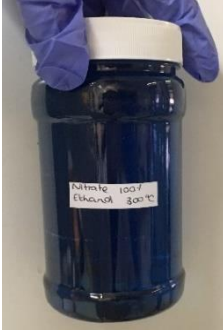

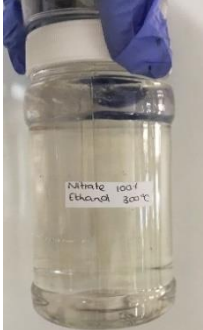

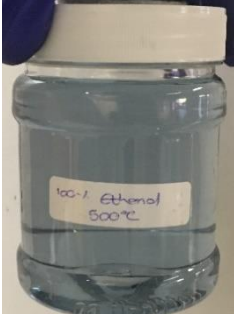
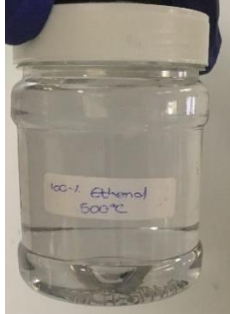
Calcination temperature [°C]		
300	400	500
		

Table 6-4: Clarity of samples after a standing time for the samples taken immediately after the colour degradation of methylene blue using the cobalt oxide catalysts synthesised from cobalt nitrate hexahydrate precursor salt

		Standing time [minutes]		
		0	30	60
100% ethanol at	400°C			
	300°C			
	500°C			

6.2 Comparative analysis

Cobalt oxide nanoparticles were successfully hydro/solvothermally synthesised for both cobalt chloride hexahydrate and cobalt nitrate hexahydrate precursor salts. The alcohols used (methanol, ethanol, propanol, butanol and octanol) within the precursor solutions, along with their concentrations, were varied by mixing with water in the ratio 1:1. Using a cobalt chloride precursor salt provided both α and β polymorphs of the cobalt hydroxide precursor used to generate cobalt oxide, while the cobalt nitrate precursor salt only provided the α -phase. Upon studying the colour and therefore the water content of the precursor solution and the resulting polymorph phase, a relationship between alcohol concentration and polymorph phase was noted – for 100% alcohols resulting in a blue cobalt solution, β -cobalt hydroxide was formed, while for precursors containing water, a red cobalt solution occurred, resulting in α -cobalt hydroxide. Ultimately, a general trend between the catalytic activity for the degradation of methylene blue dye was tested and revealed that the cobalt oxide particles calcined from β -cobalt hydroxide provided better degradation in terms of reaction rates, while the cobalt oxide particles calcined from α -cobalt hydroxide had slower reaction rates. However, an exception to the trend was encountered for the particles synthesised from 50% propanol, 50% butanol and 50% octanol for the nitrate batches. It was, however, noted that the sulphur impurity found in it could have aided the degradation process. Figures 6-14 and 6-15 display the best and worst degradation curves obtained for the cobalt precursor salts observed. It may be noted that the chloride precursor salt produced catalysts which resulted in faster degradation rates in both cases. However, the difference in results are miniscule. The chloride precursor salt results also provided a more reliable result, as only unreacted chloride ions were found in the sample, which should have hindered and not enhanced the reaction. The results revealed that the cobalt oxide which would be best suited as a catalyst in colour degradation within the textile industry would be that which was synthesised from cobalt chloride hexahydrate in 100% methanol, while the cobalt oxide which would be worst suited as a catalyst in colour degradation within the textile industry would be that which was synthesised from cobalt nitrate hexahydrate in 100% butanol.

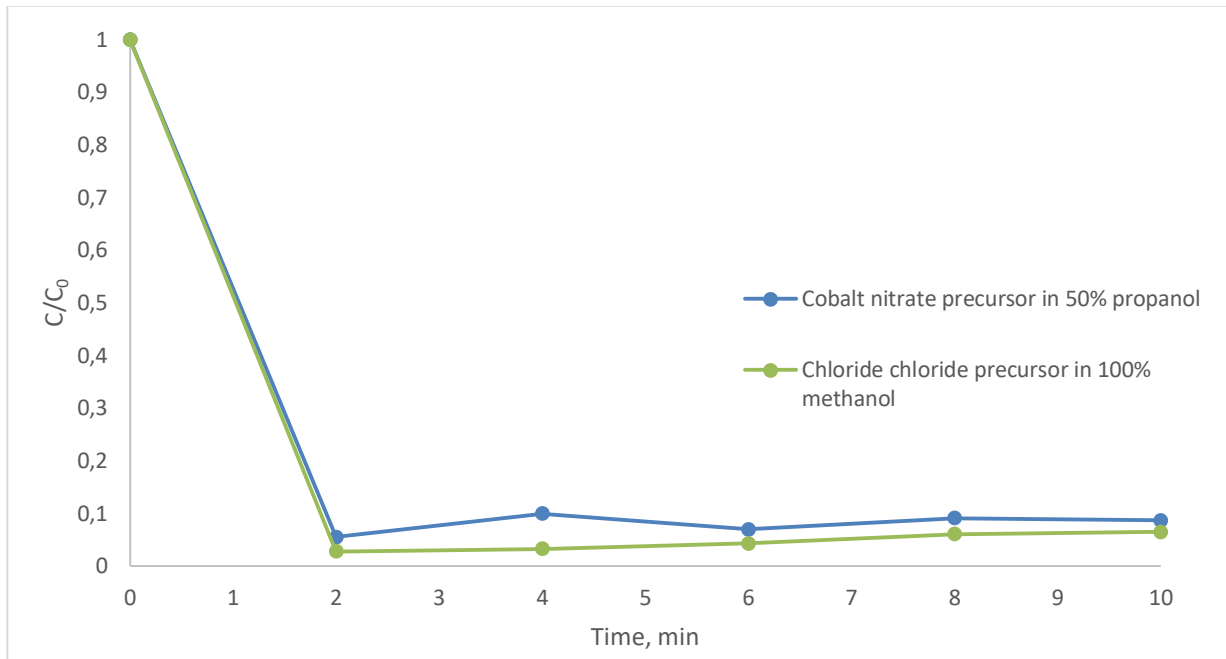


Figure 6-14: Degradation curves for the treated methylene blue solution using the cobalt oxide catalysts which produced the fastest degradation rates

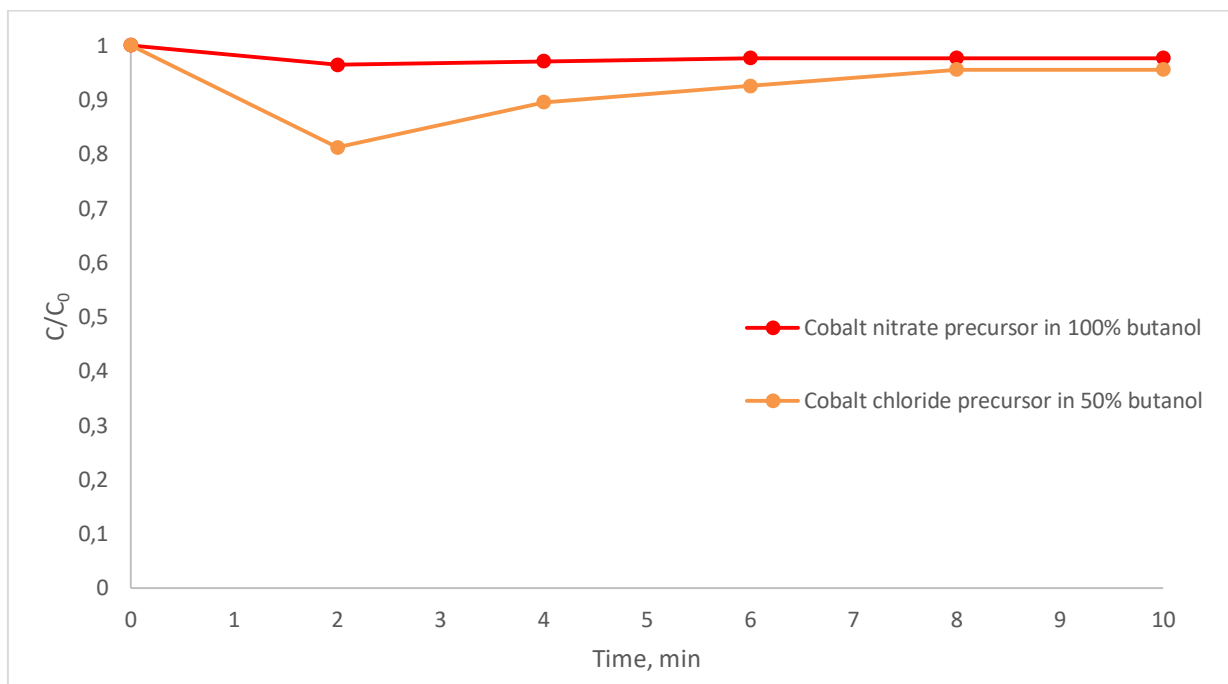


Figure 6-15: Degradation curves for the treated methylene blue solution using the cobalt oxide catalysts which produced the slowest degradation rates

Since the best suited catalyst for colour degradation was the cobalt oxide synthesised from cobalt chloride hexahydrate in 100% methanol, it was necessary to determine the ratio of cobalt valence states within its sample, along with its 50% alcohol counterpart. This analysis was done via Energy Loss Near-Edge Fine Structure (ELNEFS) analysis, as shown in Figures 6-16 and 6-17 below. Two peaks, L_2 and L_3 , were noted, which represent the Co^{2+} and Co^{3+} valence states respectively. The ratio between the two states on the active area of the catalysts plays an important role in their activity, as

the Co^{3+} has been deemed the more active species.

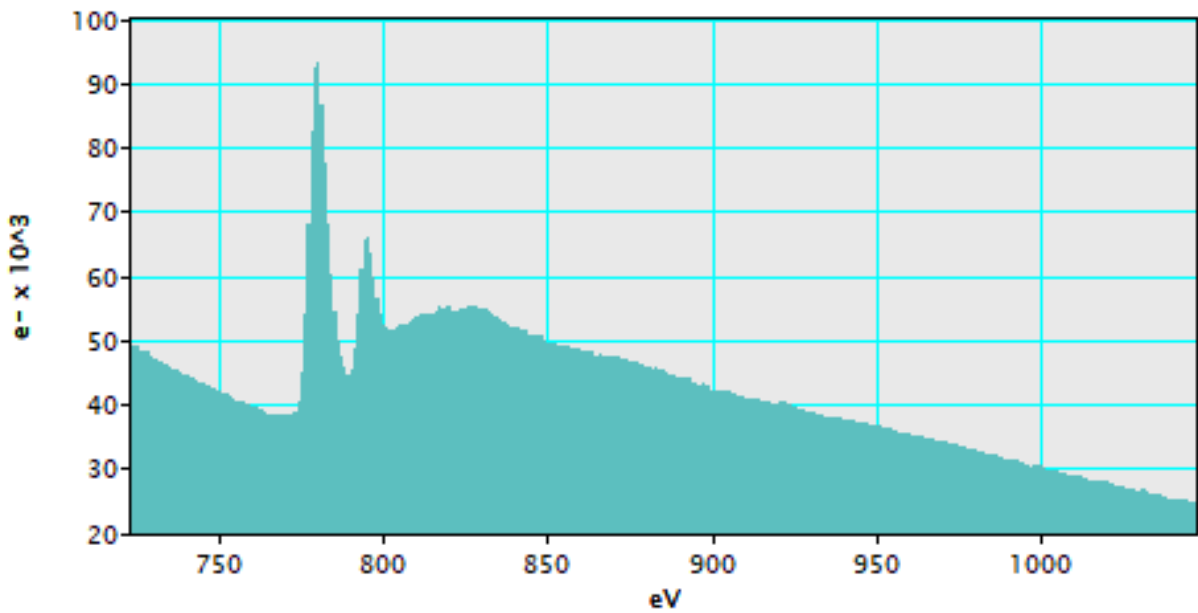


Figure 6-16: ELNEFS spectra revealing the L_3 and L_2 peaks for the cobalt oxide particles showing the best catalytic degradation properties i.e. produced from cobalt chloride hexahydrate in 100% methanol, calcined at 300°C

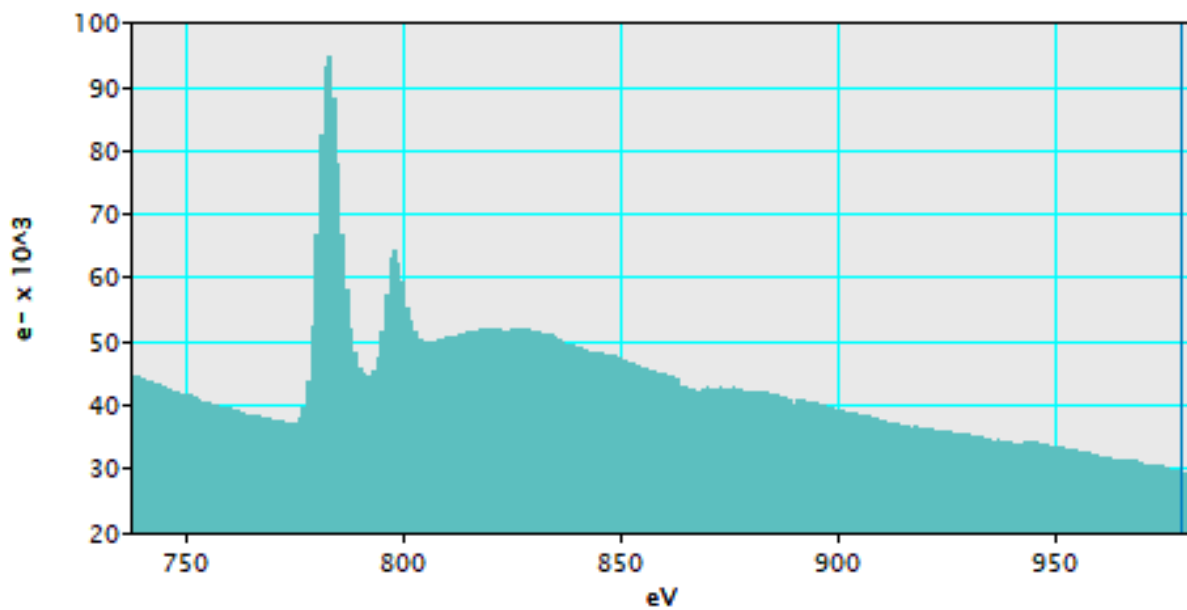


Figure 6-17: ELNEFS spectra revealing the L_3 and L_2 peaks for the 50% counterpart of the 100% methanol cobalt chloride hexahydrate particles, calcined at 300°C

The Lorentzian function is a singularly peaked function, defined by Equation 6-1, which may be used to calculate the L_3/L_2 ratio by integrating the Lorentzian functions represented by L_2 and L_3 respectively. The integration of the Lorentzian function is represented by Equation 6-2. The results of these equations reveal that the 100% methanol batch provided a L_3/L_2 ratio of 31.587, while the 50% batch a L_3/L_2 ratio of

3.209, approximately 10 times less than that of the 100% batch. This method of determining the L_3/L_2 ratio displays an accuracy within the range ± 0.3 , an adequate range for the qualification of valence states, according to Chen *et al.*, 2007. This additionally explains the reduced catalytic performance of the 50% methanol batch.

$$f(E) = \frac{h_1}{\pi} \times \left[\arctan(\pi \cdot (E - E_1)) + \frac{\pi}{2} \right] + \frac{h_2}{\pi} \times \left[\arctan(\pi \cdot (E - E_2)) + \frac{\pi}{2} \right] \quad 6-1$$

$$\frac{I(L_3)}{I(L_2)} = \frac{\int_{L_3-w/2}^{L_3+w/2} I(E) dE}{\int_{L_2-w/2}^{L_2+w/2} I(E) dE} \quad 6-2$$

6.3 Optimisation of degradation studies

The sample showing the highest degradation rate was found to be the cobalt oxide particles synthesised from cobalt chloride precursor salt in 100% methanol, calcined at 300°C. In order to see how effective these particles were, it was important to optimise the methylene blue degradation process using this catalyst. In that way, the best parameters were used to degrade various dyes as a simulation for actual textile wastewater. It should be noted that actual textile wastewater contains a lot more than just dye remnants, as many chemical additives are added for various processes, which commonly end up in one disposal sump. In addition, textile companies all have different recipes, including different chemicals. Treatment of actual textile wastewater therefore poses the risk that no generic treatment exists, as each case may be different. However, knowing how to treat various dyes at various colour spectra, is the first step to actively treating actual textile wastewater.

6.3.1 Optimisation of catalyst load

Keeping the degradation parameters constant, the catalyst load was varied in order to determine the best catalyst load for the volume of dye treated and amount of Oxone[®] used. The catalyst load was changed from 0.15 g to 0.4 g per filter. The filter making time was obviously altered, due to the increase/decrease in catalyst load. The time to make one 0.3 g filter varies from 30 minutes to 1 hour. The time almost doubled with a 30% increase of catalyst, while the decreased loads of 0.15 g or 0.2 g took an average of 10 minutes. This is an important factor to take into account for commercial production.

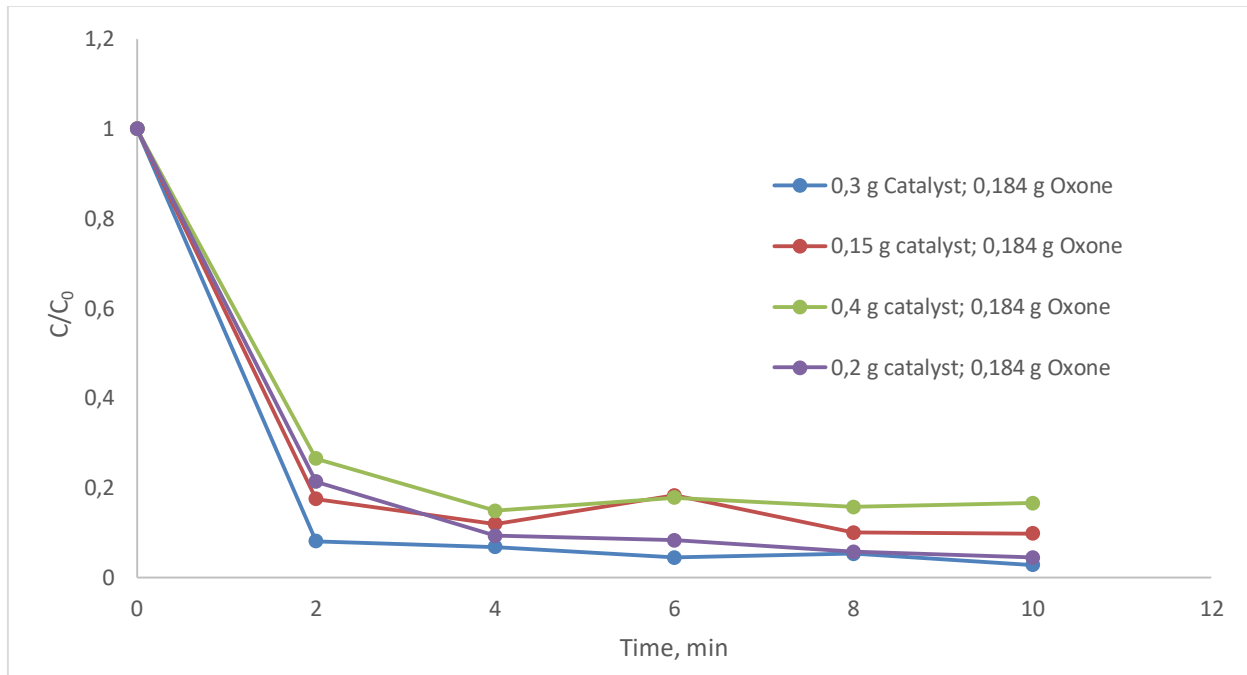


Figure 6-18: Methylene blue degradation with catalyst load variance

The filters were dried as per usual and used to degrade a standard methylene blue solution, as captured in Figure 6-18. The final samples taken at 10 minutes show the general trend of the degradation of the methylene blue solutions. The most rapid degradation rate was found when using a catalyst load of 0.3 g, shortly followed by 0.2 g, then 0.15 g and finally 0.4 g catalyst load filter. It was found that a catalyst load of 0.4 g on one filter was ineffective, mostly due to the catalyst not staying fixed to the filter. Upon treatment, the catalyst became dispersed, thus providing a denser reading for the handheld spectrometer. A catalyst load of 0.15 g proved to be less effective, as fewer active sites were provided to activate the peroxymonosulphate fed into the system. Narrowing down the catalyst load variance to between 0.2 g and 0.3 g shows a very slight difference in favour of a 0.3 g catalyst load. Although the 0.3 g catalyst load displays the highest degradation rate, it is also important to take cost into account. As the difference in degradation is very slight, it would be more economically viable to use filters containing 0.2 g over the 0.3 g. However, from a research perspective, it is important to determine the best overall conditions.

6.3.2 Optimisation of Oxone[®] concentration

Using the most effective catalyst load and maintaining it, the Oxone concentration was varied. Concentrations were increased by 0.093 g per 500 ml of methylene blue treated. Using the most efficient catalyst load, it was important to find out the Oxone concentration which would best correlate with it. The catalyst concentration therefore was maintained at 0.3 g per filter, and the process carried out as per usual.

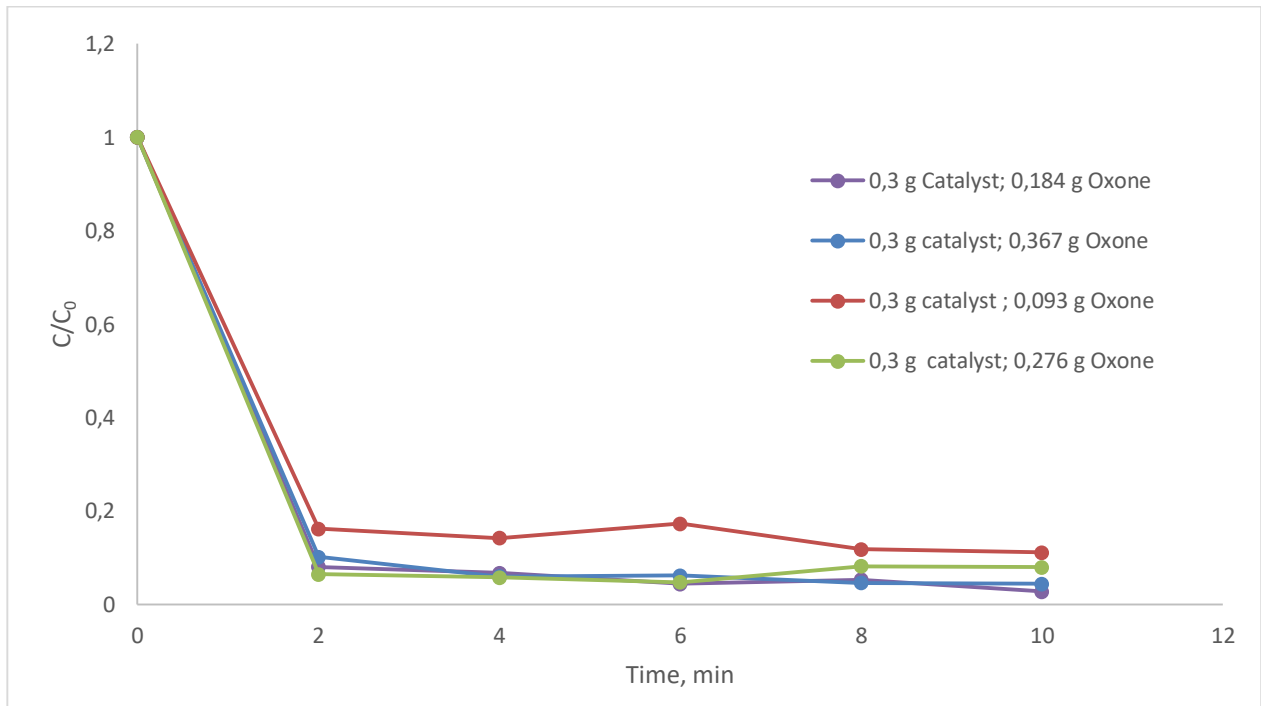


Figure 6-19: Methylene blue degradation with Oxone variance

From Figure 6-19 it can be seen that the Oxone concentration providing the lowest degradation in the allotted time was 0.093 g/500 mL. This was also the lowest concentration explored and half the amount previously explored. The highest degradation was provided by an Oxone concentration of 0.184 g. The concentration of 0.367 g provided the second highest degradation. This shows that a concentration of 0.184 g Oxone is not only preferable for degradation rate, but also for cost analysis.

6.3.3 System optimisation for dye degradation

From the previous investigation, the optimal conditions for degradation of methylene blue using this system was found to be a catalyst load of 0.3 g and Oxone concentration of 0.184 g per 500 mL methylene blue treated. Using the best conditions, various concentrations of methylene blue dye were treated, in order to determine the

highest dye concentration which can be treated using this system. The standard for the previous tests used a concentration of 10 mg/L of methylene blue dye. To test the strength of the degradation system, the dye concentration was increased five-fold.

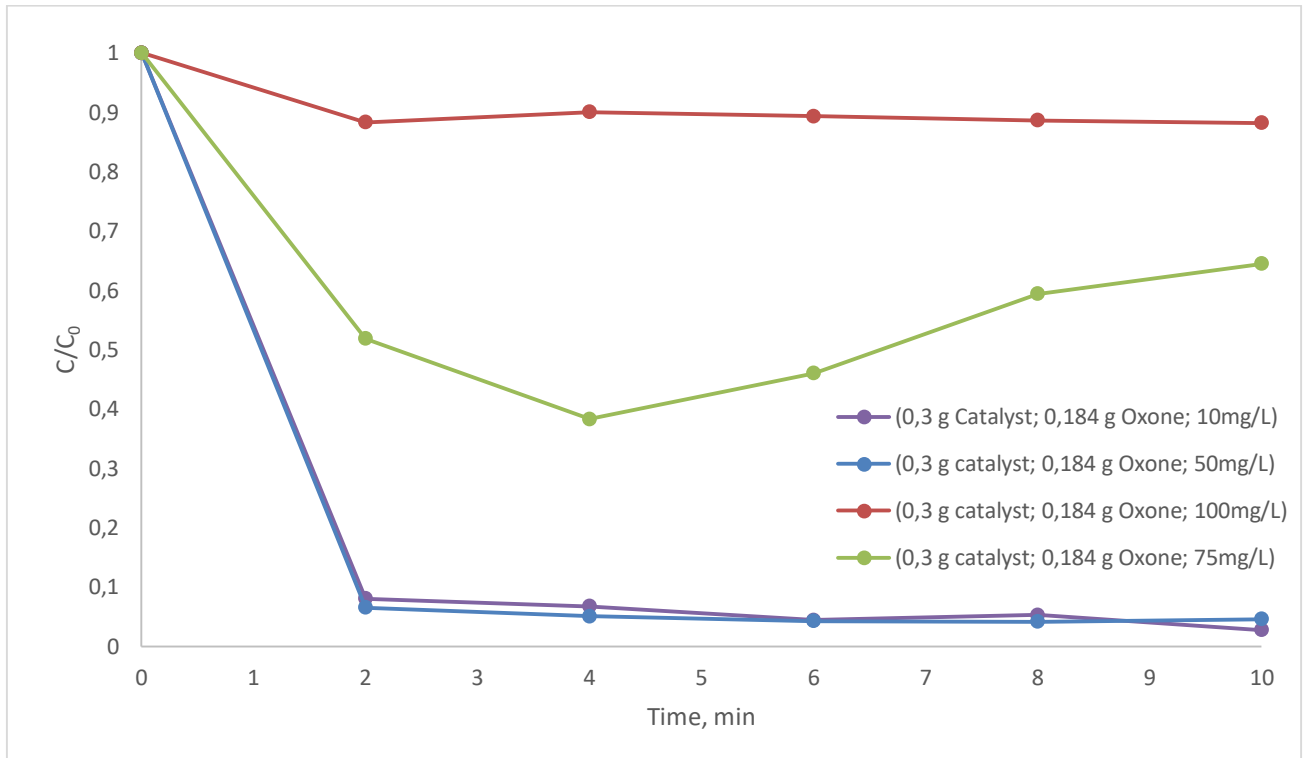


Figure 6-20: Degradation of various concentrations of methylene blue at optimum conditions (0,3 g catalyst and 0,184 g Oxone)

Figure 6-20 shows the degradation curves of the increased methylene blue dye concentrations. The highest degradation (97.26%) was achieved in the standard test using the best conditions (0.3 g catalyst and 0.184 g Oxone per 500 mL methylene blue). The concentration was then increased to 50 mg/L, which was degraded by 95.4% using the same conditions. The concentration was then increased to 75 mg/L, which displayed a major drop in degradation efficiency. A higher concentration of 100 mg/L was then tested, but remained virtually untreated. These concentrations were degraded by 35.5% and 11.82% respectively. Figure 6-21 provides visuals of the dye after treatment, which displays the degree of degradation.

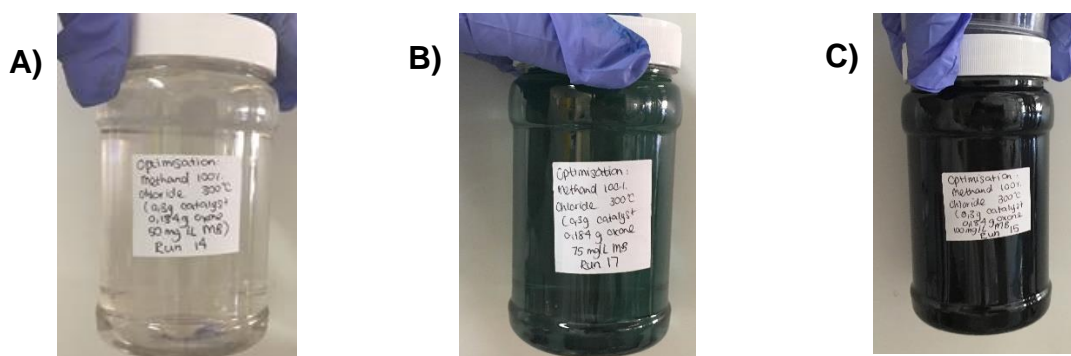


Figure 6-21: Treated methylene blue solutions at concentrations of a) 50 mg/L, b) 75 mg/L and c) 100 mg/L

The possibility that an increased catalyst surface area over a larger filter bed, made up of 3 individual filters stacked on one another, would increase the degradation of the higher concentrated dye was investigated. From the investigation, it was found that no substantial changes were made for the increased dye concentration of 75 mg/L to account for the increased cost of making more filters. Further studies were therefore maintained at the best conditions for the system: 0.3 g catalyst, 0.184 g Oxone and 50 mg/L methylene blue dye. The concentration appeared to be increasing after the 4-minute minimum obtained for the 75 mg/L sample in both experiments as shown in Figure 6-20 and 6-22. This phenomenon should be further studied as it is not clear why this has happened.

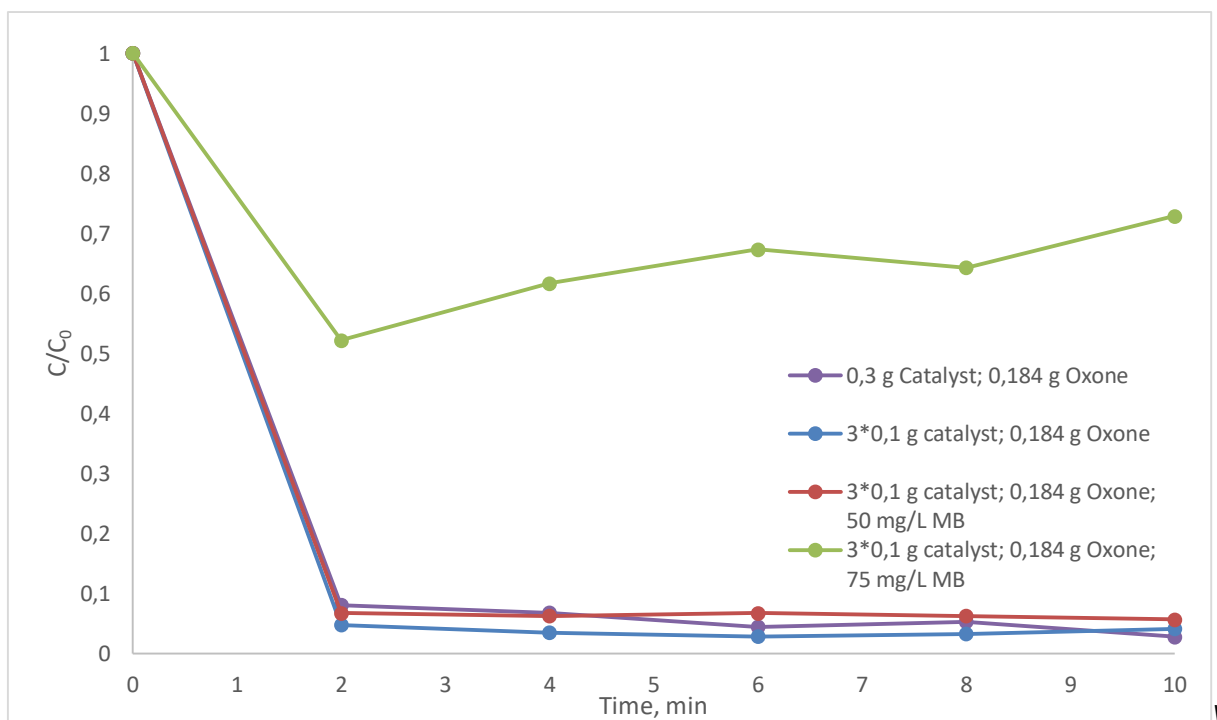


Figure 6-22: Degradation of methylene blue at various concentrations at optimum conditions and increased filter bed

The best conditions were selected to treat various dyes in order to determine the effectiveness of the 100% methanol batch. Synozol Red and Synozol Yellow were selected for the primary colours to be complete, with the addition of Methylene Orange. As 50 mg/L of methylene blue was selected, it was important for the molarity to be maintained. This translated to a concentration of 0.071 g/L, 0.043 g/L and 0.0204 g/L for Synozol Red, Synozol Yellow and Methylene Orange respectively.

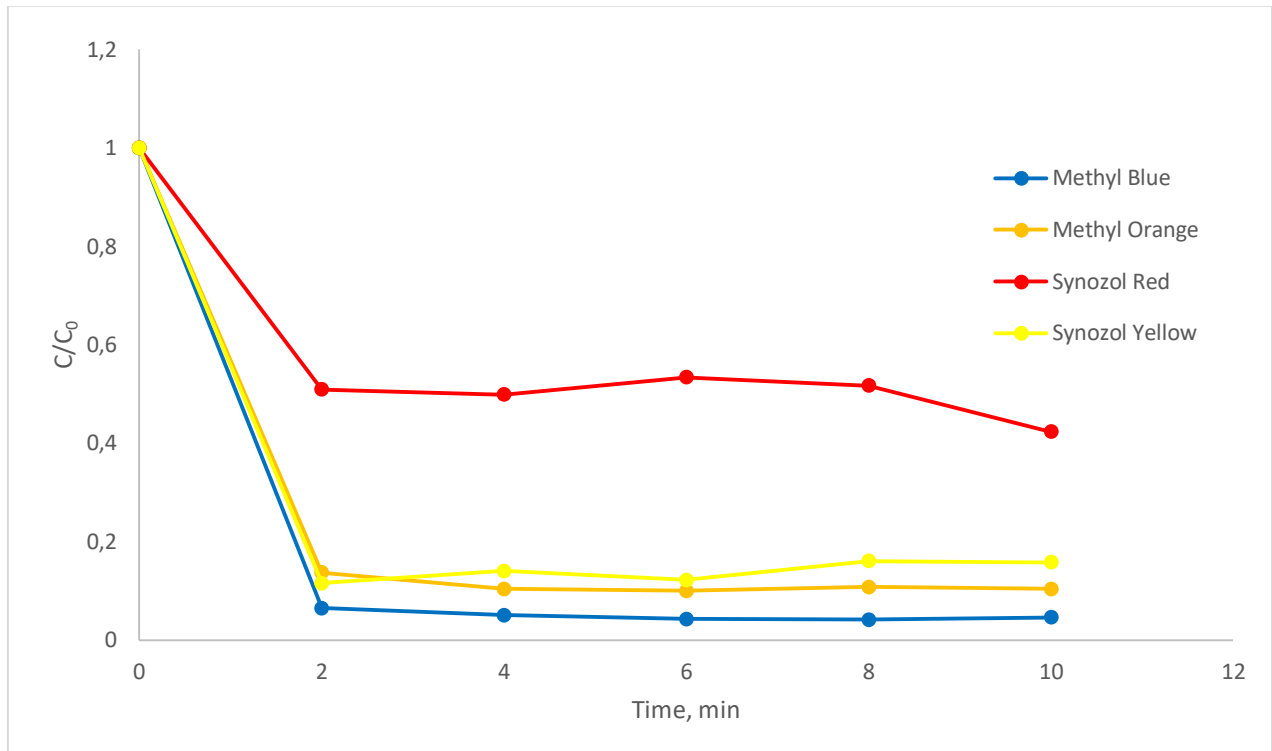


Figure 6-23: Degradation of various reactive dyes with the same molarity at the optimum conditions

The dye broken down the easiest was methylene blue, followed by methylene orange, synozol yellow and finally synozol red. It is to be noted that the chemical make-up of these dyes varies, though they all are reactive dyes. The degradation of these dyes under the same conditions presents the issues which may be encountered during the degradation of actual textile wastewater. The waste sumps at textile industries are usually a combination of various processes and dyes used. Since there are variances in the degradation of each different dye, the process of treatment should vary to optimise the degradation of each dye. It should also be noted that various additives are introduced into actual textile wastewater, both in the dyeing processes and in the sump, as discharge treatment requirements. The treatment of actual textile wastewater may therefore prove to be complicated and different for every textile dyeing process.

6.4 Conclusion

It was found that the degradation of methylene blue dye using the cobalt oxide particles calcined from β -cobalt hydroxide provided better degradation in terms of reaction rates, while those calcined from α -cobalt hydroxide had slower reaction rates. An exception to this trend was encountered for the cobalt oxide particles synthesised from cobalt nitrate precursor in 50% propanol, 50% butanol and 50% octanol. Upon investigation, it was noted that a sulphur impurity existed in these batches. The chloride precursor salt produced catalysts which provided faster degradation rates in comparison to the nitrate precursor. The catalytic activity of the produced catalysts at two minutes were plotted against the d_{50} particle sizes, the crystallite sizes and BET surface area of the most and least rapid catalyst activity achieved. From the d_{50} plot, it was found that with an increase in particle size, the degradation rate increases slightly, contrary to the notion that increased catalytic activity is dependent on increased surface area. However, degradation of only 20% occurred for the cobalt nitrate precursor samples. The particle sizes ranged between 20 and 70 nm for both the cobalt oxide synthesised from cobalt chloride hexahydrate and from cobalt nitrate hexahydrate. The crystallite size plot revealed that a large variance in crystallite size exists between the two precursor salts. However, highly active cobalt oxide particles provided crystallite sizes between approximately 8,5 and 11 nm for both cases. This was reiterated in the effect of calcination temperature on catalytic performance, as the crystallite sizes generally increased with increasing temperature, negatively affecting the catalytic ability. The exception to this finding further reiterated the effect of crystallite size range on high activity of cobalt oxide, as the cobalt oxide synthesised from the nitrate precursor in 50% octanol experienced a crystallite decrease to 9.73 nm, consequently providing a faster degradation rate than those calcined at 300 and 400°C.

Overall, the results revealed that the cobalt oxide synthesised which would be best suited as a catalyst in colour degradation within the textile industry would be that which was synthesised from cobalt chloride hexahydrate in 100% methanol, while the cobalt oxide which would be worst suited as a catalyst in colour degradation within the textile industry would be that which was synthesised from cobalt nitrate hexahydrate

in 100% butanol. The best catalyst was analysed using ELNEFS analysis in order to determine the L₃/L₂ ratios in comparison to its 50% alcohol counterpart. This was done in order to determine the ratio of Co³⁺ to Co²⁺ ions, as the Co³⁺ is the more active species. The results revealed a substantially higher Co³⁺ concentration than the Co²⁺ concentration, which was 10 times higher than its 50% counterpart.

The AOP used to degrade the methylene blue solution was then optimised using the best catalyst in order to determine the optimal process conditions under which to operate. Various factors were varied within the in-house developed reactor used in this study - the catalyst load on filter, the Oxone concentration, and filter bed thickness. The best conditions were used to treat higher concentrated methylene blue solutions, as well as various reactive dyes. It was found that a catalyst load showing the fastest degradation rate was that of 0.3 g. The 0.2 g load, however, provided very similar results and would be more viable from a cost standpoint. The Oxone concentration showing the best results was 0.364 g/L, coincidentally the amount used in the initial studies. Increased concentrations at 50, 75 and 100 mg/L were treated using the best catalyst load and Oxone concentrations. The 50 mg/L concentrated methylene blue solution was degraded by 95.4% using the same conditions, and an increase to 75 mg/L and 100 mg/L displayed a major drop in degradation. Synozol red and Synozol yellow reactive dyes, along with methylene orange, were tested at the optimal conditions at the same molarity of methylene blue. From it, it was found that the dye broken down the easiest was methylene blue, followed by methylene orange, Synozol yellow and finally Synozol red.

CHAPTER 7 CONCLUSIONS AND RECOMMENDATIONS

7.1 Introduction

The most important commodity in the world is water. Research in various industries therefore has focused on the use, reduce and reuse of water for their processes. The textile industry has become a focus in the reuse of water, due to its use of large volumes of water in practically every step of its manufacturing process. Further, conventional textile wastewater contains dye particles which often escape the treatment put in place by wastewater treatment plants, and therefore poses toxic and eutrophication threats to the environment it is pumped to.

An effective method of organic toxic waste removal, such as dye within water, has been found in Advanced Oxidation Processes (AOPs), as they convert harmful organic toxic waste to harmless H_2O and CO_2 . The use of sulphate radicals, from peroxymonosulphate, has become popular in these processes for their high reduction potential and therefore ability to mineralise the organic toxic waste with ease. Cobalt oxide has been deemed the best-known activator of peroxymonosulphate for the formation of sulphate radicals, and therefore became the focus of this research.

7.2 Conclusions

Petkova and Nedkov (2013) demonstrated different spectral behavior of CoCl_2 in water and ethanol. They found that in water, a pink/red solution was formed, while in the alcohol a blue solution was formed, attributed to the octahedral and tetrahedral complexes which form, respectively. This work confirmed this finding, with the addition that the $\text{Co}(\text{NO}_3)_2$ salt behaves differently. It was found that the nitrate anion produced only the red octahedral complex in both water and alcohol solutions. During the hydro/solvothermal synthesis, the cobalt chloride hexahydrate ($\text{CoCl}_2 \cdot 6\text{H}_2\text{O}$) precursor salt produced both green/blue α -cobalt hydroxide and pink β -cobalt hydroxide polymorphs, while only α -cobalt hydroxide was encountered for the cobalt nitrate hexahydrate precursor $\text{Co}(\text{NO}_3)_2 \cdot 6\text{H}_2\text{O}$ salt. This provided a relationship between the cobalt complex solution to the phase of cobalt hydroxide polymorph formed. A blue precursor solution (tetrahedral complex) produced pink β -cobalt hydroxide particles, while a red precursor solution (octahedral complex) produced α -cobalt hydroxide. Upon calcination, cobalt oxide nanoparticles were successfully formed from both cobalt hydroxide

polymorphs.

Shape and size variances occurred for the change in anion used, while the use of various alcohols maintained the shape and approximate size of the particles. The chloride-based particles generally produced rhombic-shaped cobalt oxide nanoparticles approximately 50 nm in size, with the exception of the water and 50% methanol batch, which produced nanorods. The nitrate-based particles were nanorod-like particles, approximately 30 nm in size, as measured from the TEM images provided. However, SEM images revealed the formation of larger particles approximately 20 μm in size for the water batch and 40 μm in size for the 50% ethanol batch. The shape and size variances shows how complex the synthesis of nanoparticles is as any change in process conditions may completely change the outcome of a synthesis process. The particle size distributions were dominated by the anion rather than the alcohol. Narrow size distributions were obtained in the presence of nitrate for all alcohol and alcohol/water solutions, in contrast to the wide particle size distributions obtained in the presence of chlorides.

The TEM images were additionally used to calculate the d-spacing of the particles, which ultimately were used to determine their main exposed facets. The chloride-based samples provided facets of [111] for all the samples apart from the 100% octanol, which provided an exposed facet of [311]. For the nitrate samples, a variety of main exposed facets for the synthesized particles were encountered. The majority of the particles had a [311] exposed facet. The XRD analysis showed that with an increase in surface tension there was a decrease in crystallite size. It also revealed that with an increase in calcination temperature an increase in crystallite size occurs.

The catalytic behaviour of the cobalt oxide particles was analysed by the degradation of methylene blue. The chloride-based samples performed better, but upon further investigation it was found that this was only true for the cobalt oxide particles synthesized from β -cobalt hydroxide, while the samples synthesized from α -cobalt hydroxide provided very little degradation. An exception to this was found to be the cobalt oxide particles synthesized from cobalt nitrate hexahydrate in 50% propanol, 50% butanol and 50% octanol. This was attributed to the niche range, in which high catalytic activity was found for crystallite sizes between 8.5 and 11 nm for both precursor salts. The effect of calcination temperature

negatively affected the degradation process. This was expected, as the crystallite sizes increased with increasing temperature, providing a lower active surface area. The crystallite niche area was confirmed by the cobalt oxide synthesized from the nitrate precursor in 50% octanol, as an unexpected decrease to 9.73 nm consequently provided a faster degradation rate than those calcined at 300°C and 400°C. It was additionally noted that although the degradation rate of methylene blue was decreased in some cases, the solutions eventually became visibly clear within a standing time. However, the standing time required for all the chloride-based samples was less than 30 minutes, while the nitrate-based samples required up to an hour of standing time to become clear.

7.3 Contributions

A comparison of the chloride and nitrate anions in the formation of cobalt complexes and its subsequent effect on the cobalt hydroxide polymorph formed has been indicated for the first time. Although it was shown in literature before that chloride results in red complex solutions in water and blue complex solutions in alcohols, it was never tested for nitrate. From this research it was found that only red octahedral cobalt complexes are formed from cobalt nitrate salts, whether in 100% alcohol solutions or in water or 50% alcohol/water solutions.

A method to control the relationship between octahedral or tetrahedral cobalt complex and cobalt hydroxide polymorph has been established. Using this synthesis route, a red cobalt complex solution with an octahedral structure produces α -cobalt hydroxide, while a blue cobalt complex solution with a tetrahedral structure produces β -cobalt hydroxide.

It was demonstrated for the first time that there is a strong relationship between the performance of the cobalt oxide catalyst and its preceding hydroxide polymorph. In colour degradation using peroxymonosulphate/AOP it was found that the β -phase is more effective than that of the α -phase.

In comparison to similar methods utilising urea instead of ammonium hydroxide, the absence of an alcohol and the same mass of cobalt salt the yield was increased from 0.5 g to approximately 5 g. Therefore, this batch synthesis method shows promise for upscaling to a continuous method.

7.4 Recommendations for future research

This study was based on 100% and 50% alcohol concentrations and may be refined and enhanced by varying the concentrations used. It may also benefit from the optimisation of the hydro/solvothermal synthesis method described in terms of the reactant quantities used, as well as temperature and reaction time. The effect of anion should further be investigated by using more cobalt salts with various anions, using this method. This study only tested the degradation of synthetic dye solutions prepared in the laboratory as a simulation for the treatment of textile wastewater. Since textile wastewater contains various additives, the catalyst prepared in this study should be evaluated using actual textile wastewater. Further, β -cobalt hydroxide particles produced cobalt oxide with a high catalytic ability in peroxymonosulphate activation, while the α -phase did not. A comparison of cobalt oxide synthesized from α - and β -cobalt hydroxide in other applications such as sensors, magnetic, electric, opto-electric and energy storage devices, should be carried out in order to ascertain whether the β -phase will always be more effective.

REFERENCES

- Al-Ghoul, M., El-Rassy, H., Coradin, T. and Mokalled, T. (2010) Reaction-diffusion based co-synthesis of stable α - and β - cobalt hydroxide in bio-organic gels. *Journal of Crystal Growth*, 312: 856-862.
- Allawdini, G., Masrinda, S. and Pudukudy, M. (2014) The effect of pH on cobalt oxide nano particles synthesis. *Aust. J. Basic & App. Sci.*, 8(19): 243-247.
- Anipsitakis, G. P. and Dionysiou, D. D. (2003) Degradation of organic contaminants in water with sulphate radicals generated by the conjunction of peroxymonosulfate with cobalt. *Environmental Science and Technology*, 37: 4790-4797.
- Athawale, A. A., Majumdar, M., Singh, H. and Navinkiran, K. (2010) Synthesis of Cobalt Oxide nanoparticles/ fibres in alcoholic medium using gamma-ray technique. *Defence Science Journal*, 60(5): 507-513.
- Beach, E., Brown, S., Shqau, K., Mottern, M., Warchol, Z. and Morris, P. (2007) Solvothermal synthesis of nanostructured NiO, ZnO and Co₃O₄ microspheres. *Material Letters*, 62: 1957-1960.
- Cao, W. and Wang, W. (2016) Three-dimensional flower-like α -(Co(OH)₂) architectures assembled by nanoplates for lithium ion batteries. *Material Letters*, 185: 495-498.
- Chani, M. T. S., Khan, S. B., Karimov, K. S., Asiri, A. M., Akhtar, K. and Arshad, M. N. (2015) Synthesis and pressure sensing properties of the pristine cobalt oxide nanopowder. *International Journal of Electrochemical Science*, 10: 10433-10444.
- Chen, K., Lo, S., Chang, L., Egerton, R., Kai, J., Lin, J. and Chen, F. (2007) Valence state map of iron oxide thin film obtained from electron spectroscopy imaging series. *Micron*, 38: 354-361.
- Cheng, J. P., Liu, L., Zhang, J., Liu, F. and Zhang, X. B. (2014) Influences of anion exchange and phase transformation on the supercapacitive properties of α -Co(OH)₂. *Journal of Electroanalytical Chemistry*, 722-723: 23-31.
- Choi, H. M., Lee, S., Moon, S.,

- Phan, T. N., Jeon, S. G. and Ko, C. H. (2016) Comparison between unsupported mesoporous Co_3O_4 and supported Co_3O_4 mesoporous silica as catalysts for N_2O decomposition. *Catalysis Communications*, 82: 50-40.
- Chowdhury, M., Oputu, O., Kebede, M., Cummings, F., Cespedes, O., Maelsand, A. and Fester, V. (2015) Rapid and large-scale synthesis of Co_3O_4 octahedron particles with very high catalytic activity, good supercapacitance and unique magnetic property. *Royal Society of Chemistry*, DOI:10.1039/C5RA20763K.
- Cushing, B. L., Kolesnichenko, V.L. and O'Connor, C.J. (2004) Recent advances in the liquid-phase syntheses of inorganic nanoparticles. *Chemical Reviews*, 104(9): 3893- 3946.
- Demond, A. H. and Lindner, A. S. (1993) Estimation of interfacial tension between organic liquids and water. *Environmental Science and Technology*, 27: 2318-2331.
- Deng, Y. and Zhao, R. (2015) Advanced oxidation processes (AOPs) in wastewater treatment. *Current Pollution Reports*, 1: 167-176.
- Egerton, R. F. (2005) *Physical Principles of Electron Microscopy*. New York: Springer Science + Business Media, Inc.
- El-Batlouni, H., El-Rassy, H. and Al-Ghoul, M. (2008) Cosynthesis, coexistence, and self- organization of α - and β -cobalt hydroxide based on diffusion and reaction in organic gels. *The journal of physical chemistry*, 112: 7755-7757.
- Filipponi, L. and Sutherland, D. (2012) *Nanotechnologies: Principles, Application, Implications and Hands-on Activities*. Luxembourg: European Union.
- Freitas de Freitas, L., Varca, G. H. C., Batista, J. G. D. S. and Lugao, A. B. (2018) An overview of the synthesis of gold nanoparticles using radiation techniques *Nanomaterials* 2018, 8 (11) 939; DOI: 10.3390/nano8110939.
- Gamonchuan, J., Poosimma, P., Saito, K., Khaorapapong, N. and Ogawa, M. (2016) The effect of alcohol type on the thickness of silica layer of $\text{Co}_3\text{O}_4@ \text{SiO}_2$ core-shell

particle. *Colloids and Surfaces A: Physicochemical and Engineering Aspects*, 511: 39-46.

Guo, J., Chen, L., Zhang, X., Jiang, B. and Ma, L. (2014) Sol-gel synthesis of mesoporous Co_3O_4 octahedra toward high-performance anodes for lithium-ion batteries. *Electrochimica Acta*, 129: 410-415.

He, T., Chen, D. and Jiao, X. (2004) Controlled synthesis of Co_3O_4 nanoparticles through oriented aggregation. *Chemistry of Materials*, 16: 737-743.

Henry, C.R. (2007) Catalysis by Nanoparticles. In *NanoScience and Technology: Nanocatalysis*. Berlin: Springer, pp. 245-268.

Hu, Z., Xie, Y., Wang, Y., Xie, L., Fu, G., Jin, X., Zhang, Z., Yang, Y. and Wu, H. (2009) Synthesis of α -Cobalt Hydroxides with difference intercalated anions and effects of intercalated anions on their morphology, Basal Plane Spacing, and Capacitive property. *Journal of Physical Chemistry*, 113: 12502-12508.

Huang, J., Ren, H., Chen, K. and Shim, J. (2014) Controlled synthesis of porous Co_3O_4 micro/nanostructures and their photocatalysis property. *Superlattices and Microstructures*, 75: 843-856.

Huang, Y., Wang, Z., Liu, Q., Wang, X., Yuan, Z. and Liu, J. (2017) Effects of chloride on PMS-based pollutant degradation: A substantial discrepancy between dyes and their common decomposition intermediate (phthalic acid). *Chemosphere*, 187: 338-346.

Jamil, S., Janjua, M.R.S.A. and Ahmad, T. (2014) The synthesis of flower shaped microstructures of Co_3O_4 by solvothermal approach and investigation of its catalytic activity. *Solid State Sciences*, 36: 73-79.

Jing, X., Song, S., Wang, J., Ge, L., Jamil, S., Liu, Q., Mann, T., He, Y., Zhang, M., Wei, H. and Liu, L. (2012) Solvothermal synthesis of morphology controllable CoCO_3 and their conversion to Co_3O_4 for catalytic application. *Powder Technology*, 217: 624-628.

- Kim, M. and Huh, Y. (2011) Morphology-controlled synthesis of octahedron and hexagonal plate of Co_3O_4 . *Materials Letters*, 65: 650-652.
- Li, H., Fei, G. T., Fang, M., Cui, P., Guo, X., Yan, P. and Zhang, L. D. 2011. Synthesis of urchin-like Co_3O_4 hierarchical micro/nanostructures and their photocatalytic activity. *Applied Surface Science*, 257: 6527-6530.
- Li, Y., Tan, H., Yang, X., Goris, B., Verbeeck, J., Bals, S., Colson, P., Cloots, R., Van Tendeloo, G. and Su, B. (2011) Well shaped Mn_3O_4 nano-octahedra with anomalous magnetic behaviour and enhanced photodecomposition properties. *Small: Nanoparticles*, 4: 475-483.
- Lu, F., Zhou, P., Han, J. and Yu, F. (2015) Fischer-Tropsch synthesis of liquid hydrocarbons over mesoporous SBA-15 supported cobalt catalysts. *The Royal Society of Chemistry*, 5: 59792-59803.
- Mahmoud, W. E. and Al-Agel, F. A. (2011) A novel strategy to synthesize cobalt hydroxide and Co_3O_4 nanowires. *Journal of Physics and Chemistry of Solids*, 72: 904-907.
- Meng, X., Feng, M., Zhang, H., Ma, Z. and Zhang, C. (2017) Solvothermal synthesis of cobalt/nickel layered double hydroxides for energy storage devices. *Journal of Alloys and Compounds*, 695: 3522-3529.
- Meriç, S., Kaptan, D. and Ölmez, T. (2004) Color and COD removal from wastewater containing Reactive Black 5 using Fenton's oxidation process. *Chemosphere*, 54: 435-441.
- Mishra, G., Dash, B. and Pandey, S. (2018) Layered double hydroxides: A brief review from fundamentals to application as evolving biomaterials. *Applied Clay Science*, 153: 172-186.
- National Geographic (2019). *Earth's Freshwater*, National Geographic, viewed 23 October 2019, <<https://www.nationalgeographic.org/media/earths-fresh-water/>>.

- Neta, P., Huie, R. E. and Ross, A. B. (1988) Rate constants for reactions of inorganic radicals in aqueous solution. *The Journal of Physical Chemistry*, 17 (3): 1027-1284.
- Ni, Y., Ge, X., Zhang, Z., Liu, H., Zhu, Z. and Ye, Q. (2001) A simple reduction-oxidation route to prepare Co_3O_4 nanocrystals. *Materials Research Bulletin*, 36: 2383-2387.
- Odularu, A. T. 2018. Metal Nanoparticles: thermal Decomposition, biomedical applications to cancer treatment, and future perspectives, *Bioinorganic Chemistry and Applications*, DOI: 10.1155/2018/9354708.
- Petkova, P. and Nedkov, V. (2013) Behavior of Co^{2+} cations in the aqueous and alcoholic solution of $\text{CoCl}_2 \cdot 6\text{H}_2\text{O}$. *ACTA Physica Polonica A*, 123 (2): 207-208.
- Rajurkar, N. and Ambekar, B. (2015) Studies on Liesegang rings of cobalt hydroxide in 1% agar gel medium. *Journal of Molecular Liquids*, 204: 205-209.
- Rivas, L., Gimeno, O., Carbajo, M. and Borrallho, T. (2009) Catalytic decomposition of potassium monopersulfate. Influence of variables. *World Academy of Science, Engineering and Technology*, 57: 218-222.
- Saputra, E., Duan, X., Pinem, J. A., Bahri, S. and Wang, S. (2017) Shape-controlled Co_3O_4 catalysts for advanced oxidation of phenolic contaminants in aqueous solutions. *Separation and Purification Technology*, 186: 213 – 217.
- Saputra, E., Muhammad, S., Sun, H., Ang, H., Tadé, M. O. and Wang, S. (2014) Shape-controlled activation of peroxymonosulfate by single crystal $\alpha\text{-Mn}_2\text{O}_3$ for catalytic phenol degradation in aqueous solution. *Applied Catalysis B: Environmental*, 154-155: 246-251.
- Sivagami, K., Sakthivel, K. P. and Nambi, I. M. (2018) Advanced oxidation processes for the treatment of tannery wastewater. *Journal of Environmental Chemical Engineering*, 6: 3656 – 3663.
- Thota, S., Kumar, A. and Kumar, J. (2009) Optical, electrical and magnetic properties of Co_3O_4 nanocrystallites obtained by thermal decomposition of sol-gel derived oxalates. *Materials Science and Engineering B*, 164: 30-37.

Vazquez, G. Alvarez, E. and Navaza, J. M. (1995) Surface tension of alcohol and water from 20 to 50°C, *Journal of Chemical and Engineering Data*, 40: 611-614.

Vinod, C. P. (2010) Surface science as a tool for probing nanocatalysis phenomena. *Catalysis Today*, 154: 113-117.

Wang, B., Lin, H. and Yin, Z. (2011) Hydrothermal synthesis of β -cobalt hydroxide with various morphologies in water/ethanol solutions. *Materials Letters*, 65: 41-43.

Warang, T., Patel, N., Fernandes, R., Bazzanella, N. and Miotello, A. (2013) Co_3O_4 nanoparticles assembled coatings synthesized by different techniques for photo-degradation of methylene blue dye. *Applied Catalysis B: Environmental*, 132-133: 204-211.

Xiong, H., Zhang, Y., Liew, K. and Li, J. (2008) Fischer-Tropsch synthesis: the role of pore size for Co/SBA-15 catalysts. *Journal of Molecular Catalysis A: Chemical*, 295: 68-76.

Xue, X., Yuan, S., Xing, L., Hui, Z., He, B. and Chen, Y. (2011) Porous Co_3O_4 nanoneedle arrays growing directly on copper foils and their ultrafast charging/discharging as lithium-ion battery anodes. *The Royal Society of Chemistry*, 47: 4718-4720.

Yang, H., Hu, Y., Zhang, X. and Qui, G. (2004) Mechanochemical synthesis of cobalt oxide nanoparticles. *Materials Letters*, 58: 387-389.

Yang, Y., Huang, K., Liu, R., Wang, L., Zeng, W. and Zhang, P. (2007) Shape-controlled synthesis of nanocubic Co_3O_4 by hydrothermal oxidation method. *Transactions of Nonferrous Metals Society of China*, 17: 1082-1086.

Yang, Y., Jiang, J., Lu, X., Ma, J. and Liu, Y. (2015) Production of sulfate radical and hydroxyl radical by reaction of ozone with peroxymonosulfate: A novel advanced oxidation process. *Environmental Science & Technology*, 49: 7330 – 7339.

Yang, Y., Liu, R., Huang, K., Wang, L., Liu, S. and Zeng, W. (2007) Preparation and electrochemical performance of nanosized Co₃O₄ via hydrothermal method. *Transactions of Nonferrous Metals Society of China*, 17: 1334-1338.

Yildiz, Y. (2017) General Aspects of the Cobalt Chemistry. *Intechopen*, DOI:10.5772/intechopen.71089.

Appendices

Appendix A. XRD Spectra for the synthesized particles

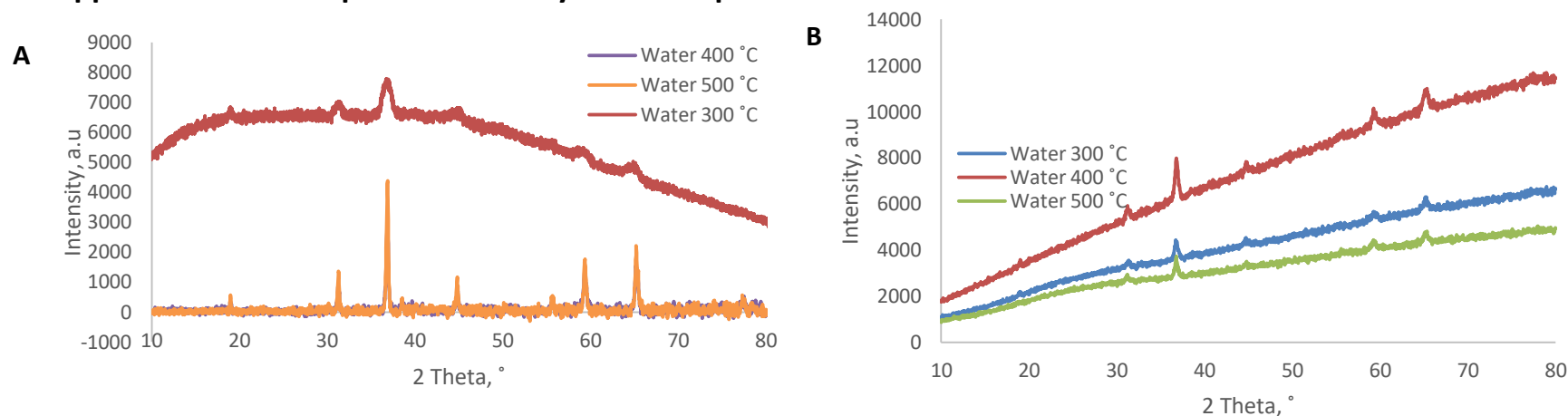


Figure A.1: XRD spectra for cobalt oxide particles synthesized from a) cobalt chloride hexahydrate base salt and b) cobalt nitrate hexahydrate base salt in water, calcined at 300, 400 and 500 °C

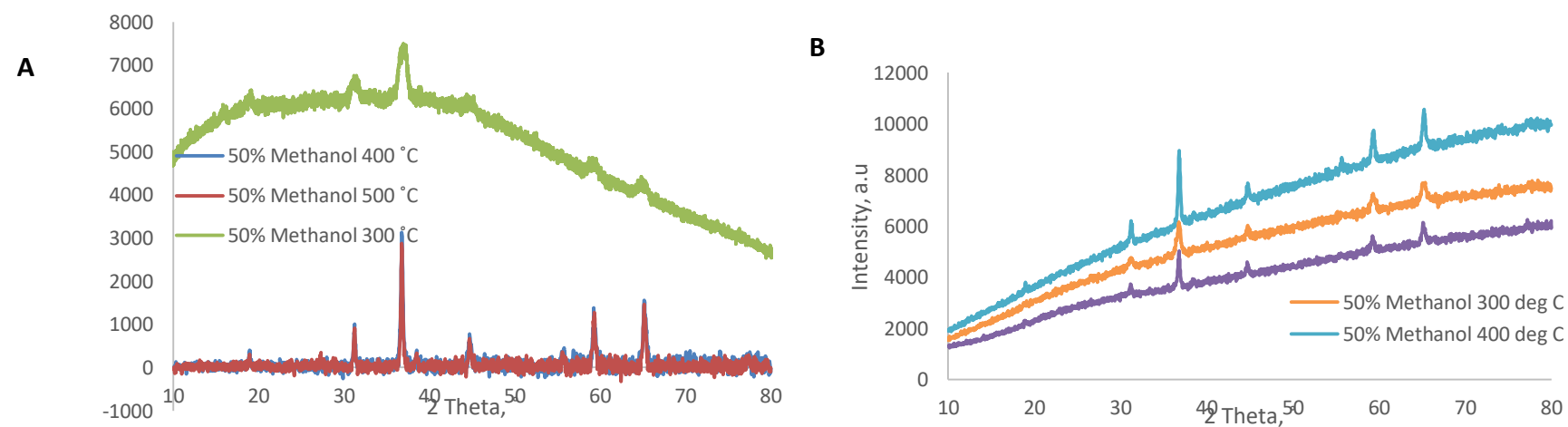


Figure A.2: XRD spectra for cobalt oxide particles synthesized from a) cobalt chloride hexahydrate base salt and b) cobalt nitrate hexahydrate base salt in 50% methanol, calcined at 300, 400 and 500 °C

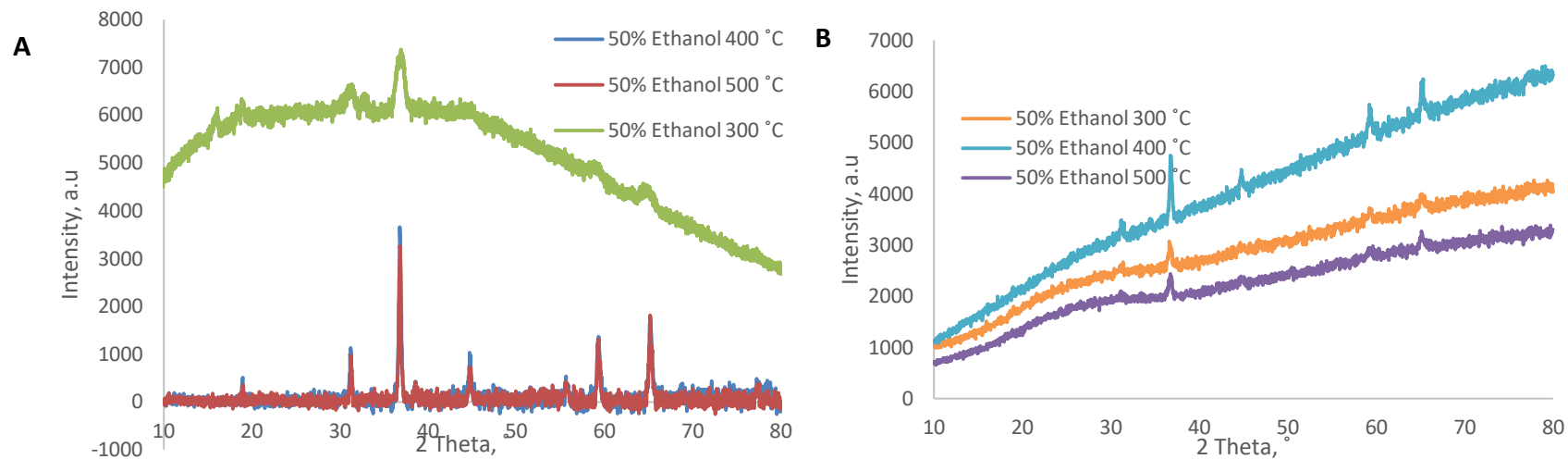


Figure A.3: XRD spectra for the cobalt oxide particles synthesized from a) cobalt chloride hexahydrate base salt and b) cobalt nitrate hexahydrate base salt in 50% ethanol, calcined at 300, 400 and 500°C

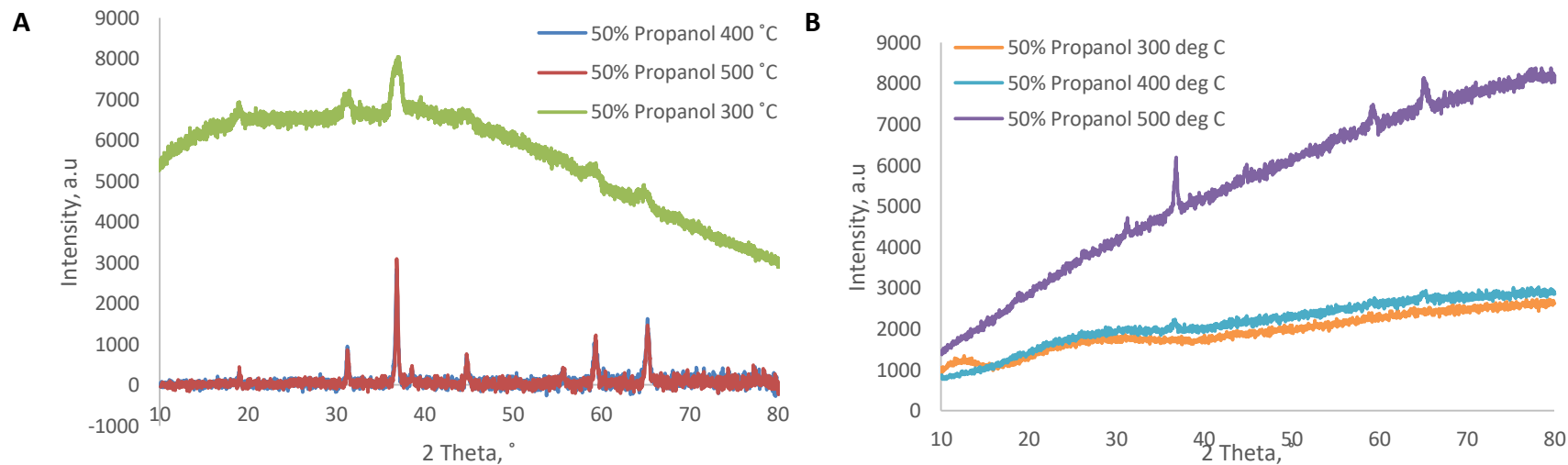


Figure A.4: XRD spectra for cobalt oxide particles synthesized from a) cobalt chloride hexahydrate base salt and b) cobalt nitrate hexahydrate base salt in 50% propanol, calcined at 300, 400 and 500°C

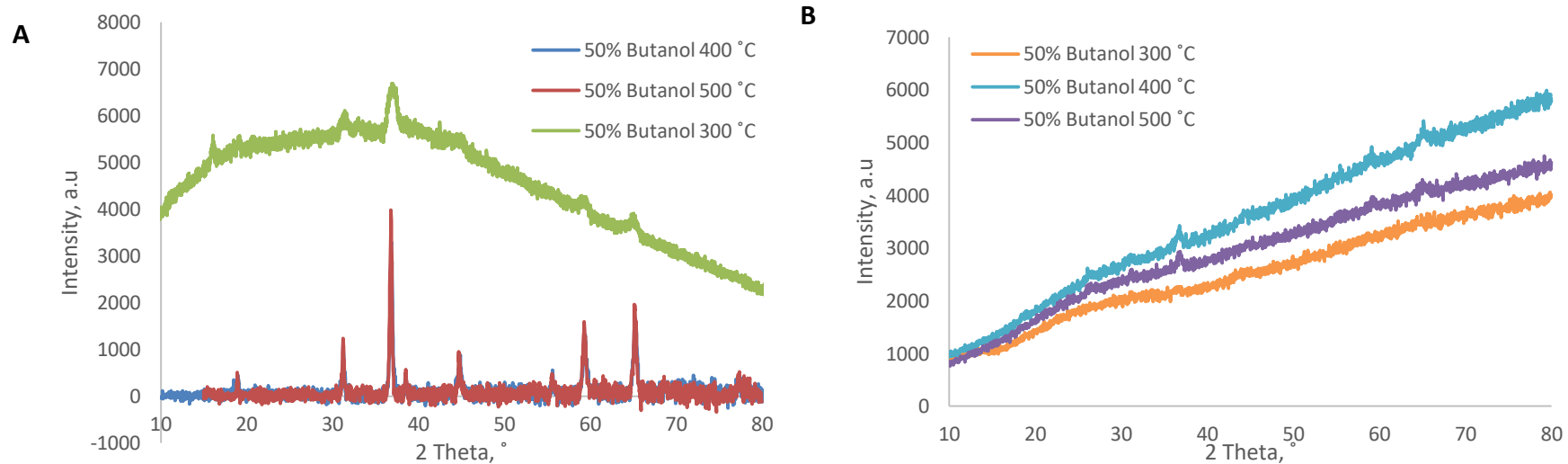


Figure A.5: XRD spectra for the cobalt oxide particles synthesized from a) cobalt chloride hexahydrate base salt and b) cobalt nitrate hexahydrate base salt in 50% butanol, calcined at 300, 400 and 500°C

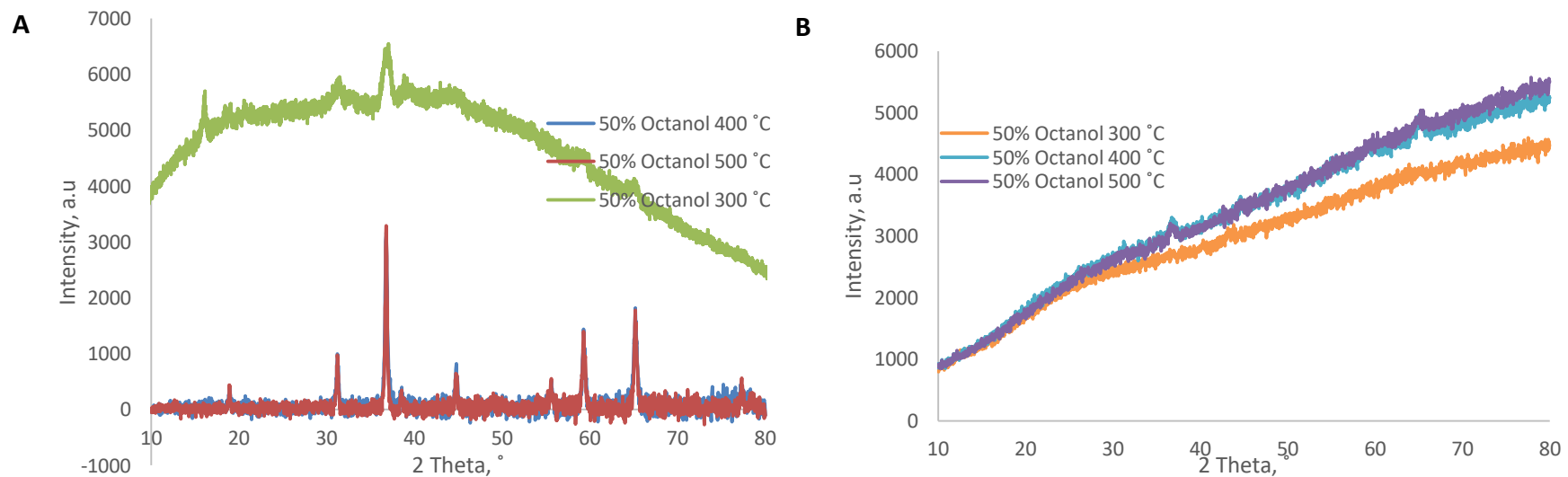


Figure A.6: XRD spectra for the cobalt oxide particles synthesized from a) cobalt chloride hexahydrate base salt and b) cobalt nitrate hexahydrate base salt in 50% octanol, calcined at 300, 400 and 500°C

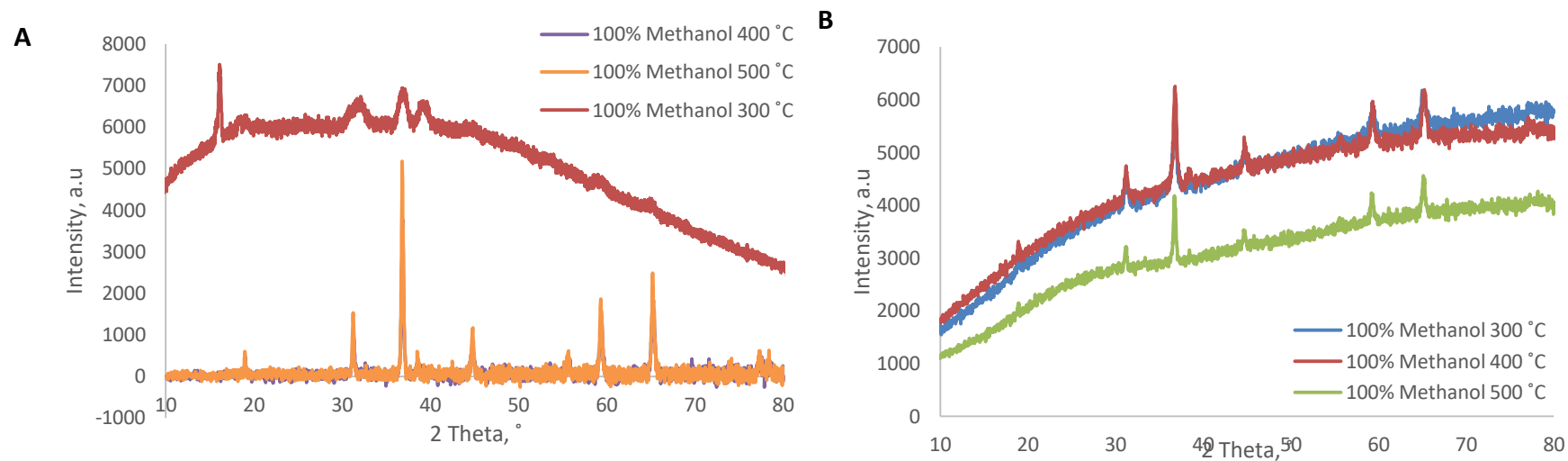


Figure A.7: XRD spectra for the cobalt oxide particles synthesized from a) cobalt chloride hexahydrate base salt and b) cobalt nitrate hexahydrate base salt in 100% methanol, calcined at 300, 400 and 500 °C

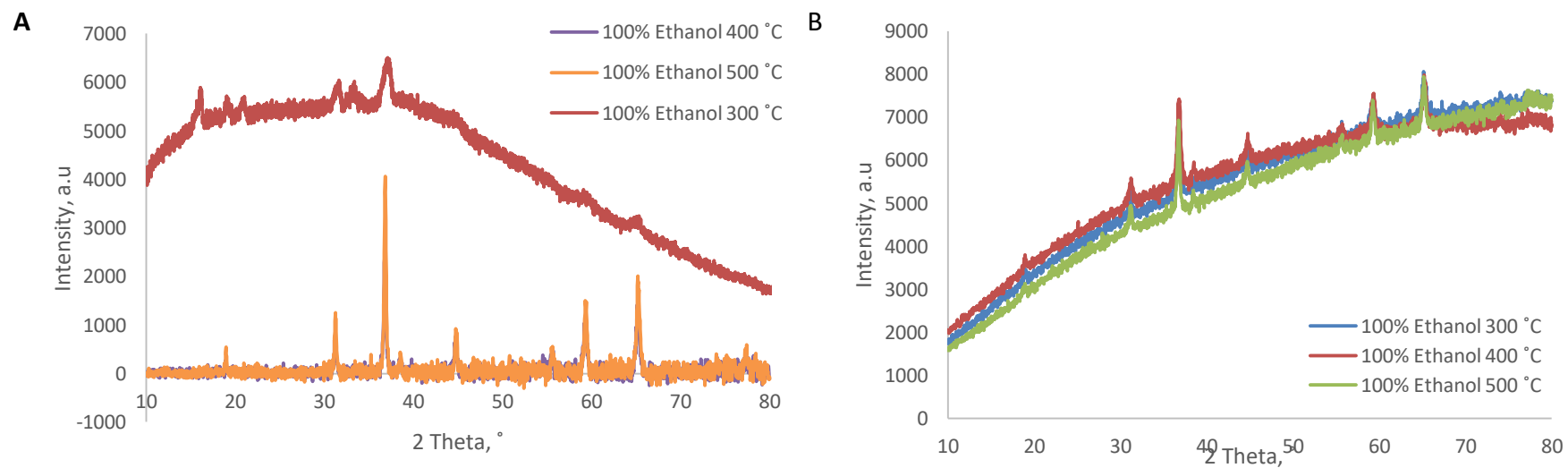


Figure A.8: XRD spectra for the cobalt oxide particles synthesized from a) cobalt chloride hexahydrate base salt and b) cobalt nitrate hexahydrate base salt in 100% ethanol, calcined at 300, 400 and 500 °C

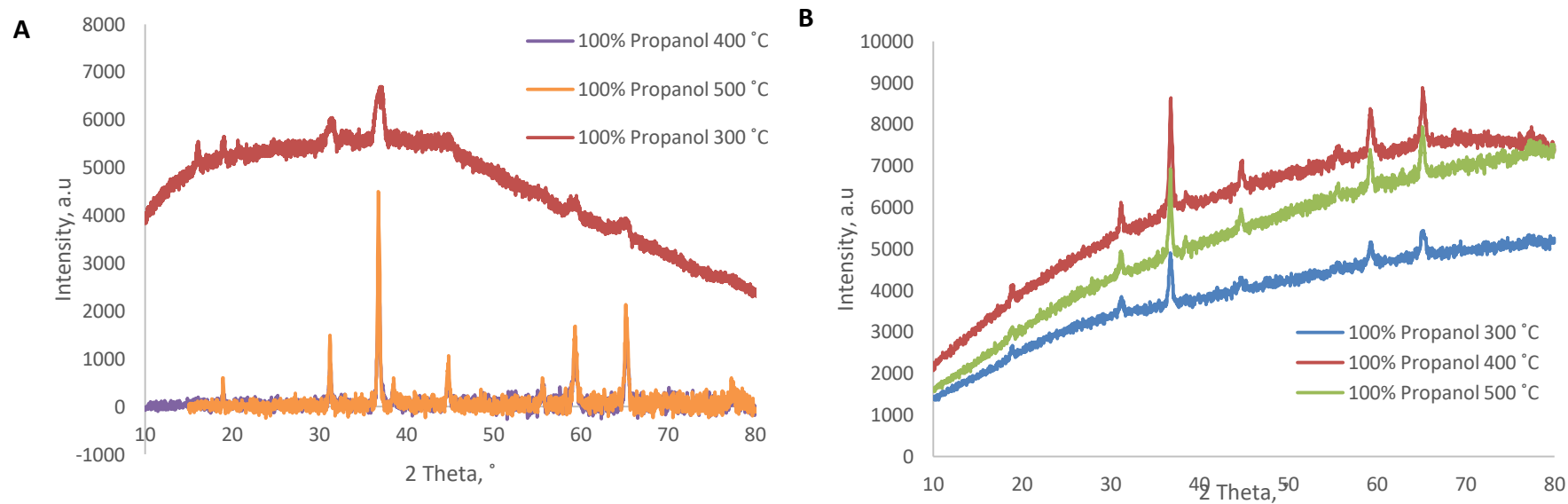


Figure A.9: XRD spectra for the cobalt oxide particles synthesized from a) cobalt chloride hexahydrate base salt and b) cobalt nitrate hexahydrate base salt in 100% propanol, calcined at 300, 400 and 500 °C

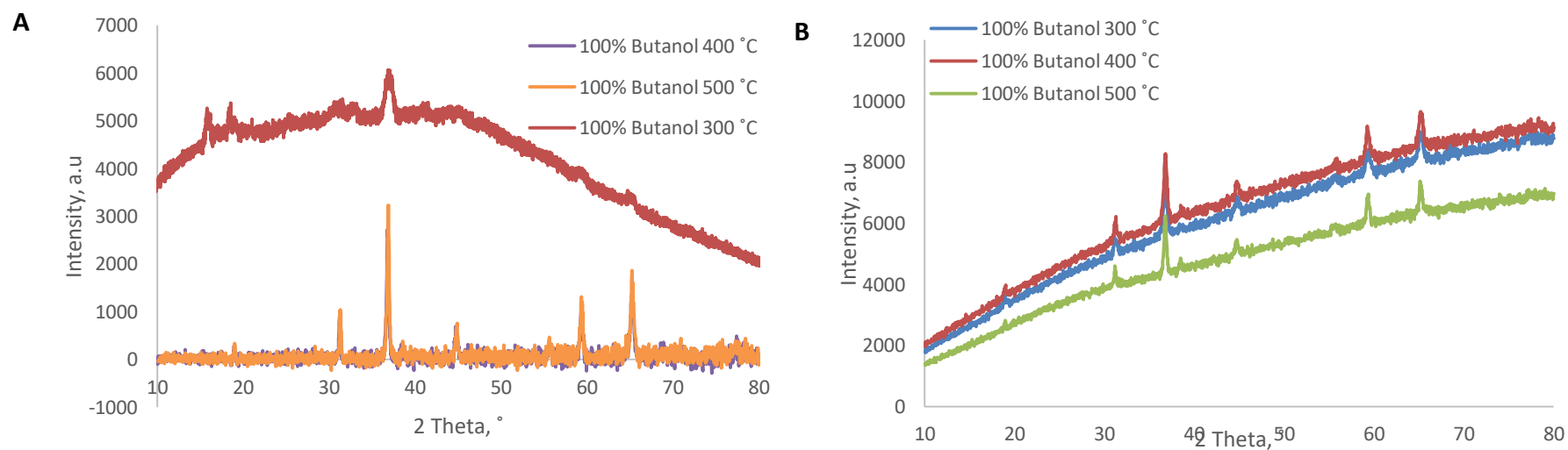


Figure A.10: XRD spectra for the cobalt oxide particles synthesized from a) cobalt chloride hexahydrate base salt and b) cobalt nitrate hexahydrate base salt in 100% butanol, calcined at 300, 400 and 500 °C

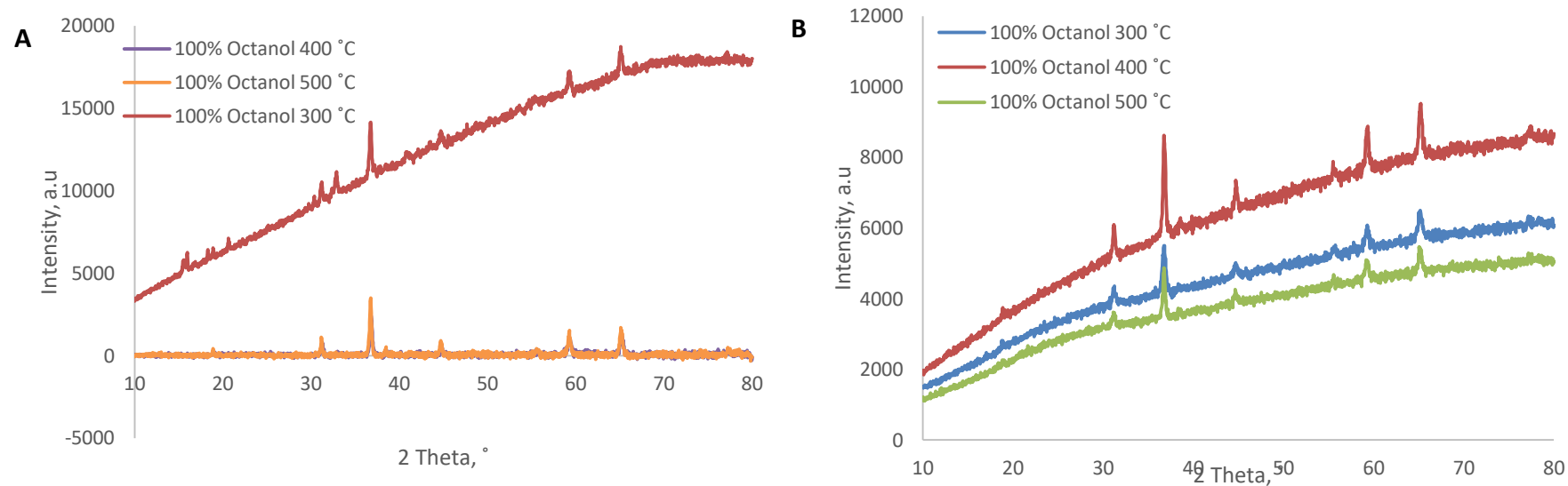


Figure A. 11: XRD spectra for the cobalt oxide particles synthesized from a) cobalt chloride hexahydrate base salt and b) cobalt nitrate hexahydrate base salt in 100% octanol, calcined at 300, 400 and 500 °C

Appendix B. FTIR spectra for the synthesized particles

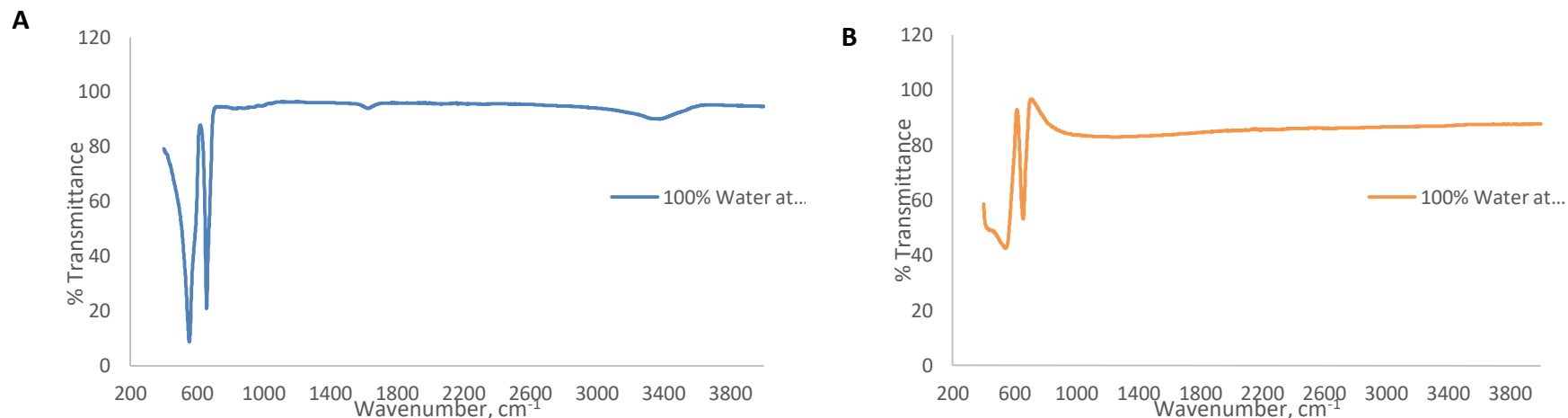


Figure B.1: FT-IR spectra for the cobalt oxide particles synthesized from a) cobalt chloride hexahydrate and b) cobalt nitrate hexahydrate in water, calcined at 300°C

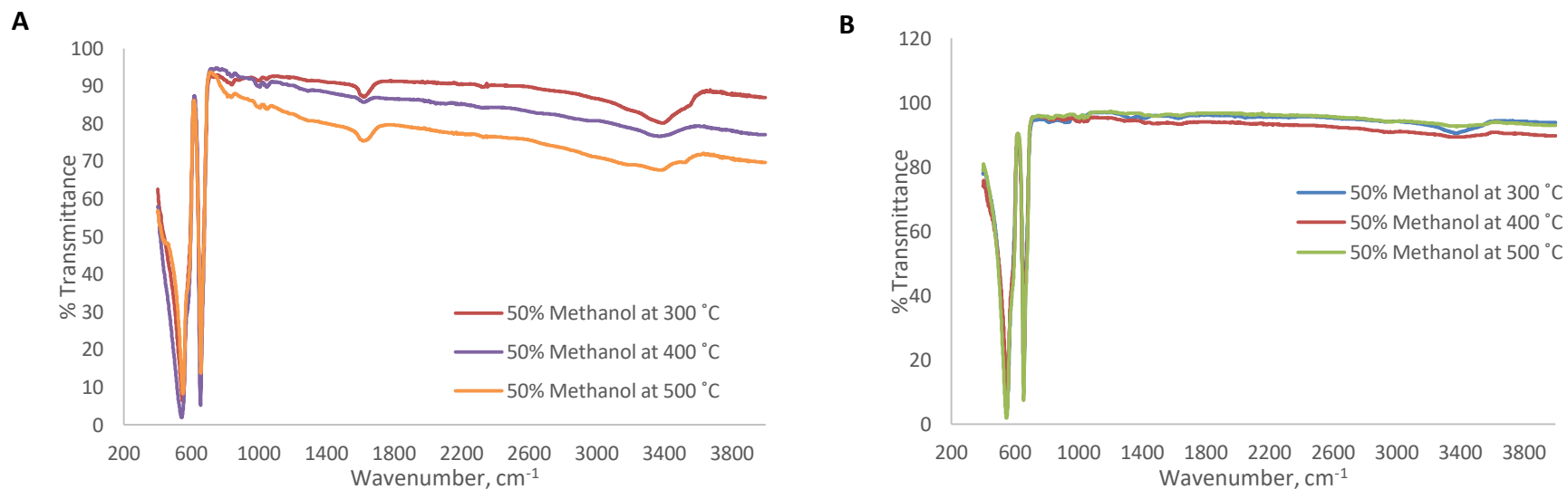


Figure B.2: FT-IR spectra for the cobalt oxide particles synthesized from a) cobalt chloride hexahydrate base salt and b) cobalt nitrate hexahydrate base salt in 50% methanol, calcined at 300, 400 and 500°C

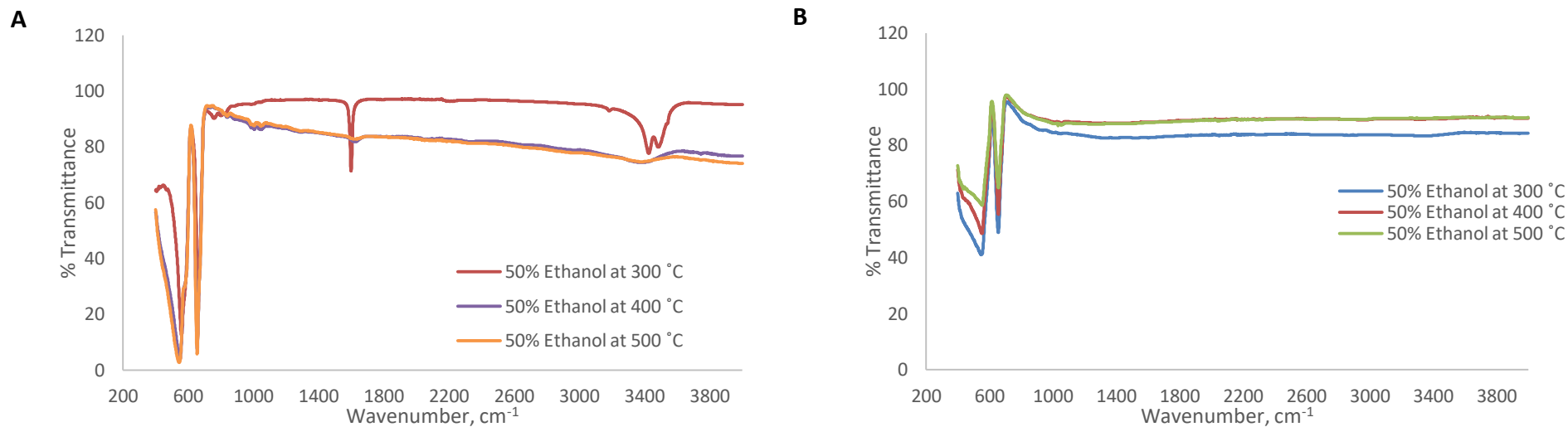


Figure B.3: FT-IR spectra for the cobalt oxide particles synthesized from a) cobalt chloride hexahydrate base salt and b) cobalt nitrate hexahydrate base salt in 50% ethanol, calcined at 300, 400 and 500 °C

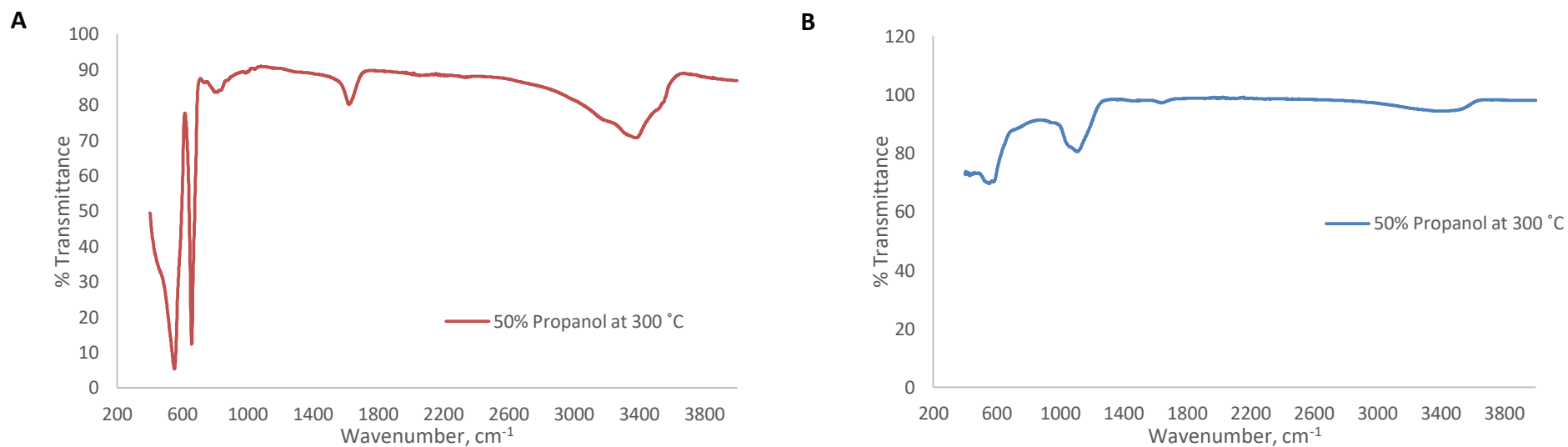


Figure B.4: FT-IR spectra for the cobalt oxide particles synthesized from a) cobalt chloride hexahydrate base salt and b) cobalt nitrate hexahydrate base salt in 50% propanol, calcined at 300 °C

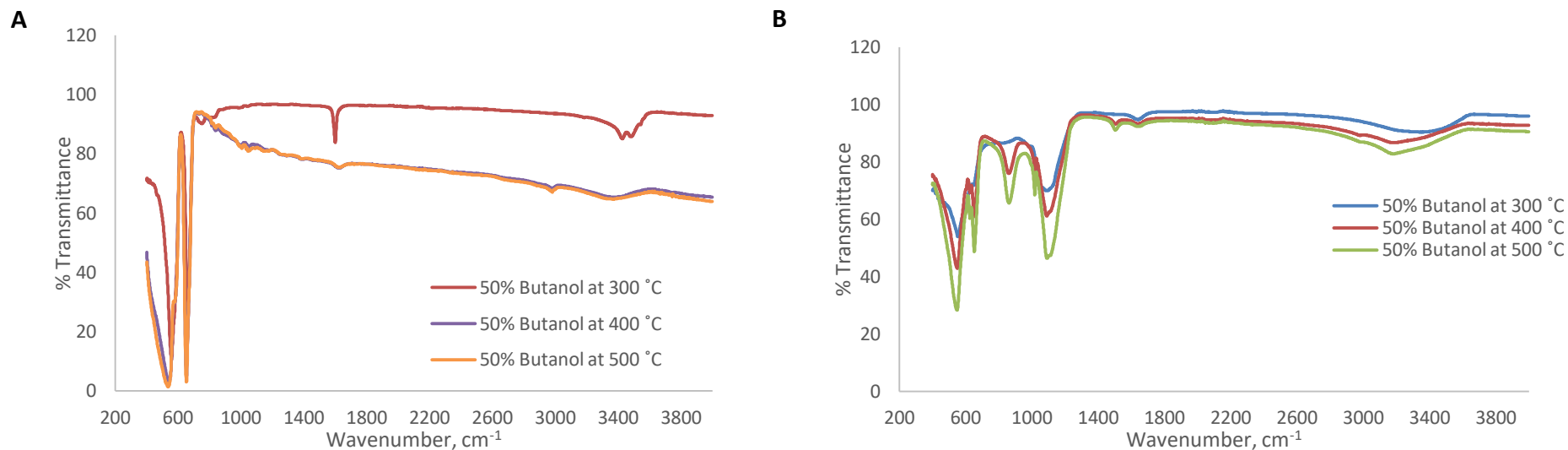


Figure B.5: FT-IR spectra for the cobalt oxide particles synthesized from a) cobalt chloride hexahydrate base salt and b) cobalt nitrate hexahydrate base salt in 50% butanol, calcined at 300, 400 and 500 °C

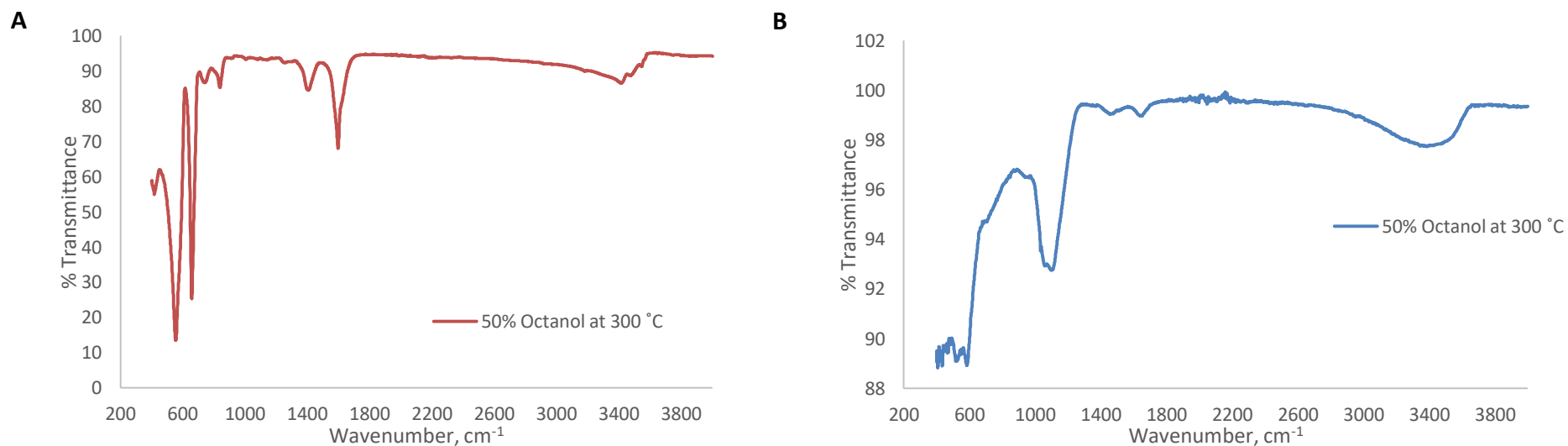


Figure B.6: FT-IR spectra for the cobalt oxide particles synthesized from a) cobalt chloride hexahydrate base salt and b) cobalt nitrate hexahydrate base salt in 50% octanol, calcined at 300 °C

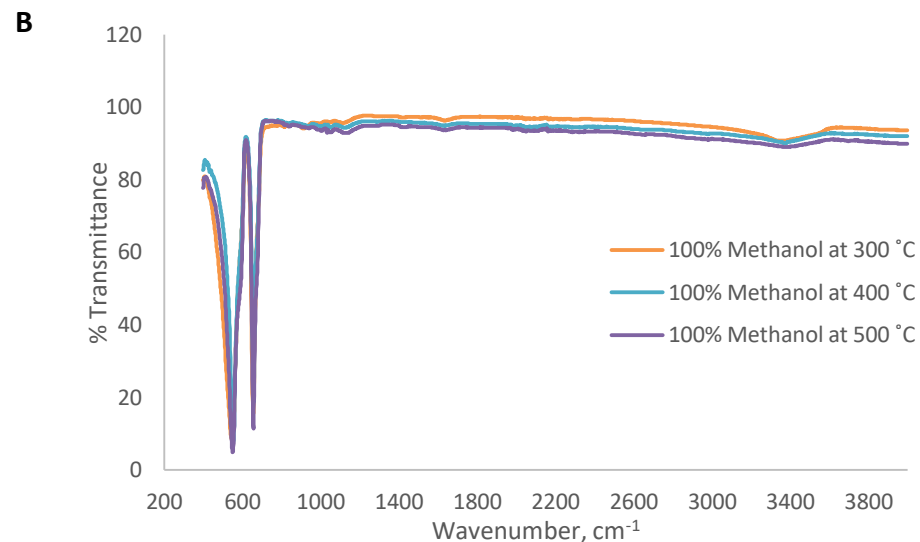
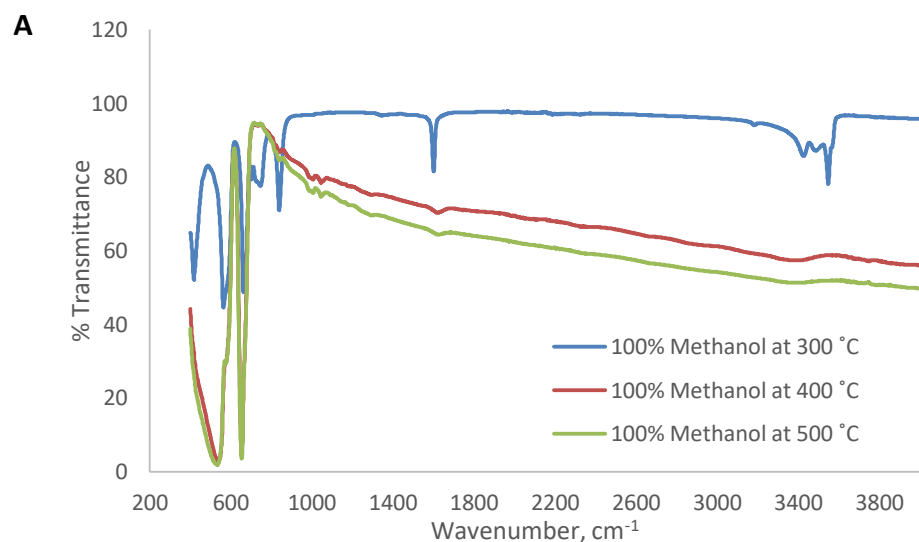


Figure B.7: FT-IR spectra for the cobalt oxide particles synthesized from a) cobalt chloride hexahydrate base salt and b) cobalt nitrate hexahydrate base salt in 100% methanol, calcined at 300, 400 and 500 °C

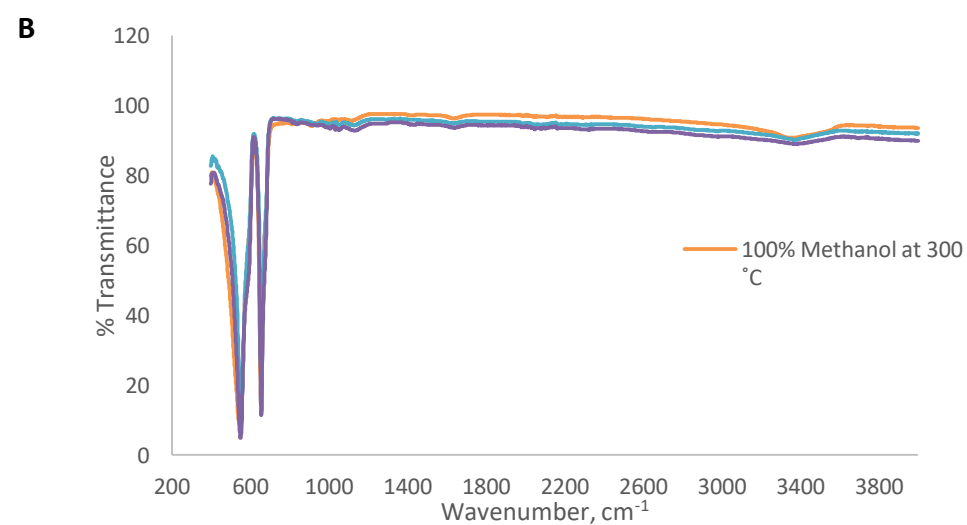
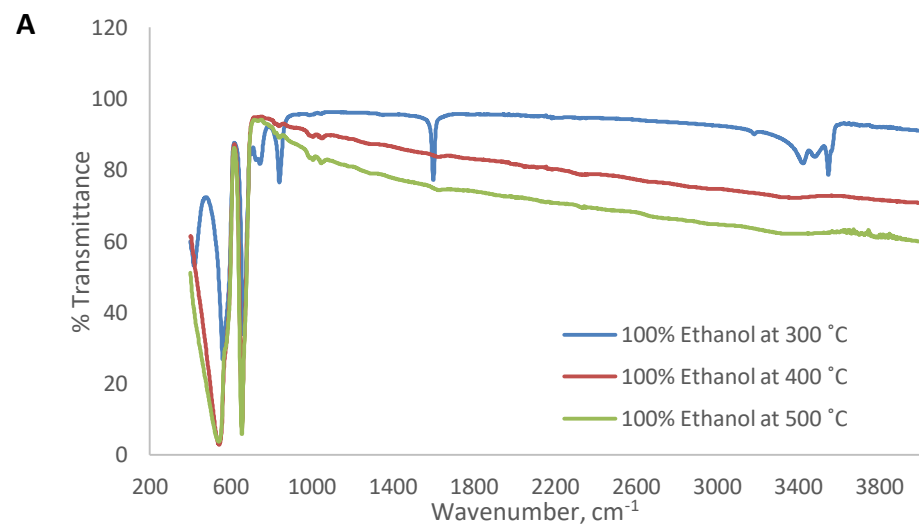


Figure B.8: FT-IR spectra of the cobalt oxide particles synthesized from a) cobalt chloride hexahydrate base salt and b) cobalt nitrate hexahydrate base salt in 100% ethanol, calcined at 300, 400 500 °C

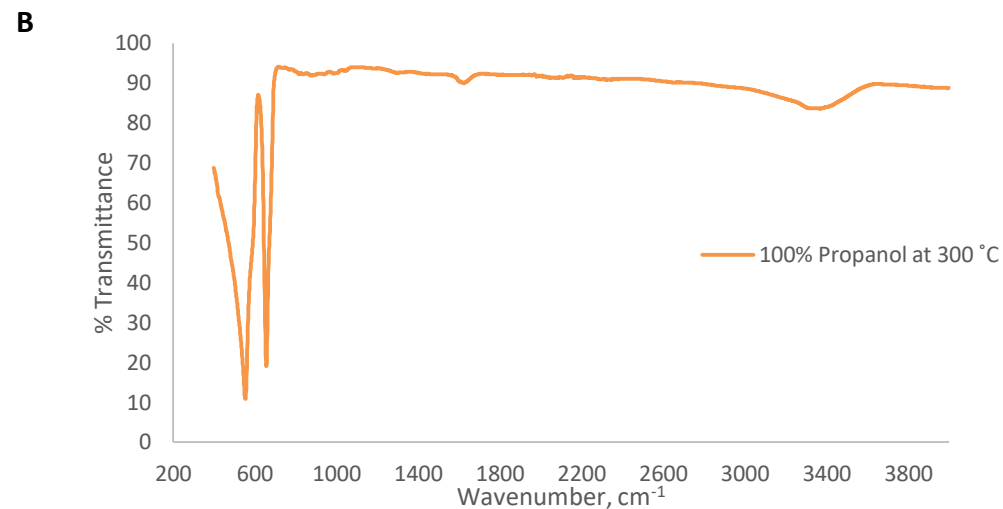
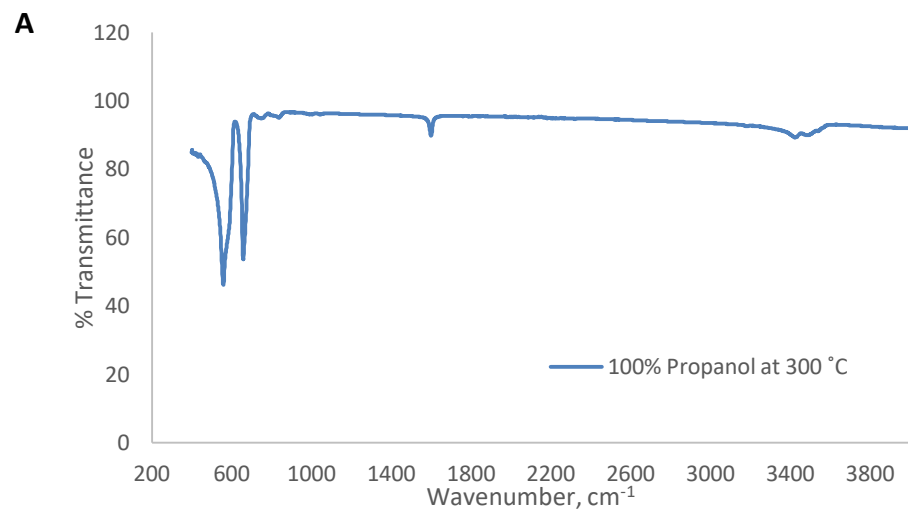


Figure B.9: FT-IR spectra for the cobalt oxide particles synthesized from a) cobalt chloride hexahydrate base salt and b) cobalt nitrate hexahydrate base salt in 100% propanol, 300°C

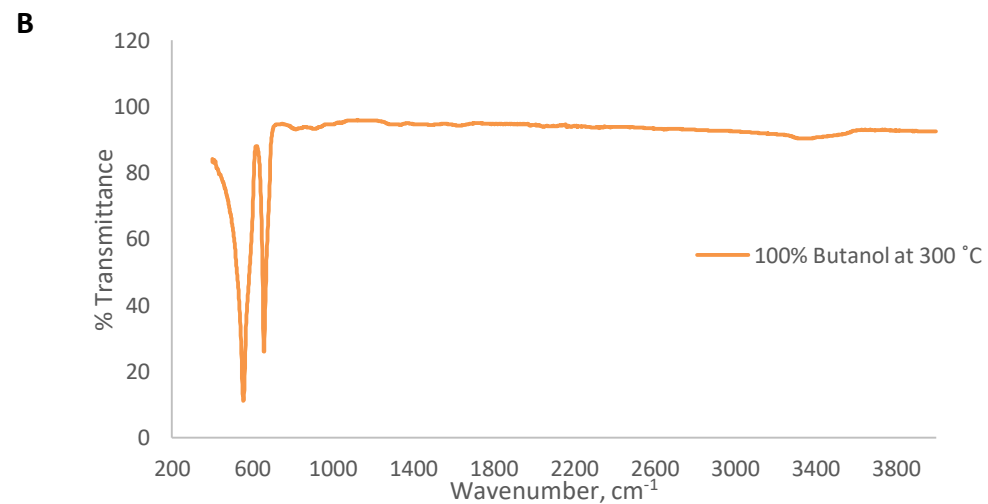
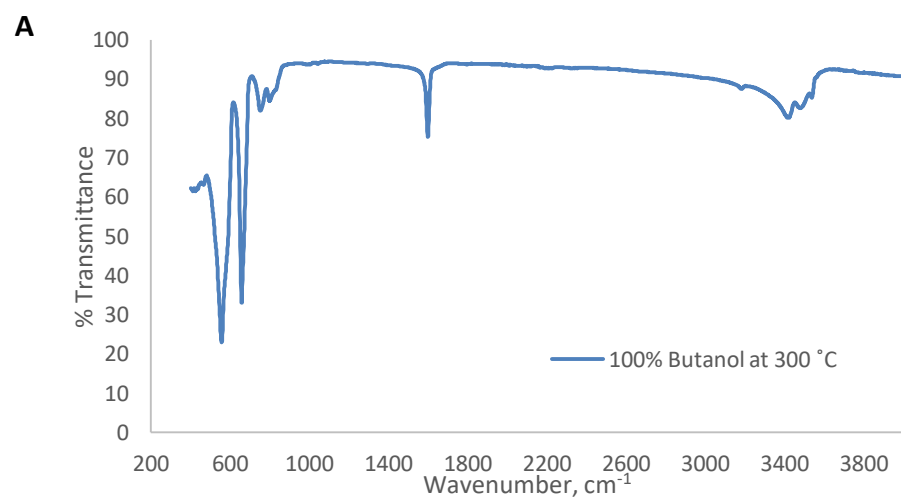


Figure B.10: FT-IR spectra for the cobalt oxide particles synthesized from a) cobalt chloride hexahydrate base salt and b) cobalt nitrate hexahydrate base salt in 100% butanol, calcined at 300°C

Appendix C. EDS spectra for the synthesized particles

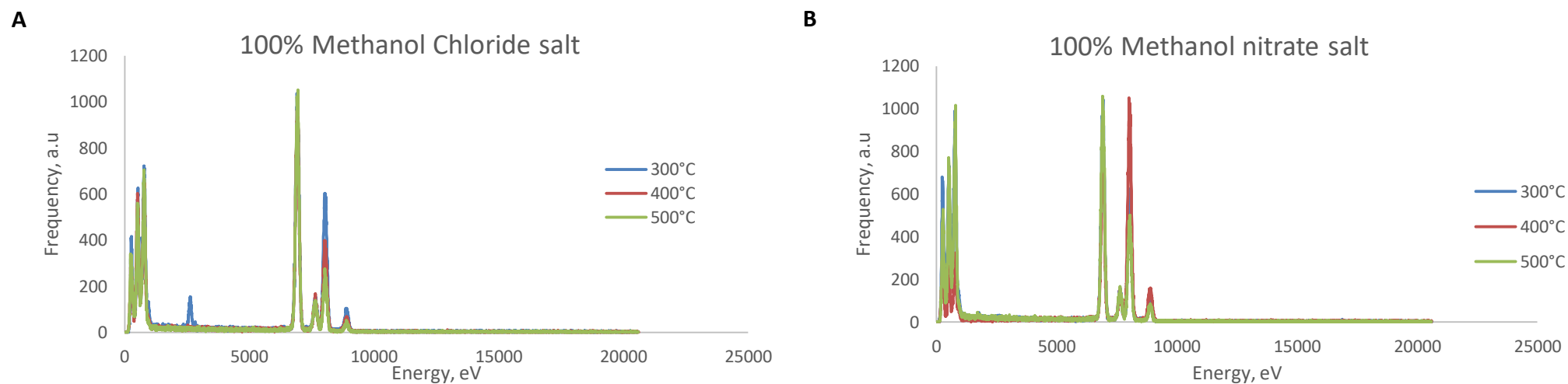


Figure C.1: EDS spectra for the cobalt oxide particles synthesized from a) cobalt chloride hexahydrate base salt and b) cobalt nitrate hexahydrate base salt in 100% methanol, calcined at 300, 400 and 500°C

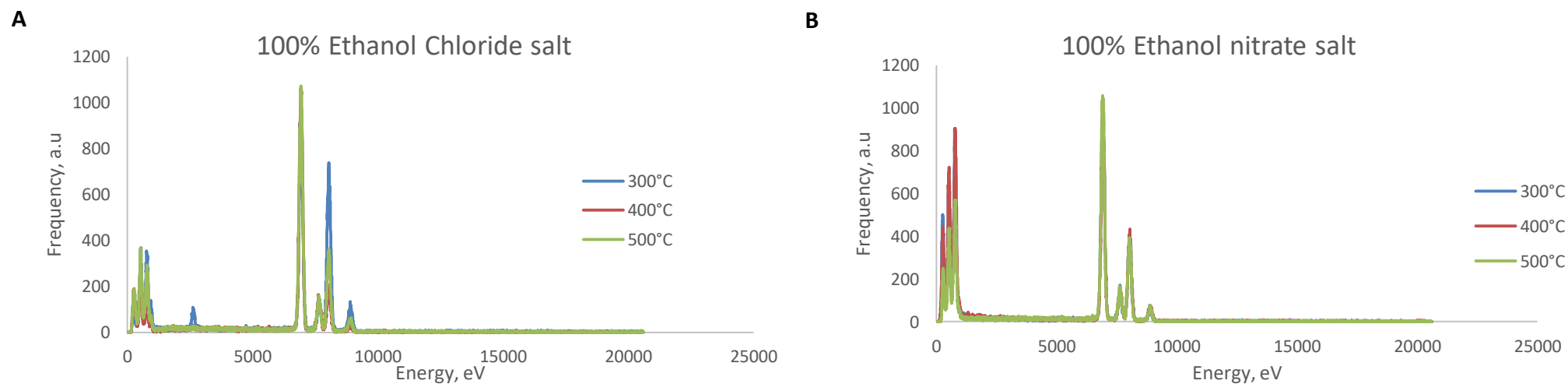


Figure C.2: EDS spectra for the cobalt oxide particles synthesized from a) cobalt chloride hexahydrate base salt and b) cobalt nitrate hexahydrate base salt in 100% ethanol, calcined at 300, 400 and 500°C

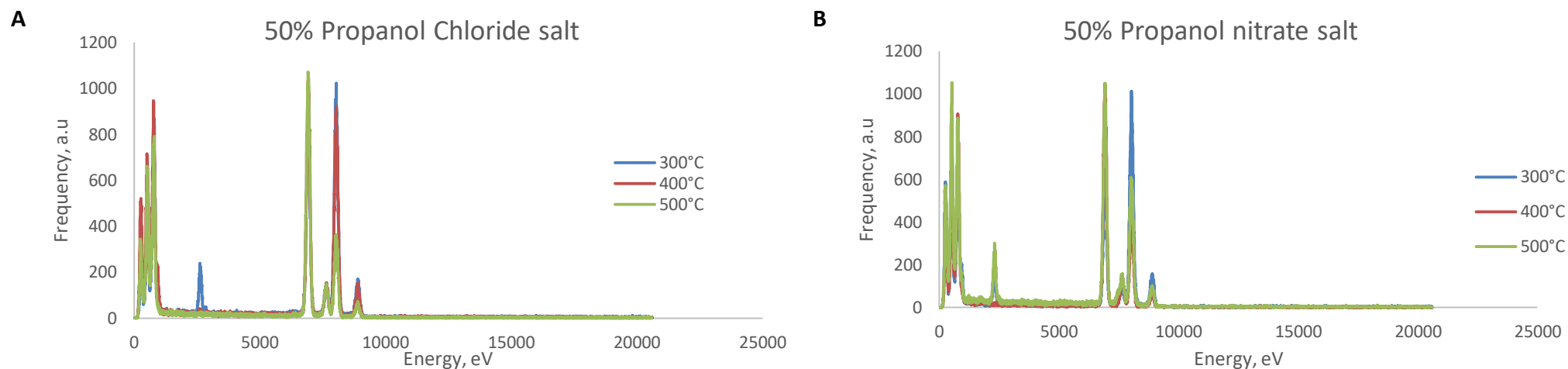


Figure C.3: EDS spectra for the cobalt oxide particles synthesized from a) cobalt chloride hexahydrate base salt and b) cobalt nitrate hexahydrate base salt in 50% propanol, calcined at 300, 400 and 500°C

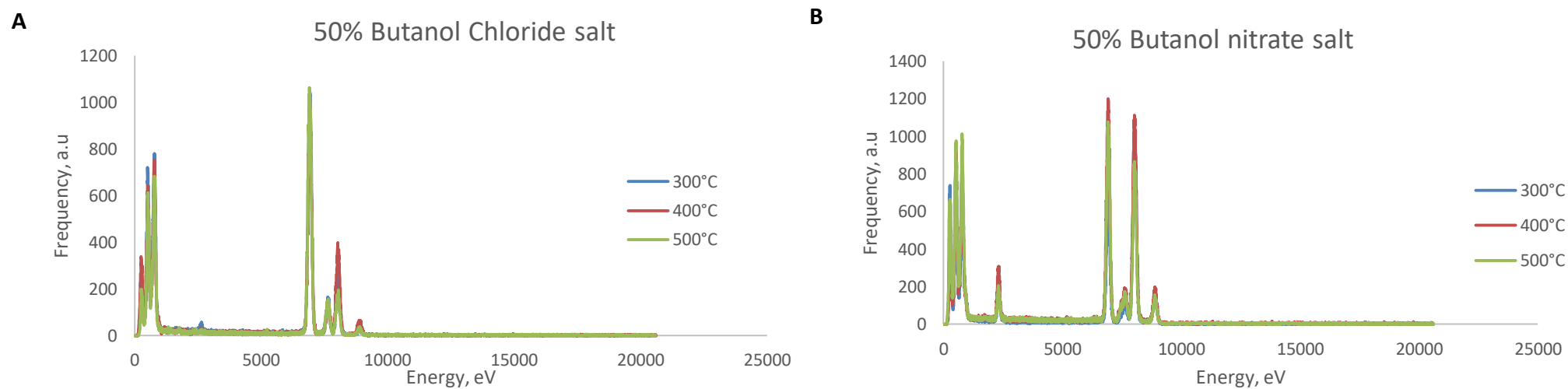


Figure C.4: EDS spectra for the cobalt oxide particles synthesized from a) cobalt chloride hexahydrate base salt and b) cobalt nitrate hexahydrate base salt in 50% butanol, calcined at 300, 400 and 500°C

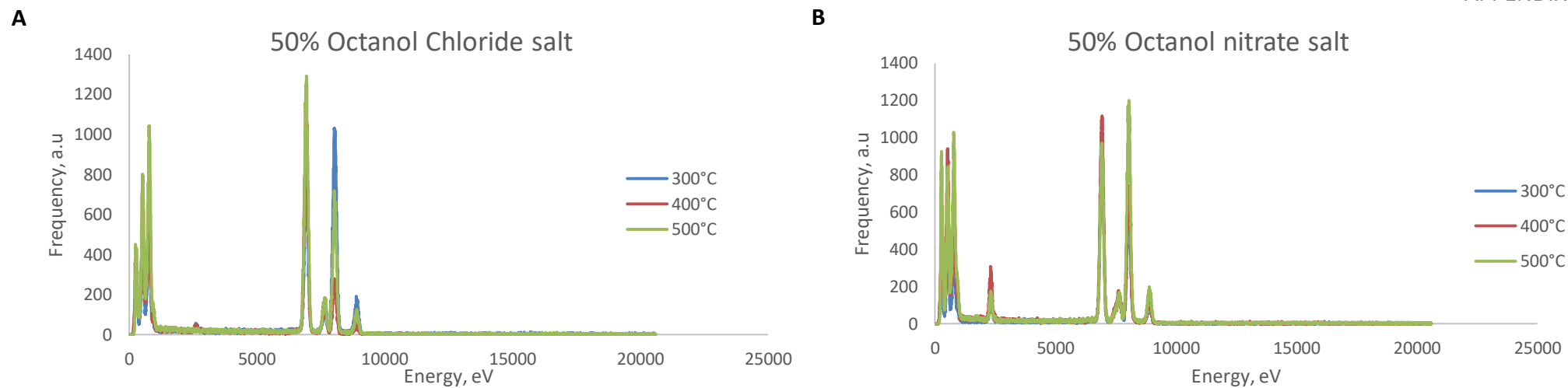


Figure C.5: EDS spectra for the cobalt oxide particles synthesized from a) cobalt chloride hexahydrate base salt and b) cobalt nitrate hexahydrate base salt in 50% octanol, calcined at 300, 400 and 500°C

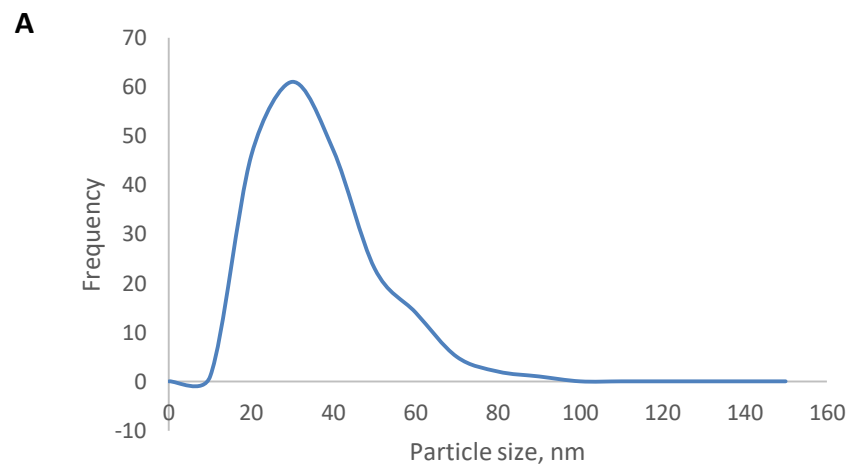
Appendix D. PSD curves for the synthesized particles

Figure D-1: PSD curves for the cobalt oxide particles synthesized from a) cobalt chloride hexahydrate base salt in 100% water, calcined at 300°C

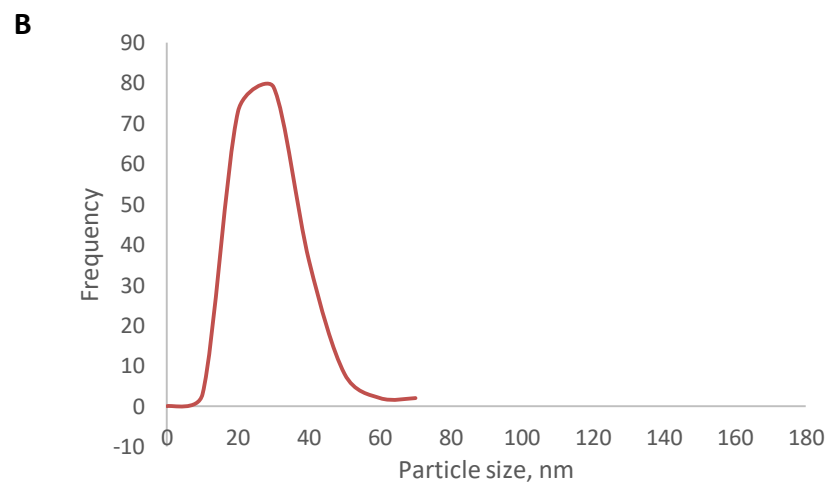
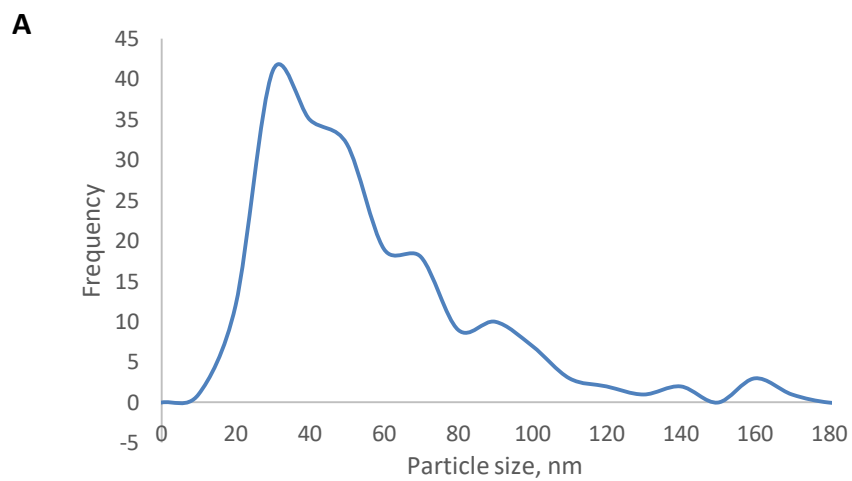


Figure D-2: PSD curves for the cobalt oxide particles synthesized from a) cobalt chloride hexahydrate base salt and b) cobalt nitrate hexahydrate base salt in 50% methanol, calcined at 300°C

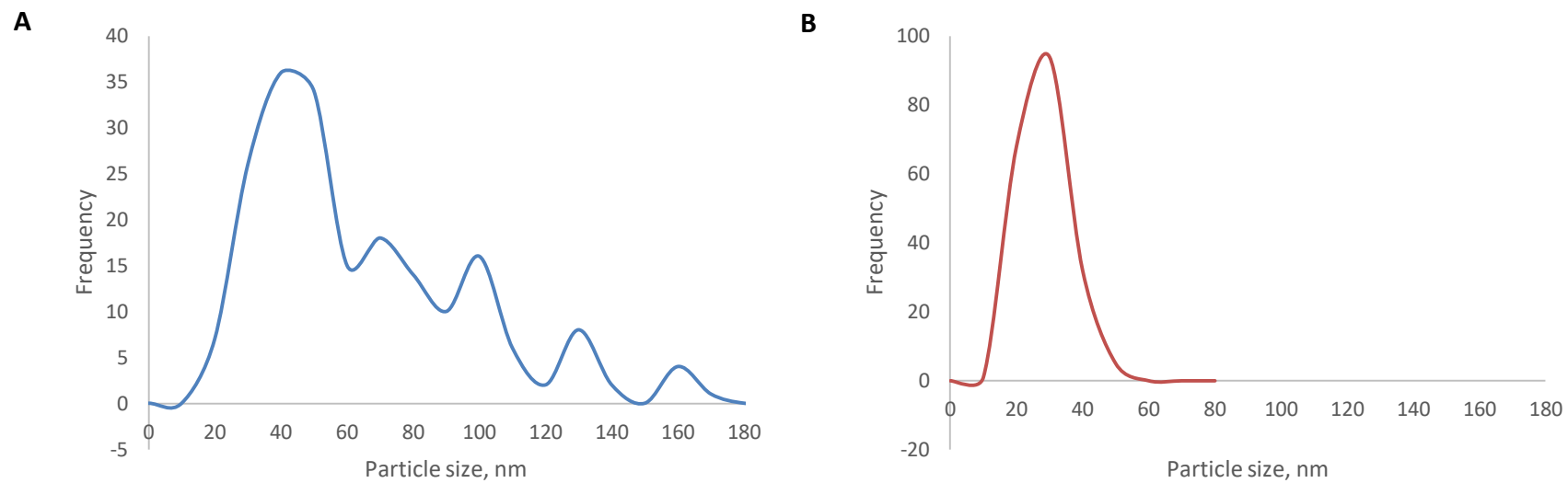


Figure D-3: PSD curves for the cobalt oxide particles synthesized from a) cobalt chloride hexahydrate base salt and b) cobalt nitrate hexahydrate base salt in 50% ethanol, calcined at 300°C

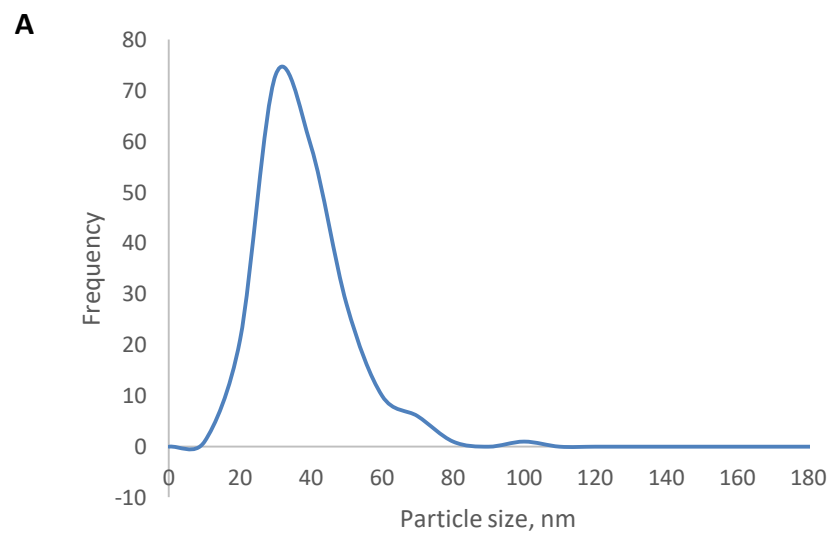


Figure D-4: PSD curves for the cobalt oxide particles synthesized from a) cobalt chloride hexahydrate base salt in 50% propanol, calcined at 300°C

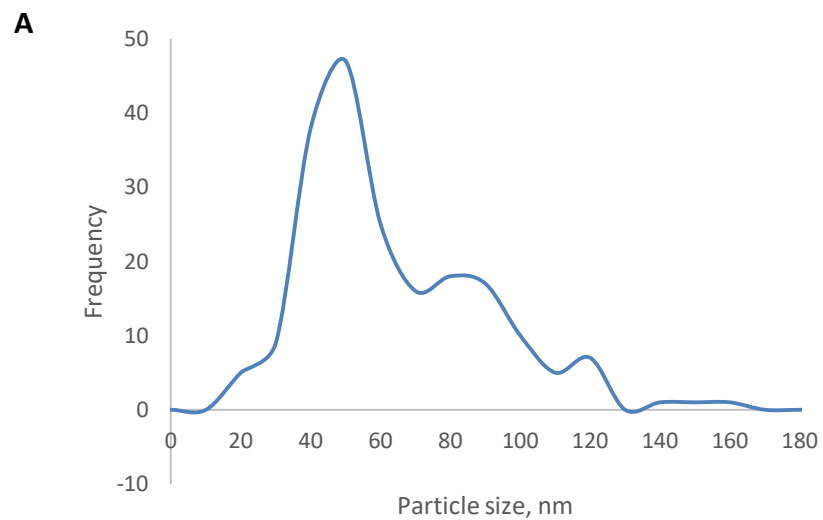


Figure D-5: PSD curves for the particles synthesized from a) cobalt chloride hexahydrate base salt in 50% butanol, calcined at 300°C

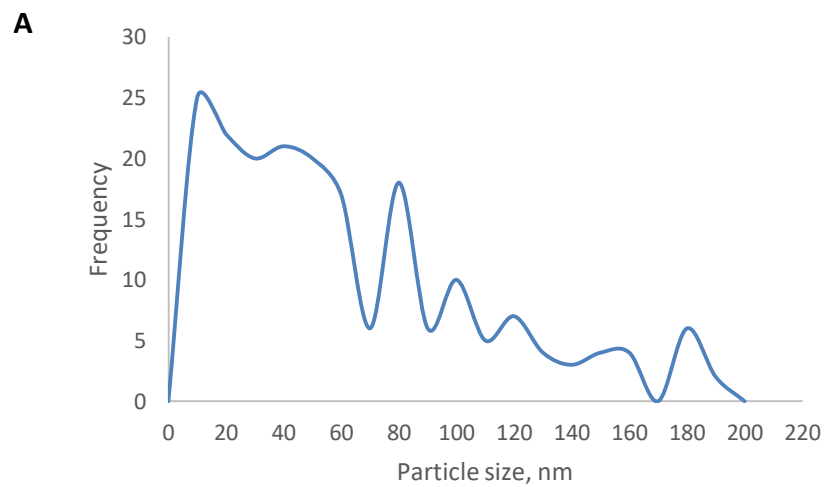


Figure D-6: PSD curves for the cobalt oxide particles synthesized from a) cobalt chloride hexahydrate base salt in 50% octanol, calcined at 300°C

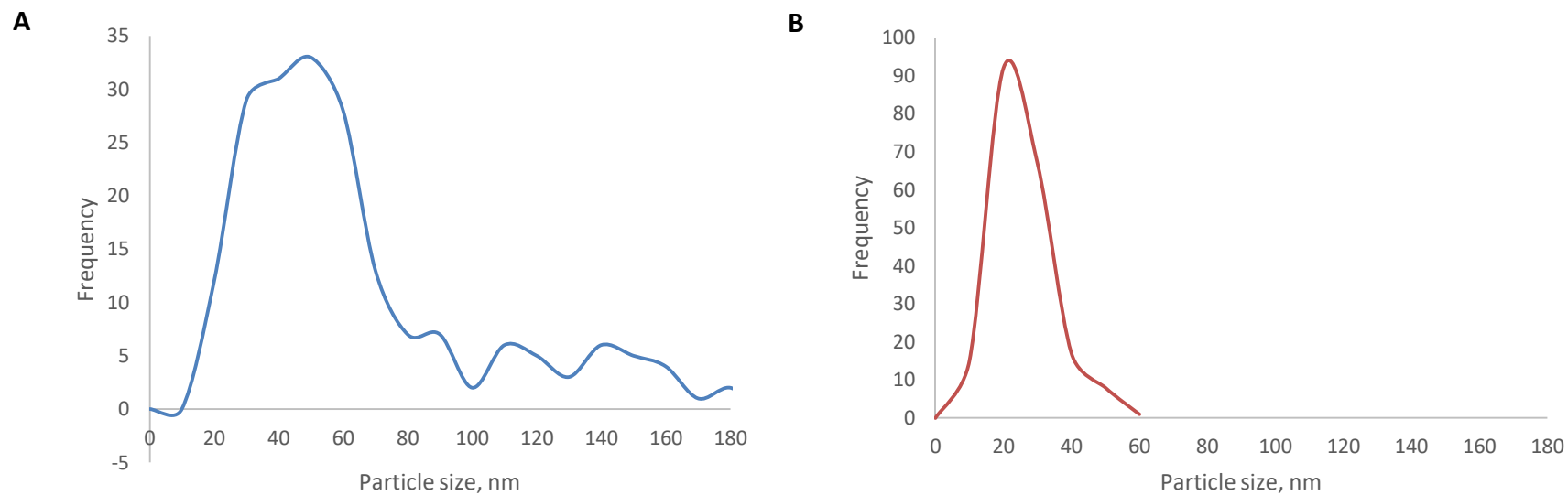


Figure D-7: PSD curves for the cobalt oxide particles synthesized from a) cobalt chloride hexahydrate base salt and b) cobalt nitrate hexahydrate base salt in 100% methanol, calcined at 300°C

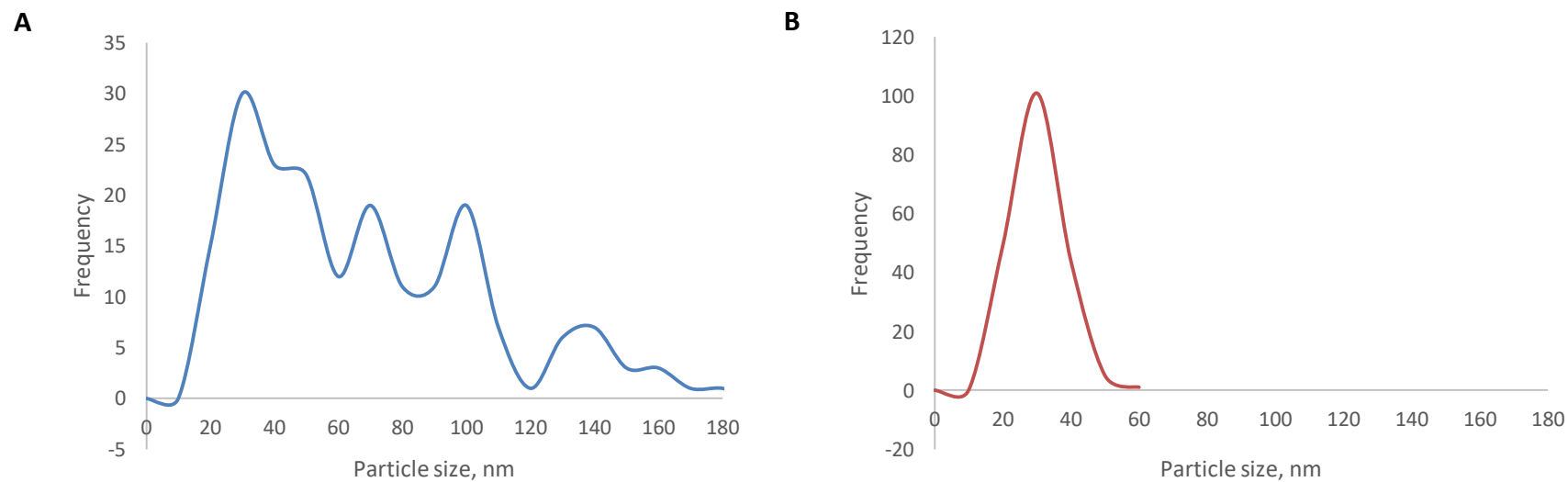


Figure D-8: PSD curves for the cobalt oxide particles synthesized from a) cobalt chloride hexahydrate base salt and b) cobalt nitrate hexahydrate base salt in 100% ethanol, calcined at 300°C

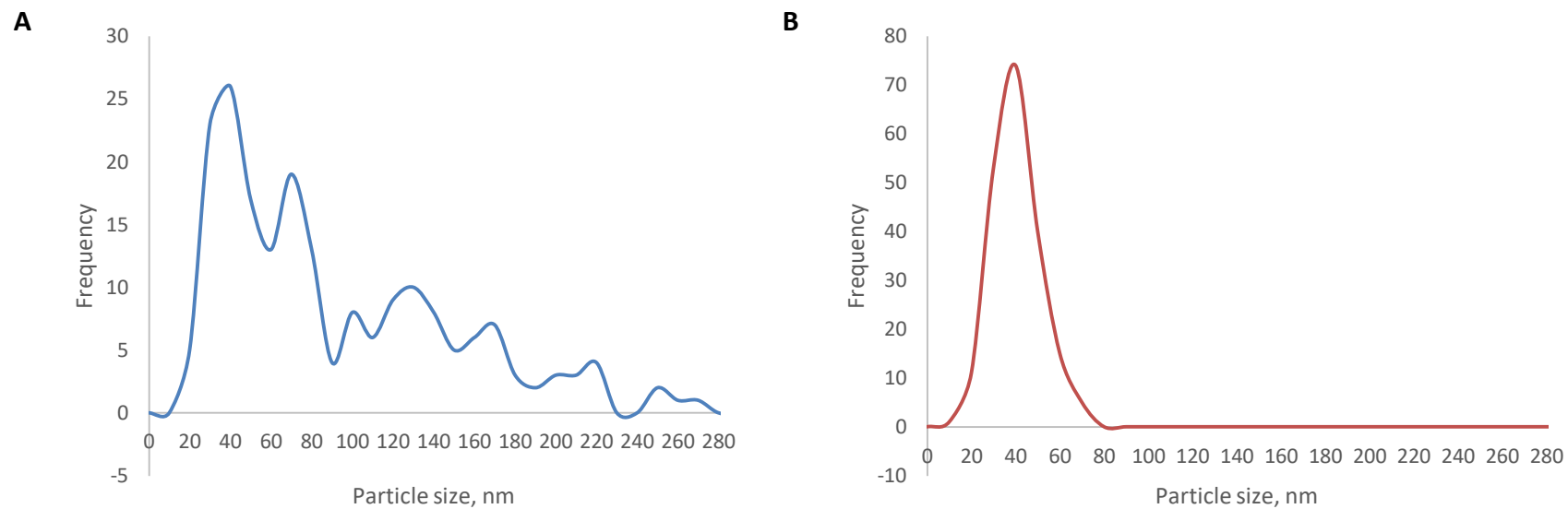


Figure D-9: PSD curves for the cobalt oxide particles synthesized from a) cobalt chloride hexahydrate base salt and b) cobalt nitrate hexahydrate base salt in 100% propanol, calcined at 300°C

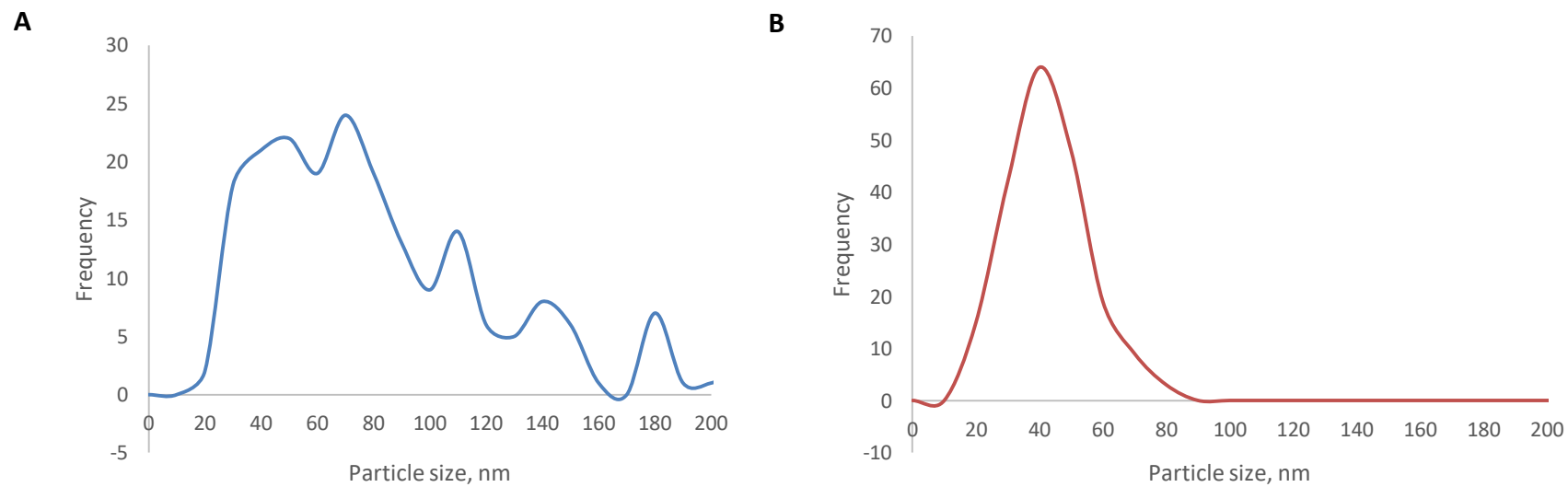


Figure D-10: PSD curves for the cobalt oxide particles synthesized from a) cobalt chloride hexahydrate base salt and b) cobalt nitrate hexahydrate base salt in 100% butanol, calcined at 300°C

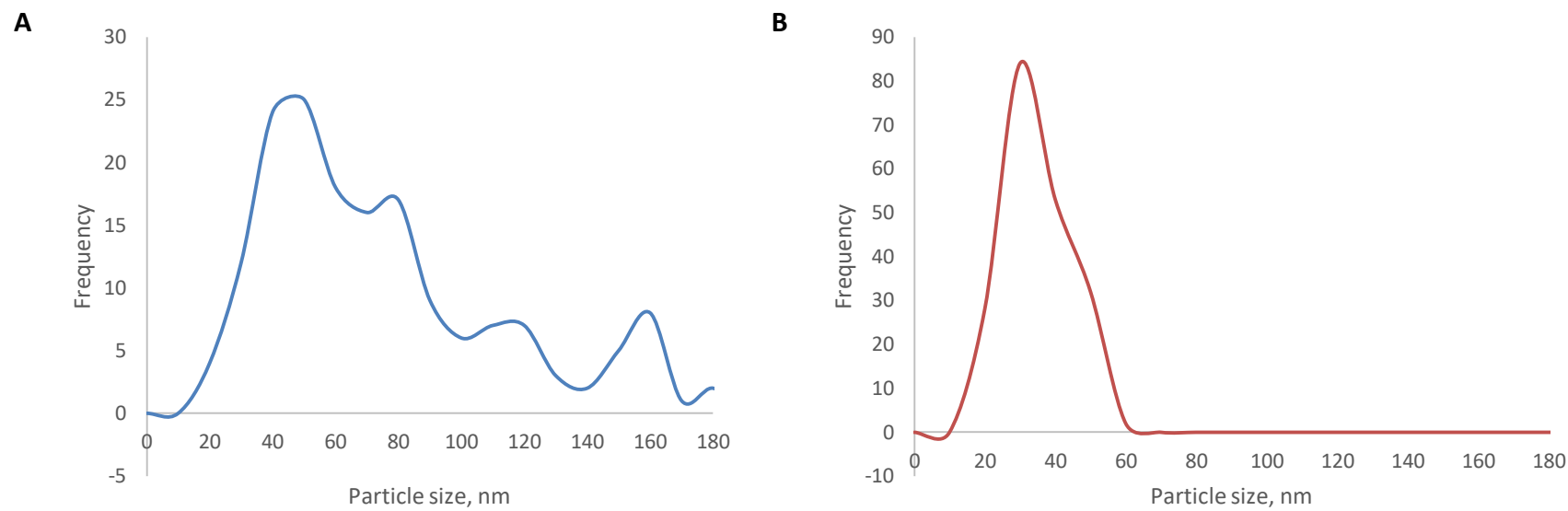


Figure D-11: PSD curves for the cobalt oxide particles synthesized from a) cobalt chloride hexahydrate base salt and b) cobalt nitrate hexahydrate base salt in 100% octanol, calcined at 300°C

Appendix E. SAED images for the synthesized particles

Table E-1: SAED images for the cobalt oxide particles synthesized in 100% water, calcined at 300°C

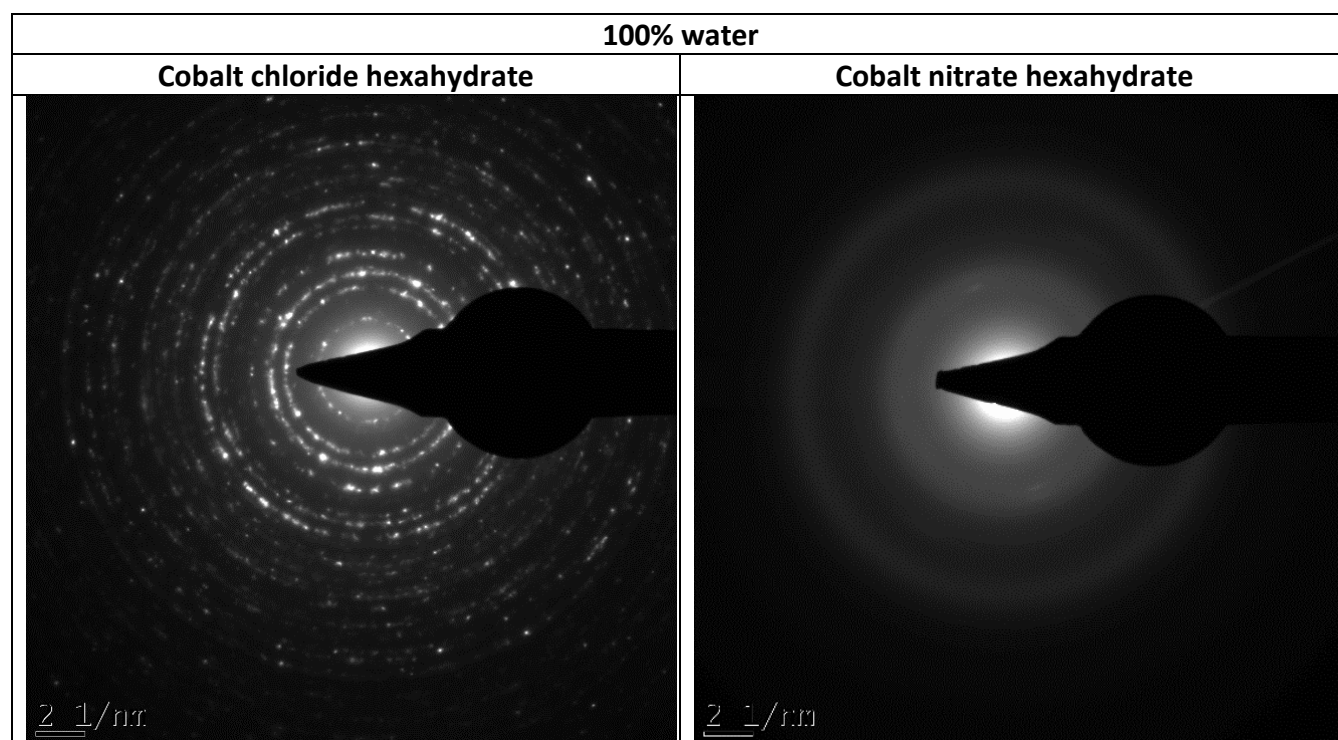


Table E-2: SAED images for the cobalt oxide particles synthesized in methanol, calcined at 300°C

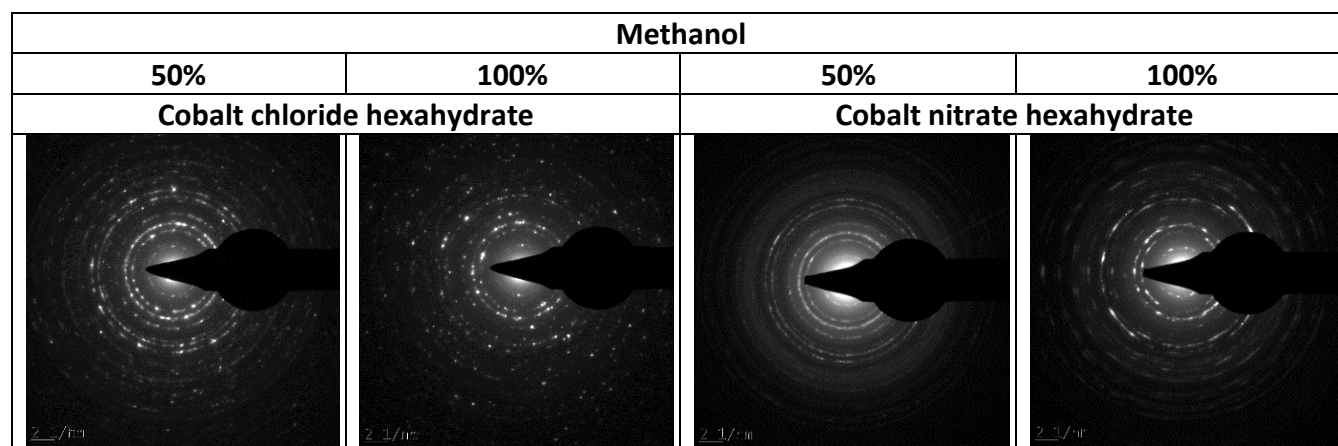


Table E-3: SAED images for the cobalt oxide particles synthesized in ethanol, calcined at 300°C

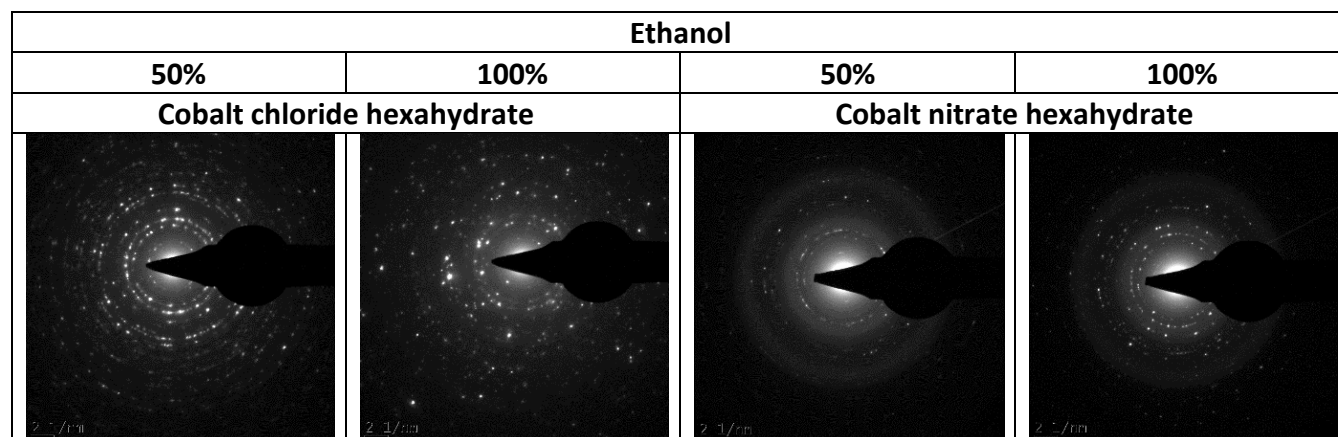


Table E-4: SAED images for the cobalt oxide particles synthesized in propanol, calcined at 300°C

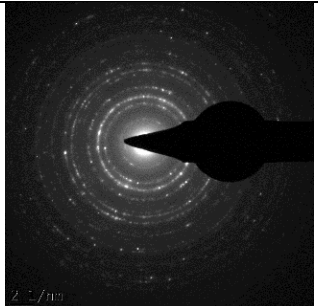
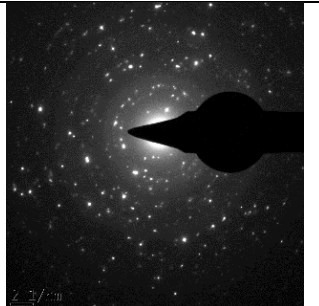
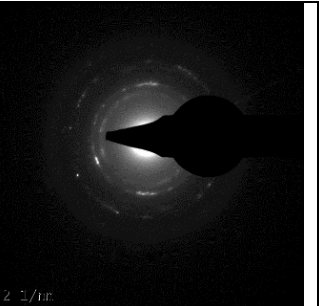
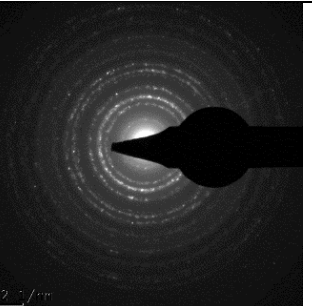
Propanol			
50%	100%	50%	100%
Cobalt chloride hexahydrate		Cobalt nitrate hexahydrate	
			

Table E-5: SAED images for the cobalt oxide particles synthesized in butanol, calcined at 300°C

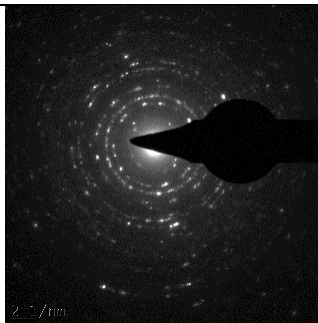
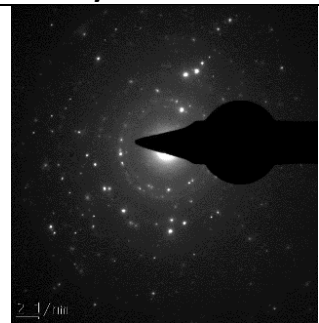
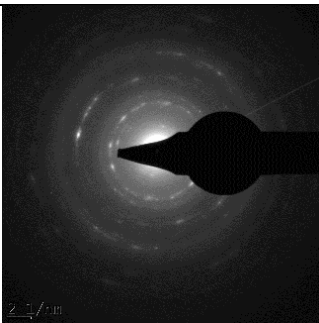
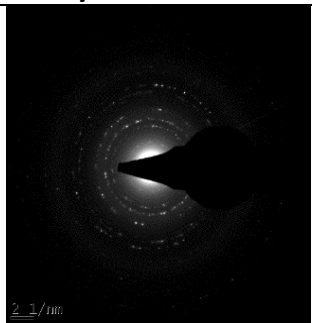
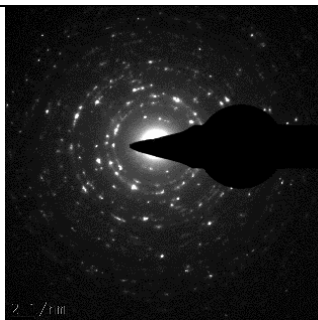
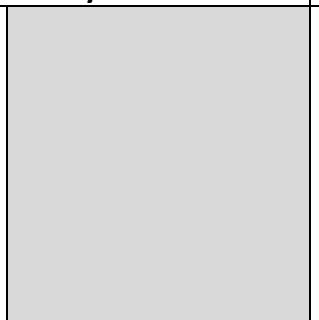
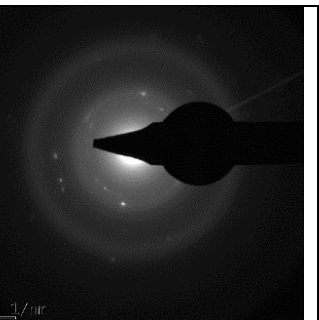
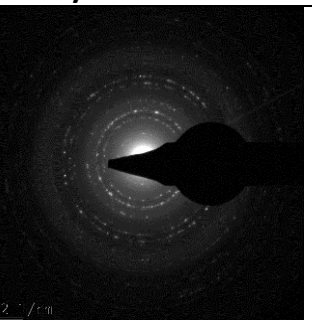
Butanol			
50%	100%	50%	100%
Cobalt chloride hexahydrate		Cobalt nitrate hexahydrate	
			

Table E-6: SAED images for the cobalt oxide particles synthesized in octanol, calcined at 300°C

Octanol			
50%	100%	50%	100%
Cobalt chloride hexahydrate		Cobalt nitrate hexahydrate	
			

Appendix F. Degradation curves

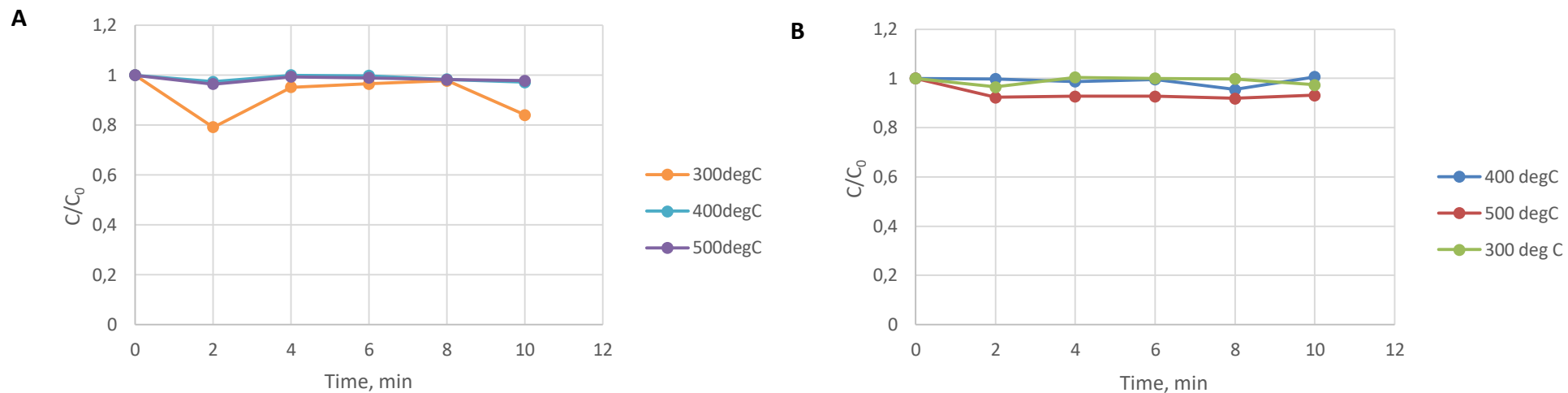


Figure F-1: Methylene blue degradation using the catalyst synthesized from a) cobalt chloride hexahydrate base salt and b) cobalt nitrate hexahydrate base salt in 50% methanol

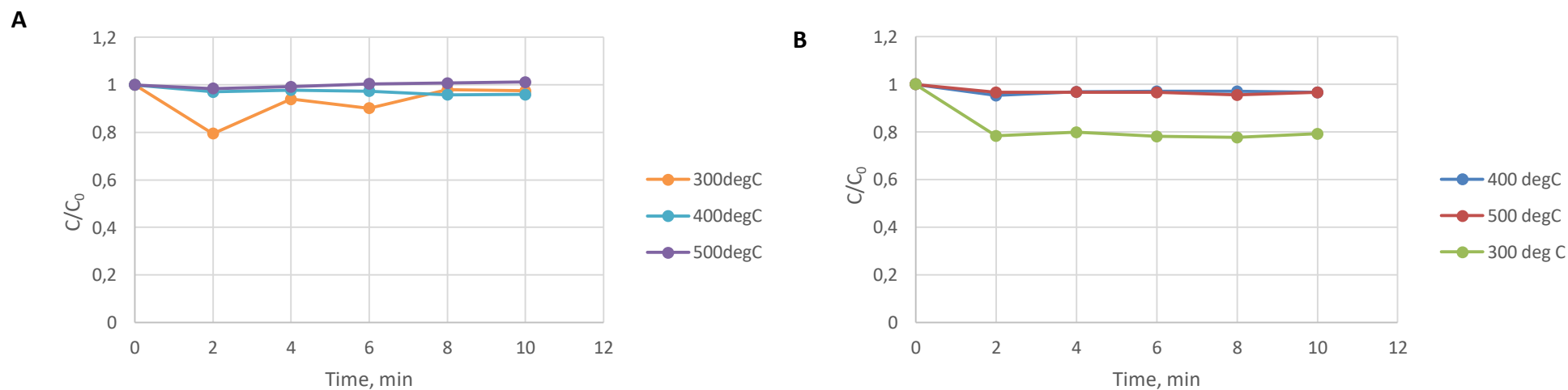


Figure F-2: Methylene blue degradation using the catalyst synthesized from a) cobalt chloride hexahydrate base salt and b) cobalt nitrate hexahydrate base salt in 50% ethanol

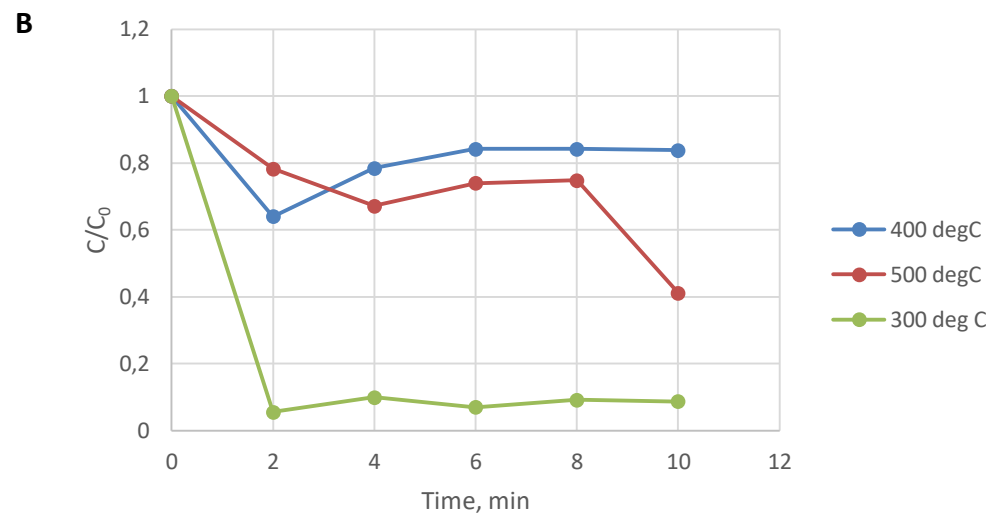
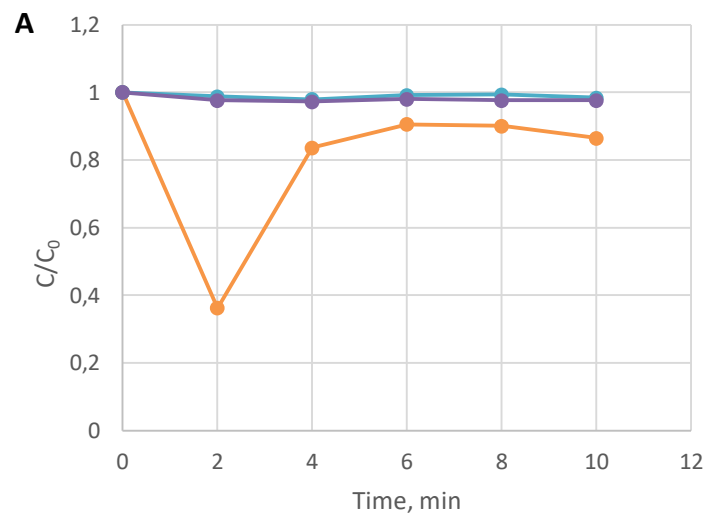


Figure F-3 Methylene blue degradation using the catalyst synthesized from a) cobalt chloride hexahydrate base salt and b) cobalt nitrate hexahydrate base salt in 50% propanol:

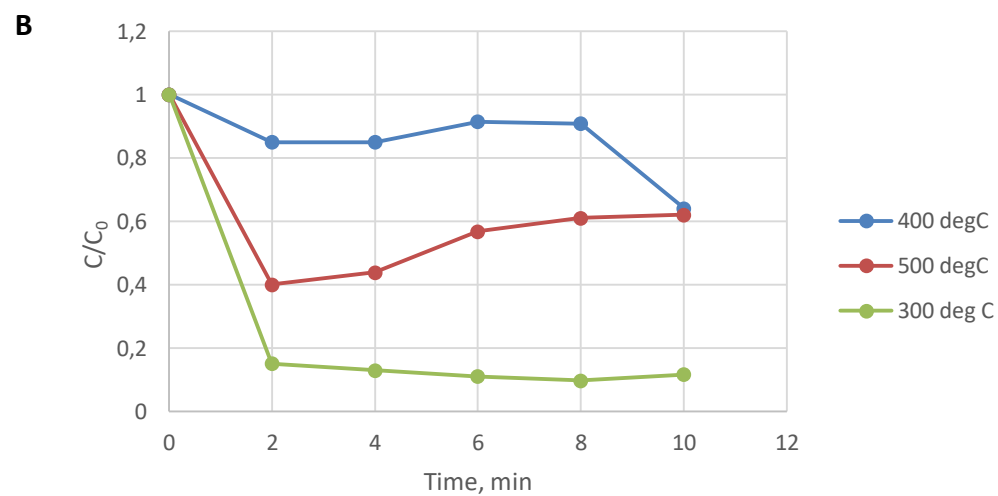
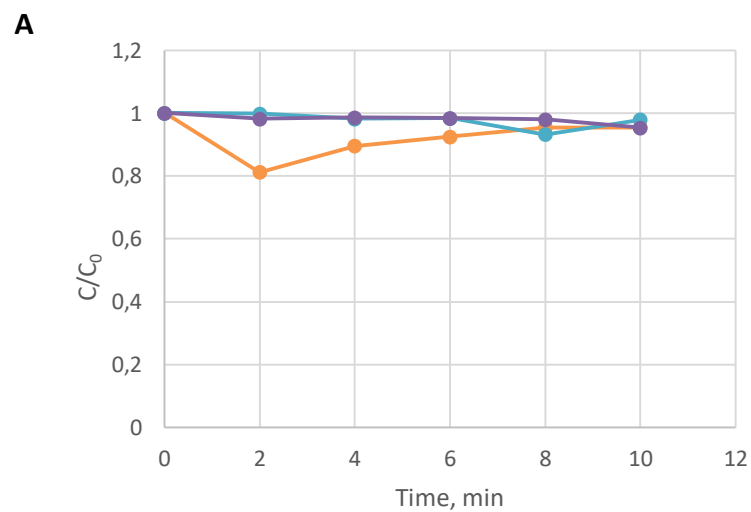


Figure F-4: Methylene blue degradation using the catalyst synthesized from a) cobalt chloride hexahydrate base salt and b) cobalt nitrate hexahydrate base salt in 50% butanol

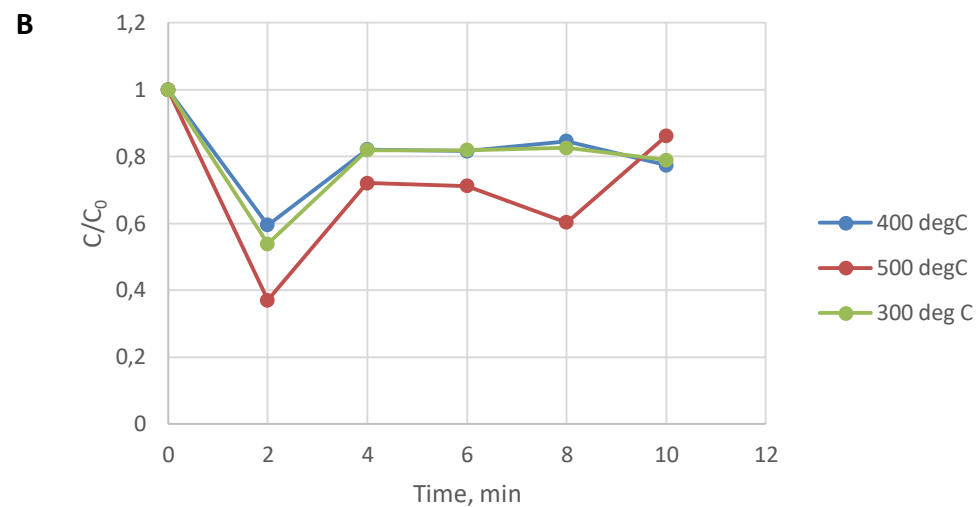
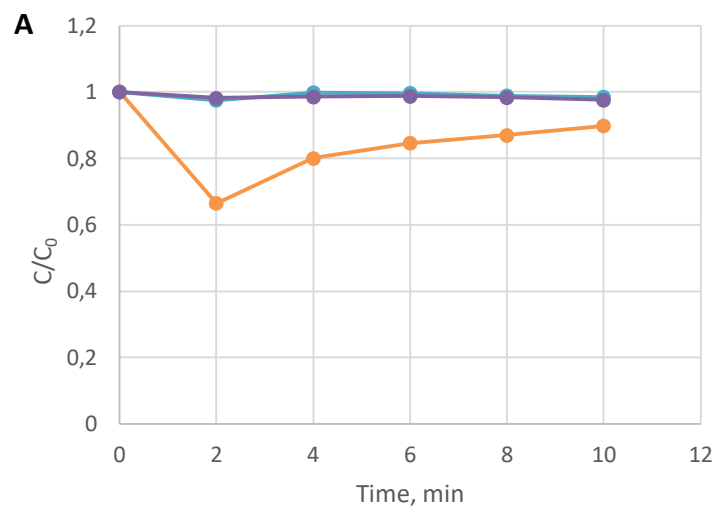


Figure F-5: Methylene blue degradation using the catalyst synthesized from a) cobalt chloride hexahydrate base salt and b) cobalt nitrate hexahydrate base salt in 50% octanol

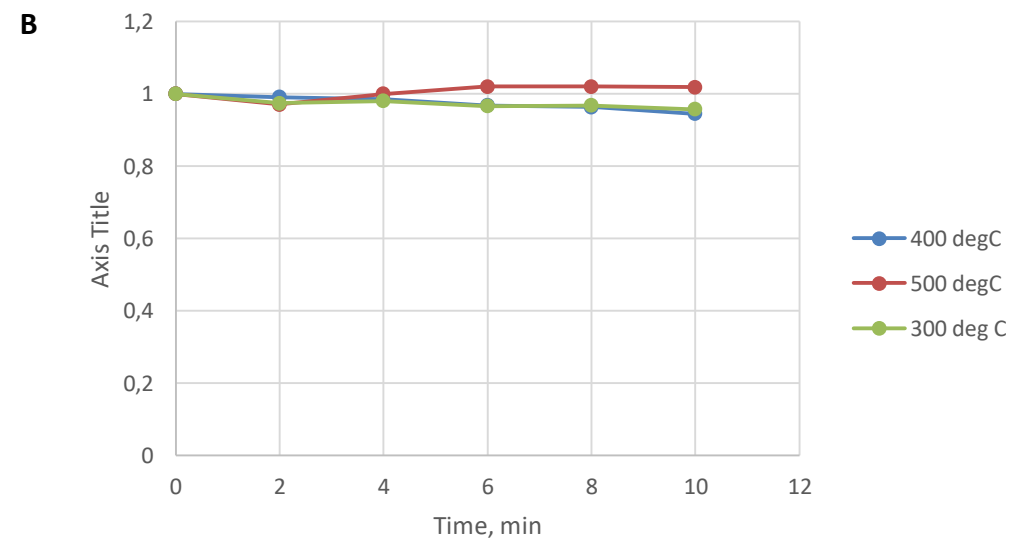
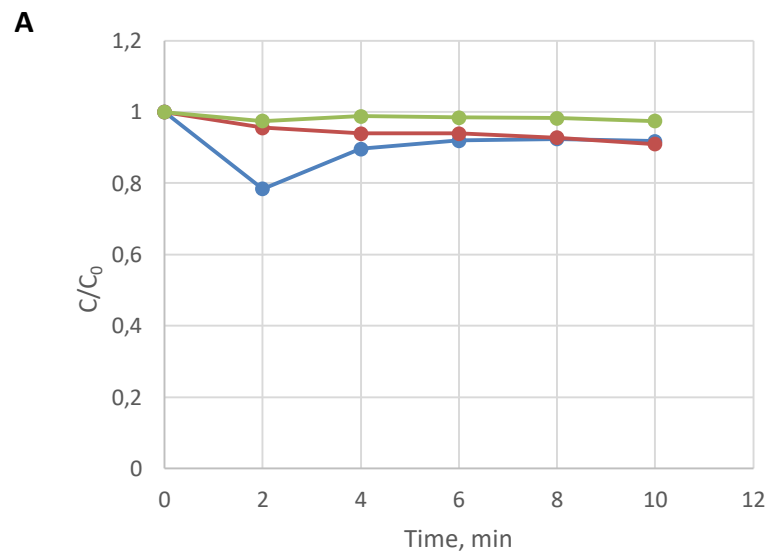


Figure F 6: Methylene blue degradation using the catalyst synthesized from a) cobalt chloride hexahydrate base salt and b) cobalt nitrate hexahydrate base salt in water

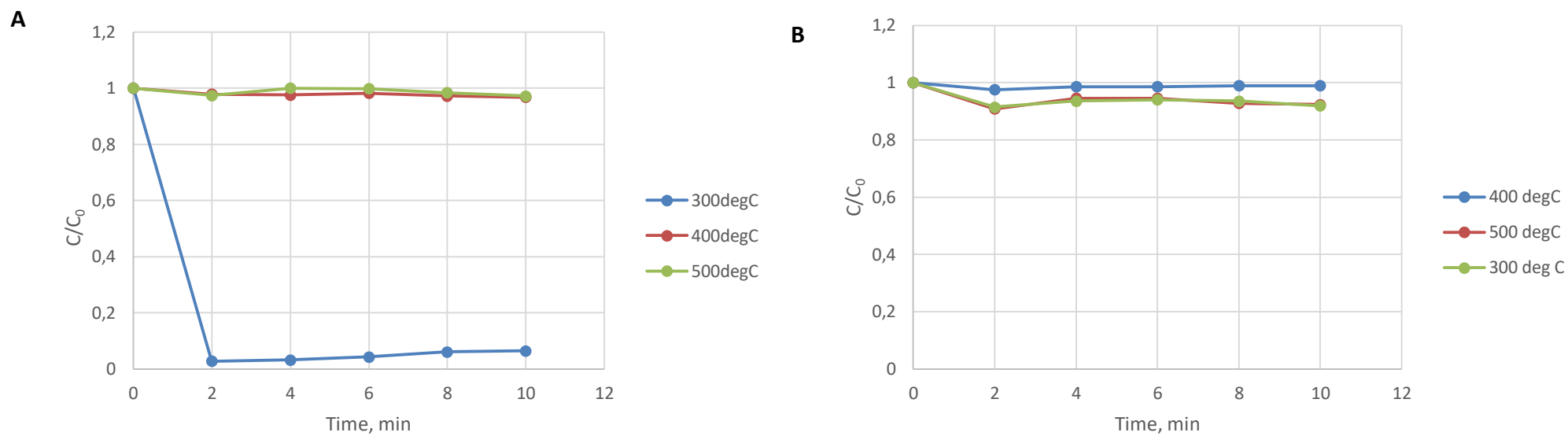


Figure F-7: Methylene blue degradation using the catalyst synthesized from a) cobalt chloride hexahydrate base salt and b) cobalt nitrate hexahydrate base salt in 100% methanol

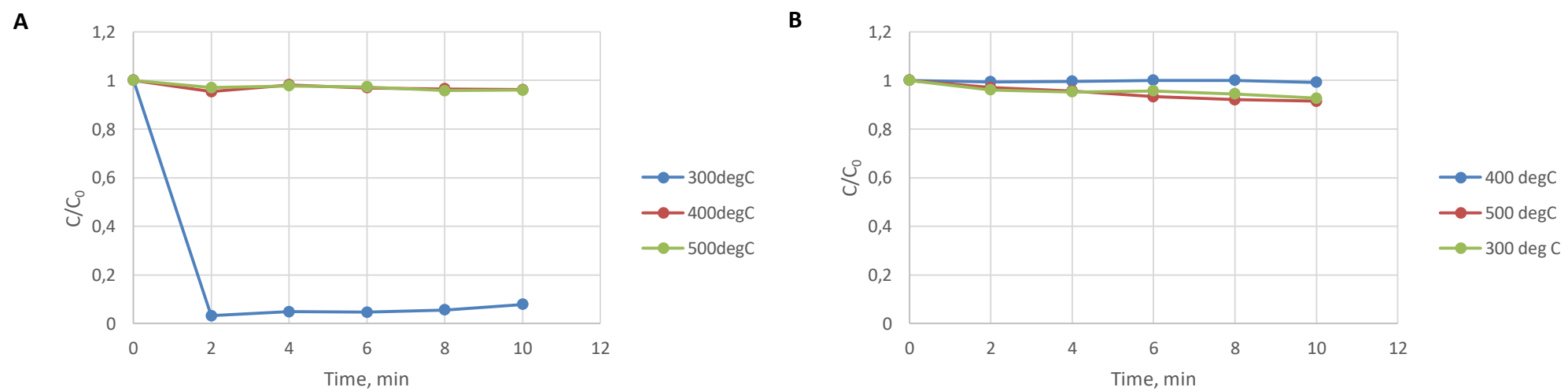


Figure F-8: Methylene blue degradation using the catalyst synthesized from a) cobalt chloride hexahydrate base salt and b) cobalt nitrate hexahydrate base salt in 100% ethanol

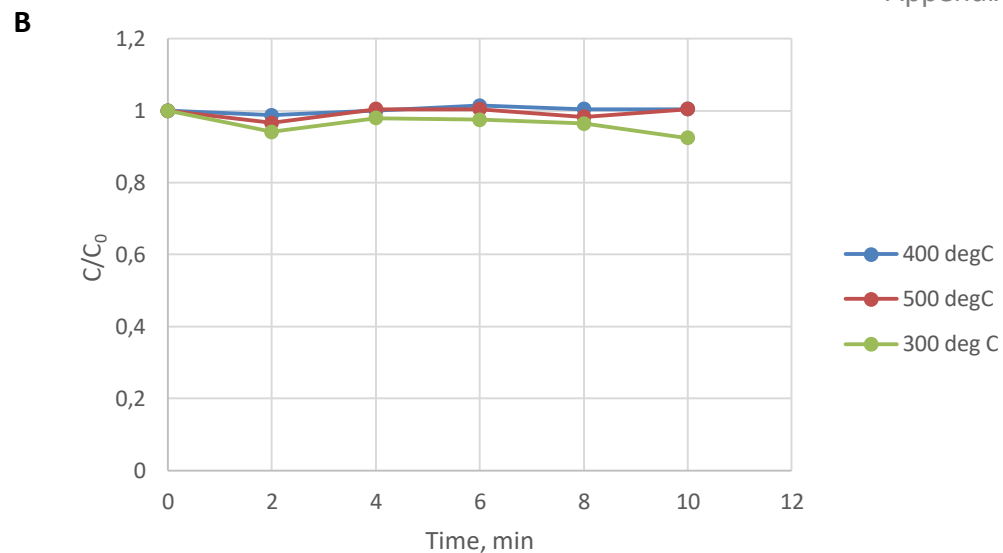
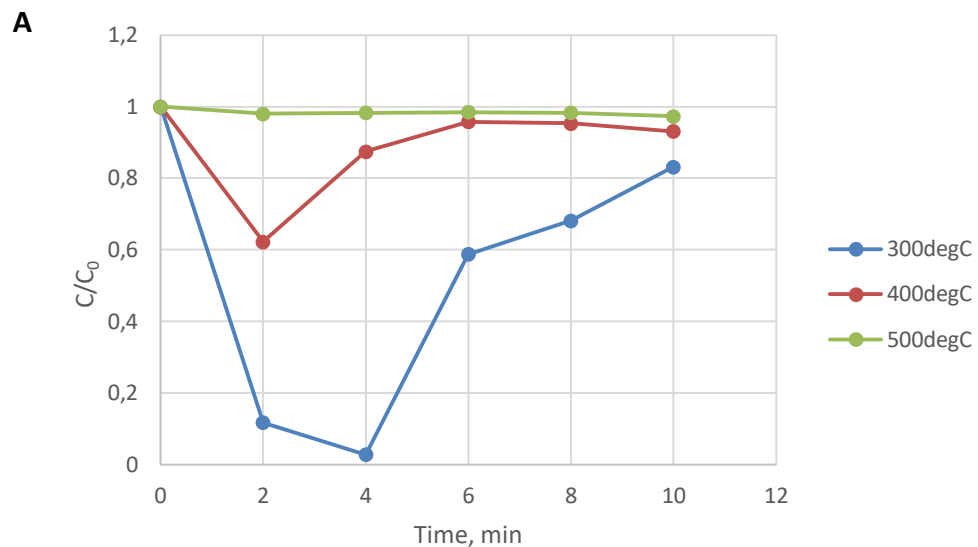


Figure F-9: Methylene blue degradation using the catalyst synthesized from a) cobalt chloride hexahydrate base salt and b) cobalt nitrate hexahydrate base salt in 100% propanol

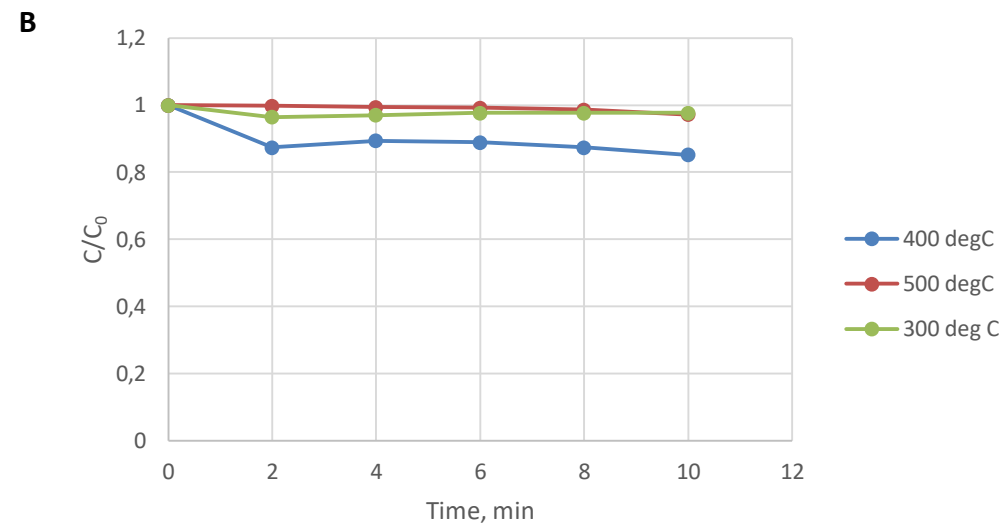
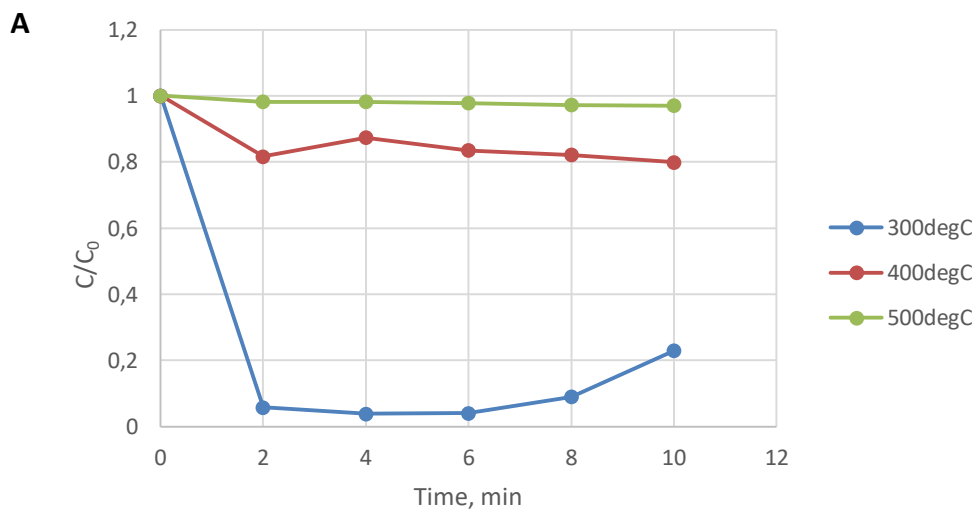
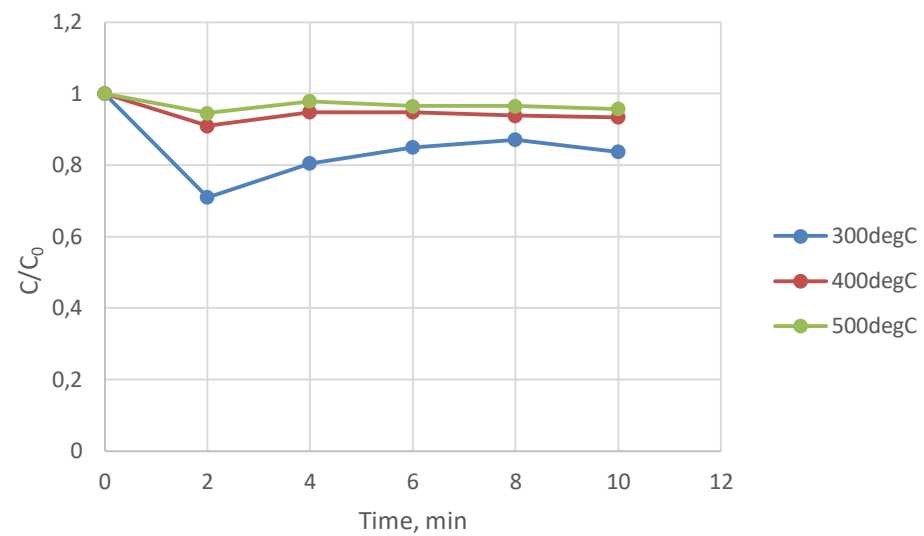


Figure F-10: Methylene blue degradation using the catalyst synthesized from a) cobalt chloride hexahydrate base salt and b) cobalt nitrate hexahydrate base salt in 100% butanol

A



B

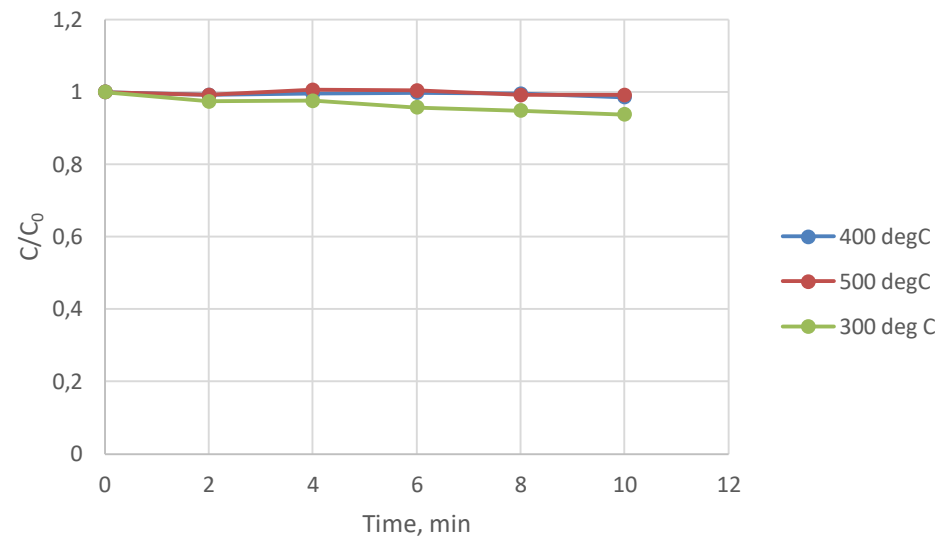


Figure F-11 Methylene blue degradation using the catalyst synthesized from a) cobalt chloride hexahydrate base salt and b) cobalt nitrate hexahydrate base salt in 100% octanol